A comprehensive study on molten conductive polymer composites under extensional deformation : relationship between filler network structure and electrical conductivity

Marjorie Marcourt

N° d'ordre NNT : 2018LYSE1097

THESE de DOCTORAT DE L'UNIVERSITE DE LYON

opérée au sein de

l'Université Claude Bernard Lyon 1

Ecole Doctorale N° accréditation
Matériaux ED34

Spécialité de doctorat : Matériaux
Discipline Matériaux innovants

Soutenue publiquement le 14/06/2018, par :

Marjorie Marcourt

Étude de l'évolution de la conductivité électrique de matériaux composites sous déformations élongationnelles: application au thermoformage

---

Devant le jury composé de :

Mme Nadia El-Kissi	CNRS Université Grenoble-Alpes	Rapporteure
Mme Paula Moldenaers	KU Leuven (Belgique)	Rapporteure
Mr. Jean-Charles Majesté	Université Jean Monnet St-Etienne	Examinateur
Dr. Olivier Lhost	Total Polymer Materials Department R&T Feluy (Belgique)	Examinateur
Prof. René Fulchiron	Université Lyon 1 – IMP	Directeur de thèse
Prof. Philippe Cassagnau	Université Lyon 1 – IMP	Co-directeur de thèse

UNIVERSITE CLAUDE BERNARD- LYON 1

Président de l'Université	**Professeur Fréderic FLEURY**
Président du Conseil Académique	Professeur Hamda BEN HADID
Vice-président du Conseil Formation et Vie Universitaire	Professeur Philippe CHEVALIER
Vice-président de la Commission Recherche	Fabrice VALLEE
Directrice Générale des Services	Dominique MARCHAND

COMPOSANTE SANTE

Faculté de Médecine Lyon Est- Claude Bernard	Directeur: Professeur G. RODE
Faculté de Médecine et Maïeutique Lyon Sud-Charles Mérieux	Directrice: Professeure C. BURILLON
Faculté d'Odontologie	Directeur: Professeur D. BOUREOIS
Institut des Sciences Pharmaceutiques et Biologiques	Directrice: Professeure C. VINCIGUERRA
Institut des Sciences e Techniques de la Réadaptation	Directeur X. PERROT
Département de formation et Centre de Recherche en Biologie Humaine	Directrice Professeure A-M. SCHOTT

COMPOSANTES ET DEPARTEMENTS DE SCIENCES ET TECHNOLOGIE

Faculté des Sciences et Technologies	Directeur : F.DE MARCHI
Département Biologie	Directeur : Professeur F. THEVENARD
Département Chimie Biochimie	Directrice C. FELIX
Département GEP	Directeur : Hassan HAMMOURI
Département Informatique	Directeur : Professeur S. AKKOUCHE
Département Mathématique	Directeur : Professeur : G. TOMANOV
Département Mécanique	Directeur : Professeur H. BEN HADID
Département Physique	Directeur : Professeur : J-C PLENET
UFR Sciences et Techniques des Activités Physiques et Sportives	Directeur : Y. VANPOULLE
Observatoire des Sciences de l'Univers de Lyon	Directeur : B. GUIDERONI
Polytech Lyon	Directeur : Professeur E. PERRIN
Ecole Supérieure de Chimie Physique Electronique	Directeur : G. PIGNAULT
Institut Universitaire de Technologie de Lyon 1	Directeur : Professeur C. VITON
Ecole Supérieure du Professorat et de l'Education	Directeur : Professeur A. MOUGNIOTTE
Institut de Science Financière et d'Assurances	Directeur : N. LEBOISNE

- Doctoral thesis -

A comprehensive study on molten conductive polymer composites under extensional deformation

Relationship between filler network structure and electrical conductivity

Marjorie Marcourt

Materials Doctoral school ED 34

University Claude Bernard, Lyon 1

Lyon, France

Supervisors

René Fulchiron and Philippe Cassagnau

January, 2018

The surest sign that intelligent life exists elsewhere in the universe is that it has never tried to contact us.

-- Bill Watterson

Ackowledgements

First and foremost, I would like to express my sincere gratitude to my supervisors for, amongst other, their dedicated time, their patience, their advices and their scientific guidance during the past three years. I've learnt a lot in the field of polymer sciences (especially rheology), composites and bio-materials. I'm grateful and lucky having the chance to take part to a many rheological congress and workshop and travelling in beautiful places. I am also thankful for their high reactivity, especially during this last writing period. Special thanks to Rene, whose maddening attention while reading my manuscript drove me to finally learn English grammar. At least, I hope so! In a nutshell, working at the IMP laboratory was a huge opportunity and a fruitful experience.

I would like to take the time to acknowledge the Total Feluy Research Center and the ANRT for funding this work. I am really grateful to my industrial supervisors Simon Karam, Olivier Lhost and Dimitri Rousseaux who gave me the opportunity to take part in their works. I thank them for their precious remarks, advices, fruitful discussion and their kindness at any time. I would especially like to thank Dimitri, who gave me the opportunity to taste his own beers and gave me a passion for Belgian beers. Thanks to Eddi, Christo and Christophe who dedicated a lot of time at respectively extruding all the composites, teaching me how to thermoform composites and introducing me to charge contrast SEM.

I would like to thank all the members of the IMP Lyon laboratory with whom I had the opportunity to work. The good progress of this work would not have been possible without their precious help and technical support of Flavien, Olivier and Laurent C. They were always available for me, providing me with all of their experiences in polymer processing and technical issues. Flavien, I will never forget the time you dedicated with me at the hospital. I wish you a pleasant and sweet retirement. Thanks to Guillaume for his technical support in light diffraction and your motivation to improve the working condition in this lab. I would also thank Thierry and especially Pierre who taught me to be patient and pugnacious while cutting polymer nanometer thick. Thanks to Béatrice and Xavier for providing me all their assistance and their precious time in Scanning Electron Microscopy analysis. Thanks also to Gisèle and Sylvie for their supports and kindness. Finally, thanks to Véro and Eliane for their affection, warm words and smile, that helped me a lot during the three years.

Now, I would like to thank my old and current office mates: Manue, Thib', (Y)MCA, Clément, Antoine (I'm glad you're back amongst us), Claire and Noémie with whom I shared a small but cozy office. I feel really lucky to have shared this working place with them during the past three years. My

coffee machine is for sure in good hands[1]. Special thanks to Pierre, Bastien and Thib' for days spent together hiking, climbing and of course playing video games. I'm always here to carry you to the top 1 (or not…). I'm also truly grateful for your dedicated time to teach me how to snowboard. Thanks to you I found a brand new addiction! I'm also appreciative to my fellow lab mates Michaël (English pronunciation), Christophe, Gui, Renaud, Imed, Nico, Yann, Marga, Fab', Mél', JiJi, Clémence, Brigand Posay, Laurent, Laura, Anaïs, Amani, Mo', Flo', Soline, Amira, Thibaut, Sara, Jimmy, Ori', Antoine (the shlag one) and so one… for all the fun we have had the last three years. I shared unforgettable moments, apero, pétanque (Antoine, Thib', Clément, Michaël) , touch rugby tournaments (Gui and Nico), concert, slacklining, (thanks Fab' I'm now addicted to!) or just chilling. I would like to take the time to thank Renaud. Your smile and your tenderness help me a lot during the last months. I'm glad to have the opportunity to meet you and fortunate to be a special member of your "vacation office". Finally, thanks the rheology congresses, especially the JJR; I had the chance to meet people with whom I had lot of fun Rudy and of course Adrien (the Belgian one).

Last but not the least; I truly thank my family and my old pales from Corrèze Sara, Marine, Lisa and Sophie. You supported me with a lot of food and warm words. The last but not the least, I would like to express my heartfelt gratitude to my sweet Romain also known as "Darling", for all the sacrifices that you've made on my behalf. You've never gave up supporting me even in the most difficult days. I'm glad, that we've managed long distance relationship. However, I wish I could have by your sides more often to help you through your grief. I will never stop supporting and encouraging you until you reach your goals.

[1] Actually it is not !

Abstract

In this work we present a complete study of the electrical conductivity evolution of molten nano-composites under extensional deformation. The Conductive Polymer Composite (CPC) analyzed is a pure Polystyrene matrix filled with Carbon Nanotubes (the model system) and a rubber modified polystyrene matrix filled with Carbon nanotubes. The conductivity properties of the composites rely on the formation of a percolated network through the material. When the composite flows, the filler network can be disrupted, altering the conductivity of the composite. Thus, after a small deformation a moderately conductive composite can turn into an insulating material. From an applied viewpoint, for instance, the thermoforming of a composite sheet with good electrical properties can lead to an insulating finished part. In the literature, the studies mainly focus on the conductivity variation of molten composites under small shear deformation at low shear rates.

This study aims at analyzing the microstructure evolution when the molten composite undergoes large deformation and especially in elongation. That is why we developed a new experiment that gives the possibility to monitor the specimen conductivity during its extensional deformation all the while recording the elongation stress. On the one hand, we highlighted a close relationship between the extensional conditions that are the specimen temperature and the extensional rate with the conductivity variation. Indeed, the conductivity variations can be described by means of the Weissenberg number that takes into account the polymer dynamics and the extensional rate. On the other hand, we have shown that the volume confinement of the filler, here achieved by the presence of polybutadiene nodules, gives the possibility to decrease the filler amount without impacting the process-ability of the composites. Finally, we propose a model that describes the conductivity evolution of CPC under extensional and planar flow. It links the structural evolution of the filler network to the macroscopic properties of the composite. Thus, this experimental work has significantly contributed to the comprehension of the conductivity variation of molten composites under extensional deformation.

Key words: Rheology, Extensional flow, Conductivity, Carbon Nanotubes, Polystyrene

Résumé

Ces travaux constituent une étude approfondie se focalisant sur l'évolution des propriétés viscoélastique et électrique de composites à matrices thermoplastiques faiblement chargés en nanotubes de carbone. Deux types de polystyrène ont été utilisés : un polystyrène vierge et un polystyrène choc dans lequel sont dispersés des nodules de polybutadiène ayant une morphologie « salami ». Un ajout suffisant de particules conductrices électriques entraine la formation d'un réseau percolant rendant le matériau conducteur électrique. Lors de l'écoulement du composite, la structure du réseau va fortement évoluer changeant ainsi les propriétés macroscopiques. Par exemple, le thermoformage d'une feuille de composite ayant initialement de bonnes propriétés électriques peut générer une pièce isolante.

La majeure partie des études référencées dans la littérature se restreignent à l'analyse rhéologique de ces matériaux dans le domaine linéaire. C'est pourquoi, nous avons mis en place une toute nouvelle expérience. Celle-ci permet de mesurer simultanément la conductivité électrique d'une éprouvette lorsqu'elle est déformée en élongation à l'état fondu. Nous avons ainsi pu mettre évidence le lien étroit entre les variations de conductivité électrique avec la dynamique moléculaire du polymère et la vitesse de déformation. Il est désormais possible de décrire les variations de conductivité par le biais du nombre de Weissenberg, produit du temps de relaxation de la matrice et de la vitesse de déformation. De plus, nous avons montré qu'il était possible de réduire la concentration massique de NTC par ajout de nodules de polybutadiène sans impacter les conditions de mise en forme. Enfin, nous proposons un modèle qui permet de décrire les évolutions de conductivité électrique de composites subissant des déformations à l'état fondu, et ce, pour une gamme très large de conditions expérimentales.

Mots clés : Rhéologie, Élongation, Conductivité électrique, Nanotubes de carbone, Polystyrène

Présentation synthétique des travaux

Ces travaux de thèse sont le fruit d'une collaboration entre le laboratoire d'Ingénierie des Matériaux Polymères (IMP) de Lyon et le centre de recherche de Total situé à Feluy en Belgique. Total est, entre autres, un acteur majeur dans la production de polyoléfines et de thermoplastiques. L'arrivée sur le marché européen de polymères issus de la production de gaz de schiste principalement importé des Etats-Unis et du Canada a forcé les acteurs européens à diversifier leurs produits. Dans ce contexte, Total élargit le domaine d'application de ses matériaux polymères en améliorant ou en leur conférant de nouvelles propriétés physiques. Deux stratégies sont envisageables pour la réalisation de composites à matrice polymère à forte valeur ajoutée en modifiant l'architecture micrométrique du matériau ou en rajoutant des particules au sein de la matrice. Dans cette étude, nous nous concentrerons sur les propriétés de composites par ajout de particules pour la réalisation de packaging respectant la norme Electrostatic Discharge (ESD).

La miniaturisation des composants électroniques a entrainé la production de packagings répondants à un cahier des charges très spécifique. Tout au long de leur fabrication, les composants électroniques sont susceptibles d'être endommagés par des décharges électrostatiques. Les frottements ainsi que la non-homogénéité des propriétés électriques sont des conditions favorables pour la formation et la stagnation de charges électriques à la surface des composants. Leur décharge engendre localement la formation de courants importants qui vont endommager les circuits électroniques. Ceci s'illustre par des baisses de capacités de stockage, de rapidité de calculs voire par une destruction complète du composant qui entrainent des pertes matérielles très élevées. La réalisation de packagings spécifiques va permettre de protéger les composants tout au long de leur processus de fabrication et de transport. Ces packagings à matrice thermoplastique doivent présenter des conductivités électriques comprises dans une gamme précise pour permettre la dissipation des charges électrostatiques tout en évitant les décharges trop brusques. La première solution a été de développer des composites à matrices thermoplastiques chargées avec du noir de carbone. Un ajout suffisant de particules permet la formation d'un réseau percolant qui va assurer le passage des électrons. Le matériau devient conducteur électrique. Cette charge inorganique est caractérisée par un facteur de forme (rapport du diamètre sur la longueur apparente) faible : ≈ 1. Ainsi, la formation d'un réseau percolant nécessite un ajout important de charges. À cela s'ajoute des phénomènes de relargage qui peuvent contaminer les composants électroniques.

Une solution est de remplacer le noir de carbone par une autre charge dérivée du carbone : les nanotubes de carbone (NTC). Cette particule, caractérisée par un facteur de forme très élevé (100 à 1000 fois supérieur à celui du noir de carbone) permet l'obtention de composites ayant de bonnes

propriétés électriques et ce avec une très faible teneur en particules. Ce type de composites a fait l'objet d'un grand nombre d'études ces dernières années. Les étapes d'incorporation des particules au sein de la matrice polymère sont maîtrisées. Ainsi, il est possible d'obtenir des semi-produits, sous forme de granulés ou de feuilles, ayant de bonnes conductivités électriques. Cependant, la mise en forme de ces semi-produits, par des procédés couramment utilisés pour les thermoplastiques (en particulier le thermoformage), ne permet pas la réalisation de produits finis ayant les propriétés souhaitées.

Ces travaux de thèse ont pour objectifs d'analyser et de comprendre l'évolution du réseau de NTC lors de la mise en forme à l'état fondu du matériau composite. Ainsi, une méthode de caractérisation innovante a été mise en place au laboratoire IMP afin de caractériser la déformation du réseau de charges lorsque le matériau à l'état fondu subit des déformations en élongation uniaxiale. La Figure 1a présente l'appareil d'élongation avec le montage électrique. La Figure 1b illustre les variations de conductivité électrique et de la contrainte élongationelle en fonction de la déformation.

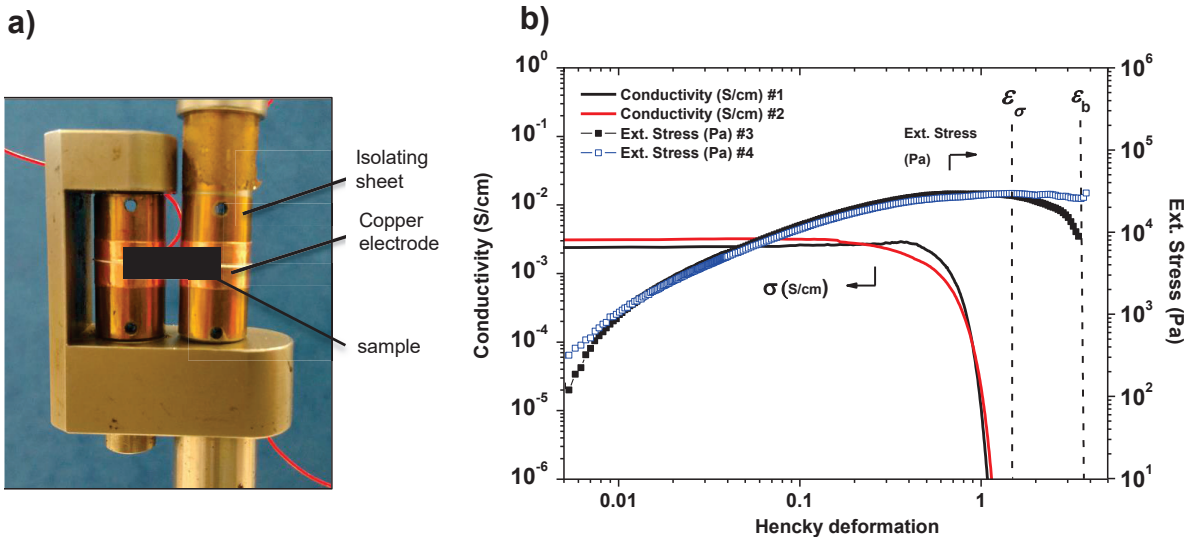

Figure 1 :Présentation du module d'élongation modifié pour permettre la mesure de conductivité électrique de l'éprouvette a). Variation de conductivité électrique et de contrainte élongationnelle pendant la déformation d'une éprouvette de PS + 0,79 vol% NTC à 160°C avec une vitesse de déformation fixée à 0,01s^{-1} b).

Cette expérience est représentative de ce que subit le matériau lors du thermoformage, procédé couramment utilisé pour la réalisation de packaging. Durant cette étude, deux types de composites ont été caractérisés à l'aide de cette expérience : une matrice polystyrène et une matrice polystyrène choc chargées toutes les deux en nanotubes de carbone. L'étude approfondie de ces matériaux a permis la réalisation d'un modèle qui rend possible la prédiction de la conductivité du matériau en fonction de la déformation.

Ce manuscrit se découpe en trois parties. La première partie se compose d'un chapitre bibliographique et d'une présentation succincte des méthodes expérimentales ainsi que les matériaux utilisés durant ces travaux de thèse. Le chapitre bibliographique expose le contexte

scientifique de l'étude et a pour objectif de présenter les notions qui ne sont pas abordées dans les chapitres scientifiques rédigés sous format publication. Ainsi, nous aborderons les problèmes d'incorporation de charges au sein de matrices polymères. Nous développerons de manière détaillée les différentes techniques de caractérisation de l'état de dispersion des charges et de leur orientation.

La deuxième partie se compose de trois chapitres scientifiques destinés à être publiés. Le premier chapitre présente une nouvelle méthode de caractérisation mise en place au laboratoire IMP. Un appareil de mesure de viscosité élongationelle a été modifié afin de mesurer la conductivité électrique de l'éprouvette pendant sa déformation à l'état fondu. Cette méthode rend possible le suivi des variations de conductivité électrique du composite tout en contrôlant la vitesse de déformation et la température et en mesurant la contrainte élongationelle. Nous avons ainsi pu observer les pertes de conductivité électrique d'un composite pendant sa déformation à l'état fondu. Ce résultat confirme des observations faites pendant le thermoformage de composites. Cette expérience a permis de mettre en exergue l'importance des conditions expérimentales sur les variations de conductivité électrique et de mettre en lumière les phénomènes de recouvrances électriques. En effet, un matériau qui a subi de grandes déformations va pouvoir retrouver, en partie ou totalement, ses propriétés électriques initiales s'il reste à l'état fondu. Ce phénomène a été expliqué par la dynamique moléculaire de la matrice. La mobilité des chaines va permettre la restructuration du réseau par le biais de la formation de connexions entre agrégats.

Pendant la déformation du matériau, une compétition entre la structuration et la destruction du réseau de nanotubes va avoir lieu. Suivant les conditions d'étirage, cette compétition sera plus ou moins importante. Nous avons montré que le nombre de Weissenberg (W_i) qui est le produit d'un temps de relaxation caractéristique de la matrice (dynamique moléculaire qui dépend de la température) et de la vitesse d'étirage permet de décrire cette compétition. Ainsi, pour des W_i élevés, la destruction du réseau sera prédominante et la limite de mise en forme dépendra uniquement de la concentration en NTCs qui régit la conductivité initiale du matériau. Au contraire, pour des faibles W_i, une forte compétition entre la structuration et la destruction du réseau a lieu. Dans ces conditions, le matériau pourra subir des déformations plus importantes avant de perdre ses propriétés électriques. Ainsi, nous avons montré qu'en jouant sur la température et la vitesse de déformation il était désormais possible d'obtenir un matériau étiré avec une conductivité électrique maitrisée.

Le second chapitre se concentre sur l'étude d'un composite à matrice polystyrène choc (HIPS) chargé en NTC. Cette matrice se compose d'une phase PS dans laquelle se trouvent des nodules de polybutadiène (morphologie type salami) issus de la réticulation de la phase élastomère. La phase polystyrène présente des propriétés rhéologiques proches de la matrice qui a été étudiée dans le premier chapitre scientifique. Pour ce composite, les charges sont exclusivement localisées dans la phase PS qui constitue un peu moins de 60% du volume total du matériau. Ce confinement des NTC permet de réduire le taux massique de charges nécessaire à la conduction. En effet, on peut réduire de moitié la masse de charges incorporé tout en ayant des propriétés électriques proches de celle du composite à matrice PS (en considérant la même concentration volumique de nanotubes de carbone

dans la phase PS). Cette étude nous a permis de confirmer les phénomènes de restructuration (sans déformation) qui sont gouvernés par la dynamique moléculaire de la matrice dans laquelle sont dispersées les charges. Nous avons également observé que la présence des nodules n'influence pas la restructuration du réseau de charges après avoir subi une forte déformation. Néanmoins, ce type de composites se distingue pendant la déformation à l'état fondu. Lorsque les mécanismes de destruction sont prépondérants, les deux composites présentent des limites de mise en forme comparables. Au contraire, lorsqu'il y a une forte compétition possible entre les mécanismes de destruction et de structuration, les composites à matrice HIPS perdent leurs propriétés électriques pour des déformations plus faibles. Nous avons expliqué ce phénomène par la présence des nodules. Lorsque le matériau est soumis à une déformation, les nodules de polybutadiène se déforment moins ce qui entraine des inhomogénéités de vitesse de déformation au sein du matériau. Au voisinage des nodules, les agrégats sont beaucoup plus déformés et ne sont pas orientés dans le sens de la déformation, ce qui ne favorise pas les phénomènes de connexion entre agrégats.

Le dernier chapitre présente un modèle qui permet de décrire l'évolution de la conductivité électrique des composites lorsqu'ils subissent des déformations. Ce modèle relie l'évolution microscopique du matériau (réseau percolant de charges qui permet le passage des électrons) à ses propriétés macroscopiques (sa conductivité électrique). L'évolution de la population de nanotubes de carbone qui participent au réseau peut être décrite par une équation cinétique. Cette équation prend en compte les mécanismes de structuration et de destruction du réseau lorsque le matériau est déformé à l'état fondu. Pour la structuration, nous avons fait l'hypothèse que l'ensemble des NTC appartenant au réseau percolant de charges sont des sites potentiels pour la formation de nouvelles connexions avec des agrégats qui sont isolés. La vitesse de formation de nouvelles connexions est proportionnelle à la proportion de NTC qui n'appartient pas au réseau percolant. La distribution du réseau, quant à elle, dépend uniquement de la déformation subie par le matériau. Tout d'abord les charges vont s'orienter et s'allonger dans le sens de la déformation. Puis, petit à petit, les agrégats vont se séparer les uns des autres. Les jonctions qui les relient vont être détruites et la conductivité électrique du composite va diminuer progressivement jusqu'à ce que le matériau devienne isolant électrique car la population de NTC qui participent au réseau sera devenue inférieure au seuil de percolation. La solution de cette équation cinétique qui décrit l'évolution de la population de NTC appartenant au réseau percolant est ensuite injectée dans une loi de percolation qui décrit l'évolution de la conductivité électrique du matériau en fonction de sa concentration en charge. On a montré que les phénomènes de structuration dépendent uniquement de la température par l'intermédiaire du temps de relaxation du polymère dans lequel les nanotubes sont dispersés. La destruction dépend uniquement de la déformation appliquée au matériau. Ainsi, en connaissant la concentration de nanotubes de carbone, la conductivité initiale du matériau (qui rend compte de l'état d'équilibre initial), la température et la vitesse d'étirage nous pouvons déterminer l'évolution de la conductivité du composite en fonction de la déformation ainsi que la déformation maximale que le matériau peut subir avant de devenir isolant. Ce modèle s'est montré performant pour une large gamme de conditions expérimentales (W_i élevés et faibles), de concentrations en nanotubes de carbone et de type de matrice.

Enfin l'annexe scientifique regroupe des résultats qui complètent les chapitres scientifiques.

Nous présentons l'application du modèle sur des matériaux HIPS chargés en nanotubes de carbone ainsi qu'une étude réalisée sur le thermoformage de feuilles de polystyrène chargés en nanotubes de carbone. A partir de feuilles épaisses de composite, des coupelles ont été thermoformées. Une cartographie précise de la déformation et de la conductivité a été réalisée sur les produits finis. Nous avons pu, in fine, montrer que le modèle donne des résultats en accord avec les variations de conductivité électrique observées en thermoformage.

Contents

Part I

Chapter 1

State of the art

I. Fillers and Polymers

A. Carbon Nanotubes

The worldwide enthusiasm of the Carbon Nanotubes (CNTs) fields occurred in the 1990's and was triggered by the works of Iijima *et al.* [1,2]. They were the first to report the catalyst-free formation of almost perfect concentric Multiwall Carbon Nanotubes (c-MWCNTs) as by-products of the formation of fullerene by electric-arc technique. Two years later, Iijima *et al.* [2] simultaneously with Bethune *et al.* [3] have observed the generation of Single Wall Carbon Nanotubes (SWCNTs). Those fillers belong to the fullerene family of carbon allotropes. They are characterized by a tubular morphology with a small diameter ~ 2.5 nm and a nanotube length only restricted by the elaboration conditions (from the micrometer to the millimeter range). It can also be found Multi Wall Carbon Nanotubes (MWCNTs) which are SWCNTs with increasing diameter coaxially arranged walls. This specific feature gives CNTs extremely large aspect ratio compared to other carbon based fillers. The structure is formed by sp^2-hybridized carbon atoms (C-C distance 1.4 Å). In addition, they are characterized by good electrical and mechanical properties (arrangement of covalent bonds oriented along the axis). Owing to their feature and physical characteristics CNTs are ideal candidates for a wide range of applications and more specifically their properties have inspired interest as fillers in polymer composites for the generation of ultra-light structural materials with enhanced electrical, mechanical, thermal and optical properties [4,6].

1. From structure to CNTs properties

The generation of Carbon Nanotubes is achieved thanks to the decomposition of carbonaceous precursor into carbon atoms on catalytic surface. When the limit of carbon solubility is reached carbon atoms start precipitating. Their crystallization induces the formation of tubular structure on the catalytic surface. The decomposition and the graphitization require specific condition and large amount of energy. Catalytic Chemical Vapor Deposition (CCVD) is commonly used to grow CNTs as it is technically simpler to carry out than laser ablation or arc discharge. The obtained product, commonly called "soot", is composed of SWCNT or MWCNT and a lot of impurities such as fullerene, amorphous carbon, graphite sheets and metal catalyst.

a. Structural description

For an easiest representation, CNTs can be visualized as graphite sheet rolls into a tube. Graphite is made of 2D carbon atoms arranged in a hexagonal array. The physical properties of CNTs are tightly bound to the atomic arrangement, both diameter and length of tube and the morphology (SWCNT or MWCNT). All the carbon atoms are involved in hexagonal aromatic rings (except in some cases for the tips), consequently the C-C bonds is no longer planar changing the carbons hybridization. The carbons are not pure sp^2 but a mix between sp^2 (i.e. graphite) and sp^3 (i.e. diamond). The percentage of sp^3 increases as the curvature radius of the tube decrease. Even if, Wang and coworkers [6] have achieved the synthesis of SWCNTs with a diameter of 0.4 nm, it is energetically more favorable to maintain tubular morphology beyond 2.5 nm. Commonly, SWCNT are found with a diameter of around 1.4 nm (suitable energetic compromise). There is no such restriction for the CNT length (from micrometer range to the millimeter range). MWCNT are coaxial nanotubes separated by 0.34 nm [7-9]. Like SWCNT, there is no specific restriction to the length.

To describe the atomic structure of CNT one uses the tube chirality/helicity defined as the $\boldsymbol{C_h}$ vector

$$\overrightarrow{C_h} = n.\overrightarrow{a_1} + m.\overrightarrow{a_2}$$

Equation 1

with

$$\overrightarrow{a_1} = \frac{a\sqrt{3}}{2}\vec{x} + \frac{a}{2}\vec{y}$$

Equation 2

and

$$\overrightarrow{a_2} = \frac{a\sqrt{3}}{2}\vec{x} - \frac{a}{2}\vec{y}$$

Equation 3

where a =2.46 Å

and

$$\cos\theta = \frac{2n+m}{2\sqrt{n^2+m^2+n.m}}$$

Equation 4

Figure 1 illustrates the representation of the vector $\overrightarrow{C_h}$. n and m are the number of steps along the zig-zag carbon bonds of the lattice and $\overrightarrow{a_1}$ and $\overrightarrow{a_2}$ are unit vectors. In contrast to graphene sheet, the chirality will have impact in both mechanical [10,11] and electrical properties [12] of the CNT. The electrical properties will be discussed more precisely in the following section. To sum up, the geometry of any nanotubes can be described by the integer pair (*n,m*) determining the chiral vector.

Figure 1: Schematic view of a single-walled zigzag, armchair and chiral carbon nanotubes

As illustrated by Figure 1, there are two limiting cases depending on the chiral angle θ (0° or 30°). On refer to a zig-zag configuration (i.e. chiral angle equals to 0°) achieved for a helicity vector perpendicular to any overall C-C bond (that is (*n,0*) or (0,*m*)) and the armchair configuration (30°) is achieved for a helicity vector parallel to one of the three C-C bond (i.e. (*n,n*)). Otherwise, SWCNT are chiral with an angle between 0 and 30° [13,14].

When talking about the physical properties of CNT one must be very cautious as they show strong anisotropy. The properties along the tube axis are way better than that perpendicular to the tube. In the following, the mechanical, thermal and electrical properties of CNT will be presented.

2. Physical properties

a. Mechanical properties

The great mechanical properties of CNTs result from the strong bonding between atoms. Indeed, carbons bonding are mostly sp^2 hybridization kind, which leads to lower C-C bond length than in diamond or graphene. To show the great potential of the CNT one will present mechanical measurements carried out on CNT with low amount of defect. For instance, the tensile strength of SWCNT has been measured equal to 45 GPa [15,16] which is twenty times higher than tensile strength of steel (~ 2 GPa.) The tensile strength is even higher for defect free perfect c-MWCNTs as the number of tubes is not detrimental to the overall tube strength. Demczyk and coworkers [17] have measured a tensile strength of 150 GPa for defect free MWCNT. Flexibility was measured equal to 3-30 GPa for MWCNT [18]. To finish, tensile modulus is also large, for instance, M.M. J. Treacy *et al.* have measured 1 TPa for MWCNT [19], Yao and coworkers. [20,21] have measured 1.3 TPa for SWCNT. One must remain careful as the characterization methods for the determination of mechanical properties of CNTs are complex to setup and not always reliable due to the size of the filler.

The addition of CNTs in polymer can be used as fiber reinforcement. For the mechanical reinforcement, one must consider, the aspect ratio, the orientation of the CNT (strong anisotropic), the dispersion and the adhesion between the fillers and matrix for a good transfer of the mechanical loads. Figure 2 shows the strong difference between long fiber and nanotubes in term of interphase. The filler size generates a huge volume of interface between polymer matrix and fillers.

Figure 2: Fraction of interphase polymer as a function of volume fraction of fiber, where t is the interphase thickness and r_f is the radius of the nanotube/fiber inclusion. Plotted from Ref [22]

One can easily imagine that considering CNTs with strong interactions with polymer matrix (covalent bonds) [23-25] and homogeneously dispersed in the matrix will drastically increase the mechanical

properties of the material. The large generated interface will withstand larger stresses than bulk polymer and consequently will increase the mechanical properties of the composite [26-28].

b. Thermal properties

CNTs show a duality in their thermal properties. They are extremely good thermal conductors along the tube axis but show insulator behavior laterally to the tube axis [29,30]. The thermal conductivity for 1 single MWCNT along its axis has been measured at room temperature; the values are wide from 600 W/(mK) [31] up to 3500 W/(mK) [32] which is almost ten times higher than copper a metal widely used as good thermal conductor (385 W/(mK)). In addition, to the difficulty to measure the thermal conductivity some simulation works have shown that the thermal conductivity depends on the carbon nanotube length [33,34]. Considering the properties laterally to the tube axis one can find values ~1 W/(mK) [35,36]. The high thermal properties might be a consequence of the small number of defect: the mean free path of phonon is large.

c. Electrical properties

In order to explain the electrical properties of CNT a parallel with graphene sheet will be made. Graphene has an unusual band structure characterized by states crossing the Fermi level at six points in K-space (Brillouin). As already mentioned; CNTs can be seen as rolled graphene sheet. The shrinkage from 2D graphene sheet to 1D CNT induces strong modification in the band structure. The confinement of electrons around the circumference of the nanotube generates an additional level of quantization. Then the component of the wave-vector k_c must fulfill a new condition:

$$C_h . k_c = 2\pi j$$

Equation 5

where $\boldsymbol{C_h}$ is the chiral vector (see Equation 5) and j is an integer. This equation means that each graphene band is split into additional subbands indexed by j with energy states corresponding to slice in the graphene band structure. The position of the slices in the graphene Brillouin zone will generate different physical properties. If slices pass through one of the six K-point of the graphene Brillouin zone the CNT will be metallic otherwise the CNT will behave as semiconductor. That is why knowing the chiral indices (*n,m*) gives the possibility to predict the electrical properties of CNT. When *n=m*, nanotubes are metallic, when *n-m = 3i* (*i* is a nonzero integer) the tube is a semiconductor with a small gap and all other values of (*n,m*) lead to semiconductor CNTs. Generally, the band gap is inversely proportional to the nanotube diameter [37,38]. The conduction mechanism for c-MWCNTs is not strongly different from SWCNT. The conduction mainly occurs on the external wall [13]. However, the interactions between the internal walls can generate variation in electronic properties. For small diameter MWCNT (i.e. DWCNT), the electrical properties relies on the superposition of the two structures.

Considering metallic CNT, the resistance can be deduced from the electric conductance unit as $R=1/G$, with $G=4e^2/h$. G is determined from the Landauer-Buttiker formula [39] for a one-dimensional conductor, considering that there is no scattering inside the nanotube or at the contacts and there is two propagating modes. That is why transport in metallic CNTs can be considered as ballistic over a distance of ~ microns.

Due to reduced scattering, metallic SWCNT can support large current densities. Yao *et al.* [40] have measured a current densities of 109 A/cm^2 without damaging CNT which is higher than Cu (106 A/cm^2).

CNTs are fillers with huge potential. In the next section, one will present a specific application of CNT: the generation of composites with electrically properties. But first, polymers that are generally used for the generation of electrically conductor composites will be presented.

B. Polymers

1. Polystyrene and High Impact Polystyrene

Crystal Polystyrene is a linear thermoplastic obtained by radical polymerization and characterized by a fully atactic molecular structure. This is an amorphous and transparent material.

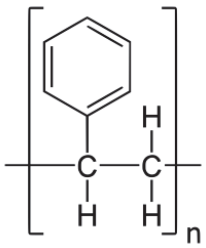

Figure 3: Chemical structure of Polystyrene

The polymer chain is characterized by the presence of a benzene ring that prevents the mobility of the chain. Consequently the material is very brittle and rigid at room temperature (impact resistance 20-30 J/m Izod impact strength) [41]. This material has a glass transition at around 100°C with a very large rubbery plateau. This characteristic is, for instance, adequate for thermoforming as the material has a large window of forming temperature. In order to improve its mechanical properties, elastomers with a lower modulus is dispersed within the matrix. This addition of rubber nodules prevents the crack propagation by large energy dissipation.

High Impact Polystyrene (HIPS) is a heterophasic polymer made of dispersed Polybutadiene phase in continuous polystyrene phase. This composite is obtained by radical polymerization by bulk

or bulk-suspension method from a solution of Styrene and Polybutadiene [42-45].

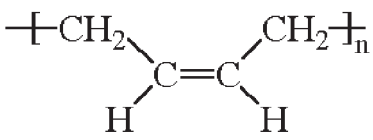

Figure 4: Chemical structure of Polybutadiene

Due to non-miscibility between polystyrene and the elastomeric phase, a phase separation occurs at low styrene conversion. Polystyrene-Styrene droplets are dispersed in the Polybutadiene-Styrene phase (Styrene Rubber Phase). Grafted copolymers (PB-g-PS) are found at the interface and act as emulsifying agent. As the polymerization goes on, the volume of the rubber phase decreases. A new phase inversion occurs when the volume of the SRP and polystyrene become close. This leads to the formation of SRP domains dispersed in continuous polystyrene phase. Depending on the temperature, the radical initiator concentration, the elastomer concentration, the mixing speed or the rubber precursor various morphologies can be obtained. For instance, Echte *et al.* [46] have found that larger stirring rates lead to smaller particles.

In addition, Copolymer Styrene Butadiene can be used as rubber precursor. This copolymer will be grafted during the polymerization. The obtained morphology will directly depend on the styrene composition of the copolymer [47]. For small amount of PS in the copolymer Styrene Butadiene, the morphology will be of the salami type represented in Figure 5. Multiple PS phases are trapped in a rubber shell. With larger PS content in the copolymer, the salami type becomes a core shell type (mono inclusion).At larger content, the morphology becomes of a “labyrinth” kind.

The mechanical properties will be linked to the morphology type and the volume concentration of the elastomeric phase. For the “salami” morphology type, larger nodules and larger content of elastomeric phase will lead to better impact resistance [48,49]. To conclude, in order to generate materials with tailored mechanical properties, PS and HIPS can be blended to generate additional levels of rubber.

Figure 5: Transmission Electron micrograph of HIPS with a salami morphology type. The PB nodules have been chemically treated with Osmium solution in order to rigidify their structure and facilitate the specimen preparation. Plotted from Ref [50]

2. Rheological properties

In the literature, a few have studied the influence of the nodules on the composites melt behavior under uni-axial extensional and on the dynamic rheology. One can cite the work of Barosso *et al.* [41] who has analyzed pure PS, HIPS and a blend of PS and HIPS (50-50wt%). Figure 6 shows the master curve built at T_{ref} =150°C of the three matrices. They have shown that in the terminal region, the viscosity of the PS is lower than the HIPS matrix. The rubber phase has moderate influence at long time scale solicitation. However, the dynamic moduli of the two matrices are quite comparable.

Figure 6: Master curve built at T_{ref} = 150°C for pure PS, HIPS and blend PS HIPS (50-50 wt%). Plotted from Ref [41]

They have also analyzed the strain-at-rupture, i.e. when the deformation triggers a loss of integrity of the specimen, for PS, HIPS matrices and blend of PS and HIPS matrices (see Figure 7). PS matrix has larger strain-at rupture than HIPS matrix or blend of PS and HIPS matrices. Surprisingly, the PS and the blend follow the same evolution.

Figure 7: Strain-at-break variation as a function of the strain rate at 150°C for three PS based matrices under extensional deformation. Plotted from Ref [41]

3. Thermoforming

The thermoforming is a forming method commonly used for the generation of packaging on a large scale. This method uses polymers as extruded or calendared sheet. The polymer sheet is heated by radiation to a softened state and then melt processed. There are two main forming methods: drap forming or vacuum forming. The first one uses a positive or male mold. The sheet is pressed against the cold mold. Then differential pressure is applied to finish the part shape. The vacuum forming uses a negative or female mold. Under vacuum, the sheet is forced against the mold. The sheet will undergo biaxial deformation at high strain rate [51, 52].The wall thickness is not controlled especially at the edge. Indeed, the sheet parts that are first in contact with the mold will be less deformed than the parts that come into contact last. This area will be thinner. To avoid such differential thickness and especially for the generation of parts with large depth, plug-assisted negative mold is privileged. Figure 8 illustrates the plug-assisted thermoforming. The plug will first stretch the sheet to near the bottom of the negative mold and then a combination of vacuum and compressed air will force the sheet against the mold. The stretch induced by the plug gives the possibility to a better control sheet thickness. The sheet deformation and the sheet thickness is described by combination of the Ogden

model [53] (a hyperelastic constitutive relationship) and the K-BKZ model (a viscoelastic relationship) [54-57]. This model can simulate isothermal and non-isothermal vacuum or plug-assisted thermoforming. Indeed, prestretching induced by the plug-assisted thermoforming is best described as viscoelastic.

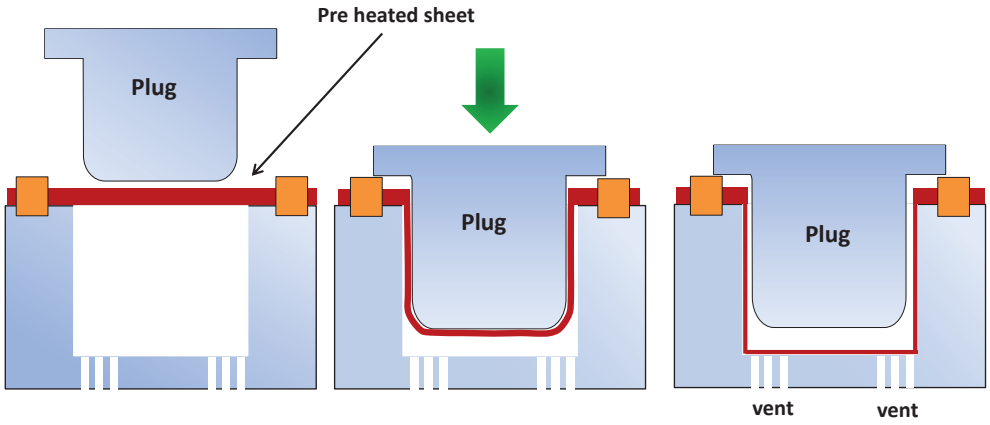

Figure 8: Schematic of a plug assisted thermoforming

The thermoforming conditions and especially the temperature will be intimately linked to the polymer properties. The choice of the temperature is a compromise between polymer resistances to applied stress, elongation at break and sheet sagging. The two first parameters mark the lower temperature out whereas the last one determines the upper working temperature. A large temperature range will be suitable for thermoforming. That is why amorphous polymers that have a sufficient “hot strength” or High Density Polyethylene that has good elasticity in the melt state are privileged polymers for thermoforming. They have a larger thermoforming window than crystalline polymer. A combination of Extensional viscosity for determining the strain-at-rupture and Dynamic Mechanical Rheology Analysis allows determining the thermoforming range. For instance, Figure 9 illustrates the variation of the elastic modulus as a function of the temperature.

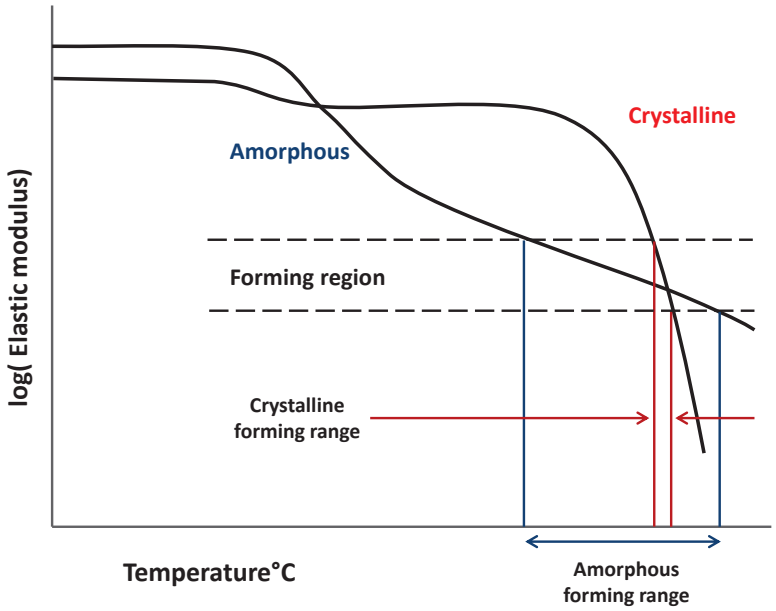

Figure 9: Schematic of the temperature-dependent elastic moduli of an amorphous and a crystalline polymer. The forming regions are detailed for the two polymers

With the increase of the temperature, the elastic modulus of the amorphous polymer significantly decreases before stabilizing and forming a plateau. The value of the plateau must be coherent with the pressure generated during the thermoforming in order to be properly stretched. The large rubbery plateau of the PS makes it suitable for thermoforming applications. Moreover, (Figure 6) the addition of PB nodules does not influence the dynamic modulus. Consequently, the thermoforming window remains unchanged by the presence of the elastomeric phase.

The large demand of packaging with specific properties such as tailored surface conductivity has urged the development of new composites made of polymer matrix filled with electrically conductor fillers. However, the transposition of melt processing such as thermoforming on such specific composites is not as easy as expected. Indeed, a composite sheet with moderate conductivity will generate, most of the time, an electrically insulating composite part after thermoforming. Moreover, composites will have different viscoelastic behavior and the addition of fillers will change the thermal properties of the sheet. For instance the addition of Carbon Nanotubes (CNTs) can dramatically change the heating steps as fillers change the thermal properties of the sheet. Indeed, if the dispersion is not fully controlled, large aggregates can generate over heating of the matrix. For now, the generation of composite parts with tailored electrical properties remains a thorny challenge.

In the following, the generation of such composites and their characterization will be tackled.

C. CNTs as fillers for the generation of electrically conductor composites

In the last decades, electrically conductive polymer composites (CPCs) have attracted tremendous attention in both academic and industrial fields. The addition of fillers with electrical properties can generate composites with extremely large tunable electrical properties in comparison to intrinsic conductive materials and consequently can be used in a large panel of application such as chemical and biological sensors, photovoltaic devices, flexible and transparent plastic electronics, printable circuit wiring, variable resistors and actuators [58-61]. Figure 10 illustrates the large range of resistivity (i.e. conductivity) and their specific applications.

Figure 10: Classification of Conductive Polymer Composite materials according to their electrical resistivity and application ranges. Plotted from Ref [62]

Conductive Polymer Composites are employed in two major fields: Electromagnetic Interference (EMI) shielding and Electrostatic Dissipation (ESD) as moderate conductivity are required (respectively $\sigma > 1$ S.m^{-1} for EMI and $\sigma = 10^{-4}$- 10^{0} S.m^{-1} for ESD) [59,60].

In this section, the electrical properties of such composites and the challenges for their elaboration will be presented.

1. Electrical properties of nanocomposites

a. From insulating polymer to electrically conductor composites

Polymer matrix are insulating materials characterized by a conductivity of around 10-16 S.cm^{-1}. The addition of electrically conducting particles to polymer has been investigated a lot recently [62-64]. This strategy opens the possibility to increase their panel of applications by generating electrically conductor composites. Figure 11 introduces the difference in physical properties resulting

from the addition of fillers.

Figure 11: AC conductivity as a function of frequency for PC with different MWCNT content. Plotted from Ref [159]

For ultra-low amount of CNT (between 0.5 and 1 wt%), the pure matrix and the composites behave the same way. However, from a certain amount of fillers, the conductivity σ' dramatically rises and becomes independent to the frequency. This gives an insight of the transition between electrically insulator material (pure matrix or filled with low amount of CNT) and electrically conductor material for concentration in CNT larger than 1 wt%. This is called the "percolated-governed" conductivity and is a standard behavior when adding fillers with electrical properties to polymer matrices [65,66].

In the last decades, the generation of composites with electrical properties thanks to the addition of CNT has been widely investigated. In the review [66], the authors have listed a large number of generated composites. One will use this review to present the challenges for the generation of plastic parts with tailored electrical properties.

b. Percolation threshold

The electrons conduction through the material is only possible thanks to the fillers and their organization in the material. A composite becomes electrically conductor when a sufficient network of filler is formed within the material. Each elements of the network must be in direct contact in order to enable the electrons conduction. Those composites made of a polymer matrix filled with CNT can be described by the percolation theory. [63,67] The percolation theory describes the formation of a lattice made of connections at the nanoscale and its effect on the macroscale properties of the system. From a certain amount of bonds at the percolation threshold, the bonds form an infinite lattice through the material. Figure 12 illustrates the formation of a percolated network.

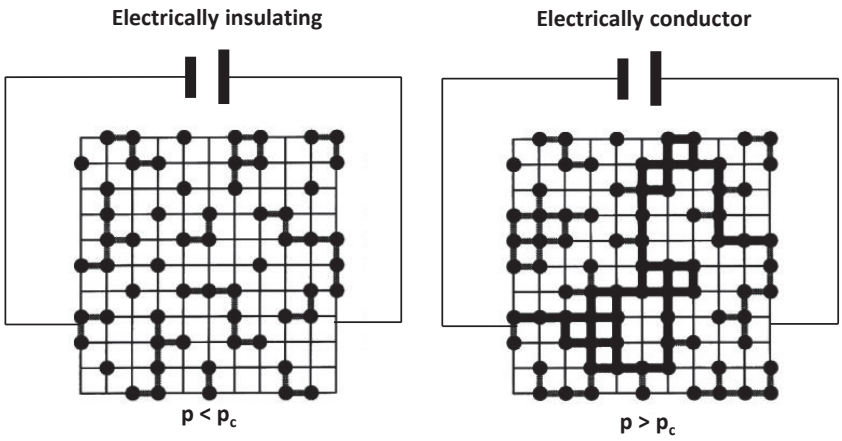

Figure 12: Generation of an electrons path for p lower than p_c (left) and larger than p_c (right)

Under the percolation threshold, the bonds form isolated clusters and the material conductivity is governed by the polymer conductivity. At higher concentration (above the percolation threshold) the bonds sufficiently connect the clusters generating a percolated network. The filler network governs the material conductivity.

The percolation theory has been successfully applied to describe the evolution of the electrical conductivity of polymer composites as a function of the filler fraction. The evolution of the Direct Current (DC) conductivity ($\lim_{\omega\to\infty}\sigma'$) can be expressed as a function of the percolated threshold p_c and the concentration p of bonds as:

$$\sigma_{DC}\infty\ (p_c - p)^{-s}\ p< p_c$$

Equation 6

$$\sigma_{DC}\infty\ (p - p_c)^{t}\quad p>p_c$$

Equation 7

with t a critical exponent which only depends on the dimension of the percolated system and not on the fillers geometry. In the literature one can find accepted values for the critical exponent [68]. For a three dimensions network, the exponents are respectively $s \approx 0.73$ and $t \approx 2$. Usually, Equation 6 and Equation 7 are written as a function of the filler volume fraction ϕ and from a geometrical point of view ϕ is proportional to p:

$$\sigma_{DC}\infty\ (\phi - \phi_c)^{t}\quad \phi > \phi_c$$

Equation 8

The percolation threshold is intimately linked to the filler geometry. Figure 13 represents the

evolution of the volume of filler at percolation in function of the aspect ratio of the filler. The aspect ratio is the ratio of the length to the diameter of the filler.

Figure 13: Theoretical evolution of the percolated threshold in function of the aspect ratio of the filler. Plotted from Ref [69]

Figure 13 illustrates one of the main advantages of CNT for the generation of electrically conductor composites. They have nanoscale diameter and length up to the millimeter scale. Their high aspect ratio compared to Carbon Black (CB) gives the possibility to obtain electrically conductor composites at ultra-low filler concentration. From a practical point of view, the percolation threshold can be seen as Equation 9

$$\phi_c \sim \frac{D}{L}$$

Equation 9

Fillers with high aspect ratio will percolate at lower percolation threshold as the formation of an efficient network is achieved with fewer contacts.

In the literature, a large number of works were aimed at investigating the generation of Polymer Conductor Composites with different matrices and methods. All authors have determined the percolation threshold of their systems via conductivity measurements. The different publications are reported in the following Table 1 and dispersed MWCNT with an aspect ratio of 1000 in different matrices and with different methods. The matrix, the filler, the aspect ratio the dispersion methods and the percolation threshold expressed in wt% are resumed in the Table 1.

Table 1 : Recapitulative of nanocomposites generated with different matrix filled with MWCNT characterized by an aspect ratio of d/L = 1000, with different dispersion strategy and their percolation threshold [63]

Matrix	Dispersion	Φ_c wt%	Ref.
Polycarbonate	Extruded	1	[70]
Polycarbonate	Extruded	5	[71]
PET	Extruded, hot pressed	0.7	[72]
Polystyrene	Extruded	0.45	[73]
Epoxy	Stirred	0.4	[74]
Epoxy	Calendered and stired	0.3	[75]

The percolation thresholds reported in the different publications are truly scattered and even similar to a hypothetic percolation threshold for particles of aspect ratio of about 10. For given aspect ratio (1000), the theoretical percolation threshold should be in the range of 0.1 vol%. The difference between experimental and theoretical values highlights one of the main drawbacks of CNTs. The percolation theory considers straight tubes, isotropic orientation, homogeneously dispersed in the materials and direct contact between the fillers. CNT are flexible and can be seen as cooked spaghetti. This not straight structure drastically reduces their lengths. In addition, they are not isolated but generally found as bundle and they aggregate instead of being perfectly distributed within the matrix.

Nevertheless, such composites exhibit a power law dependence of the conductivity in function of the filler concentration. Percolation theory is a useful tool for composites comparison however if one knows the aspect ratio of the fillers after the generation of the composites.

2. Nano-fillers in polymer matrix

In this section, we will set aside the geometrical point of view and will focus on one of the major problem to overcome for the generation of nanocomposite: the high tendency of CNT to agglomerates.

a. Strong interaction between CNTs

CNTs are sold as powder made of bundles, clusters or large agglomerates. Figure 10 illustrates the characteristic powder after the purification step. Figure 14a is Scanning Electron Microscopy

image of primary agglomerate. This primary agglomerate; made of dried MWCNT; is characterized by a strong cohesive force. Indeed, due to the size of the fillers and their high specific surface area, Van der Walls and electrostatic forces are extremely strong.

Figure 14: SEM of as received NC 7000 powder (a) primary agglomerate and (b) at higher magnification

Huaung *et al*. [76] have proposed a method for the determination of the cohesive energy of CNT agglomerates. To do so, they have shown that for SWCNT, only considering van der Walls forces are sufficient to sense the interaction. They have considered two parallel mesoscopic cylinder with a diameter d and a length L, considering that $d>>z$, with z the distance between the two SWCNTs and z_0 the distance separation at the closest approach (for the graphite 0.34 nm).

$$E_{||} \approx -\frac{HLd^{1/2}}{24z^{3/2}} \text{ with } z \geq z_0$$

Equation 10

where *H* is the Hamaker constant [77] (~2x10^{-19} J for nanotubes in a low-permittivity medium [78]). Considering a diameter of 10nm Equation 8 gives energy per unit length of -0.09 eV/Å. Their results are closed to the calculation of Girofalco who has found -0.095 eV/Å [79]. However, this equation suggests that MWCNT, with larger diameter have larger cohesive energy and should be found as tightly packed parallel bundles. The opposite is found in practice. They have argued that in bundles, MWCNTs must adjust their conformation in function of their closest neighbors and consequently are in contact. This contact junction can be seen as two perpendicularly crossed rods of diameter *d* and gap size *z*. Then, the contact energy can be simplified as:

$$E_{\perp} \approx -\frac{Hd}{12z} \text{ for } z < d$$

Equation 11

Considering tubes with a diameter of 10 nm spaced by 0.34 nm, they have found energy of -10 eV per contact which is closed to the -15 eV obtained by [80] who has calculated the energy based on the surface integral of rolled graphene layers.

Then, the density energy can be deduced for the two kinds of CNT. On the one hand, the separation of two parallel SWCNTs bound by an attractive potential $E_{tot} \approx E_{||}$, the density energy υ can be expressed as:

$$\upsilon \approx \frac{E_{tot}}{Ld^2}$$

Equation 12

leading to $\upsilon \approx$ 100 MPa for SWCNT with a length L = 1 µm and diameter d = 1 nm.

On the other hand, the number of binding contacts between MWCNTs must be first taken into account in order to determine the density energy. They have considered that the number of contact increases with the length of the fillers and introduced a spacing distance ζ between direct crossing junctions. They have estimated the number density of contacts c_t as inversely proportional to ζ to a third power. Then the density energy can be expressed as:

$$\upsilon \approx c_t E_{tot}$$

Equation 13

with $E_{tot} = E_{\perp}$. Considering MWCNTs with 10nm diameter and a spacing distance between MWCNT junctions in the range of 100 nm (the authors have estimated this distance thanks to SEM observation) one obtains $\upsilon \approx$ 1 kPa [76]. Even if the spacing distance is an estimated value, one can sense the strength difference between SWCNT and MWCNT.

At a larger scale, the agglomerates strength made of a large number of CNTs will depend on the cohesive strength between CNTs. Carbon Nanotubes with extremely large aspect ratio will give birth to agglomerates with very large cohesive strength. The challenge to decrease this strong cohesive strength is to increase the distance between CNT to decrease the van der Walls interactions.

b. Carbon Nanotubes functionalization

One way to decrease the inter-particles interaction is the addition of a functionalization step before the mixing with the polymer [81-83]. There are two kinds of functionalization: the non-covalent and the covalent functionalization. The first one generates a layer of functional groups (surfactants or small organic molecules) on the filler surface whereas the second one induces the generation of chemical bonding between the filler surface and the functional molecules. The functionalization methods will be not much detailed as this technique is not used in the present work.

The covalent functionalization of the CNT surface generates defects that reduce the electrical properties of the filler and the non-covalent functionalization generates a thin layer that prevents good contact between fillers for the electrons conduction. However, for mechanical properties where good adhesion is required functionalization is a viable solution as it can generate compatibility between CNT and polymer matrix via covalent bonding. Hence, good interfacial adhesion between polymer and fillers is required for efficient load transfer. However, this can be detrimental to the electrical transmission from one CNT to another. Thus, for electrical applications the non-covalent functionalization will be privileged.

The non-covalent functionalization is achieved by the adsorption on the filler surface of surfactant [84,85] or of polymer chains [86]. A thin layer on the filler surface will drastically reduce the filler-filler interactions. However, it will prevent a direct contact between fillers and consequently will generate some deviation from a theoretical percolation threshold.

Conclusion

To conclude, isolated CNTs show promising mechanical, electrical and thermal properties and seems to be ideal fillers to polymers to improve and give them new properties and so to expand their spectrum of application. This optimistic perspective is sullied by the strong interaction between CNTs which forces them to bundle and form strong agglomerates that dramatically tarnish their physical properties.

The dispersion at the nanoscale has a crucial impact on the mechanical and electrical properties of the materials. One must find the appropriate way to process nanocomposites in order to obtain the end-product with tailored properties. This will be the topic of the next section where the different strategies developed to overcome the challenges for the incorporation of CNT to polymer matrix will be presented. In addition, one will pay attention to the different methods for the characterization of the filler network.

II. Processing of polymer filled with CNT nanocomposites and their characterization

The generation of nanocomposites with tailored physical properties is strongly linked to the mixing method for the incorporation of the nano-filler into the polymer matrix. The main challenge is to disperse the fillers from their agglomerated structure. In this section, the mechanisms of the filler incorporation to polymer matrix will be presented. Then, the different strategies will be highlighted. To conclude this section, techniques for the characterization of the composites after their elaboration will be presented.

A. Incorporation of CNTs into polymer matrix

1. Mixing challenges

CNT are fund into different structures: isolated nanotubes, small bundles of CNTs, dense aggregates and primary agglomerates. Most of the time, CNTs are delivered into powder made of large primary agglomerates with high strength. The challenge of the dispersion is to decrease the size of the primary agglomerate into smaller aggregates and then homogeneously distributes the entities into the polymer matrix. Figure 15 illustrates the most encountered dispersion and distribution concept for composites processing (details in the Figure description). For electrical properties, the challenge is to obtain homogeneously distributed broadly dispersed structures in order to enhance the formation of a percolated network made of connected aggregates (i.e. case Figure 15d). The main strategy for the dispersion of nano-fillers is via mechanical forces.

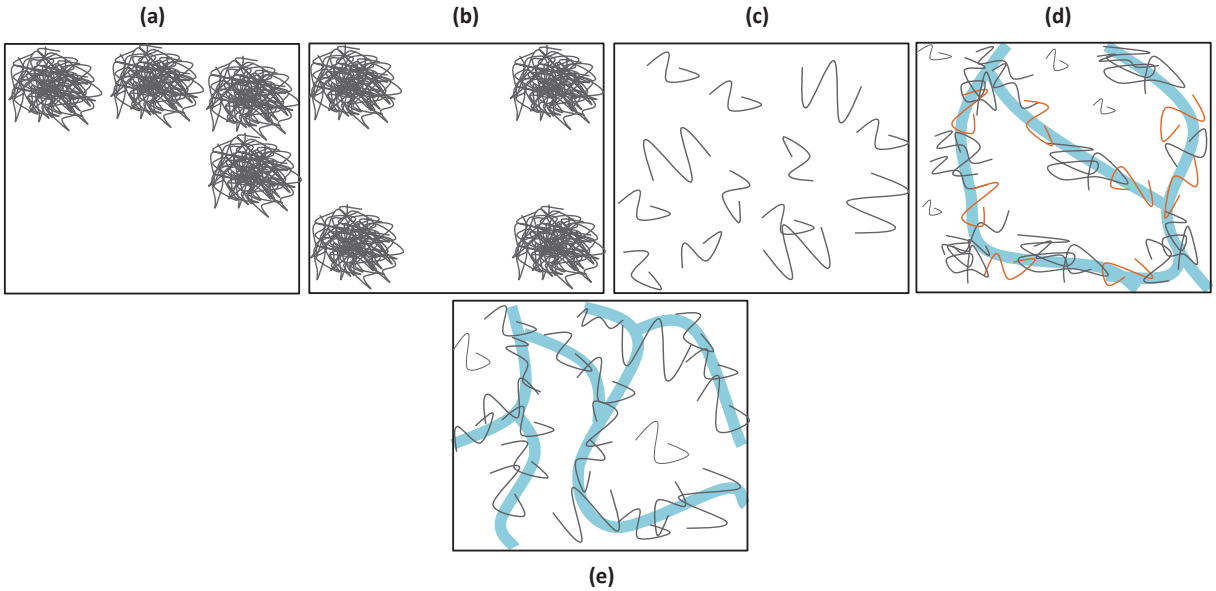

Figure 15: Achievable state dispersion/distribution of fillers in polymer matrix: (a): poorly dispersed and non-homogeneously distributed in the matrix, (b) poorly dispersed and homogeneously distributed, (c) homogenously distribution and highly dispersed, (d) broadly dispersed and distributed, (e) highly dispersed and homogeneously distributed. The orange lines show the junctions between the CNTs bundles and the large blue lines illustrate the percolated network. Not percolated network: (a), (b),(c); percolated network : (d) and (e).

Agglomerates with high cohesive strength will be hard to break into smaller particles. The fillers will be poorly dispersed in the matrix and the generated nanocomposites will show poor physical properties. During the mixing, different mechanisms can induce the destruction (break-down) of the agglomerates and their fragmentation into smaller particles: compressive loads or agglomerates-agglomerates and wall-agglomerates impacts. For polymer processing, the fragmentation by hydrodynamic forces is the most relevant phenomenon.

A great amount of studies has been carried out for the description of agglomerates break-down under hydrodynamic forces. The mechanism is characterized by the fragmentation number F_a as the ratio between hydrodynamic force and cohesive force of the agglomerate. [87-91]

$$F_a = \frac{F_{hydrodynamic}}{F_c} = \frac{\eta \dot{\gamma} R^2}{F_c}$$

Equation 14

with η the medium viscosity, $\dot{\gamma}$ the applied shear rate R the radius of the agglomerate and F_c the cohesive force of the agglomerate. The hydrodynamic forces must overcome the cohesive strength of the agglomerate in order to disperse it. Different mechanism can occur in function of the fragmentation number. For large hydrodynamic forces, (F_a>> 1) the agglomerates will break into two entities, whereas if F_a<< 1 the agglomerates will erode. In the literature, there are two main models

for the description of the agglomerates rupture. One model that takes into account homogeneous agglomerates with a planar rupture surface [92,93] and another that considers inhomogeneous agglomerates made of primary particles bound together. This heterogeneity is described with the porosity of the agglomerate [94].

The erosion is a kinetic phenomenon. Small entities (<10% of the volume of the primary particle) will detach from the agglomerates surface. A large number of kinetical laws are found in the literature for the characterization of erosion mechanisms [95-97]. Figure 16 illustrates the rupture and erosion mechanisms.

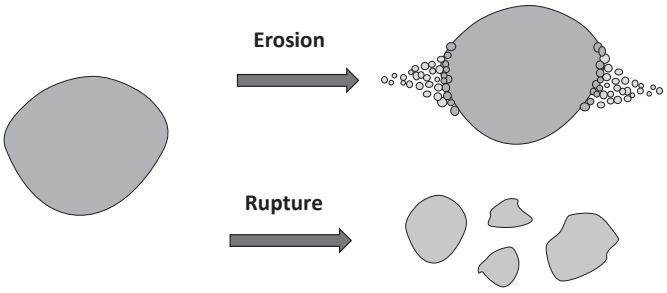

Figure 16: Schematic view of rupture and erosion of particles

In order to reach the state illustrated in Figure 15 (d), one must play on the agglomerate strength and the applied stress to have different mechanisms.

One solution to decrease the strength of the agglomerates and to obtain disentangled CNTs is to wet the primary particles by organic macromolecules. When the agglomerate surface is wetted by polymer chains, the polymer chains can infiltrate the agglomerate. The wetting will decrease the cohesive forces between the MWCNT and the infiltration will decrease the packing density of the agglomerates [98]. The time dependent length of the infiltration mechanism can be determined in the case of a fully wettable capillary as:

$$h(t)^2 = \frac{r\Upsilon \cos(\theta)\, t}{2.\eta}$$

Equation 15

where t is the time, Υ is the interfacial tension, θ the contact angle and r the pore radius. The infiltration depends on the type of the polymer chains.

The infiltration will increase the distance between the fillers. The filler-filler interactions decrease and consequently, the agglomerate cohesive strengths drastically collapse. Then, mechanical forces can easily overcome the cohesive strength of infiltrated agglomerates and break or erode the agglomerates into smaller aggregates which can be dispersed and homogeneously distributed into the polymer matrix. The infiltration mechanism relies on the characteristic of the polymer chains.

Yamada *et al.* [99,100] have worked on the infiltration of CB by polymers. Considering agglomerates with similar porosity, they have found that the molecular weight, the branching of the polymer can drastically hinder infiltration on the agglomerate. They have concluded that lower melt viscosity can enhance the infiltration of CB agglomerates, which is in good agreement with Schubert (Equation 16). The mixing of fillers into polymer matrix can be resumed by the following steps:

- Filler incorporation
- Wetting of the primary agglomerates by the polymer
- Infiltration of polymer chains into the primary agglomerates to weaken them
- Dispersion of the agglomerates by rupture and erosion
- Distribution of the small aggregates and loosely CNTs into the matrix

In the following sections, different strategies for the generation of MWCNT filled polymers will be presented. First, the generation of composites with low viscosity matrix will be presented and then the case of highly viscous polymer will be discussed more in details.

2. Mixing strategies

For the incorporation of CNT into low viscous polymer matrices there are two main routes: solution mixing and in-situ polymerization. For those specific cases, the influence of the polymer for the infiltration is limited.

a. Solution mixing

The solution mixing involves three major steps: the dilution, the dispersion and the precipitation. This strategy is used for low viscous medium. First, the fillers are dispersed separately in a suitable solvent. The matrix is dissolved or suspended in the same solvent used for the CNT dispersion. The dispersion of CNTs in a low-viscosity media requires external forces to overcome the substantial energy barrier for the desagglomeration mechanism. That is why; it is common to use mechanical mixing, magnetic agitation or sonication for the fillers dispersion in the solvent. Sonication is the most effective way in debunbling CNT as it involves large forces. The application of sound wave (with frequency above 20 kHz) in a media will generate low and high pressure area. The two pressure stage will trigger cavitation in the media. The low pressure stage leads to the formation of bubbles which will collapse in the high pressure stage. The shear rate involved during the bubble collapsing has been estimated as high as 10^7 to 10^9 s^{-1} [101,102]. Considering a typical low viscosity solvent of 0.1 Pa.s, the shear stress $\sigma_{shear} = \eta.\dot{\gamma}$ is in the range of ten of MPa. This means that for higher viscosity medium the sonication can lead to CNT break as the tensile strength of CNT is of tens GPa or to polymer degradation if the polymer matrix and the CNTs are dispersed together [103]. Good debundling is possible by controlling the ultrasonic amplitude and frequency and the amount of dissolved gases in the solution.

Subsequently, the dispersed CNTs solution and the dissolved or precipitated polymer solution are mixed together at room temperature or high temperatures. This method can lead to good dispersion

for a wide range of systems. However, one can add that the use of dispersant is possible to reduce the external forces and enhance the dispersion even for large amount of CNTs [104,105]. Dispersant molecules wrap or adsorb onto CNTs and decrease the internal forces in the agglomerates. A large amount of studies have been carried out on the kind of surfactants used for CNT dispersion in organic or inorganic solvent. For an appropriate use of dispersant, they have shown that one must consider the time required for the diffusion of the dispersant molecules to the surface of the nanotubes and consequently adjust the applied shear rate.

Then the mixture is casted. A major issue of this process is the solvent removal. During this stage, CNTs can re-agglomerate forming aggregates smaller than the primary aggregates. There are two main routes for this stage. The solvent is removed by evaporation (with or without heat assisted) which is a slow mechanism but gives the possibility to directly make films or fibers. A faster way is to quickly add the solvent-polymer-NTCs mixture to an excess of liquid that is only miscible with the solvent. This technique can be used for two fiber-processing: gel spinning and electrospinning [106-108]. For mechanical properties the coagulation process will be privileged as it prevents CNT agglomeration. For electrical properties and lower percolation threshold the evaporation way is privileged as re-agglomeration can happen.

b. Dispersion-reaction route

The dispersion-reaction route includes in-situ polymerization route and the generation of thermosets composites. The dispersion-reaction route is closed to the solution mixing strategy. For the same reasons presented in the solution mixing strategy, the direct mixing of the CNTs to the monomer must be avoided. To obtain a good mixing, the CNTs are first dispersed in a liquid and then this mixture is added to the monomers (miscible in the liquid). The polymerization is triggered by the addition of initiator or another monomer. The molecular weight of the composite is controlled by the amount of incorporated initiator, the temperature and duration of the polymerization. It must be kept in mind that initiation with ultraviolet (UV) is ineffective as CNT are UV absorbing. One the other hand, the use of microwaves radiation to trigger the polymerization has been recently investigated [109,110]. CNTs absorb microwaves inducing local increase of the temperature initiating the polymerization. The control of the produced heat remains a challenge to be tackled [111]. In situ polymerization can be applied to thermoplastics that have liquid monomers such as polystyrene [112,113] and acrylates [114-116]. This strategy is also adopted for the generation CNT-epoxy composites. The fillers are dispersed in the resin and then the resin is cured with hardener [117,118], vinyl ester [119,120] and polyimide [121,122]. The use of dispersant is not recommended as it can remain with the solid polymer and consequently decreases the mechanical properties. In this work, the matrix used is Polystyrene. In-situ polymerization is an essential route for the generation of thermoset or rubber-based composites; however for the generation of nanocomposites, the privileged way for industrial application is the melt mixing strategy

c. Melt mixing

The melt mixing strategy is the most attractive technique for the generation of nanocomposites using a large variety of polymers. The advantage of the technique is the reduction of time and steps compared to the other techniques introduced earlier and that no solvent are involved in the processing. The fillers are incorporated in the molten matrix. Melt processing can generate a large amount of nanocomposites and the semi-products can be directly processed by means of calendaring, injection molding, fibers spinning blow molding etc... . This is why this strategy is mainly privileged in the industry. The melt mixing route can be composed of a unique step (direct incorporation of the filler to the melt matrix) or composed of two or multiple stages (called masterbatch dilution). A masterbatch is a matrix containing high loading of CNTs (typically between 10-15 wt%). For the masterbatch dilution, the filler is first incorporated in the matrix to obtain a highly filled masterbatch. This masterbatch is then diluted (melt mixing) by the addition of pure polymer in order to decrease the filler concentration. It must be added that, in that case, the polymer in the masterbatch may be of different molar mass than of the composite matrix.

In this case, the parameters of the polymer have a strong influence on the generated composites. Contrary to the solution mixing strategy lately presented, where CNTs are dispersed into low-viscous materials, thanks to large amount of energy generated during the sonication stage, the mechanical forces generated with the extruder are lower than that via sonication mixing. For a pragmatic point of view, high speed shear mixing in a high viscosity melt deliver an energy density lower than the GPa observed for sonication. This means that contrary to solution mixing the dispersion quality relies on a large amount of parameters such as the screw profile, screw speed, temperature, residence time, polymer nature, viscosity etc…, which can lead to a large panel of dispersion states. Figure 17 illustrates the influence of the mixing conditions on the obtained composites. In order to highlight the influence of the main parameters, one will first present results on nanocomposites generated in small-scale mixers (direct incorporation of the fillers) and then show some results obtained at a larger scale.

As mentioned earlier, the infiltration of the matrix mainly depends on the polymer characteristics. First, the affinity between the polymer chains and the filler surface must be taken into account. A good affinity, between the two components will favor the wetting of the polymer onto the filler surface. The affinity is determined by calculating the interfacial energy between the two components.

P. Pötschke and coworkers have tackled this topic a lot [123]. They have, amongst others, analyzed the influence of the interfacial energy on the dispersion mechanism. One must mention, before presenting the results that the nanocomposites are not made with exactly the same type of CNTs. There is a small variation in there aspect that does not have dramatic impact on the dispersion.

They have characterized the nanocomposites by the determination of the agglomerates surface (see Figure 17 black entities). Large area ratio of agglomerates characterizes poorly dispersed composites. This characterization method will be presented more in details in the following section. Figure 17 shows the obtained nanocomposites, and Figure 18 summarizes the area ratio calculated from the optical micrographs as a function of the interfacial energy between the polymer and the filler. One

can observe that there is no direct relation between the dispersion state and the interfacial energy.

Figure 17: Optical micrographs of 1vol% MWCNT composites produced by using (a) PA66 (265˚C); (b) PET (290˚C); (c) PC (300˚C); (d) PA 12 (220˚C); (e) PP (200˚C); and (f) LDPE (170˚C). Composites produced at 100 rpm, 5 min, processing temperature indicated beside the name of the polymer, section thickness 20µm. Plotted from Ref [124]

Figure 18: Area ratio of undispersed CNT agglomerates AA versus interfacial energy (dotted line is only a guide). Plotted from Ref [124]

Thus, the interfacial energy is not the only accounting parameter for the infiltration mechanism. The energy generated by the shear must be also taken into account for the dispersion of the agglomerates. The viscosities of the matrices presented in Figure 17 are very different. However, the results presented in Figure 17 and 18 are not sufficient to draw conclusion.

The influence of the molar mass of the polymer has been studied by Yamada *et al.* [99,100] for the infiltration of CB. They have shown that a lower viscosity melt will infiltrate faster the agglomerates than a higher viscosity. This was confirmed by Kasaliwal *et al.* [125,126] for the infiltration of CNTs. They have analyzed the dispersion of MWCNT with different molar mass PC matrices. The agglomerate area ratio for different molar mass PC is plotted as a function of the applied shear stress during the melt mixing in Figure 19. They have applied different mixing speeds to obtain different shear stress.

Figure 19: Area ratio A_A vs. applied shear stress for composites of PCs with different viscosity and 1wt% Baytubes C150HP. The mixing speed is fixed at 150 rpm. Plotted from Ref [127]

First, Figure 19 confirms the fact that infiltrated agglomerates (low viscosity) require a lower shear stress to be broken. This result shows that an infiltrated agglomerated will not be broken into smaller agglomerates if the applied stress is not large enough to overcome its cohesive strength. The total amount of generated energy during the mixing must also be taken into account. For instance, the solution for low viscosity matrix is the increase of the mixing speed or the mixing time in order to generate sufficient energy to properly disperse the fillers [128].

After the comprehension of the different parameters for the dispersion of CNT into polymer matrix this can be scaled up to larger extruders. By adjusting the extruding conditions one can control the applied shear and the residence time to obtain well dispersed nanocomposites with a much better dispersion than in microcompounder. By this way, Andrew *et al.* [129] achieved a good dispersion of MWCNT in a Polystyrene matrix and generated nanocomposites with a low percolation threshold of 0.45 wt%, whereas Pötschke *et al*. [124] obtained only poorly dispersed nanocomposites with obviously a higher percolation threshold (see Figure 18) by using a micro-compounder.

Villmow *et al*. [130] have tested a lot of configuration for the incorporation of CNT into PCL. Their work has outlined some important results on the dispersion states as a function of the residence time, the dispersive and distributive configuration of the screw. For the realization of masterbatch, a distributive mixing will show a better dispersion than a dispersive configuration for similar residence time. However, the distributive configuration is quite limited for the dispersion of highly filled masterbatch. Playing on the residence time is not sufficient for the destruction of primary agglomerates. Nevertheless, they have shown that the dilution of their masterbatches filled with 7wt% can lead to well dispersed composites with a very low percolation threshold.

Finally, this incorporation method shows a drawback. The stress applied for the filler dispersion can also induced irreversible damage of the filler. Nanotubes will break and they will lose one of their major quality: their very high aspect ratio.

One can easily understand that there is no ideal matrix that can fulfill every condition presented in the melt mixing strategy. The use of extruder gives the possibility to adapt the mixing condition as a function of the CNT characteristics and of the matrix. That is why; the masterbatch dilution is the more appropriate strategy as it gives the possibility to adapt the processing conditions of the different steps in order to enhance the filler incorporation. For instance, for the realization of the masterbatch, one can prefer the use of small molar mass with a good affinity with the filler surface in order to enhance the wetting and infiltration of the agglomerates, then, for the dilution step, one can use a larger molar weight matrix to disperse more easily the agglomerates. However, this strategy shows limits for the dispersion of SWCNT with extremely large aspect ratio. The primary agglomerates are so dense, that the mechanical forces are not enough to significantly reduce the average bundle size. For such fillers, the solvent mixing with dispersion carried out with sonication and functionalization steps will be more appropriate. For the generation via melt mixing, a sonicated pre-dispersion of the filler might be considered.

B. Nanocomposites characterization

Once the nanocomposite is elaborated its characterization should be done in order to understand the influence of the processing conditions on the physical properties of the material. The precise characterization of the CNT dispersion in the polymer matrix has faded into a thorny challenge especially when using fillers of nanometer scale as no classical observation technique seems to be totally appropriate.

1. Microscopy

For fillers of nanometer size the dispersion must be described at different length scale: the nanometer scale of the filler diameter for the description of the entanglement state the micrometer scale, describing the aggregates and agglomerates population and a scale at a larger length scale: millimeter length scale describing the resulting network. This implies the combination of different characterization techniques in order to well describe the filler network structure (disentangled structure, population of aggregates, population of agglomerates, junctions between aggregates, orientation of the fillers) and *in fine* to understand the resulting macroscopic properties. For instance, aggregates of CNT can be oriented but if the aggregate domains are not oriented the orientation of the primary structure is not relevant for predicting the macroscopic properties.

a. Optical microscopy

From a practical point of view, the characterization of the processing parameters can be easily achieved with Optical Microscopy. This technique uses a thin layer (around tens microns) of materials cut with a diamond knife and observed through light microscopy. This method is limited to the observation of large aggregates and cannot give information on the submicron dispersion. However, combined with image analysis, one can quantify the dispersion state of nanocomposites and then correlate them with the processing parameters (see Figure 20).

Figure 20: Feature-based algorithm for segmentation of grey scaled light microscopy micrographs with carbon nanotube agglomerates: (a) this is binarized with grey scale thresholds of (b) 100, (c) 138, and (d) 175. With the increasing threshold value the number of agglomerates and thus A_A increases. Plotted from Ref [131]

This method relies on the segmentation of the image. In other words, the polymer matrix and the CNT aggregates are distinguished in order to determine the surface occupied by the aggregates. One can analyze every aggregate and obtain its aspect ratio using images analysis software. The total area fraction of the agglomerates is also obtained.

Moreira *et al*. observed the formation of a percolated network of CNT dispersed in PDMS thanks to optical microscopy observation. Figure 21 shows the formation of a percolated network after a long-time rest.

Figure 21: Optical micrographs of MWCNT dispersed in Polydimethylsiloxane: a) just after the sample implementation, b) after 24h of time rest. Plotted from Ref [132]

These pictures presented in Figure 21 have been correlated with conductivity measurements from 10^{-9} S.cm^{-1} for Figure 21a to 10^{-2} S.cm^{-1} Figure 21b. The poor conductivity of the sample (a) is due to the CNT dispersion. The CNTs are too dispersed and too far from each other. However, after a long-time rest, the network is build; the material becomes electrically conductor with a good conductivity.

To describe nanocomposites at a lower scale, other characterization techniques such as Atomic Force Microscopy (AFM), Transmission Electron Microscopy (TEM) or Scanning Electron Microscopy (SEM) must be used. In this section, the TEM and SEM techniques will be only presented as they are the only techniques used in this work.

b. Transmission electron microscopy

TEM analysis often requires tedious specimen preparation especially for a thermoplastic matrix with low T_g. TEM is an imaging technique where an electron beam passes through an ultra-thin film of composite. Examples of TEM micrographs are presented in Figure 22.

Figure 22: Transmission electron micrographs from PC-MWCNT plates with 0.6vol% MWCNT (a) well dispersed state conductivity $\sigma<10^{-16}$ S/cm, pressed at 265°C and (b) conductive state $\sigma= 5x10^{-4}$ S/cm aggregates connected together. Plotted from Ref [133]

The observed contrast comes from the interaction of the electrons with the thin film specimen. The absorption will be different depending on the atomic number of the material and on the thickness of the sample resulting in the formation of bright or dark area. For non-homogenous composite this technique gives the possibility to observe the fillers from the nanometer to micrometer scale. The contrast between CNTs and the matrix is low as carbon is a major component of the matrix and obviously of the filler. For such nanocomposites the contrast observed is due to diffraction difference. It can be noticed that, the observation of isolated CNT is easier considering MWCNTs than SWCNTs. With TEM observation, one can easily underestimate the CNT length as illustrated in Figure (a). The CNT is embedded in the matrix or has been cut during the thin preparation. The solution to properly measure the CNT length is to remove the matrix with the appropriate solvent; drop the suspension on a TEM grid off and then analyze the images. Figure 23 shows the evolution of the length distribution of the MWCNT during the melt mixing. The commercialized Nanocyl NC7000 has a broad size distribution. After the melt extrusion, the population above 1500 nm has disappeared.

Figure 23: Length distribution of as-grown and processed MWCNTs (Nanocyl™ NC7000) dissolved from PC composites (3wt% MWCNT, melt extruded at 500 rpm, 5kgh^{-1}. Plotted from Ref [134]

This technique is very time consuming however it brings precious information on the evolution of CNT length during the composite elaboration.

Nevertheless, due to larger diffraction and local intensity difference of the beam, one can easily observe dense aggregates and distinguish disentangled structures (see Figure 22b). One can apply the same protocol introduced in the optical microscopy section to obtain segmented images. Caution must be paid for a correct distinction of the filler and the matrix. Indeed, the contrast of the matrix is uneven (not perfectly homogeneous thickness, knife marks) and can induce artifacts. Considering a sufficient number of analyzed images to be representative of the specimen one can deduce precious information on the orientation the dispersion and connection between the fillers [135].

A tremendous work has been carried out in order to characterize the orientation of the CNT in melt processed composites. Among them, one can cite the work of Villmow *et al.* [136] observing the filler orientation after injection molding. They have made consecutive cuts in the injection molded specimen. Figure 24 illustrates two TEM micrographs of thin films taken at different localization in

the injection molded part. One can observe the evolution of the dispersion and orientation of the CNT as a function of their relative position in the mold [137]. This analysis will be more detailed in the last section.

Figure 24: TEM micrograph of ultrathin cuts (cuts perpendicular to the plate surface) of an injection molded plate with 2 wt% MWCNT in PC for different depths from the surface; left figure 2 µm and right figure 23 µm. The flow direction is indicated by red arrows. Plotted from Ref [138]

c. Scanning electron microscopy

Classical SEM observations are carried out with a metallized specimen and the detector Anthon Thevenard. This experimental protocol is quite useful for the characterization of nanocomposites filled with long fibers, or for the characterization of highly filled materials. However, for the characterization of nanofillers, the experimental conditions must be adjusted. The observation of composites relies on two main techniques: the topographic contrast and the compositional contrast. Those techniques analyze the Secondary Electron (SE) and Back Scattering Electron (BSE) created after the interaction of the Incident Electron and the specimen surface [138].

The topographic contrast can be achieved using SEM in secondary electrons (SE). Those electrons emitted from the specimen surface are originated from inelastic scattering, which is a transfer of energy of the specimen atom and a potential expulsion of an electron from that atom. They have a low energy level and, by consequence, can only escape from a volume near the specimen surface. The SE detector is located near the specimen surface but oriented with a specific angle. The signal variation (different quantity of SE) will correspond to a specific geometrical feature of the specimen surface. The other contrast mainly relies on the BSE signal analysis. It results from the direct interaction of incident electrons with the nuclei of the atoms of the observed specimen. They have higher energy levels. The composition contrast will lead to an image with different grey-scale levels. One can easily understand that the composition contrast analysis is quite limited for polymer matrix filled with CNT as the two components of the material: CNT (carbon element) and polymer matrix (carbon as a constituent element) have low contrast.

However, Campbell [139] has firstly achieved to observe Carbon Black (CB) dispersed in Polyvinylchloride without any coating of the specimen. By varying the applied voltage, they have observed a difference in the SE emission. This is the voltage contrast in SEM, now widely used for the characterization of electrically conductor composites [140-145]. This method relies on the inhomogeneity of the material and more specifically on the permittivity difference between the filler and the polymer matrix. In this paragraph, the main studies carried out for the comprehension and development of this method will be presented.

The observation method principles will be first presented with an ideal case of MWCNT dispersed in an epoxy matrix. SEM observation technique is based on the analysis of SE emitted by the specimen surface. To enhance the analysis it is recommended to use the in-lens detector instead of a classical detector. The in-lens detector is located in the focusing beam lens. The location of this detector excludes most of the BSE, and SE generated after BSE scattering (SE3). In addition, the Working Distance (WD), which is the distance between the detector and the specimen surface, is set to a low value in order to increase the number of collected SE from the sample.

As mentioned earlier, the voltage contrast observation is possible if the specimen is not coated with metal particles. This implies that the acquisition will be possible if the charge state (negatively, positively or neutralized state) of the specimen is appropriate. First, one must consider the different electron flux generated during the acquisition in order to determine the resulting charge state of the specimen. The process can be summarized as a flux of primary electron (PE), a generation of SEs resulting from the interaction of PE with the specimen and the leakage current. One can write a law of charge conservation as a function of time t:

$$I_{PE}(1-(\delta+\vartheta)]-I_L=\frac{\partial Q}{\partial t}$$

Equation 16

where $\partial Q/\partial t$ is the charge build-up rate, δ and ϑ respectively describe the generation of SEs and BSE and I_L is the leakage current. The specimen will be negatively charge if the current sent by the PEs is greater than the total generated current and leakage current [146]. Charges will stack on the specimen surface and will deflect and defocus the PE beam inducing strong distortion during the image acquisition.

A composite with a well formed percolated network will be characterized by a sufficient electrical conductivity. The PE will interact with the CNT, doing so they will dissipate their energy avoiding the whole charging of the specimen. However, some electrons will not be fully dissipated. Due to the difference of dielectric properties, those electrons will be trapped in the specimen more precisely at the interface between the fillers and the polymer matrix.

Considering CNTs of (χ_{CNT}) embedded in a polymeric matrix (χ_{matrix}), this susceptibility gradient will generate a local density of polarization charges creating a potential barrier in which carriers can be trapped. According to Cazaux and cowrokers the primary electrons have sufficient energy to overcome this potential. However, an electron which was submitted to scattering will be trapped at the interface as its energy is too small [147]. Those trapped electrons will then generate a negative

potential enough to locally enhance the emission of SE. The area will consequently appear bright. The electrons are trapped on the polymer side, as the polymer matrix of lower permittivity. That is why; charge contrast increases the diameter of the CNT.

Figure 25 illustrates the different mechanisms which can occur during charge contrast observation. One considers calendared composites (CNT/epoxy matrix) filled with different amount of CNT and observed under varying accelerating voltage. According to the author [144,145] the material with 0.5 wt% has a lower conductivity than the composites filled with 0.7 wt% and 1.3 wt%.

Figure 25: SEM images of calendered composites MWCNT in epoxy matrix: Column 1) 0.5 wt%-composite; Column 2) 0.7 wt% composite; Column 3) 1.3 wt%-composite. Large scalebar is 2 μm; small scale bar is 400 nm. Plotted from Ref [144]

First, it can be noticed that the observation of the 0.5 wt% specimen is not possible at low voltage. By increasing the concentration of CNT, (i.e increasing the whole conductivity of the specimen) the observation of the CNT are possible and even more pronounced when increasing the accelerating voltage. The clouds observed respectively at 5 kV and 7 kV for the specimens of 0.7 wt% and of 0.5 wt% are distortions induced by the stacking of charges on the specimen surface. The CNT network is not dense enough to dissipate the PE. However, at higher accelerating voltage, PE can penetrate deeper in the material and can interact with CNT located deeper in the specimen. At higher concentration and low accelerating voltage the penetration depth is small but PE can be dissipated by CNT located near the surface. The case of 5 kV for 0.5 wt% is explained by Li and coworkers [144,145] as a negatively charged materials and the bright area correspond to polymer matrix. This is a specific case of the technique and will not be more explained here.

By depositing a thin layer of PS (80 nm) on their specimen Li *et al.* [144,145] have highlighted the depth penetration of both PE and SE emitted in the specimen. At 7 kV, one can observe large distortions that are not observed for uncoated samples (for composites 0.5 wt%, 0.7 wt% and 1.3

wt% see Figure 26) they tend to disappear with the increase of the accelerating voltage. Usually, SEs have low energy and their maximum escape depth is around 50 nm. The observation of CNTs with a coating layer of 80 nm highlights the energy level of the produced SEs. Some have explained this by a local electric field that accelerates the SE emitted and increasing their escape depth. Charge contrast SEM gives also the possibility to sense relatively deeper in the specimen.

Figure 26: SEM images of calendered-composites MWCNT in epoxy matrix coated with 80 nm-PS film: Column 1) 0.5 wt%-composite; Column 2) 0.7 wt%-composite; Column 3) 1.3 wt%-composite. Large scale bar is 2 μm; small scale bar is 400 nm. Plotted from Ref [144]

Figure 27 illustrates the main mechanisms occurring during charge contrast SEM observation.

Figure 27: Illustration of imaging mechanism for MWCNT filled polymer. Plotted from Ref [148]

Charge contrast SEM is based on different phenomena which must be taken into account in order to

well interpret the contrast charge images. First, this method can sense deeper in the material than classical observation (2D-observation) and gives information on the specimen conductivity (macroscopic information). The local emission of SE located deeper in the material will appear less bright than this occurring near the edge of the specimen. Second, this technique induces overestimation of the CNT diameter, because SE generated in the polymer matrix near the CNT will appear. One cannot be sure if an observed CNT belongs to the whole CNT network or if it is isolated. To facilitate charge contrast SEM, attention to the specimen surface preparation must be paid. A smooth surface will avoid any additional topographic contrast and will enhance the CNT visualization. To finish, the choice of the accelerating voltage to generate good images depends on the specimen conductivity, the type of SEM, and the detectors. It can be kept in mind that high conductivity specimen can be observed with high accelerating voltage and low accelerating voltage is for low conductivity specimen.

2. Rheological analysis

For fillers in the nanometer range different kind of interactions must be taken into account. The filler-filler interaction (percolated network), already mentioned, which is very strong for the case of filler with very large specific area. One must also consider the interaction between the polymer chains and the filler and also the temporary polymer network. For a processing point of view, the analysis of the behavior of such nanocomposites under flow is crucial. Indeed, during the processing steps for the elaboration of plastic parts, the melt is submitted to large deformation at high speed that can dramatically impact the orientation of the polymer chains but also on the filler network structure. In most cases, after the processing, one obtains final parts with uncontrolled or inhomogeneous electrical properties. The rheological measurement and more specifically, the rheometry combined with Direct Current (DC) measurement has paved the way for a better comprehension of the mechanism occurring in the melt. First, in this section the rheometer as a tool for the determination of the percolation threshold will be presented. Then, rheological experiments combined with conductivity measurement as a tool to probe the structural evolution under quiescent and under deformation will be presented.

a. Determination of the percolated threshold

A great deal of work on the rheological properties of such materials can be found in the literature. The analysis of the melt viscoelastic properties using both strain-controlled and stress-controlled rheometers in the linear domain (strain or stress chosen in the linear viscoelastic range of the material) has highlighted a change in the rheological behavior of the material with the addition of CNT.

With the presence of CNTs the material behavior changes from purely viscous to solid-like. The formation of a percolated network in the nanocomposite generates an increase of the complex shear

modulus *G* (ω)*. At low frequencies, the apparition of an equilibrium modulus G_e in the storage modulus variations is observed. The rheological behavior is not dominated by the polymer matrix any more. The increase of the G_e modulus is very important for a wide range of filler concentrations. This result is commonly known in the field of filled polymers. One can find a large number of studies showing a dramatic change in the rheological behavior for different kinds of matrix and fillers [149-157]. The value of the G_e follows a power law as a function of the filler concentration [158,159]. The interfacial forces between the fillers are so strong that the filler compaction is limited and the filler network adopts a fractal-like conformation well described in the literature. [132,160-163]

As for electrical conductivity measurement, the rheology analysis can be a useful technique for the determination of the percolation threshold. For a better sensitivity, the use of the van Gurp-Palmen plot [164] can be used to determine the rheological percolation threshold. The phase angle δ is plotted versus the absolute value of the complex modulus *G** [156]. Valentino *et al*. have highlighted the slight difference between the evolution of the complex viscosity, the storage modulus and the van Gurp Palmen Plot with the increase of the MWCNT concentration in HDPE matrix. The different evolutions are depicted in Figure 28.

Figure 28: (a) Complex viscosity () vs. frequency (ω) and (b) storage modulus (G') vs. frequency (ω) and (c) phase angle δ vs. the absolute value of the complex modulus |G| for the MWNT/HDPE composites and the pure HDPE (T = 200 °C). Plotted from Ref [155]*

The rheological analysis has also highlighted the strong sensitivity of the filler network to the flow conditions. Nobile *et al.* [165], Somma *et al.* [166], Pötschke *et al*. [167] and Iervolino *et al.* [168] have observed an evolution of the percolation threshold as a function of the measurement temperature. Lowering the measurement temperatures shifts the rheological percolation threshold to higher filler concentration. Hence, Pötschke *et al.* [169] have observed for MWCNT dispersed in PC a percolation threshold drop from 5 to 0.5 wt% for temperatures increasing from 170 to 280°C. They have argued that the network includes both CNT and polymer. It was indeed, the first observation of the huge capability of CNT network to change when composite is in molten condition. It must be added that the structuring of the network take a long time and this also depends on the polymer temperature. This phenomenon can lead to percolation threshold difficulty measurements.

b. Structural evolution in molten-state: combined rheology/electrical measurements

The combination of rheological analysis with conductivity measurement enables to better probe the structural change of the network in molten condition. The electrical measurements are carried out using the parallel-plates which act as electrodes. More precisely, the rheological cell geometry is made of isolated ring-plate electrodes connected to a power source. The upper and lower plates are equipped with ring electrodes (inner diameter 22 mm, outer diameter 25 mm). In those conditions, quasi-homogeneous shear rate and deformation throughout the sample volume are applied. The electrical conductivity is measured perpendicular to the direction of shear [170].

Migler and coworkers [170] were the first to use this specific set-up and observe the structural change under shear stress. Figure 29 shows the evolution of conductivity as a function of the shear rate for a PP matrix filled with different MWCNT concentrations.

Figure 29: Conductivity as a function of the shear rate for PP filled with MWCNT (X_m weight percent) T= 190°C. Plotted from Ref [170]

They were the first to observe the conductor-insulator transition by destruction of the filler network under shear stress. Their works have triggered the analysis of the structural change of composites with this specific set-up. [132,152,171-173]

Figure 30: DC conductivity during annealing T=230°C, transient shear deformation (t=10s, $\dot{\gamma} = 1\ s^{-1}$) and isothermal conductivity recovery after shear at T=230°C PC filled with 0.6vol% MWCNT. Plotted from Ref [174]

The conductivity evolution observed in Figure 30 illustrates the structural evolution of the filler network while the material exists as a melt. The experience starts from a non-equilibrium state. The specimen has a low conductivity. The percolated network is not constituted of all the fillers present in the material. Under quiescent condition, the filler network can be developed thanks to new connections between the aggregates. When stress is applied to the filler network, the connections break and the aggregates are strained apart. The material becomes electrically insulating. Directly after the end of the deformation the conductivity increases again. The state after the shear can be compared to Figure 31a, whereas the state after the annealing step is illustrated in Figure 31b. Later, Alig and coworkers presented additional work on the structural evolution of the filler network in molten conditions [160].

Figure 31: Time-dependent conductivity for initially agglomerated (a) and well dispersed (b) composites of MWCNT (0.6 vol%) in PC under steady shear deformation ($\dot{\gamma} = 0.02\ s^{-1}$ for 1 h) and during quiescent annealing after shear at 230 C. The inserts schematically show the state of nanotube dispersion and the measuring cell with the sample. Plotted from Ref [160]

They have even observed conductivity increase when small steady shear is applied (Figure 31b). The deformation brings aggregates closer to each other triggering agglomeration between isolated CNT or between small aggregates. The formed agglomerates are not broken as the viscous forces are too small to disrupt the formed connections. Moreira *et al*. [132] have also observed the same phenomenon for PDMS filled with MWCNT. With TEM analyses of their samples, Alig *et al*. [160] have explained their results. A well-formed network will be very sensitive to stress. In Figure 30, the forces involved are high enough to break all the connections of the network. However, at lower steady shear (in Figure 31), the forces partially disrupt the network and the specimen confinement gives the possibility to the system to stabilize by competition between restructuration and destruction mechanisms.

c. Application for composites processing

The rheological analyses have shown the huge structural change of nanocomposites when existing as a melt. That is why manufacturing plastic part with tailored and homogenous electrical properties is a thorny challenge. The melt processing induces large deformation at high rate and consequently, induces dramatic changes in the filler morphology. The same team also tried to make in-line measurements during continuous mixing and injection. For instance, Alig *et al*. [175] have shown the same conductivity recovery after cessation of extrusion (see Figure 32).

Figure 32: Time-dependent conductivity measurements of a PC-CNT composite with 0.6vol% MWCNT in a measurement slit die during melt extrusion at different melt temperatures (screw speed 175 rpm) and after the extrusion has stopped. Plotted from Ref [175]

On the other hand, Lellinger *et al*. [176], have analyzed the conductivity of materials as a function of the injection conditions by both in-line and off-line measurements. The different methods were carried out at the same locations. Figure 33 illustrates the works carried out for injection molding of PC/ Styrene-co-acrylonitrile blend filled with 4wt% MWCNT.

Figure 33: Influence of injection speed v (left), melt temperature (right) on the in-line and off-line measured electrical conductivity of a polycarbonate/ styrene-co-acrylonitrile blend (Bayblend) containing 4 wt% MWCNT. Plotted from Ref [176]

The flow condition generates different electrical conductivity levels. The stronger the mechanical deformation induces larger destruction of the percolated network. In addition, the low difference between in-line (melt state) and off-line (under T_g) shows that the melt processing step defines the filler network structure of the final parts (i.e the physical properties).They have observed similar results on PC/MWCNT, PA/MWCNT materials for different processing conditions.

In addition, CNTs are highly flexible fillers that can easily be aligned when the polymer matrix flows during composite processing stages. Villmow *et al.* [137] have observed the strong orientation of MWCNT during injection molding (see Figure 24). They have observed thanks to TEM analysis, that the orientation is more pronounced as the stress increases. Indeed, MWCNTs are more oriented in the area near the wall where the shear is higher than in the middle of the mold. Surface of end-product will present a lower conductivity than the core.

d. Modeling conductivity variation

In addition to experimental observation, some studies have dealt with simulation approaches (in 2D and 3D) on rod-like fillers to model the effect of orientation on the conductivity and the percolation threshold. Firstly, lowest percolation is obtained for isotropic or slightly anisotropic systems [177,178]. Indeed, Chang and coworkers [179] have observed under uniaxial and biaxial deformation a decrease of the percolation threshold with the deformation. Then, the percolation threshold increases with larger deformation. Even if rod-like structure is a poor description of CNT, they have observed large decrease of the specimen conductivity with the increase of the alignment [177,180]. Moreover, they have both put in the light a critical alignment when the percolated

network is broken and a power law dependence of the conductivity as a function of the alignment. However, Silva *et al.* [181] who conducted similar simulations have observed conductivity decrease but without such critical values or power law dependence. The simulation of such complex dispersion is quite difficult.

The experimental results (TEM observation Figure 24 left) steer the thought that the conductivity decrease is not only due to the filler alignment but also due to the fact that particles are strained apart from each other. Clearly, the destruction of the percolated network is very hard to precisely model. That is why; Skipa *et al*. [172,173] have privileged a phenomenological approach to model the conductivity evolution. They have used a structural network model with a kinetic equation to characterize the network evolution under quiescent and shear. This strategy was useful but shows some limitations when there is strong competition between structuration and destruction of the network. Their work will be more precisely presented in Chapitre 5 and transposed for the prediction of conductivity variation under extensional deformation.

Conclusion

The addition of CNTs to polymer has urged scientists to develop and adapt existing characterization techniques in order to understand the relation between the nanostructure and the macroscopic properties. Thanks to OM, TEM and SEM one can analyze the dispersion state of the filler in the polymer matrix and consequently improve the mixing steps. Indeed, the physical properties of the composite directly rely on the appropriate population and dispersion of CNT in order to generate a percolated network of filler. However, every melt processing steps can dramatically modify this network and the filler. For instance, TEM analysis has given the possibility to observe the orientation of the filler during injection molding.

However, the major breakthrough remains the development of a new set-up that combines conductivity measurement and rheology analysis. The observation of conductor-insulating transition under small shear deformation confirms the encountered difficulties for the realization of plastic parts with controlled electrical properties.

III. Conclusion

Since their discovery in the early 90's, Carbon Nanotubes have generated unprecedented excitement in the academic and industrial fields. Their promising intrinsic properties make them the perfect candidate as filler for the generation of high added value composites. For instance, in polymer matrix, it gives the possibility to increase their panel of activity by the achievement of Conductor Composites Polymer.

However, their strong interaction forces make the mixing steps more difficult than encountered for other kind of fillers.

This thorny problem has urged scientists to develop and adapt existing characterization technique in order to understand the relation between the nanostructure and the macroscopic properties. Indeed, the physical properties of the composite directly rely on the appropriate population and dispersion of CNT in order to generate a percolated network of filler. The filler network, when the polymer exists as a melt, can dramatically change leading to composites with better or worth properties. Indeed, CNT can orient under external forces but most important is that the connections that make the percolated network can break leading to insulating composites. That is why the achievement of final parts with tailored electrical properties remains a tricky challenge.

The combination of the rheology analysis to conductivity measurement has paved the way to a better comprehension of the structural evolution of the filler network under shear stress of under quiescent conditions. This set-up has given the possibility to observe the transition of modest conductor to insulating under shear. There is still a gap to fill in as most of the studies have dealt with shear deformation which is not transposable for thermoforming where the composites undergo purely large extensional deformation.

That is why; the aim of this work was to develop a new combined method for the comprehension of the network deformation under extensional deformation. Nevertheless, there is a lack of experimental data on nanocomposites under large extensional deformations. The few studies have been done with post-mortem conductivity measurement. To date, none have carried out in-line measurement during extensional deformation when nanocomposite exists as a melt. This will be the challenge of this work.

References

[1] Iijima, S., Helical Microtubules of Graphitic Carbon Nature; *London* 354.6348 (**1991**): 56.

[2] Iijima S., T. Ichihashi : Single-shell carbon nanotubes of 1-nm diameter, *Nature* 363 (**1993**) 603-605

[3] Bethune D. S., C. H. Kiang, M. S. de Vries, G. Gorman, R. Savoy, J. Vasquez, R. Bayers : Cobalt-catalyzed growth of carbon nanotubes with single-atomic-lawer walls, *Nature* 363 **1993** 605-607

[4] Kim, P., Shi, L., Majumdar, A., McEuen, P. L. Thermal transport measurements of individual multiwalled nanotubes, *Phys. Rev. Lett.* **2001**, 87, 215502.

[5] Fujii, M., Zhang, X., Xie, H. Q., Ago, H., Takahashi, K., Ikuta, T., Abe, H., Shimizu, T. (2005). Measuring the thermal conductivity of a single carbon nanotube, *Phys. Rev. Lett.* **2005**, 95, 065502.

[6] Wang N., Z. K. Tang, G. D. Li, J. S. Chen : Single Walled 4 Å carbon nanotubes arrays, *Nature* 408 **2000** 50-51

[7] K. I. Tserpes and P. Papanikos Finite element modeling of single-walled carbon nanotubes. *Composites Part B: Engineering* **2005**, Volume 36, Issue 5, Pages 468-477

[8] Chunyu Li and Tsu-Wei Chou Single-walled carbon nanotubes as ultrahigh frequency nanomechanical resonators. *Phys. Rev. B 68*, 073405 –2003

[9] Dresselhaus M. S., G. Dresselhaus, and R. Saito, Carbon 33, 883–891 (1995).

[10] Yakobson, B.I. , C.J. Brabec, J. Bernholc Nanomechanics of carbon tubes: instabilities beyond linear response. *Phys. Rev. Lett.* **1996**, 76, 2511

[11] Yakobson, B.I., G. Samsonidze Atomistic theory of mechanical relaxation in fullerene nanotubes. *Carbon*, 38 (11-12) **2000**, pp. 1675-1680

[12] Dresselhaus, M.S. , G. Dresselhaus, P.C. Eklund, Science of fullerenes and carbon nanotubes (1996)

[13] Saito, R., G Dresselhaus, MS Dresselhaus, Physical properties of carbon nanotubes. *Imperial College Press* **1998**

[14] Iijima, S. , C. Brabec, A. Maiti, J. Bernholc Structural flexibility of carbon nanotubes; *J Chem Phy*, **1996** 104, pp. 2089-2092

[15] Walters, D. A. , L.M. Ericson, M.J Casavant, J. Liu, D. T. Colbert, K.A. Smith, R. E. Smalley: Elastic strain of freely suspended single-wall carbon nanotube ropes, *Appl. Phys. Lett.* **1999**,74 3803-3805

[16] Yu, M.-F. , O. Lourie, M. J. Dyer, K. MOloni, T. F. Kelley, R. S. Ruoff : Strenght and breaking mechanism of multiwalled carbon nanotubes under tensile load, *Science* **2000**,287 637-640

[17] Demczyk, B. G. , Y. M. Wang, J. Cumingd, M. Hetamn, W. Han, A. Zettl, R. O. Ritchie: Direct mechanical measurement of the tensile strength and elastic modulus of multiwalled carbon nanotubes, *Mater. Sci. Eng. A* **2002**,334, 173-178

[18] Gao, R.P. Z.L. Wang, Z.G. Bai, W.A. De Heer, L.M. Dai, M. Gao: Nanomechanics of individual carbon nanotubes from pyrolytically grown arrays, *Phys. Rev. Lett.* **2000** ,85,622-625

[19] Treacy, M.M.J T.W. Ebbesen, J.M. Gibson: Exceptionnaly high Young's modulus observed for individual carbon nanotubes, *Nature* **1996** ,381,678-680

[20] Yao, N. V. Lordie : Young's modulus of single-wall carbon nanotubes, *J. Appl. Phys.* 84 (**1998**) 1939-1943

[21] Lourie, O. H. D. Wagner: Transmission electron microscopy observations of fracture of single-wall carbon nanotubes under axial tension, *Appl. Phys. Lett.* **1998** , 73, 3527- 3529

[22] Eitan, A., F.T. Fisher, R. Andrews, L.C. Brinson, and L.S. Schadler, *Composites Science and Technology*, **2006,** Vol. 66, p. 1159.

[23] Thostenson, E. T. , R. Zhifeng, and T.-W. Chou, Advances in the science and technology of carbon nanotubes and their composites: a review, *Compos. Sci. Technol.* **2001,** 61,1899

[24] Hull, D. , An Introduction to Composite Materials, 2nd ed. (Cambridge University Press, Cambridge, **1996**)

[25] Li, F., H. M. Cheng, S. Bai, G. Su, and M. S. Dresselhaus, Tensile strength of single-walled carbon nanotubes directly measured from their macroscopic ropes, *Appl. Phys.Lett.* **2000,** 77, 3161.

[26] Asa H. Barber, S R Cohen, H. D. Wagner, measurement of carbon nanotube-polymer interfacial strength. *Applied Physics letters* **2003,** vol 82, nb 23

[27] Liao, K. and S. Li, Interfacial characteristics of a carbon nanotube–polystyrene composite system, *Appl. Phys. Lett.* **2001,** 79, 4225

[28] Frankland, S. J. V. , A. Caglar, D. W. Brenner, and M. Griebel, Molecular simulation of the influence of chemical cross-links on the shear strength of carbon nanotube− polymer interfaces, *J. Phys. Chem. B* **2002,** 106, 3046

[29] Hone, J., Whitney, M., Piskoti, C. & Zettl, A. Thermal conductivity of single-walledcarbon nanotubes. *Phys. Rev. B* **1999,** 59, R2514-R2516

[30] Che, J., C¸a˘gın, T. & Goddard III, W. A. Thermal conductivity of carbon nanotubes. *Nanotechnology* **2000** 11, 65–69.

[31] Berber, S., Kwon, Y.-K. & Tománek, D. Unusually high thermal conductivity of carbon nanotubes, *Physical Review Letters,* **2000** 84, 4613–4616.

[32] Pop, E., Mann, D., Wang, Q., Goodson, K. & Dai, H. Thermal Conductance of anIndividual Single-Wall Carbon Nanotube above Room Temperature. *Nano Lett*. 6, 96–100 (**2006**).

[33] Shiomi, J., Maruyama, S., Molecular dynamics of diffusive-ballistic heat conduction in single walled carbon nanotubes, *Jpn. J. Appl*. *Phys.* . **2008**, 47, 2005–2009.

[34] Wang, J. A.,Wang, J. S.. Carbon nanotube thermal transport: ballistic to diffusive, *Appl. Phys. Lett*., **2006** 88, 111909.

[35] Hone, J. : Phonons and thermal properties of carbon nanotubes. In: Carbon Nanotubes: Synthesis, Structure, Properties, and Applications, ed by M.S. Dresselhaus, G. Dresselhaus, P. Avouris (Springer Verlag, Berlin **2001**)

[36] Sinha, N., Yeow JT-W Carbon nanotubes for biomedical applications. *IEEE Trans Nanobiosciences* (2005) 4:180–195

[37] Weisman, R. B.: "Fluorescence Spectroscopy of Single-Walled Carbon Nanotubes", Chapter 8, Springer **2004**

[38] O'Connell, M. , S.M. Bachilo, C.B. Huffman, V. Moore, M.S. Strano, E. Haroz, K. Rialon, P.J. Boul, W.H. Noon, C. Kittrell, J. Ma, R.H. Hauge, R.B. Weisman, and R.E. Smalley: *Science* **2002,** 297, 593

[39] Landauer, R. , Electrical resistance of disordered one-dimensional lattices, *Taylor and Francis Philos. Mag.* **1970** 21, 863

[40] Z. Yao, C.L. Kane, and C. Dekker, High-field electrical transport in single-wall carbon nanotubes, *Phys. Rev. Lett.* **2000**, 61, 2941

[41] V.C. Barroso Æ S.P. Ribeiro J.M. Maia Unusual extensional behavior of a polystyrene/HIPS blend. *Rheol Acta* **2003** 42: 483–490

[42] Molau, G. E. , H. Keskkula,J., Heterogeneous polymer systems. IV. Mechanism of rubber particle formation in rubber-modified vinyl polymers, *Polym. Sci., Part A-1* **1966**,4, 1595.

[43] K. Sardelis, H. J. Michels, G. Allen, F. R. S. XX *Polymer* **1987**,28, 244–2250

[44] M. Fisher, G. P. Hellman, On the evolution of phase patterns during the high-impact-modified polystyrene process, *Macromolecule*s **1996**,29,2498–2509

[45] M. Lambla, "Initiation à la chimie et à la physico-chimie macromoléculaires" G. F. P.; chimie des polymères volume 3 , 337 **1980**

[46] A. Echte, Angew., Teilchenbildung bei der Herstellung von kautschukmodifiziertem Polystyrol,

Makromol. Chem., 58/59, 175 **1977**

[47] R. Wirth, "Initiation à la chimie et à la physico-chimie macromoléculaires" G. F. P.; mélange de polymères volume 6 , 239 **1986**

[48] C. B. Bucknall, Brittle-tough transition temperatures in impact tests on rubber-toughened plastics, *Makromol. Chem. -Makromol Symp*. **1988** ,16, 209.

[49] J.P. Dear, J.C., Graham Measurement of the effect of toughening agents in polystyrene *Polym. Test*., 17 **1998**, p. 3

[50] F. Ramsteiner, W. Heckmann, G.E. McKee, M. Breulmann Influence of void formation on impact toughness in rubber modified styrenic-polymers *Polymer* 43 (**2002**) 5995–6003

[51] Throne, J. L., "Thermoforming:", Hanser, New York (**1987**).

[52] Aliza Erner Etude expérimentale du thermoformage assisté par poinçon d'un mélange de polystyrènes submitted July **2005** Id: pastel-00001313 pastel.archives-ouvertes.fr/pastel-00001313

[53] Ogden, R. W., Proc. R. Soc. Lond. A., 326,565, (**1972**).

[54] Kouba, K., Vlachopoulos, J., *SPE ANrEC Tech Papers*, 50, 114 **1992**.

[55] VJachopoulos. J., Kouba, K., Ghafur, M. 0., Founh European Rheology Conference - Sevilla. Spain (**1994**).

[56] Kouba, K., Bartos, 0., Vlachopoulos, Computer simulation of thermoforming in complex shapes, *J. Polym. Eng. Sci.*, 32, 699 **1992**.

[57] Koziey, B., Ghafur, M. 0., Vlachopoulos, J., Mirza, F. A., "Computer Simulation of Thermoforming" ,Chapter 2 in "Thermoplastic Sheet Forming", Bhanacharyya, D., (ed.), EIsvier

[58] Moniruzzaman M, Winey KI. Polymer nanocomposites containing carbon nanotubes. *Macromolecules* **2006**; 39 :5194-205

[59] Strümper R, Glatz-Reichenbach J, Conducting polymer composites J. Electroceram **1999**; 3:329-46

[60] Byrne MT. Gun'ko YK. Recent advances in research on carbon nanotube-polymer composites. *Adv. Mater* **2010**; 22:1672-88

[61] Grossiord N, Loos J. Regev O, Koning CE. Toolbox for dispersing carbon nanotubes into polymers to get conductive nanocomposites. Chem Mater **2006**; 18: 1089-99

[62] Huan Pang, Ling Xu, Ding-Xiang Yan, Zhong-Ming Li Conductive polymer composites with segregated structures *Progress in Polymer Science* 2**014**, 39,1908–1933

[63] Stauffer D, Aharony A. Introduction to Percolation Theory. London:Taylor and Francis; **1994** p. 192

[64] Xu S, Rezvanian O, Peters K,Zikry MA. The viability and limitations of percolation theory in modeling the electrical behavior of carbon nanotube–polymer composites. *Nanotechnology* **2013** ;24:155706/1–155706

[65] Kirkpatrick S. Percolation and conduction. *Rev Mod Phys* **1973** ;45:574–88.

[66] Wolfgang Bauhofer , Josef Z. Kovacs A review and analysis of electrical percolation in carbon nanotube polymer composites *Composites Science and Technology* **2009** , 69, 1486–1498

[67] Stauffer, D., Scaling theory of percolation clusters, *Physics Reports*, **1979** 54, 1–74.

[68] De Gennes PG., On a relation between percolation theory and the elasticity of gels*, J Phys* **1976**;37:1–2.

[69] Balberg, I., Binenbaum, N. & Wagner, N. Percolation thresholds in the 3-dimensional sticks system, *Physical Review Letters*, **1984** , 52, 1465–1468.

[70] Pötschke P, Abdel-Goad M, Alig I, Dudkin S, Lellinger D. Rheological and dielectrical characterization of melt mixed polycarbonate-multiwalled carbon nanotube composites. Polymer **2004** ; 45(26):8863–70

[71] Chen L, Pang XJ, Yu ZL. Study on polycarbonate/multi-walled carbon nanotubes composite produced by melt processing. *Mater Sci Eng A* **2007** ;457(1-2):287–91.

[72] K AA, Agarwal US, Joseph R. Carbon nanotubes-reinforced PET nanocomposite by melt-compounding. *J Appl Polym Sci* **2007**;104(5):3090–5.

[73] Andrews R, Jacques D, Minot M, Rantell T. Fabrication of carbon multiwall nanotube/polymer composites by shear mixing. *Macromol Mater Eng* **2002** ;287(6):395–403.

[74] Li J., Ma PC, Chow WS, To CK, Tang BZ, Kim JK. Correlations between percolation threshold, dispersion state, and aspect ratio of carbon nanotubes. *Adv Funct Mater* **2007**;17:3207–15.

[75] Gojny F.H., Wichmann MHG, Fiedler B, Kinloch IA, Bauhofer W, Windle AH, Evaluation and identification of electrical and thermal conduction mechanisms in carbon nanotube/epoxy composites. *Polymer* **2006** ;47(6):2036–45

[76] Yan Yan Huang and Eugene M. Terentjev Dispersion of Carbon Nanotubes: Mixing, Sonication, Stabilization, and Composite Properties *Polymers* **2012**, 4, 275-295

[77] Hamaker, H.C. The London van der Waals attraction between spherical particles. *Physica* **1937**, 4, 1058-1072.

[78] Shvartzman-Cohen, R., Nativ-Roth, E., Baskaran, E., Levi-Kalisman, Y., Szleifer, I., Yerushalmi- Rozen, R. , Selective dispersion of single-walled carbon nanotubes in the presence of polymers: the role of molecular and colloidal length scales, *J. Am. Chem. Soc*., **2004** 126, 14850–14857.

[79] Girifalco, L.A.; Hodak, M.; Lee, R.S. Carbon nanotubes, buckyballs, ropes, and a universal graphitic potential. *Phys. Rev. B* **2000**, 62, 13104-13110

[80] Zhbanov, A.I.; Pogorelov, E.G.; Chang, Y.C. Van der Waals interaction between two crossed carbon nanotubes. *ACS Nano* **2010**, 4, 5937-5945

[81] Geng, Y., Liu, M. Y., Li, J., Shi, X. M., Kim, J. K.. Effects of surfactant treatment on mechanical and electrical properties of CNT/epoxy nanocomposites, *Compos. Part A*, **2008**, 39, 1876–1883

[82] Lillehei, P. T., Kim, J. W., Gibbons, L. J., Park, C.. A quantitative assessment of carbon nanotube dispersion in polymer matrices, *Nanotechnology*, **2009**, 20, 325708

[83] Lee, J. Y., Kim, J. S., An, K. H., Lee, K., Kim, D. Y., Bae, D. J., Lee, Y. H.. Electrophoretic and dynamic light scattering in evaluating dispersion and size distribution of single-walled carbon nanotubes, *J. Nanosci. Nanotechnol.*, **2005**, 5, 1045–1049

[84] Geng, Y., Liu, M. Y., Li, J., Shi, X. M., Kim, J. K.. Effects of surfactant treatment on mechanical and electrical properties of CNT/epoxy nanocomposites, *Compos. Part A*, **2008** 39, 1876–1883

[85] Chen, H., Muthuraman, H., Stokes, P., Zou, J. H., Liu, X., Wang, J. H., Huo, Q., Khondaker, S. I., Zhai, L. Dispersion of carbon nanotubes and polymer nanocomposite fabrication using trifluoroacetic acid as a co-solvent, *Nanotechnology*, **2007**. 18, 415606.

[86] Liu, X. Q., Chan-Park, M. B.. Facile way To disperse single-walled carbon nanotubes using a noncovalent method and their reinforcing effect in poly(methyl methacrylate) composites, *J. Appl. Polym. Sci.*, **2009**. 114, 3414–3419.

[87] Bolen, W. R., Colwell, R. E., Intensive mixing, *Soc. Plast. Engng J.,* August, pp. 24-28 **1958**

[88] McKelvey, J. M., Mixing, chapt. 12 , *Polymer Processing*, John Wiley & Son, Inc, NY, pp. 299-339 **1962**

[89] J. M. Ottino and D. V. Khakhar Mixing and Segregation of Granular Materials *Annual Review of Fluid Mechanics* Vol. 32:55-91 (Volume publication date January **2000**

[90] Leblanc, J., Rhéologie des élastomères et leur mise en forme, ARTEL, Namur **1996**

[91] White, J. L.,Elastomer rheology and processing, *Rubber Chem. Technol.,* 42, pp. 257-338 **1969**

[92] Rumpf, H., Agglomeration, W. A. Knepper ed., New York, pp. 379-417 **1962**

[93] Bagster, D. F., Tomi, D., The stresses within a sphere in simple flow fields, *Chem. Engng Sci.,* 29, pp. 1773-1783 **1974**

[94] Horwatt, S. W., Manas-Zloczower, I., Feke, D. L.,The influence of structural heterogeneities on the cohesivity and break-up of agglomerates in simple shear flows, *Powder Technol.,* 72(1), pp. 113-119 **1992**

[95] Manas-Zloczower, I., Model and analysis of kinetics erosion in simple shear flows, *Rubber Division Meeting*, Savannah, Georgia, april 28th –may 1st , **2002**

[96] Rwei, S. P., Feke, D. L., Manas-Zloczower I., Observation of carbon black agglomerate dispersion in simple shear flows, *Polym. Engng Sci.,* 30, pp. 701-706 **1990**

[97] Bohin, F., Feke D. L. and Manas-Zloczower, I.,Penetration of silicone polymers into silica agglomerates and its influence on dispersion mechanism, *Rubber Chem. Technol.,* 67, pp. 602-609 **1994**

[98] Schubert, H. Principles of agglomeration, *Chemie Ingenieur Technik*, **1979** 51, 266–277

[99] Yamada, H., Manas-Zloczower, I. and Feke, D.L. The influence of matrix viscosity and interfacial properties on the dispersion kinetics of carbon black agglomerates, *Rubber Chemistry and Technology*, **1998** 71, 1–16

[100] Yamada, H., Manas-Zloczower, I. and Feke, D.L. Influence of matrix infiltration on the dispersion kinetics of carbon black agglomerates, Powder Technology, **1997** 92, 163–169

[101] Nguyen, T. Q., Liang, O. Z., Kausch, H. H.. Kinetics of ultrasonic and transient elongational flow degradation: a comparative study, *Polymer*, **1997**. 38, 3783–3793.

[102] Kuijpers, M. W. A., Iedema, P. D., Kemmere, M. F., Keurentjes, J. T. F. **2004**. The mechanism of cavitation-induced polymer scission; experimental and computational verification, *Polymer*, 45, 6461–6467

[103] Lu, K. L., Lago, R. M., Chen, Y. K., Green, M. L. H., Harris, P. J. F., Tsang, S. C. 1**996**. Mechanical damage of carbon nanotubes by ultrasound, *Carbon*, 34, 814–816.

[104] S. Cui, R. Canet, A. Derre, Characterization of multiwall carbon nanotubes and influence of surfactant in the nanocomposite processing, *Carbon* 41 **2003** 797

[105] R. Sen, B. Zhao, D. Perea, Preparation of single-walled carbon nanotube reinforced polystyrene and polyurethane nanofibers and membranes by electrospinning, *Nano Lett.* 4 **2004** 459

[106] Saeed, K., Park, S.Y., Lee, H. J., Baek, J. B., Huh,W. S. . Preparation of electrospun nanofibers of carbon nanotube/polycaprolactone nanocomposite, *Polymer*, **2006**, 47, 8019–8025.

[107] Näbe, M., Lin, T., Staiger,M. P., Dai, L. M.,Wang, X. G.. Electrospun single-walled carbon nanotube/polyvinyl alcohol composite nanofibers: structure–property relationships, *Nanotechnology*, **2008**, 19, 305702

[108] Y. Dror, W. Salalha, R.L. Khalfin, Y. Cohen, A.L. Yarin, E. Zussman, *Langmuir* **2003** 7012

[109] Chowdhury, S. R., Chen, Y., Wang, Y., Mitra, S.. Microwave-induced rapid nanocomposite synthesis using dispersed single-wall carbon nanotubes as the nuclei, *J. Mater. Sci*., **2009**, 44, 1245–1250.

[110] Yuan, J. M., Fan, Z. F., Chen, X. H. C., X. H., Wu, Z. J., He, L. P.. Preparation of polystyrene–multiwalled carbon nanotube composites with individual-dispersed nanotubes and strong interfacial adhesion, *Polymer*, **2009**, 50, 3285–3291

[111] Higginbotham, A. L., Moloney, P. G., Waid, M. C., Duque, J. G., Kittrell, C., Schmidt, H. K., Stephenson, J. J., Arepalli, S., Yowell, L. L., Tour, J. M.. Carbon nanotube composite curing through absorption of microwave radiation, *Compos. Sci. Technol.,* **2008**, 68, 3087–3092.

[112] Choi, H. J., Zhang, K., Lim, J. Y.. Multi-walled carbon nanotube/polystyrene composites prepared by in-situ bulk sonochemical polymerization, *J. Nanosci. Nanotechnol.,* **2007**, 7, 3400–3403.

[113] Liu, P., Facile graft polystyrene onto multi-walled carbon nanotubes via in situ thermoinduced radical polymerization, *J. Nanopart. Res.*, **2009**, 11, 1011–1016

[114] Blond, D., Barron, V., Ruether, M., Ryan, K. P., Nicolosi, V., Blau, W. J., Coleman, J. N. . Enhancement of modulus, strength, and toughness in poly(methyl methacrylate)-based composites by the incorporation of poly(methyl methacrylate)-functionalized nanotubes, *Adv. Funct. Mater*., **2006**, 16, 1608–1614

[115] Kwon, S. M., Kim, H. S., Myung, S. J., Jin, H. J. . Poly(methyl methacrylate)/multiwalled carbon nanotube microspheres fabricated via in-situ dispersion polymerization, *J. Polym. Sci. Polym. Phys.*, **2008** 46, 182–189

[116] Xia, H. S., Qiu, G. H., Wang, Q. . Polymer/carbon nanotube composite emulsion prepared through ultrasonically assisted in situ emulsion polymerization, *J. Appl. Polym. Sci.,* **2006**, 100, 3123–3130.

[117] Gojny, F. H.,Wichmann, M. H. G., Fiedler, B., Kinloch, I. A., Bauhofer,W.,Windle, A. H., Schulte, K.. Evaluation and identification of electrical and thermal conduction mechanisms in carbon nanotube/epoxy composites, *Polymer*, **2006**, 47, 2036–2045

[118] Pumera, M., Merkoci, A., Alegret, S. . Carbon nanotube–epoxy composites for electrochemical sensing, Sens. Actuators B, **2006** 113, 617–622.

[119] Gryshchuk, O., Karger-Kocsis, J., Thomann, R., Konya, Z., Kiricsi, I.. Multiwall carbon nanotube modified vinylester and vinylester-based hybrid resins, *Compos. Part A*, **2006** 37, 1252–1259.

[120] Grujicic, M., Sun, Y. P., Koudela, K. L.. The effect of covalent functionalization of carbon nanotube reinforcements on the atomic-level mechanical properties of poly-vinyl-ester-epoxy, *Appl. Surf. Sci.,* (**2007**) 253, 3009–3021

[121] Park,C.,Ounaies, Z.,Watson,K.A.,Crooks, R. E., Smith, J., Lowther, S.E.,Connell, J.W., Siochi, E. J., Harrison, J.S., Clair,T. L. S. .Dispersion of singlewall carbonnanotubes by in situ polymerization under sonication, *Chem. Phys. Lett.,* **2002**, 364, 303–308

[122] Zhu, B. K., Xie, S. H., Xu, Z. K., Xu, Y. Y.. Preparation and properties of the polyimide/multiwalled carbon nanotubes (MWNTs) nanocomposites, *Compos. Sci. Technol.,* **2006**, 66, 548–554.

[123] T. McNally, P. Pötschke Polymer-carbon nanotube composites Preparation, properties and applications Woohead Publishing **2011**

[124] T. McNally, P. Pötschke Polymer-carbon nanotube composites Preparation, properties and applications Woohead Publishing **2011** pp 107

[125] Kasaliwal, G., Göldel, A., Pötschke, P. and Heinrich, G. Influences of polymer matrix melt viscosity and molecular weight on MWNT agglomerate dispersion, (**2010b**) submitted.

[126] Kasaliwal, G., Göldel, A., Pötschke, P., Pegel, S. and Heinrich, G. Analysis of agglomerate dispersion mechanisms of multiwalled carbon nanotubes during melt mixing in polycarbonate, *Polymer*, (**2010a**) , 51, 2708–2720.

[127] Gaurav R. Kasaliwal Sven Pegel Andreas Göldel PetraPötschk Gert Heinrich, Analysis of agglomerate dispersion mechanisms of multiwalled carbon nanotubes during melt mixing in polycarbonate, *Polymer* 2010, Volume 51, Issue 12, 28, Pages 2708-2720

[128] Kasaliwal, G., Göldel, A. and Pötschke, P. (**2009**) Influence of processing conditions in smallscale melt mixing and compression molding on the resistivity and morphology of polycarbonate-MWNT composites, *Journal of Applied Polymer Science*, 112, 3494–3509

[129] Andrews R, Jacques D, Minot M, Rantell T. Fabrication of carbon multiwall nanotube/polymer composites by shear mixing. *Macromol. Mater. Eng.,* (**2002**);287(6):395–403

[130] Villmow, T., Potschke, P., Pegel, S., Haussler, L. & Kretzschmar, B. Influence of twin-screw extrusion conditions on the dispersion of multi-walled carbon nanotubes in a poly(lactic acid) matrix, *Polymer*, (**2008b**), 49, 3500–3509.

[131] McNally, P. Pötschke Polymer-carbon nanotube composites Preparation, properties and applications Woohead Publishing (**2011**) Polymer–carbon nanotube composites pp 272

[132] L. Moreira, R. Fulchiron, G. Seytre, P. Dubois, P. Cassagnau, Aggregation of Carbon Nanotubes in Semi-dilute Suspension, *Macromolecules*, 43(3), 1467-1472, **2010**

[133] Pegel, S., Pötschke, P., Petzold, G., Alig, I., Dudkin, S. M. & Lellinger, D. Dispersion, agglomeration, and network formation of multiwalled carbon nanotubes in polycarbonate melts, *Polymer*, **2008**, 49, 974–984

[134] B. Krause, R. Boldt and P. Pötschke, A method for determination of length distributions of multiwalled carbon nanotubes before and after melt processing, *Carbon* **2011**, 49, 1243–1247

[135] Pegel S, Pötschke P, Villmow T, Stoyan D & Heinrich G., Spatial statistics of carbon nanotube polymer composites, *Polymer* **2009** , 50, 2123–2132

[136] Lellinger, D., Skipa, T., Böhm, W. & Alig, I. Spatial decorrelation of the conductive nanotube network in

a polymer melt, *Physica Status Solidi B: Basic Solid State Physics,* **2009** , 246, 2667–2670

[137] Villmow, T., Pegel, S., Pötschke, P. & Wagenknech, U., Influence of injection molding parameters on the electrical resistivity of polycarbonate filled with multiwalled carbon nanotubes, *Composites Science and Technology,* **2008a**, 68, 777–789.

[138] G. H. Michler Electron Microscopy of Polymers Springer Laboratory Part II Preparation technique, 2008, pp 241-259

[139] Campbell, E. R.; Reisner, J. H.; Chung, K. T. Charging Phenomenon in Conductor-Insulator Composites as Displayed by the Scanning Electron Microscope, *J. Appl. Phys.* **1983**, 52, 1133-1134.

[140] K.T. Chung, J.H. Reisner and E.R. Campbell, Charging phenomena in the scanning electron microscopy of conductor-insulator composites: A tool for composite structural analysis, *J. Appl. Phys*., **1983**, vol. 54, p. 6099

[141] J. Loos, A. Alexeev, N. Grossiord, C.E. Koning and O. Regev, Visualization of single-wall carbon nanotube (SWNT) networks in conductive polystyrene nanocomposites by charge contrast imaging, Ultramicroscopy, **2005**, vol. 104, p. 160

[142] J.Z. Kovacs, K. Andresen, J.R. Pauls, C.P. Garcia, M. Schossig, K. Schulte and W. Bauhofer, Analyzing the quality of carbon nanotube dispersions in polymers using scanning electron microscopy, *Carbon*, **2007** vol. 45, p. 1279

[143] P.T. Lillehei, J.-W. Kim, L.J. Gibbons and C. Park, A quantitative assessment of carbon nanotube dispersion in polymer matrices, *Nanotechnology*, **2009**, vol. 20, p. 325708,

[144] W. Li, S.T. Buschhorn, K. Schulte and W. Bauhofer, The imaging mechanism, imaging depth, and parameters influencing the visibility of carbon nanotubes in a polymer matrix using an SEM, *Carbon* **2011**, vol. 49, p. 1955-1964,

[145] Li, W.; Bauhofer, W. Imaging of CNTs in a polymer matrix at low accelerating voltages using a SEM. *Carbon* **2011**, 49, 3891-3898.

[146] J. Cazaux, Scanning, Charging in scanning electron microscopy “from inside and outside”, **2004** vol. 26, p. 181,.

[147] Cazaux, J. The Electric Image Effects at Dielectric Surfaces. *Trans. Diel. Elec. Insul.* **1996**, 3, 75-79

[148] Polymer Nanotube Nanocomposites, Synthesis, Properties, and Applications 2nd Edition Edited by Vikas Mittal Wiley **2014** ISBN 978-1-118-94592-6 pp 405-424

[149] Meincke O., Kaempfer D., Weickmann H., Friedrich C., Vathauer M. and Warth H., Mechanical properties and electrical conductivity of carbon-nanotube filled polyamide-6 and its blends with acrylonitrile/butadiene/styrene, *Polymer*, **2004** , 45, 739–748.

[150] Pötschke P., Abdel-Goad M., Alig I., Dudkin S. and Lellinger D., ‘Rheological and dielectrical characterization of melt mixed polycarbonate-multiwalled carbon nanotube composites’, *Polymer* 24, **2004** , 8863–8870

[151] Kim J. Y. and Kim S. H. ‘Influence of multiwall carbon nanotube on physical properties of poly(ethylene 2,6-naphthalate) nanocomposites’, *J. Polym. Sci: B Polym. Phys.* **2006***,* 44, 1062–107

[152] Lin B., Sundararaj U and Pötschke P, ‘Melt mixing of polycarbonate with multiwalled carbon nanotubes in miniature mixers’, *Macromol. Mater. Eng.*, **2006** , 291, 227–238.

[153] Wu D., Wu L and Zhang M ‘Rheology of multi-walled carbon nanotube/ poly(butylene terephthalate) composites’, *J. Polym. Sci: B Polym. Phys*., **2007a** , 45, 2239–2251.

[154] Bose S., Bhattacharyya A R, Bondre A P, Kulkarni A R and Pötschke P ‘Rheology, electrical conductivity, and the phase behavior of cocontinuous PA6/ABS blends with MWNT: correlating the aspect ratio of MWNT with the percolation threshold’, *J. Polym. Sci: B Polym. Phys.*, **2008** , 46, 1619–1631.

[155] Valentino O, Sarno M, Rainone N G, Nobile M R, Ciambelli P, Neitzert H C and Simon G P ‘Influence of the polymer structure and nanotube concentration on the conductivity and rheological properties of polyethylene/CNT composites’, *Physica E* **2008***,* 40, 2440–2445.

[156] Mitchell C. A., Bahr J L, Arepalli S, Tour J M and Krishnamoorti R., 'Dispersion of functionalized carbon nanotubes in polystyrene', *Macromolecules*, **2002** 35, 8825–8830.

[157] Mitchell C. A. and Krishnamoorti R., 'Dispersion of single-walled carbon nanotubes in poly(ε caprolactone)', *Macromolecules*, **2007** 40, 1538–1545.

[158] M. Klüppel and G. Heinrich, Fractal structures in carbon black reinforced rubbers, *Rubber Chem. Technol.* 68, 623 **1995**

[159] R. Hjelm,W.Wampler, and P. Serger, in ACS Rubber Division Meeting, 21–24 May 1991 (American Chemical Society, **1991**).

[160] I. Alig, P. Pötschke, D. Lellinger, T. Skipa, S. Pegel, G. R. Kasaliwal, and T. Villmow, "Establishment, morphology and properties of carbon nanotube networks in polymer melts," *Polymer* 53, 4–28 **2012**.

[161] A. W. K. Ma, F. Chinesta, and M. R. Mackley, "The rheology and modeling of chemically treated carbon nanotubes suspensions," *J. Rheol.* **2009** 53, 547–573.

[162] Jouault N, Vallat P, Dalmas F, Said S, Jestin J, Boué F. Well-dispersed fractal aggregates as filler in polymer-silica nanocomposites: long-range effects in rheology. *Macromolecules* **2009**; 42:2031-40.

[163] Jouault N, Dalmas F, Boué F, Jestin J. Multiscale characterization of filler dispersion and origins of mechanical reinforcement in model nanocomposites. *Polymer*, **2012**; 53:761-5.

[164] Van Gurp M., and Palmen J., 'Time-temperature superposition for polymeric blends', *Rheol. Bull*., **1998** , 67, 5–8.

[165] Nobile M. R., Simon G. P., Valentino O. and Morcom M., 'Rheological and structure investigation of melt mixed multi-walled carbon nanotube/PE composites', *Macromol.Symp*., **2007** , 247, 78–87.

[166] Somma E, Valentino O., Iervolino R., Simon G. P., Hsiao B. S. and Nobile M. R., 'Temperature effect on the percolation network of multi-walled carbon nanotubes polymer nanocomposites', in Proceedings of the 5th Annual European Rheology Conference, Cardiff, United Kingdom **2009**

[167] Pötschke, P., Abdel-Goad, M., Alig, I., Dudkin, S., Lellinger, D., Rheological and dielectrical characterization of melt mixed polycarbonate–multiwalled carbon nanotube composites, *Polymer*, **2004**. 45, 8863–8870

[168] Iervolino R., Somma E., Nobile M. R. and Hsiao B. S., 'The combined effect of multiwalled carbon nanotubes and shear flow on the crystallization of isotactic poly(1-butene)', Proceedings of the 5th Annual European Rheology Conference, Cardiff,United Kingdom. **2009a**

[169] Pötschke P., Abdel-Goad M, Alig I, Dudkin S and Lellinger D., 'Rheological and dielectrical characterization of melt mixed polycarbonate-multiwalled carbon nanotube composites', *Polymer*, **2004**, 24, 8863–8870.

[170] Obrzut, J., Douglas, J. F., Kharchenko, S. B., Migler, K. B., Shear-induced conductor–insulator transition in melt-mixed polypropylene–carbon nanotube dispersions, *Phys. Rev. B*, **2007**, 76, 195420

[171] Alig, I., Skipa, T., Lellinger, D., Bierdel, M. & Meyer, H., Dynamic percolation of carbon nanotube agglomerates in a polymer matrix: comparison of different model approaches, *Physica Status Solidi B:Basic Solid State Physics*, **2008c**, 245, 2264–2267

[172] Skipa, T., Lellinger, D., Böhm, W., Saphiannikova, M. & Alig, I., Influence of shear deformation on carbon nanotube networks in polycarbonate melts: interplay between build-up and destruction of agglomerates, *Polymer*, **2010**, 51, 201–210.

[173] Skipa, T, Lellinger, D. Saphiannikova, M & Alig I. Shear-stimulated formation of carbon nanotube networks in polymer melts, *Physica Status Solidi B : Basic Solid State Physics*, **2009**, 246, 2453-2456

[174] I. Alig, T. Skipa, D. Lellinger, P. Pötschke Destruction and formation of a carbon nanotube network in polymer melts: Rheology and conductivity spectroscopy *Polymer* 49 **2008** 3524-3532

[175] Alig, I., Lellinger, D., Engel, M., Skipa, T. & Pötschke, P., Destruction and formation of a conductive carbon nanotube network in polymer melts: in-line experiments, *Polymer*, **2008a**, 49, 1902–1909

[176] Lellinger, D., Xu, D. H., Ohneiser, A., Skipa, T. & Alig, I., Influence of the injection moulding conditions on the in-line measured electrical conductivity of polymer-carbon nanotube composites, *Physica Status Solidi B: Basic Solid State Physics*, **2008** , 245, 2268–2271.

[177] Sadie I. White Brian A. DiDonna Minfang Mu Tom C. Lubensky Karen I. Winey Simulations and electrical conductivity of percolated networks of finite rods with various degrees of axial alignment Physical Review B, Volume 79, Issue 2, Article 024301, (January **2009**).

[178] Rahatekar SS. Shaffer MSP, Elliot JA, Mesoscale modeling of electrical percolation in fiber-filled systems. *J. Chem Phys* **2005**; 123, 134702/1-5

[179] Eunse Chang, Amir Ameli, Lun Howe Mark, and Chul B. Park, Effects of uniaxial and biaxial orientation on fiber percolation in conductive polymer composites AIP Conference Proceedings 1695, 020027 (2015)

[180] Du F, Fischer J, Winey K, Effect of nanotube alignment on percolation conductivity in carbon nanotube/polymer composites. *Phys Rev B.* **2005**; 72 121404/1-5

[181] Silva J, Ribeiro S. Lanceos-Mendez S. Simeos R. The influence of matrix mediated hopping conductivity, filler concentration, aspect ratio and orientation on the electrical response of carbon nanotube/polymer nanocomposites. *Compos Sci Technol* **2011**; 71; 643-6

Chapitre 2

Materials and methods

I. Materials

This thesis has been written in articles format, in all chapters the specific materials and methods used will be detailed. That is why; this chapter aims to present the most important information of the materials and methods used in the whole study.

A. Composites

1. Polymers

The polymer matrices used in this work are respectively a commercial amorphous polystyrene (PS) and a commercial High Impact Polystyrene (HIPS) both supplied by Total. They are characterized by a Melt Flow Index of 2.4 g/10 min and 2.8 g/10 min (200°C - 5kg). The glass transition of the pure polystyrene is around 100°C. The zero-shear viscosity of the matrices are respectively η_0 = 1.0x10^4 Pa.s and η_0 = 2.4x10^4 Pa.s at 200°C. The complex viscosities and the moduli are depicted in Figure 1.

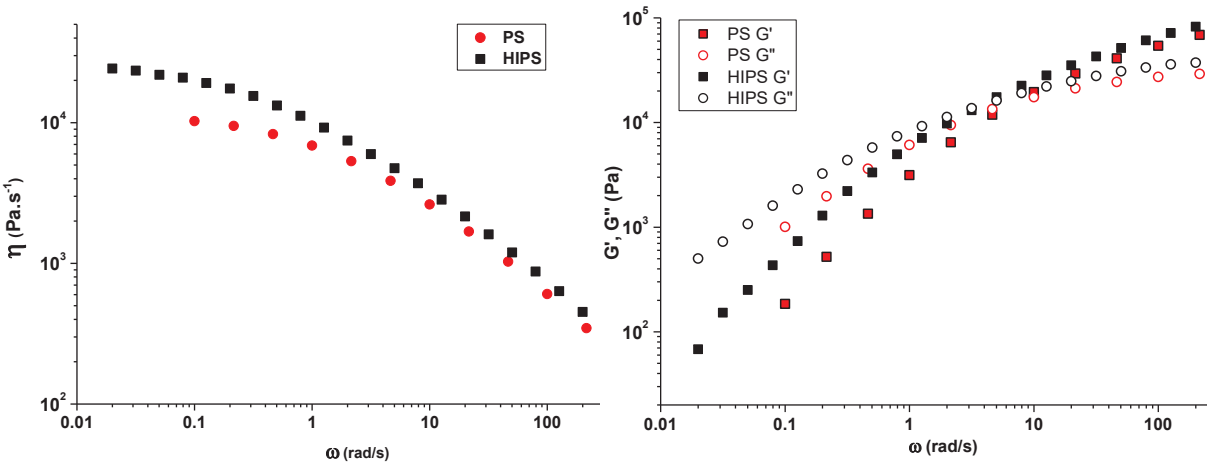

Figure 1: (Left) Complex viscosity (left) and storage and loss moduli (right) as a function of angular frequency (200°C) for pure PS and HIPS matrices.

2. Carbon Nanotubes

The Carbon Nanotubes NC7000 (CNTs) were supplied by Nanocyl™ a Belgian company. The CNTs are more precisely MWCNTs characterized by a diameter *d* around 10 nm. The length dispersion has been determined after the blending of CNT and PS. Indeed, during the incorporation in the molten polymer the CNTs can be broken due to the large shear applied during the extrusion. The length measurement has been achieved after dissolving the matrix in an adequate solvent. The mixture is then put on a grid to be observed through Transmission Electron Microscopy. The length distribution is presented in Figure 2. The aspect ratio υ that is defined as the length *L* over the diameter *d* has been estimated to 140 (considering the average length *L*(0.5) equal to 1.4µm).

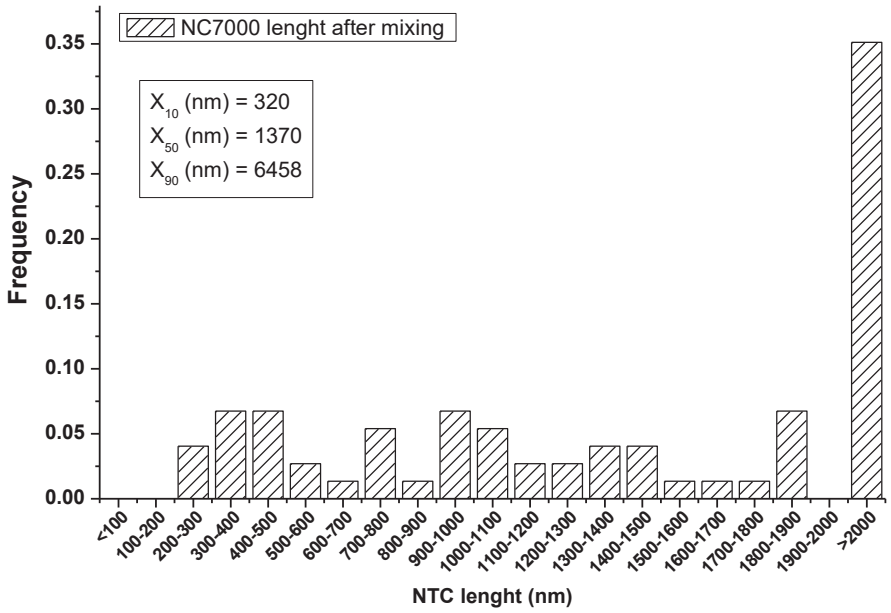

Figure 2: Length distribution of processed NC7000 dissolved from the PS matrix

B. Elaboration process

1. Masterbatch dilution

The elaboration process is the melt mixing. The composites are obtained from a highly filled composite (called masterbatch) that is diluted in an extruder by the addition of pure matrix. The masterbatch dilution follows the protocol presented in patent WO2015014897 [1]. For the HIPS filled with CNTs composite, we start from a masterbatch made with pure PS filled with CNT. The dilution is achieved by the addition of pure HIPS matrix.

2. Sample preparation

All the specimens used in this work were compression molded in order to control the filler network structure. The goal is to minimize as much as possible the orientation of the CNTs and enhance the connections between CNTs for the formation of a well percolated network. The compression molded protocol is made of three steps. First the specimen is compression molded using a hydraulic press at 210°C. The force is controlled in order to apply on the sample a pressure of 20 bars for 10 minutes followed by a pressure ramp 18 bar/min. The specimen is held for around 5 min under 200 bars. Then, the specimen is cooled down at room temperature.

II. Composites characterization

A. Microscopy

1. Transmission Electron Microscopy

The filler dispersion was investigated by Transmission Electron Microscopy. Figure 3 and Figure 4 show TEM micrographs of CNTs dispersed within the polymer matrix. The micrographs were carried out on 500 nm thick film of PS filled with 0.79 vol% CNT. The accelerating voltage was fixed to 300 kV. The voltage was high due to the large thickness of the specimen.

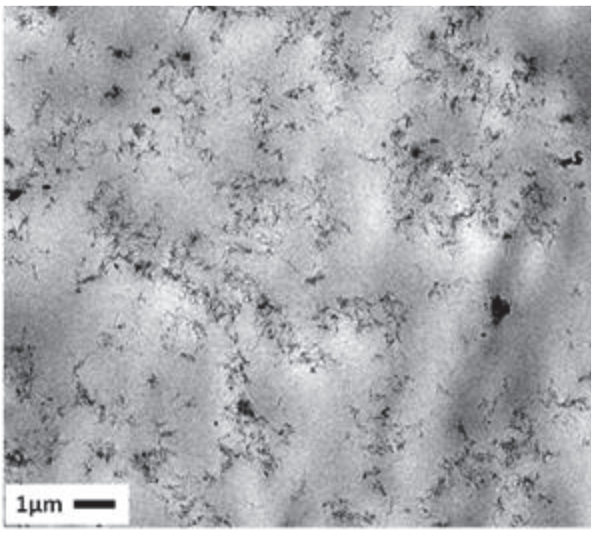

Figure 3: TEM micrograph of PS filled with 0.79 vol% CNT

Figure 3 shows the filler network made of aggregates. In addition, the connections between the aggregates are displayed in Figure 4.

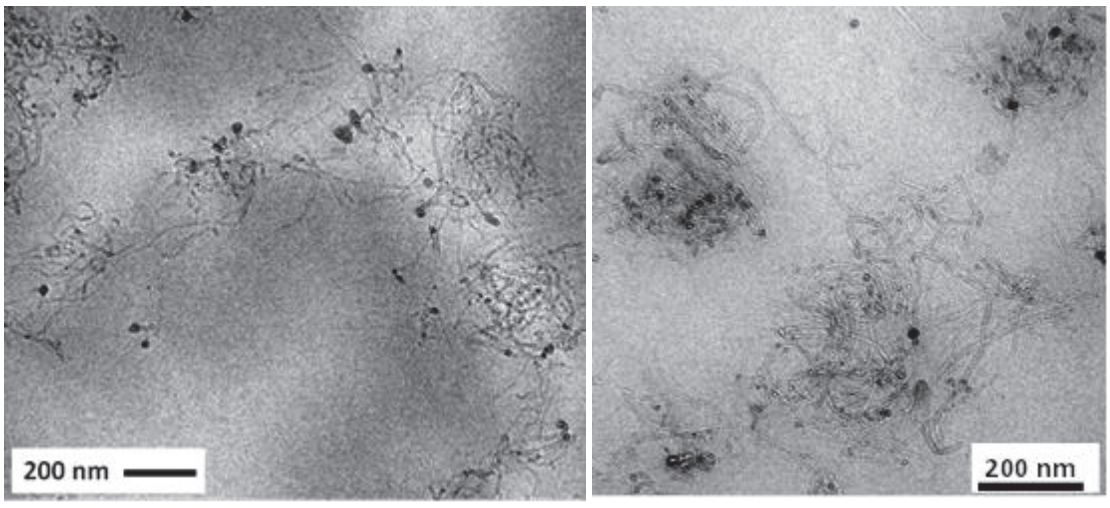

Figure 4: TEM micrograph of PS filled with 0.79vol% CNT, details of the connections between agglomerates and single CNTs

2. Scanning Electron Microscopy

In addition to TEM micrographs, Scanning Electron Microscopy has been carried out on composites in order to characterize the filler dispersion at a larger resolution. The device used is a LSM800 supplied by Zeiss. Figure 5 illustrates the location of the in-Lens detector inside the beam focusing lens. The working distance *WD* which is the distance between the surface sample and the final condenser lens is around 5 mm. The distance must be as small as possible in order to optimize the signal reception (electron emitted from the specimen surface). The aperture size was fixed at 30 µm. As the in-Lens detector is very sensitive to surface roughness, the sample surface has been cut with diamond knife to remove any roughness and promote the contrast between electrically conductor filler and insulating matrix [2-4]. For HIPS composites, the specimen surface must be first functionalized in OsO_4 solution in order to strengthen the PB nodules and enhance the surface cutting.

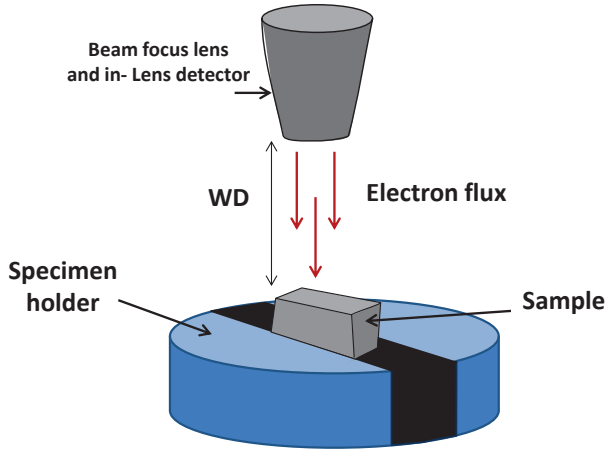

Figure 5: details of the SEM observation carried out on smooth specimen surface

The accelerating voltage is chosen between 15 and 20 kV. The accelerating voltage (and the WD) must be adjusted and directly depends on the specimen conductivity. In Figure 6 are displayed three SEM micrographs of PS 0.4 vol% CNT. The WD is fixed to 6 mm and the accelerating voltage varies from 5 kV to 20 kV. The observation at low voltage (5 kV) is not possible. There are distortions induced by the staking of charges on the specimen surface that blur the observation. With the increase of the accelerating voltage, the distortion disappears and is replaced by isolated clouds. At large voltage 20 kV, the specimen observation is possible with a clear distinction between the CNTs and the matrix. For each specimen, the voltage and the WD must be adjusted in order to properly observe the filler dispersion.

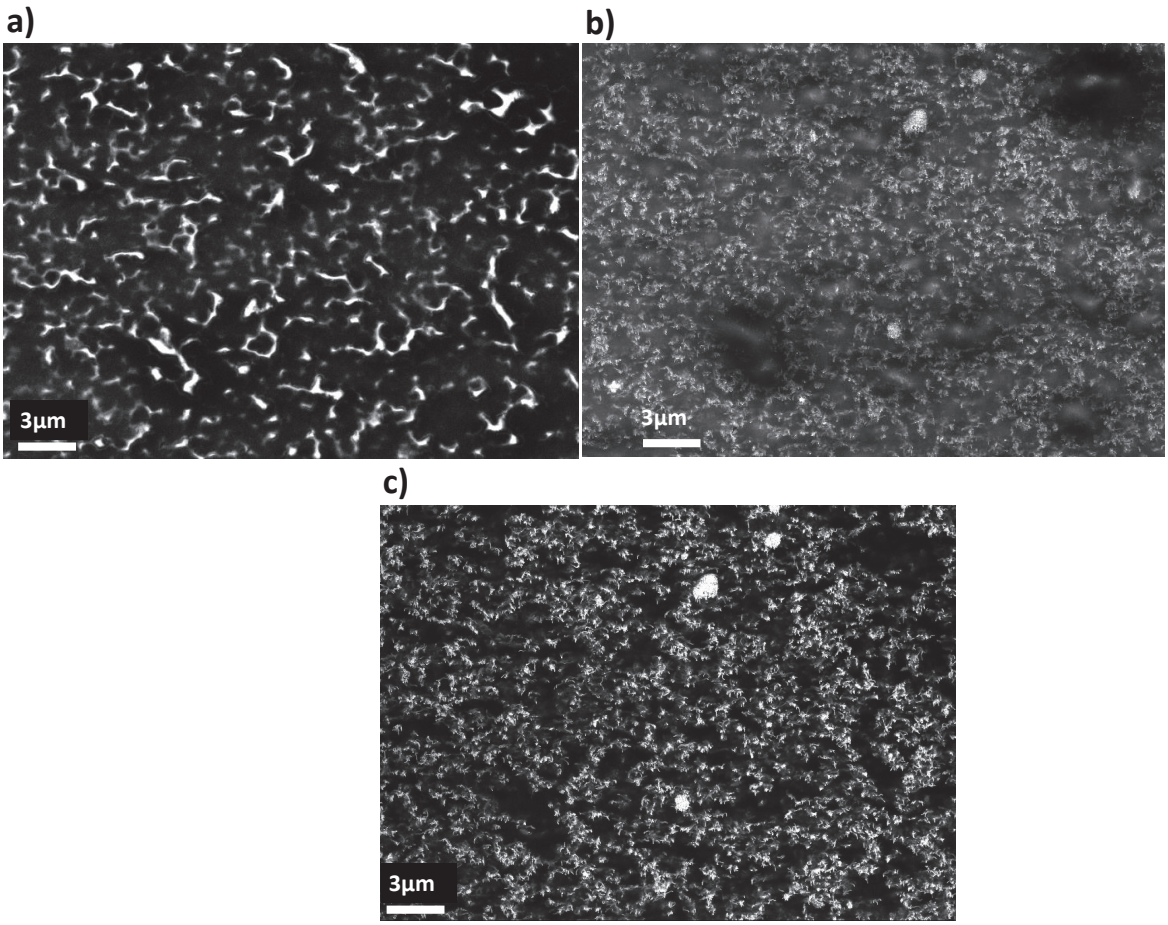

Figure 6: SEM observation with inLens detector, WD fixed at 5.8mm, magnification x2000 of PS filled with 0.4 vol% CNT (compression molded). The accelerating voltage is fixed at 5kV a), 10kV b) and 20 kV c).

B. Conductivity characterization

Electrical conductivity analysis has been conducted on compression molded samples with a post annealing at 200 °C for around 20 min. This annealing ensures a thermodynamic equilibrium state with a well-developed filler network. The surface and the volume conductivities of composites have been measured.

1. Surface conductivity

First, colloidal silver paste is applied on the surface sample to obtain a good electrical contact between the electrodes. Figure 5 depicts the surface conductivity measurement. The colloidal silver paste is applied with a stencil. The surface resistivity is measured owing to an Ohmmeter.

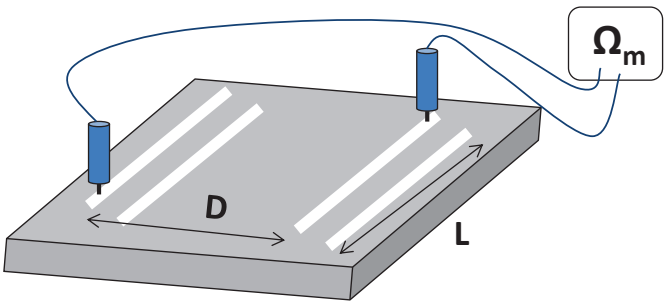

Figure 7: Surface conductivity meausrement of composite

Knowing the characteristic lengths L and D and the measured electrical resistance R_m the surface resistivity can be deduced as:

$$\rho_S = \frac{R_m L}{D}$$

Equation 1

The surface conductivity σ_S is defined as

$$\sigma_S = \frac{1}{\rho_S}$$

Equation 2

2. *Volume conductivity*

For the volume conductivity measurement, owing to a Keithley 237 power supply a Direct Current (DC) of 10 volts is applied on the opposite surfaces of the specimen and the current passing through the material is measured.

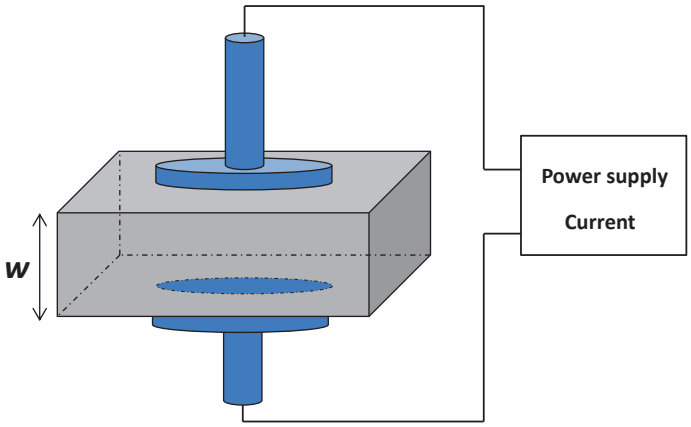

Figure 8: Volume conductivity measurments of the composite

The conductivity can be determined as:

$$\sigma = \frac{w.I}{S.U}$$

Equation 3

with U the applied voltage, I the measured current, w the specimen thickness and S the surface of the electrodes.

C. Rheological characterization

1. Dynamic rheology

Rheological experiments in dynamic frequency sweep mode with parallel plates geometry (diameter 25 mm, gap of approximately 1 mm) were conducted using an ARES rheometer (TA instruments) and an ARES G2 (TA instruments). The strain was chosen in the linear domain for the whole range of frequencies and was fixed to 1%. The filler network characterization has been carried out at 200°C. Before launching the experiment, the specimens are maintained 20 min at 200 °C. This sample conditioning allows to control the filler dispersion and to characterize a well aggregated network. In Figure 7 is displayed the storage modulus variation for the PS a) and the HIPS b) matrices filled with CNTs. The concentration is the CNT concentration in the PS phase. A plateau emerges at low frequencies illustrating the presence of the percolated network of CNTs.

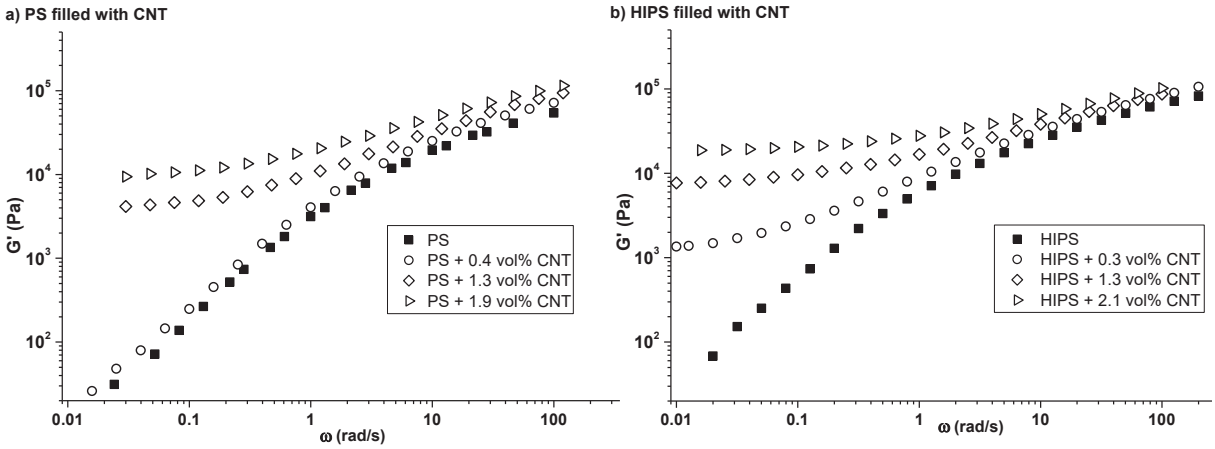

Figure 9: Storage modulus as a function of angluar frequency for a) pure and filled with CNT PS matrix and b) pure and filled HIPS matrix. The filler concentration is the concentration of CNT in the PS phase.

2. Extensional viscosity fixture

Extensional experiments were carried out with a commercialized Extensional Viscosity Fixture (TA instruments) mounted on the ARES rheometer. This set-up is based on the Meissner concept [5]. It is made of two drums: a fixed one connected to the torque sensor making possible the measurement of the extensional force, and a rotating one moving on a circular orbit centered on the fixed drum. The edges of the specimen are clamped on each drum. The extensional rate $\dot{\varepsilon}$ is defined as:

$$\dot{\varepsilon} = \frac{\dot{\theta}(t)R}{L_0}$$

Equation 4

$\dot{\theta}$ is the angular rotation speed, R is the drum radius and L_0 is the distance between the two drums. The extensional stress and the extensional viscosity are respectively defined by:

$$\sigma_E(t) = \frac{F_E(t)}{S(t)}$$

Equation 5

$$\eta_E = \frac{\sigma_E(t)}{\dot{\varepsilon}}$$

Equation 6

where F_E is the force required to stretch the sample, obtained from the torque measured by the rheometer C_E ($F_E = CE/(2.R)$) and S is the instantaneous cross-section of the sample. The drums are first heated at the working temperature and then a sample having 25x10x0.5 mm^3 is placed and clamped onto the drums. The sample is maintained around 100 s in order to ensure the stabilization of the temperature in the chamber and the sample relaxation. Figure 10 illustrates the extensional viscosity of pure PS and of the PS filled with 0.79 vol% of CNT specimens at 160 °C and an extensional rate fixed to 0.01 s^{-1}. The linear viscoelastic behavior (LVE) calculated from the relaxation spectrum obtained with the frequency sweep measurements is also displayed.

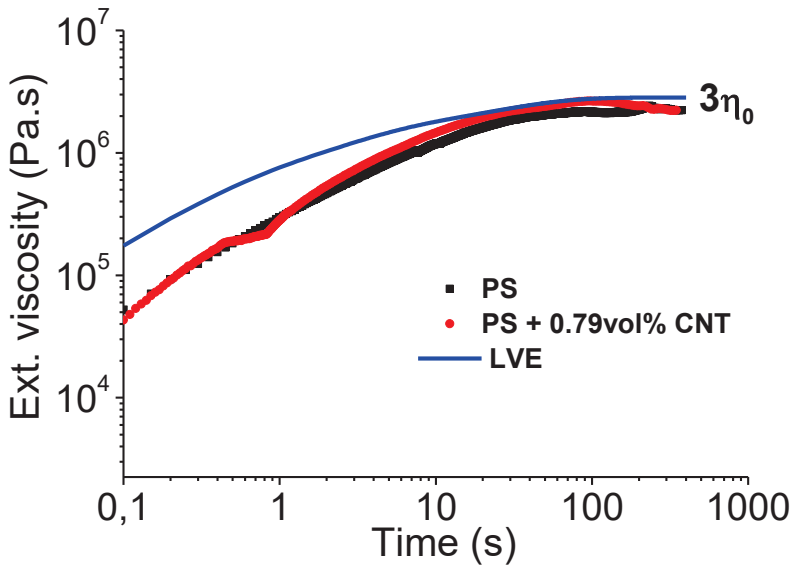

Figure 10: Extensional viscosity of pure PS and filled PS with 0.79vol% CNT at 160°C and extensional rate fixed to 0.01s^{-1}

D. Extensional rheology combined with conductivity measurement

1. Presentation of the home made set-up

Home-made modifications have been done to allow us to monitor the specimen conductivity during the extensional test. First, the two metallic drums (see Figure 11) have been electrically isolated with a Kapton film (adhesive tape with a high fusion temperature). The Kapton layer avoids any short-circuit. Then, copper thin film of 10 mm width has been rolled around each drums (see Copper electrode in Figure 11). The electric cables are welded on it. The weld is lead-free solder[1] with a T_f around 230 °C. The two drums are electrically powered through electric cables connected to a Keithley 237 power supply delivering a DC of 10 V and measuring the current passing through the specimen (see Figure 11 and Figure 12).

[1] Copper 0.7%, Tin 99.3%

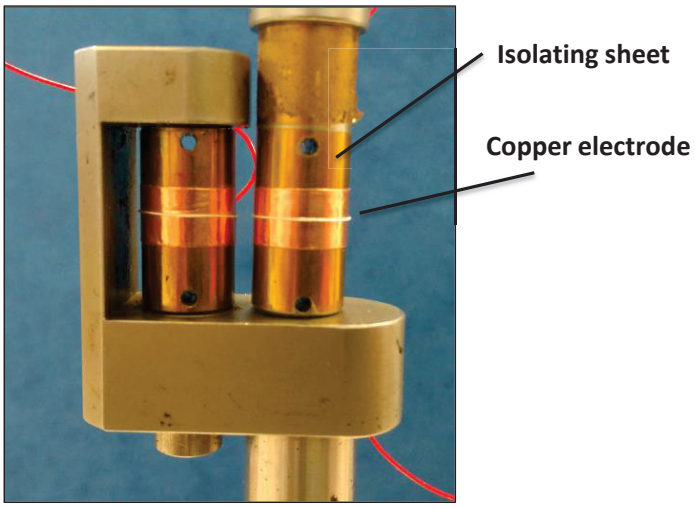

Figure 11: EVF with the electrical set-up that ensures the conductivity measurement of the specimen

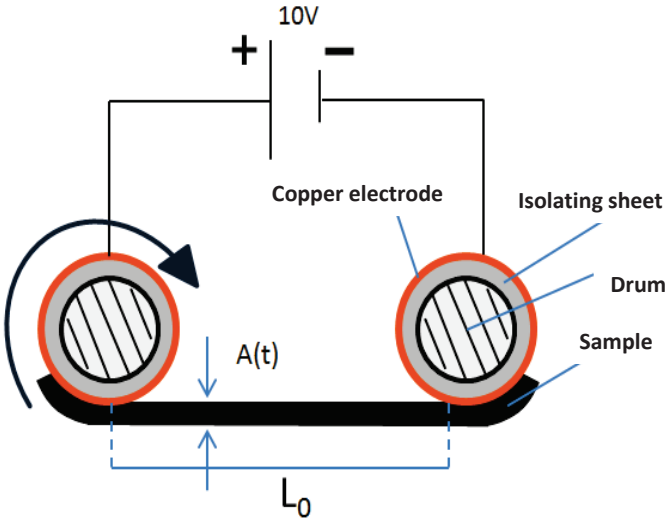

Figure 12: Cross section view of the experimental set-up

The specimen is clamped on the heated drums so that the specimen melts on them. Molten sample closely fits to the barrels and ensure a good and homogeneous contact between the specimen surface and the electrodes (see Figure 12). *A(t)* represents the sample thickness as a function of time *t*. The electrical potential difference is taken at the distance noted L_0 between the two drums which remain unchanged as the sample is rolled up on the electrode.

2. Specimen conductivity under extensional deformation

The time-dependent conductivity can be determined from the measured current and the specimen geometry as:

$$\sigma(t) = \frac{1}{\rho(t)} = \frac{L_0.I(t)}{U.S(t)}$$

Equation 7

with L_0. is the sample length between the two drums, $I(t)$ is the current passing through the specimen, U is the applied DC voltage and $S(t)$ is the effective cross-section of the specimen. Between the two drums, we assume a uniform deformation of the specimen. This area can be expressed as a function of time and the initial section of the specimen S_0 as:

$$S(t) = S_0 e^{-\varepsilon_H} = S_0 e^{-\dot{\varepsilon}t}$$

Equation 8

By combining Equation 7 and Equation 8, the conductivity, as a function of time can be deduced.

$$\sigma(t) = \frac{L_0.I(t)}{U.S_0 e^{-\dot{\varepsilon}t}}$$

Equation 9

The extensional rates are taken between 0.005 s^{-1} and 0.4 s^{-1}. The extensional rates are limited to 0.4 due to the electrical acquisition. This could be improved by changing the acquisition set-up. In Figure 13 is displayed the conductivity variation of a specimen (PS filled with 0.79 vol% of CNT). At *t* = 0 the pre-heated specimen is clamped onto the two drums. The specimen is first quiescent annealed during 140s in order to stabilize the chamber temperature. Then, the extensional test starts at *t* = 140 s.

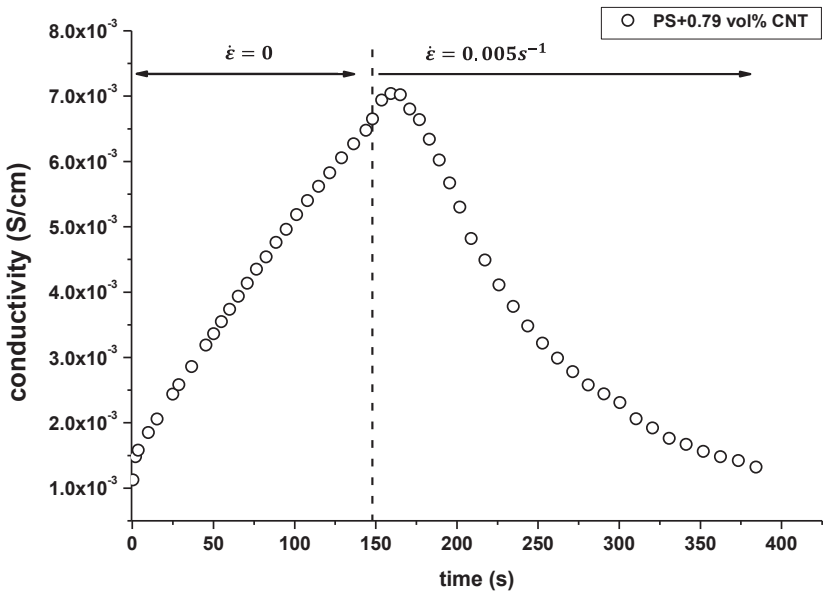

Figure 13 : Detail of the protocol followed for each extensional test. The Polystyrene filled with 0.79 vol% of CNT specimen is first quiescent annealed during 140 s and then deformed at a fixed extensional rate. The experience is carried out at 200°C.

References

[1] ROUSSEAUX, D., O. Lhost, P. Lodefier and E.Scandino, “Masterbatches for preparing a composite materials with enhanced conductivity properties, process and composite materials produced,” (2015); Available from: google.com/patents/WO2015014897A1?cl=en_2

[2] Li, W., S.T.Buschhorn., K. Schulte and W. Bauhofer, “The imaging mechanism, imaging depth, and parameters influencing the visibility of carbon nanotubes in a polymer matrix using an SEM,” J. Carbon, 49(6) (2011)

[3 Li, W.and W.Bauhofer, “Imaging of CNTs in a polymer matrix at low accelerating voltages using a SEM,” Carbon, 49(12), 3891-3898 (2011)

[4] Li, W., Y.Zhou, H.-J. Fitting and W. Bauhofer, “Imaging mechanism of carbon nanotubes on insulating and conductive substrates using a scanning electron microscope,” J. Mat. Sci.,46 (2011)

[5] Meissner J.and J.Hostettler, “A new elongational rheometer for polymer melts and other highly viscoelastic liquids,” Rheol Acta, 33(1), 1-21 (1994).

Part II

Chapter 3

Conductive polymer composites under extensional deformation

Abstract

In the last decades, nanocomposites made of polymer matrix filled with CNT have been a great topic of studies, particularly as concerns the rheological behavior and the electrical property under shear. In contrast, this work focuses on the deformation of the CNT network in elongated polymer melts by a combination of conductivity monitoring and extensional rheological measurement. For this specific purpose, an Extensional Viscosity Fixture accessory of a rotational rheometer ARES has been modified to allow the sample conductivity measurement. This new set-up gives access to the measurement of the electrical conductivity simultaneously with the extensional stress under extensional deformation. First results have shown that the conductivity of CNT/polystyrene nanocomposites can present a sharp decrease before the sample break and this decrease appears more rapidly for higher extensional rates and lower temperatures. The results have been correlated to experimental conditions via the introduction of the Weissenberg number.

Keywords: Nanocomposites; Extensional Viscoelasticity; Electrical conductivity.

Reformatted version of paper originally published in:

Journal of Rheology, 2017, Volume 61 N°5 pp 845-857

An Original Combined Method for Electrical Conductivity Measurement of Polymer Composites under Extensional Deformation.

Marjorie Marcourt, Philippe Cassagnau, René Fulchiron[a)],

Univ Lyon, Université Claude Bernard Lyon 1, CNRS UMR 5223, Ingénierie des Matériaux Polymères, F-69622, Villeurbanne Cedex, France

Dimitri Rousseaux, Olivier Lhost, Simon Karam

Total Research and Technology Feluy Zone Industrielle Feluy C 7181 Feluy, Belgium

I. Introduction

The addition of Carbon Nanotubes (CNT) to a polymer matrix has paved the way of ultra-low filled nanocomposites characterized by both electrical and mechanical specific properties generally due to the percolation network formed by the fillers [1-3]. From the abundant literature on the topic, some general trends can be recalled. Theoretically, the large aspect ratio (*L/d*) leads to nanocomposites with an insulator/conductor transition for an ultra-low filler amount. However, this achievement of nanocomposites with tailored conductivity properties remains a challenge. As CNT are fillers with dimension in the range of polymer chains size, the interactions are predominant. Therefore, the mixing and the dispersion processes of CNT in the polymer matrix are crucial issues in elaborating the nanocomposites and thus, in controlling its properties [4-7]. Moreover, after its elaboration, the material may be subjected to very large deformation during the forming process (thermoforming, injection molding, melt blowing…) leading to drastic modification or even destruction of the network. In this regard, the present study is devoted to the analysis of the electrical behavior of nanocomposites submitted to extensional forces.

Electrical properties are governed by the filler dispersion state and the filler-filler connections. Indeed, when fillers are too well dispersed, the material will present a poor electrical conductivity as these fillers do not constitute an electron pathway. A good, electron conductor network is made of homogeneous dispersion of interconnected CNT aggregates [8-11]. However, well above T_g the flow can drastically modify the whole filler structure through aggregation and disaggregation mechanisms and, consequently alter the electrical properties of the final parts [8, 12, 13]. In order to understand those phenomena, a great deal of studies have been carried out on nanocomposites with highly viscous polymer matrix like Skipa *et al*. [14] and Pegel *et al*. [11] (PMMA/ CNT), Abbasi *et al.* [15]

(PC/MWCNT) and Kota *et al*. [16] (PS/MWCNT). Other studies are reported on low viscous thermoplastic or uncured thermoset resin filled with CNT [8, 17, 18]. Using a rheometer set-up with DC conductivity monitoring, they have shed light on noticeable conductivity variations revealing the filler network evolution. For well dispersed and distributed fillers (electrically insulating material), a quiescent annealing at temperature above T_g will lead to a significant conductivity increase. Through diffusion and filler-filler interactions, the formation of the percolated network will be triggered. Under external forces the conductivity variation are more complex. The majority of reported studies carried out on highly viscous systems have highlighted a conductivity decrease under both high and low shear stresses. Under shear stresses, the fillers connections break and the aggregates are subjected to some erosion. However, Hilarius *et al*. [6] have dealt a consistent work in this field. They have shown that, under a low steady shear of $0.02s^{-1}$, the conductivity of the material can decrease until it reaches an equilibrium state and can even increase. Those phenomena have been attributed to the superposition of buildup and destruction of connections. They have also experienced conductivity increase under low shear rate. However, the last case is highly dependent on the initial dispersion state and shear rate applied.

Few works have tackle nanocomposites under extensional deformation. One can cite, the work of Grillard *et al*. [19] on the melt-spinning of Polyamide 12 fibers filled with CNT and more recently the work of Johannsen *et al.* [20] on poly(hydroxyether of bisphenol A) fibers filled with MWCNT. They both observed severe conductivity decrease when the material is submitted to large deformation and large strain rates. The large deformations are transmitted to the aggregates scale; they are separated and stretched [21]. The filler network is broken as a result the material becomes electrically isolative. That is why the use of such materials at industrial scale remains a thorny challenge. Indeed, most of industrial processes imply large deformations at very high rate. For instance, during thermoforming when the plug comes into contact with the sheet it induces large biaxial deformation at a constant strain rate.

This work aims at bringing some additional results to the abundant literature on thermoplastic filled with CNT and more specific is focused on the behavior of such nanocomposites under extensional deformation. To go further in the comprehension of network deformation/destruction under extensional flow, a commercialized Extensional Viscosity Fixture (EVF) system has been modified to monitor the electrical properties of nanocomposites with the extensional viscosity during the melt deformation. As the polymer matrix is electrically insulating, the measured current is characteristic of the CNT network giving the opportunity to follow the network evolution under extensional forces.

II. Materials and methods

A. Matrix and fillers

Multi Wall Carbon Nanotubes Nanocyl^{TM} NC7000 supplied by Nanocyl S.A Belgium have been used in this work. They are characterized by a diameter (*d)* of 10 nm and a length distribution (*L)* mainly between 300 nm and 2 µm. The matrix is a pure Polystyrene Crystal 1160 (PS) supplied by Total Petrochemicals. Masterbatches of PS filled with 15 wt% MWCNTs were melt–mixed and diluted with the pure PS to reach the desired concentration [22].

B. Characterization

1. Scanning Electron Microscopy

The filler dispersion has been investigated by Scanning Electron Microscopy (SEM) using a device LSM800 from Zeiss. The detection was ensured owing to in-Lens detector which is located inside the beam focusing lens. The observations have been carried out with a distance between the surface sample and the final condenser lens (the working distance WD) of around 5 mm, an aperture size fixed at 30 µm and the accelerating voltage ranging from 15 kV to 20 kV. As the in-Lens detector is very sensitive to surface roughness, the sample surface has been cut with diamond knife to remove any roughness and promote the contrast between electrically conductor filler and insulating matrix. This observation technique will be not detailed in the paper; however the reader can refer to studies on this method [23-25].

2. Electrical characterization

Electrical properties analysis has been conducted on compression molded samples with a post annealing at 200°C for 20 min. This ensures a thermodynamically equilibrium state with a well – developed filler network. Colloidal silver paste is applied on the surface sample to obtain a good electrical contact between the electrodes and the materials. Owing to a Keithley 237 power supply a 10 volt DC is delivered and the current passing through the sample is measured.

3. Rheology

a. Dynamic rheology

Rheological experiments in dynamic frequency sweep mode with parallel plates geometry (25mm) were performed using an ARES rheometer (TA instruments) at various temperatures between 200°C and 240°C under nitrogen atmosphere. The strain was chosen in the linear viscoelastic domain, was fixed to 1%. The master curves were established at a reference temperature of 200°C (see Figure 1). The master curve obtained for the sole PS was fitted with a classical Maxwell *N* modes model [26] as:

$$G'(\omega) = \sum_{i=1}^{N} \frac{G_i \omega^2 \lambda_i^2}{1 + \omega^2 \lambda_i^2}$$

Equation 1

$$G''(\omega) = \sum_{i=1}^{N} \frac{G_i \omega \lambda}{1 + \omega^2 \lambda_i^2}$$

Equation 2

where G_i is the modulus contribution corresponding to the relaxation time λ_i. The λ_i parameters were fixed over the range of time constants corresponding to the reverse of the experimental frequency range. The G_i were obtained by means of an iterative method minimizing the following criterion [26]:

$$\sum_{j=1}^{M} \left(\frac{G'(\omega_j)}{G'_j} - 1 \right)^2 + \left(\frac{G''(\omega_j)}{G''_j} - 1 \right)^2$$

Equation 3

where *M* is the number of G'_j and G''_j experimental values. The number of modes was fixed to 5 as the best compromise between satisfying fit of the experimental curves and physically proper values of the G_i (maximum modes before negative modulus contribution).

Furthermore, the composites behavior exhibits a plateau on the *G'* curve in the low frequency domain as currently observed [8, 12, 15, 16, 18]. This is due to the percolated network of CNT. The behavior was described on the basis of the Maxwell-Wiechert model which is the Maxwell model plus a parallel purely elastic strand. This model is currently used for soft materials presenting a solid-like, weakly elastic behavior at low frequencies [27-29], just like the nanocomposite considered in the present work. Moreover, it must be mentioned that, for describing the behavior, the previously obtained relaxation spectrum of the pure PS matrix was not changed and the supplementary elastic

modulus G_e was simply inserted in the G' equation leading to:

$$G'(\omega) = G_e + \sum_{i=1}^{N} \frac{G_i \omega^2 \lambda_i^2}{1 + \omega^2 \lambda_i^2}$$

Equation 4

It should be noticed that the expression of $G''(\omega)$ remains unchanged (Eq. 2).

The good agreement between the model and the experimental data is shown in the inset of Figure 1. Thus, it can be considered that the molecular mobility of the PS is practically unaffected by the CNT network.

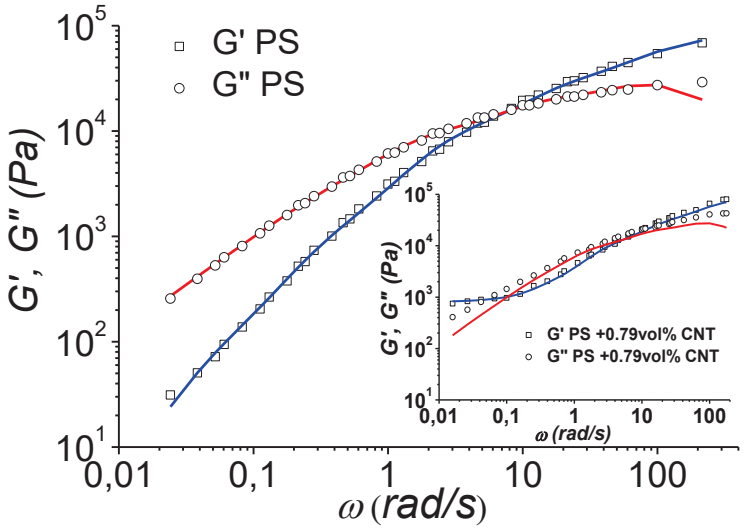

Figure 1 : Master curve for PS at a reference temperature of 200°C. Experimental data G'(□) and G" (○) and discrete Maxwell model (solid line). In inset: master curve of the PS filled with 0.79 vol% of CNT (reference temperature 200°C) fitted with the same relaxation times contributions G_i plus a constant value G_e in the expression of G'.

Moreover, concerning the relaxation spectrum of the PS matrix, since the λ_i values were arbitrarily chosen, it would be meaningless to consider a relaxation mechanism associated to each of these values. That is why, it is more appropriate to handle meaningful values as the number or weight average relaxation times, (respectively, λ_n and λ_w) [30] that are deduced from the λ_i and G_i parameters by Equation 5 and Equation 6.

$$\lambda_n = \frac{\sum_{i=1}^{n} G_i \lambda_i}{\sum_{i=1}^{n} G_i} = \frac{\eta_0}{G_N^0}$$

Equation 5

$$\lambda_w = \frac{\sum_{i=1}^{n} G_i \lambda_i^2}{\sum_{i=1}^{n} G_i \lambda_i} = \eta_0 J_e^0$$

Equation 6

The zero shear-viscosity η_0 at 200°C is 1x10^4 Pa.s, the compliance J_e^0 is 4x10^{-4} Pa^{-1} and the modulus G_N^0 is 8x10^4 Pa. In the literature it can be found a modulus G_N^0 equal to 2x10^5 Pa [31]. However, it can be pointed out that the plateau is not reached in the storage modulus curve of Figure 1 (it should be at higher frequencies). This is generally the case for the melt polymer with broad molecular weight distribution like the presently used commercial polystyrene. Indeed, the narrower is the molar mass distribution; the sharper is the transition between the flow zone and the rubbery plateau [31]. Thus, the obtained fitted value of G_N^0 is underestimated. Nevertheless, this is without any consequence for the following.

From the building of the master curve the shift factors a_T were determined and it was verified that they fulfill the WLF (Williams-Landel-Ferry) equation [30, 32]:

$$\log(a_T) = \frac{-C_1^{T_{ref}}(T - T_{ref})}{C_2^{T_{ref}} + (T - T_{ref})}$$

Equation 7

For pure PS, the WLF coefficients C_1^{200} and C_2^{200} are respectively 3.5 and 110°C for a reference temperature T_{ref} fixed to 200°C.

From the relaxation time of the reference temperature, one can deduce the relaxation times at other temperatures (see Equation 8) [26]. The values are displayed in Table I and will be used in section III part b).

$$\lambda_{n-w}(T_0) = \frac{\lambda_{n-w}(T_1)}{a_{T_1}}$$

Equation 8

Table I: Rheological parameters of pure Polystyrene obtained with a T_{ref} fixed to 200°C

T°C	λ_n (s)	λ_w (s)	a_T
200	1.42x10^{-1}	4.19	1
180	8.74 x10^{-1}	26.2	6.24
170	3.11	93.2	22.2
160	16.2	4.83 x10^2	1.15 x10^2

The ratio between the weight and number average relaxation time is characteristic of broadness of the relaxation time spectrum and the obtained value ˜30 is common for a commercial polymer of a relatively wide molecular weight distribution. For the following, the weight average relaxation time (λ_w) will be used because it is recognized as more reflecting the polymer behavior than the number average relaxation time. As a matter of fact, it contains the effect of both the average molar mass and the molar mass distribution [33,34]. Besides, it is more linked to the behavior in the terminal zone and, in that sense, is closer to the longest relaxation time of the polymer. Thus, in the following, only the weight average relaxation time will be considered. It must be added that the obtained shift factors are in agreement with values found in the literature [26]

b. Extensional viscosity

Extensional experiments were carried out with a commercialized EVF (TA instruments) mounted on the ARES rheometer. This set-up is based on the Meissner concept [35]. It is composed of two drums: a fixed one connected to the torque sensor making possible the measurement of the extensional force, and a rotating one moving on a circular orbit centered on the fixed drum. The edges of the specimen are clamped on each drum. Using such a system, the extensional rate $\dot{\varepsilon}$ is defined as:

$$\dot{\varepsilon} = \frac{\dot{\theta}(t)R}{L_0}$$

Equation 9

$\dot{\theta}$ is the angular rotation speed, R is the drum radius and L_0 is the distance between the two drums. The extensional stress and the extensional viscosity are respectively defined by:

$$\sigma_E(t) = \frac{F_E(t)}{S(t)}$$

Equation 10

$$\eta_E(t) = \frac{\sigma_E(t)}{\dot{\varepsilon}}$$

Equation 11

where F_E is force required to stretch the sample, obtained from the torque measured by the rheometer C_E ($F_E = C_E/(2.R)$) and S is the instantaneous cross-section of the sample. The drums are first heated at the working temperature, and then a sample having dimension of 25x10x0.5 mm^3 is placed and clamped onto the drums. The sample is maintained for around 100 s in order to ensure the stabilization of the temperature in the chamber and the sample relaxation. The extensional test

is made of two steps. First, the sample is pre-stretched at $\dot{\varepsilon} = 0.001\ s^{-1}$ for 10 s and then stretched at constant strain rate. The EVF is limited to three quarters of a revolution. Indeed, after one total revolution of the drums the sample winds on itself making the measurement unusable. As a result, the highest Hencky ε strain reachable is limited to about 4. For their characterization, the samples are taken off right after the end of the test and cooled down with compressed air in order to keep their structures.

4. Extensional viscosity combined with conductivity set-up

Home-made modifications have been carried out on the commercialized EVF system to give access to the conductivity measurement during the extensional test. First, the two metallic drums have been electrically isolated to avoid any short-circuit. Copper thin film with 10 mm width has been rolled around each drum to constitute an electrode and then electric cables are welded on it. The two drums are electrically powered through electric cables connected to a Keithley 237 power supply delivering a DC 10 V and measuring the resulting current.

When the sample is clamped on the two drums it closes the electrical circuit so that the measured current is the current passing through the sample. Molten sample closely fits to the barrels and ensure a good and homogeneous electrical contact between the sample surface and the electrodes. Figure 2 illustrates the experimental set-up with *A(t)* representing the sample thickness as a function of *t*.

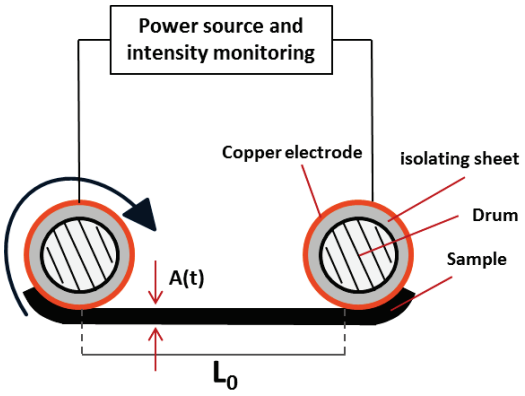

Figure 2: Cross section view of the experimental set-up.

The potential difference is taken at the distance noted L_0 between the two drums which remains unchanged as the sample is rolled up on the electrode. The time-dependent conductivity is deduced from the measured current as:

$$\sigma(t) = \frac{1}{\rho} = \frac{L_0 . I(t)}{U . S(t)}$$

Equation 12

where L_0 is the sample length between the drums, *I(t)* is the measured current, *U* the applied DC voltage, and *S(t)* the effective cross-section area of the sample. Assuming a uniform deformation of the sample and a constant volume this area can be expressed as a function of time and the initial section S_0 as:

$$S(t) = S_0 e^{-\varepsilon_H} = S_0 e^{-\dot{\varepsilon} t}$$

Equation 13

Combining Equation 12 and Equation 13, the conductivity, as a function of time, can be expressed by:

$$\sigma(t) = \frac{L_0 . I(t)}{U . S_0 e^{-\dot{\varepsilon} t}}$$

Equation 14

Samples were deformed at strain rates between $0.005 \leq \dot{\varepsilon} \leq 0.1$ s^{-1}. These values are taken small enough to facilitate the electrical acquisition and to monitor the structure evolution of the conductor network. The conductivity monitoring configuration makes possible reliable measurements for quite high Hencky deformations. However, for deformation above 2 the electrical cables prevent the drum to rotate and, by consequence, a false upturn of the stress is shown whereas it is the case without the wire (see Figure 3). In addition, the specimen's width dimension has been observed during extensional test in order to certify the proper adhesion of the clamped specimen with the drums and the homogeneous deformation of the sample.

First, the conductivity monitoring has been tested on systems with a relatively high initial electrical conductivity. A satisfying reproducibility test is presented in Figure 3. The conductivity variation and the extensional viscosity displayed in Figure 3 were carried out at 160°C with an extensional rate of $0.01 s^{-1}$ on the same system: PS filled with 0.79 vol% CNT. For the sample 1 (#1) and the sample 2 (#2) the measurements were carried out with the electrical system whereas, for the sample 3 (#3), it was conducted only with the classical EVF device. The extensional stresses for #1 and #2 display a deviation because the electrical cables disturb the torque monitoring.

For the following, in order to discriminate the samples behavior the variable ε_σ will be introduced. It represents the Hencky deformation when the conductivity falls down and reaches 10^{-6} $S.cm^{-1}$ (taken arbitrarily). The EVF shows limitation for the fully characterization of the material. Indeed, the system cannot reach the Hencky strain-at-rupture for this material. The experiment has been stop before the sample starts wrapping on the two drums. This Hencky deformation does not represent a characteristic of the material. In the literature, one can find specimens of General Purpose Polystyrene break after a Hencky deformation of around 4. This was achieved by using a modified a modified rotational rheometer at 150°C [36].

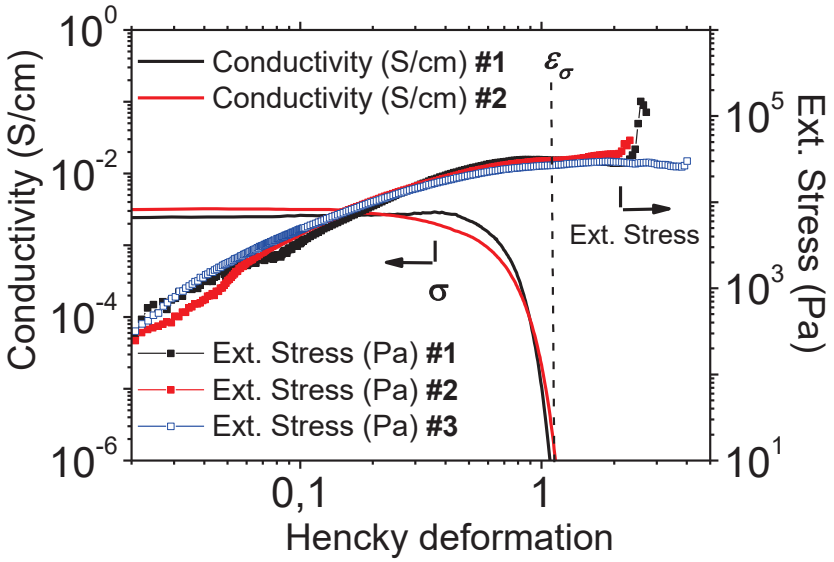

Figure 3 : Polystyrene filled with 0.79 vol% of CNT deformed at 160°C under extensional rate fixed to 0.01s^{-1}. The extensional stress curves #3 has been monitored on a EVF without the electrical set-up to reach higher Hencky deformation and highlights the impact on the electrical set-up on the stress monitoring (see #1 and #2).

Figure 3 clearly shows that the measured conductivity strain limit ε_σ is reproducible: the obtained values are within 10%. However, it must be mentioned that the deviation is slightly more important for higher extensional rates (about 20%).

In addition to the reproducibility, it is necessary to check that the experimental set-up does not take part in the filler deformation and orientation by electrophoresis mechanism as experienced by Martin *et al.*[17]. To do so, the hydrodynamic forces must be compared to the electrostatic polarization force [37]. The hydrodynamic force acting on a spherical particle (here a spherical aggregate) can be expressed as:

$$F_H = 6\pi\eta_0 a^2 \dot{\varepsilon}$$

Equation 15

with η_0 being the zero shear viscosity of the pure matrix, a the radius of the particle and $\dot{\varepsilon}$ the strain rate. On the other hand, the electrostatic polarization force exercised on a spherical particle is expressed as:

$$F_{El} = 12\pi\varepsilon_0\varepsilon_r a^2 \beta^2 E^2$$

Equation 16

where ε_0 = 8.8542 x 10^{-12} F/m is the permittivity of the free space, ε_r is the relative dielectric constant of the continuous phase, a the particle radius, β is the relative polarizability [= $(\sigma_f-\sigma_p)/(\sigma_f-2\sigma_p)$] where σ_p and σ_f are the conductivity of respectively the polymer phase and the filler. E is the electric field

fixed to 1kV/m. Combining Equation 15 and Equation 16 the Mason number (M_n) [37] may be defined as:

$$M_n \equiv \frac{F_H}{F_{El}} = \frac{\eta \dot{\varepsilon}}{2\varepsilon_0 \varepsilon_r \beta^2 E^2}$$

Equation 17

In this work, extensional rates are taken in the range of 0.005 s^{-1} to 0.1 s^{-1} ; the M_n factor is much greater than 1. Therefore, it can be concluded that the electric field does not take part in the fillers alignment and will be neglected in the study.

III. Results and discussion

A. CNTs dispersion and resulting conductivity

Carbon nanotubes are rod-like shape fillers. Without any functionalization, the surface energy is predominant and forces them to form aggregated structures. SEM observations have been performed on the nanocomposite made of PS filled with 0.79 vol% of CNT. The obtained picture reveals bright and dark areas. The bright areas highlight the electrically conductor fillers: privileged area for secondary electron emission. The dark area is the insulating matrix. This observation method will not be detailed in the paper; however the reader can refer to studies on this method [23-25]. It is relevant to note that the brightness among all aggregates is not homogeneous. This is explained by the depth penetration of the incident electrons. The secondary electrons flow will be more important for aggregates near the surface sample (bright area) than the aggregates located deeper in the material (grey scaled area).

Those observations give access to the 2-D picture of the filler dispersion. In Figure 4, a percolated network of CNT in the PS matrix can be observed. The structure obtained is homogenous (at macroscopic scale) and does not present any favored orientation. Based on the SEM observation the CNT entities seem to form an infinite percolated network.

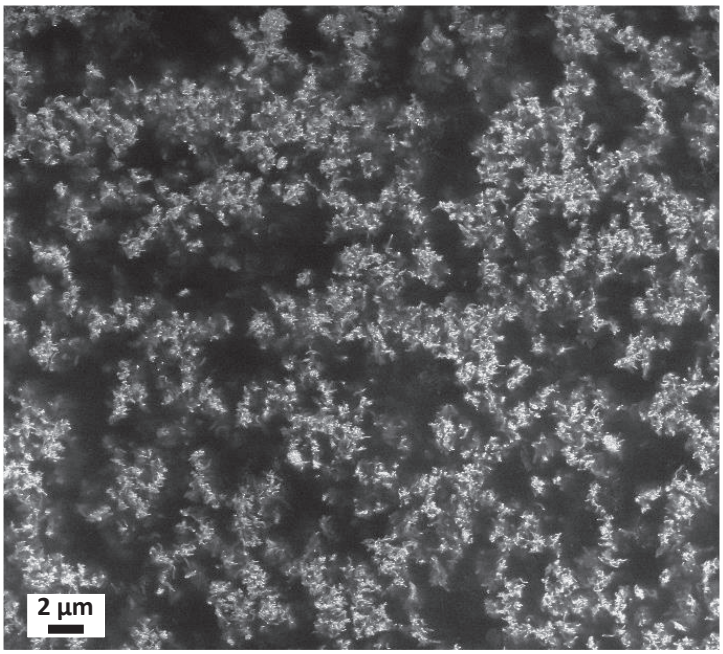

Figure 4: SEM observation with in-Lens detector, WD fixed at 5.4mm, ETH = 20kV, magnification x2000 of PS filled with 0.79 vol% CNT (compression molded).

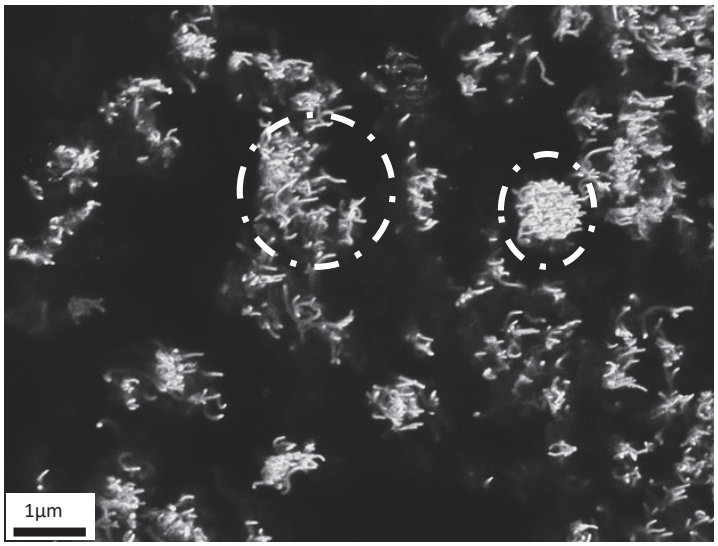

Figure 5: SEM observation at higher magnification x10 000 of PS filled with 0.79 vol% of CNT (compression molded).

Details of the structure can be observed at higher magnification (see Figure 5). This structure can be outlined as a population of aggregates and agglomerates interconnected together by smaller structures (i.e. small disentangled bundles). In Figure 5, the dense aggregates are highlighted by white dotted circles.

With the addition of fillers, the connections between clusters become predominant, and by consequence, the formed percolated network is more electrically conductor. The conductivity evolution with the filler concentration illustrates this phenomenon (see Figure 6).

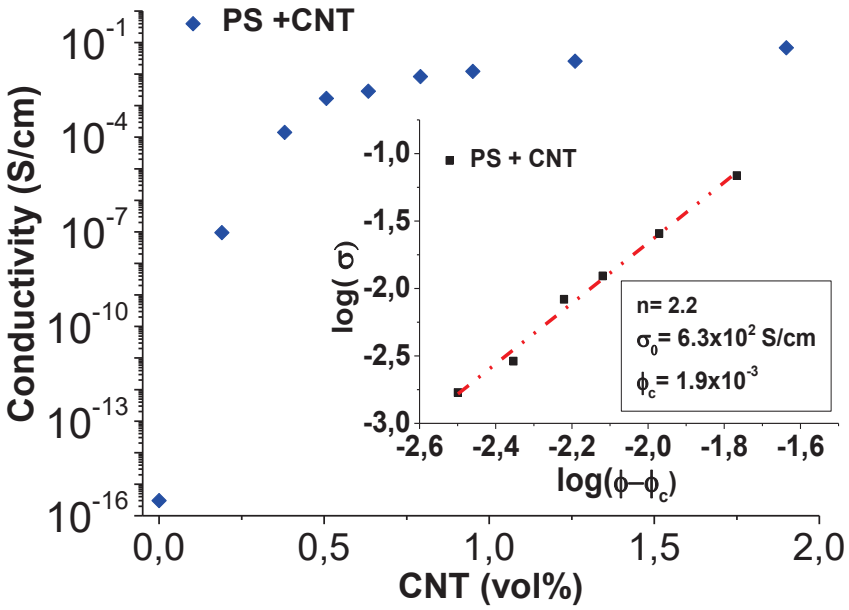

Figure 6: Evolution of the volume conductivity of PS filled with CNT as a function of the filler concentration (measured on compressed samples). As inset, is plotted linearized expression of the conductivity.

The electrical characterization of the different nanocomposites over a wide filler concentration range highlights the electrical insulator-conductor transition with the addition of a very low amount of filler. The formation of an infinite conductive path can be determined by classical percolation law. For a filler concentration higher than the percolation threshold, the evolution of the conductivity can be expressed as $\sigma = \sigma_0(\Phi - \Phi_c)^n$, with Φ the CNT volume fraction and Φ_c the volume fraction at the percolation threshold. The electrically insulator-conductor transition occurs for a concentration around 0.19 vol%. The obtained *n* exponent is equal to 2.2 (see the inset in Figure 6) and is in good agreement with the universal critical exponent 2 for the description of 3-D lattices [38,39]. The majority of the experiments will be carried out with specimens filled with 0.79 vol% of CNT, which is well above the percolation threshold. The electrical percolation threshold is significantly lower than the concentration needed for the formation of an elastic network. The formation of a percolated network made of mechanical bound, can be achieved at a larger filler concentration. The rise of a plateau at low frequencies in the storage modulus evolution occurs from a filler concentration of 0.37 vol%. This result is quite common and is explained by the capability of electrons to go through a network by tunneling effect [40]. More pragmatically, it can be also invoked that, near the percolation threshold, the formed network is very weak, and thus, difficult to be mechanically characterized without being destroyed (which can lead to an overestimation of the threshold). Obviously, this is not the case for an electrical measurement.

B. Nanocomposites under extensional deformation

The different materials have been characterized with a common EVF device. In Figure 7 is plotted the extensional viscosity of the pure matrix and the nanocomposite filled with 0.79 vol%. The two curves superimposed relatively well with the Linear Viscoelastic Envelope (LVE in Figure 7). The slight deviation in early stage might be accounted to the use of relaxation spectrum and moduli taken from a master curve built at 200°C. Nevertheless, the response is governed by the flow of the matrix and is not perturbed by the filler network. Thus, the evolution of the network during the deformation cannot be asses from the stress measurement. This motivates the coupling of the EVF accessory with conductivity measurement in order to highlight the network variation under extensional deformation.

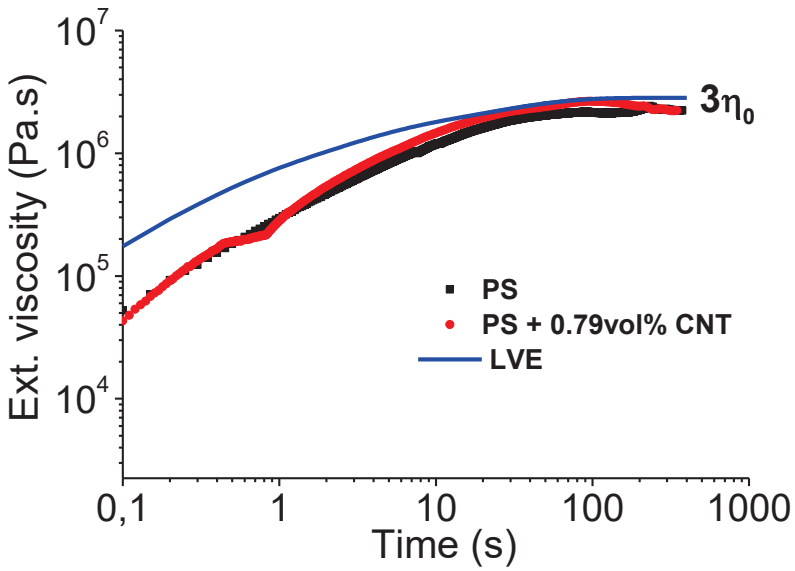

Figure 7: Extensional viscosity of pure PS and PS filled with 0.79vol% CNT at 160°C and extensional rate fixed to 0.01s^{-1}

Moreover, as the extensional rates are quite small, it is relevant to describe the competition between relaxation mechanism and stretching of the polymer chains. In this work, the use of the Weissenberg number defined for extensional deformations [41-43] will be used.

$$W_i = \lambda . \dot{\varepsilon}$$

Equation 18

where λ is the relaxation time of the pure matrix and $\dot{\varepsilon}$ is the extensional rate. The different Weissenberg numbers have been determined at 160°C and 180°C for the whole range of extensional rates (Table II) using the weight average relaxation times of the pure PS (see Equation 6).

Table II : Temperatures and extensional rates used for extensional tests and corresponding Weissenberg number W_i of the Polystyrene.

Temperature (°C)	Extensional rate (s^{-1})	Weissenberg number (W_i)
160	0.005	2.4
	0.01	4.8
	0.1	48
180	0.005	0.13
	0.01	0.26
	0.1	2.6

1. Conductivity variation under extensional deformation

In Figure 3 the variation of the conductivity is plotted as a function of the Hencky deformation. This test has been carried out on samples filled with 0.79 vol% of CNT at 160°C and an extensional rate fixed at 0.01 s^{-1}. First, it is relevant to note that ε_σ is far lower than the strain-at-break of the specimen. A smooth decrease of the conductivity is triggered at a strain of around 0.15. Then, the conductivity keeps on decreasing until the system reaches a conductor-insulator transition. This experiment highlights the highest uniaxial extensional deformation that the system can endure before becoming electrically insulator. This is a first distinction from the studies carried out under steady shear [14]. Indeed, under shearing, the conductivity can reach a stable non-zero value resulting from the establishment of an equilibrium regime between destruction and restructuration mechanisms. Under extensional stresses, the aggregates are dragged apart from each other and stretched in the deformation direction causing the break of the inter-aggregates connections. The structure obtained after a uniaxial deformation of ε=1 is presented in Figure 8. The white arrow indicates the deformation direction. The aggregates network is oriented and deformed within the flow direction (see white circle). However, some aggregates present no preferential orientation or deformation (see white dotted circle in Figure 9). This shows that only isolated carbon nanotubes or highly disentangled bundles presenting a structure more flexible can be deformed under external forces.

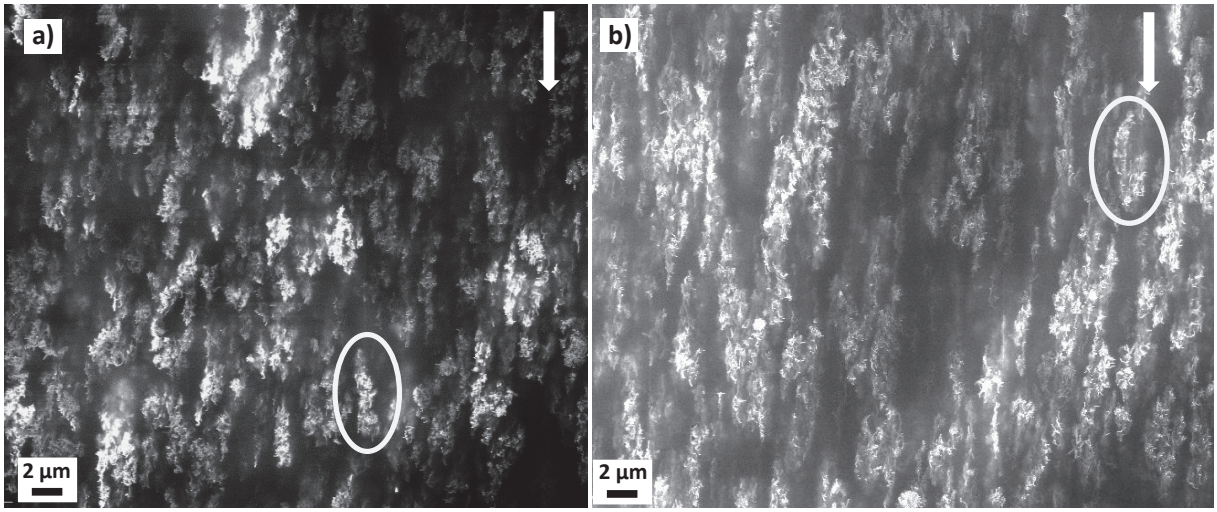

Figure 8: SEM observation with in-Lens detector 20kV, WD=5mm, magnification x 2 000. PS filled with 0.79 vol% of CNT after a Hencky deformation of 1 at 160°C for an extensional rate of (a) 0.01s^{-1} and (b) 0.1 s^{-1}.

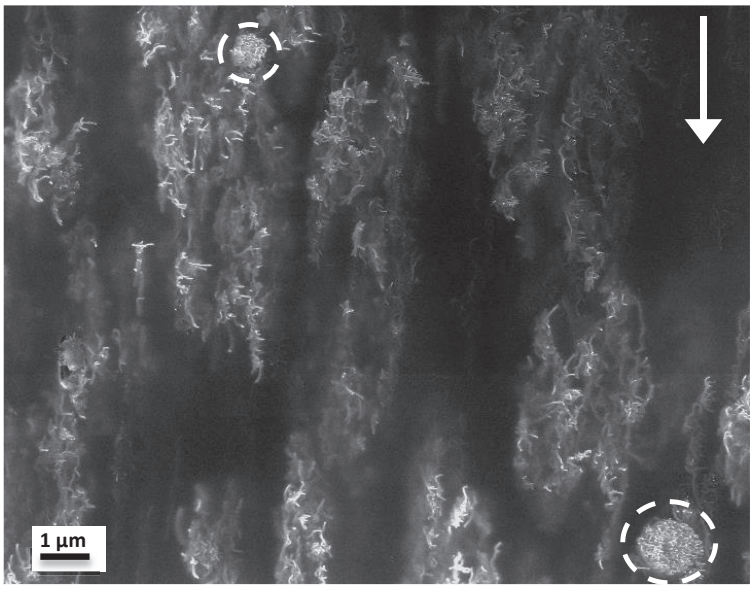

Figure 9: SEM observation with in-Lens detector 20kV, WD=5mm, magnification x 5 000. PS filled with 0.79 vol% of CNT after a Hencky deformation of 1 at 160°C for an extensional rate of 0.1 s^{-1}.

The deformations implied under extensional stresses are more effective in the network deformation than those induced by shear. However, stopping the deformation before reaching the critical ε_σ gives rise to the recovery of the sample conductivity. This result has been obtained from a two-step experiment which is illustrated in Figure 10. The samples are first deformed at an extensional rate fixed to $0.01s^{-1}$ at, respectively 160°C, 170°C and 180°C. Then, the first step is stopped after a Hencky deformation of 1 for the experiment carried out at 160°C, 1.4 for the one carried out at 170°C and 1.8 for the last one carried out at 180°C. These deformations were chosen to obtain approximately the same conductivity decrease. Finally, the samples are subjected to a quiescent annealing at the same temperature (160°C, 170°C and 180°C respectively). The conductivity recording is continued during this quiescent treatment. To characterize the structural evolution occurring during the quiescent treatment, SEM observations have been carried out before and after the quiescent treatment (see Figure 11).

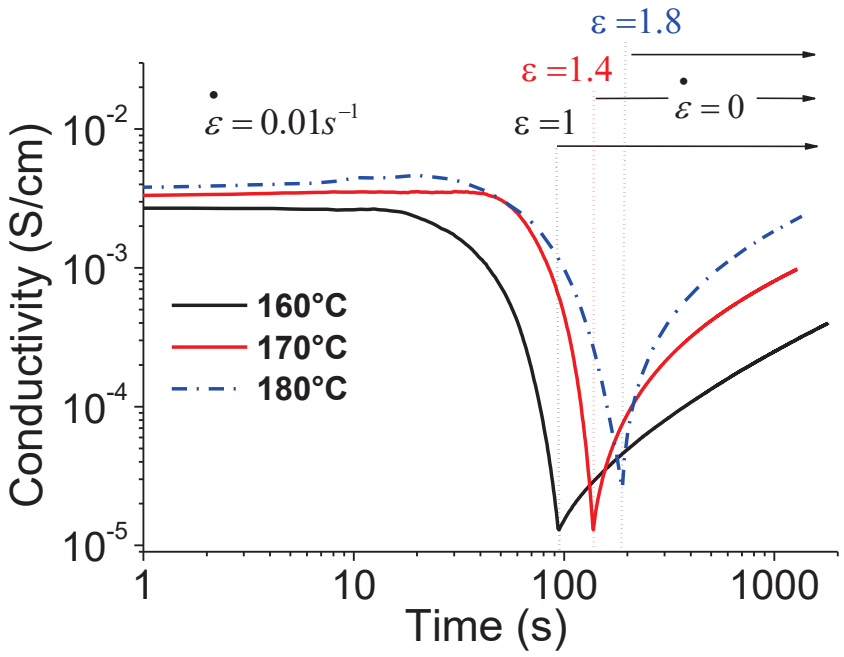

Figure 10: A two-step extensional experiment carried out at 160, 170 and 180°C (PS filled with CNT 0.79 vol%). First, an extensional deformation at a rate of 0.01s^{-1} up to a Hencky strain of 1, 1.4 and 1.8 respectively, followed by quiescent treatments at same temperatures.

In Figure 10, one can observe that the conductivity starts to increase right after the deformation interruption. The conductivity value when the quiescent treatment starts is respectively 2.5x10^{-5} S/cm at 180°C and 1.3x10^{-5} S/cm at both 170°C and 160°C, which gives the possibility to compare the three experiments. The conductivity recovery is significantly faster at higher temperature. Because of the very long duration of the total recovery, the conductivity measurement has been stopped before being stabilized. Anyway, this type of experiment illustrates the reversibility of the CNT network damaging mechanism as observed after shear. Even if the entities are drawn apart they remain sufficiently closed to each other and that make easier the network restructuration. Other tests have been carried out by stopping the deformation at different Hencky values where the conductivity ranged between 10^{-3} and 10^{-6} S/cm. All have shown the same recovery mechanism which is illustrated in Figure 10.

The structures obtained respectively at 160°C and ε=1 and at 180°C and ε=1.8 are utterly similar. The agglomerates are stretched and oriented within the flow direction. However, after the quiescent treatment the structures obtained are significantly different and illustrate the conductivity variation in Figure 10. At 160°C; the structure after the quiescent treatment is still oriented within the flow. Under higher temperature, the aggregates are significantly less stretched and the network orientation is less pronounced.

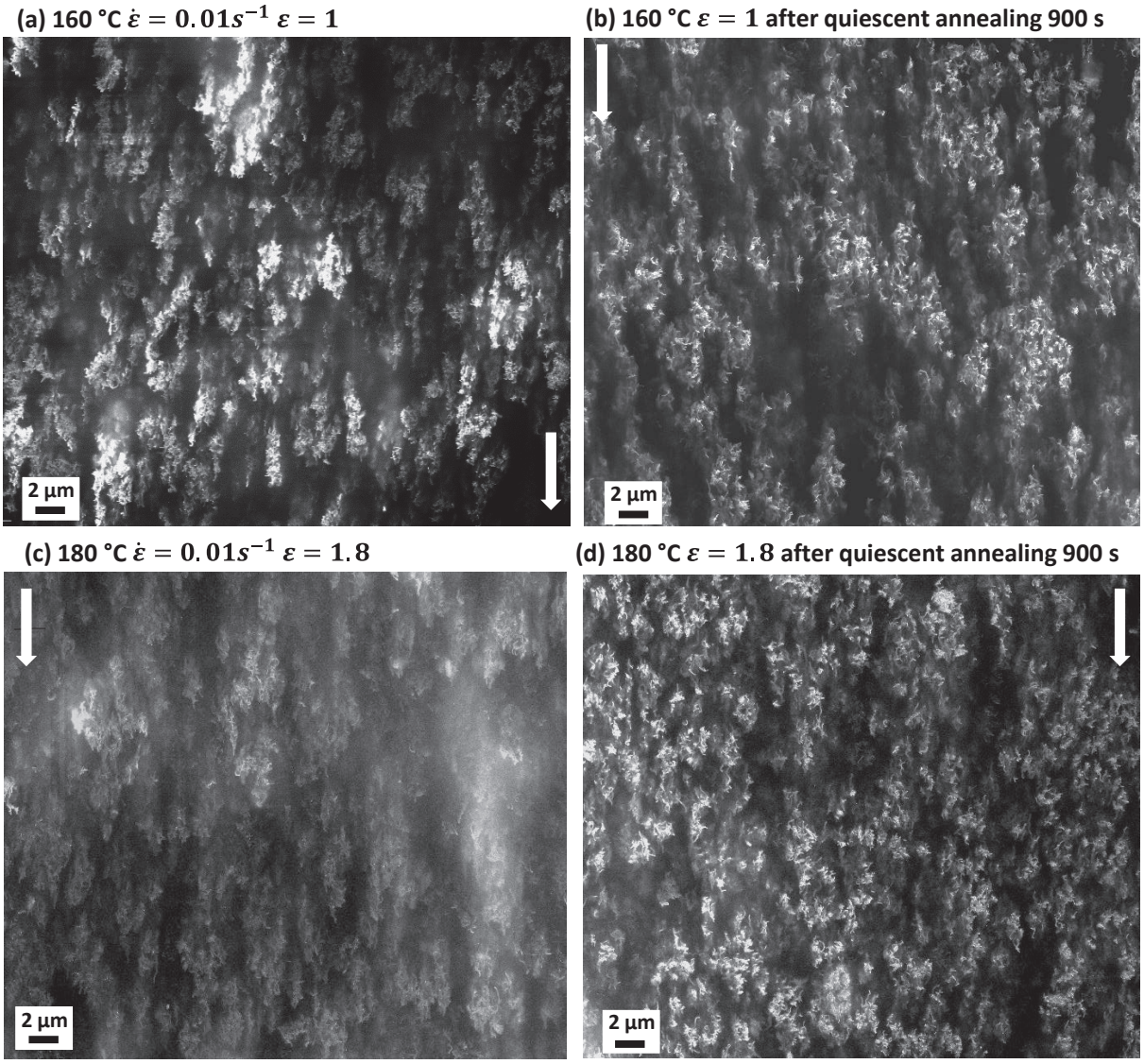

Figure 11: SEM observation with in-Lens detector 20kV, WD=5mm, magnification x 2 000. (a) and (b) structural evolution of PS filled with 0.79 vol% of CNT after a Hencky deformation of 1 at 160°C at an extensional rate of 0.01 s^{-1}: (a) immediately after elongation, (b) after quiescent annealing at 160°C during 900s, (c) and (d) structural evolution after a Hencky deformation of 1.8 at 180°C at an extensional rate of 0.01 s^{-1}: (c) immediately after deformation, (d) after quiescent treatment at 180°C during 900s.

The conductivity recovery has also been observed in others studies carried out on nanocomposites under quiescent conditions [11,14]. This phenomenon is explained by the restoration of connections between aggregates. However, the driven forces are not well understood. In order to understand the network structure evolution during the quiescent step the master curve of the quiescent annealing has been built. The three curves have been set to the same starting point to facilitate the building of the master curve at a T_{ref} fixed to 170°C (see Figure 12). The $a_{T\sigma}$ (shift factor for the quiescent treatment) are deduced from the building of the master curve and they fulfill the WLF. The obtained WLF coefficients $C_1'^{170}$and $C_2'^{170}$are respectively equal to 4.8 and 87°C for a T_{ref} fixed to 170°C. For practical reasons, the experiments couldn't have been carried out at 200°C (sagging). However, from the obtained WLF coefficients the coefficients at a different reference temperature can be deduced

[26,27]. For a temperature of 200°C, $C_1'^{200}$ and $C_2'^{200}$ are respectively equal to 3.6 and 120°C. They can henceforth be compared to the WLF coefficients C_1^{200} and C_2^{200} obtained from the master curve built at a T_{ref} fixed to 200°C (see part 3.a. **Dynamic rheology**) equal to respectively, 3.5 and 110°C. The WLF coefficients obtained from the conductivity master curve of the quiescent experiment are in good agreements with those obtained in dynamic rheology at the same T_{ref}. This result is meaningful and highlights the prevailing role of the polymer viscoelasticity for the network restructuration. After the deformation, the polymer phase tends to reach an equilibrium state via chains relaxation mechanism. This gives mobility to the filler network and triggers the restructuration. The molecular dynamic will be tackled more specifically in the next section.

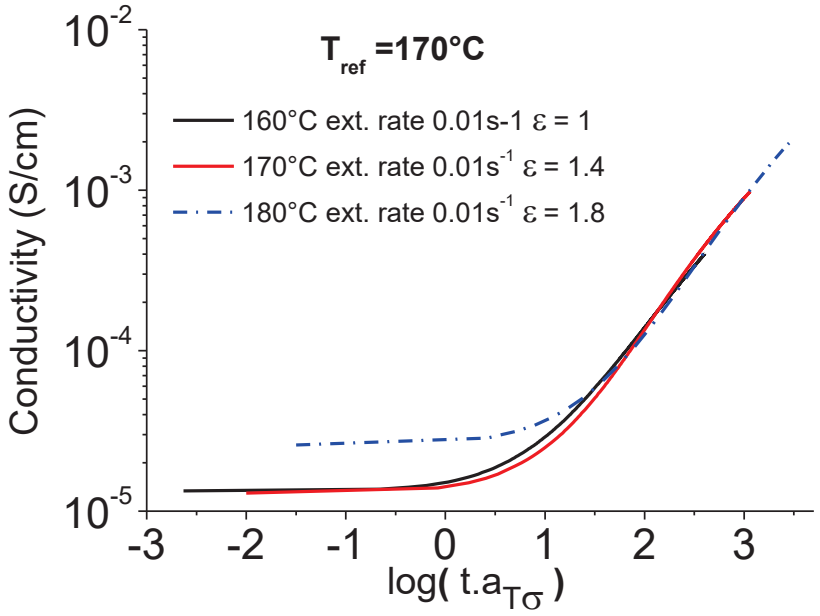

Figure 12: Master curve of the conductivity recovery during quiescent step built at a T_{ref} fixed to 170°C.

In addition, materials with varying amount of CNT have been tested. In Figure 12 is plotted the evolution of ε_σ for different CNT concentrations obtained at 160°C with an extensional rate fixed to 0.01 s^{-1}. First of all, it is relevant to point out that for all the concentrations tested, the conductivity limit ε_σ is reached before the sample breaks. The difference between ε_σ and the supposed strain at sample's break (higher than a deformation of 3.5) is quite significant and shows that the weakness of the CNT network is the real limiting factor for manufacturing conductive parts by thermoforming. With the addition of CNT, a slight but significant increase of ε_σ is observed (x2). This highlights the capability of more filled materials to undergo uniaxial elongation.

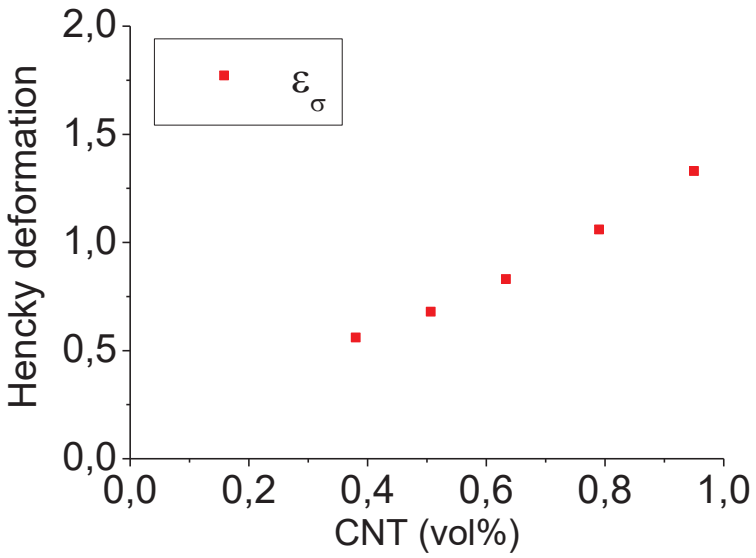

Figure 13: Evolution of ε_σ as a function of CNT concentration. Experiments carried out at 160°C with an extensional rate of 0.01s^{-1}

2. Influence of the temperature during extensional deformation

The influence of the temperature has been briefly highlighted in the previous section in Figure 10. In the following, this influence will be more expressly investigated on the PS filled with 0.79 vol% material. For this purpose, the material has been tested at three distinct extensional rates for two specific working temperatures: 160°C and 180°C. Figure 14 shows experiments the conductivity variations (a) and (c) for extensional experiments carried out at respectively 160°C and 180°C. The extensional viscosities are plotted in Figure 14 (b) at 160°C and Figure 14 (d) at 180°C.

First of all, the extensional viscosities presented in Figure 14 (b) and (d) are similar with the ones of the pure matrix (not presented here for sake of clarity) respecting the Trouton ratio of 3. Looking to the conductivity variations, one can notice that the extensional rate plays a non-negligible role in the ε_σ values. Indeed, for both temperatures tested, the decreasing of the extensional rate leads to a shift of ε_σ to higher Hencky deformations. This is even more significant at 180°C as illustrated in Figure 14 (c). Indeed, at this temperature, the conductivity variations for extensional rates of 0.005 s^{-1} and 0.01 s^{-1} are truly contrasting with the variation obtained with an extensional rate of 0.1 s^{-1}. For the formers, the conductivity decrease is really smooth. For all the systems analyzed, a conductivity decrease is triggered between 0.2 and 0.5 of Hencky deformation. However, the sample extended at 0.005s^{-1} presents first a slight increase of the conductivity (from 4.8x10^{-3} S.cm^{-1} to 8.2x10^{-3} S.cm^{-1}). The decrease stage is shifted at a higher Hencky deformation of 0.7. Moreover, the conductivity decrease is really smooth whereas at 0.1 s^{-1}, the conductivity sharply plummets. Hence, by dividing the extensional rate by a factor 20, the Hencky limits ε_σ are increased by a factor greater than 2.

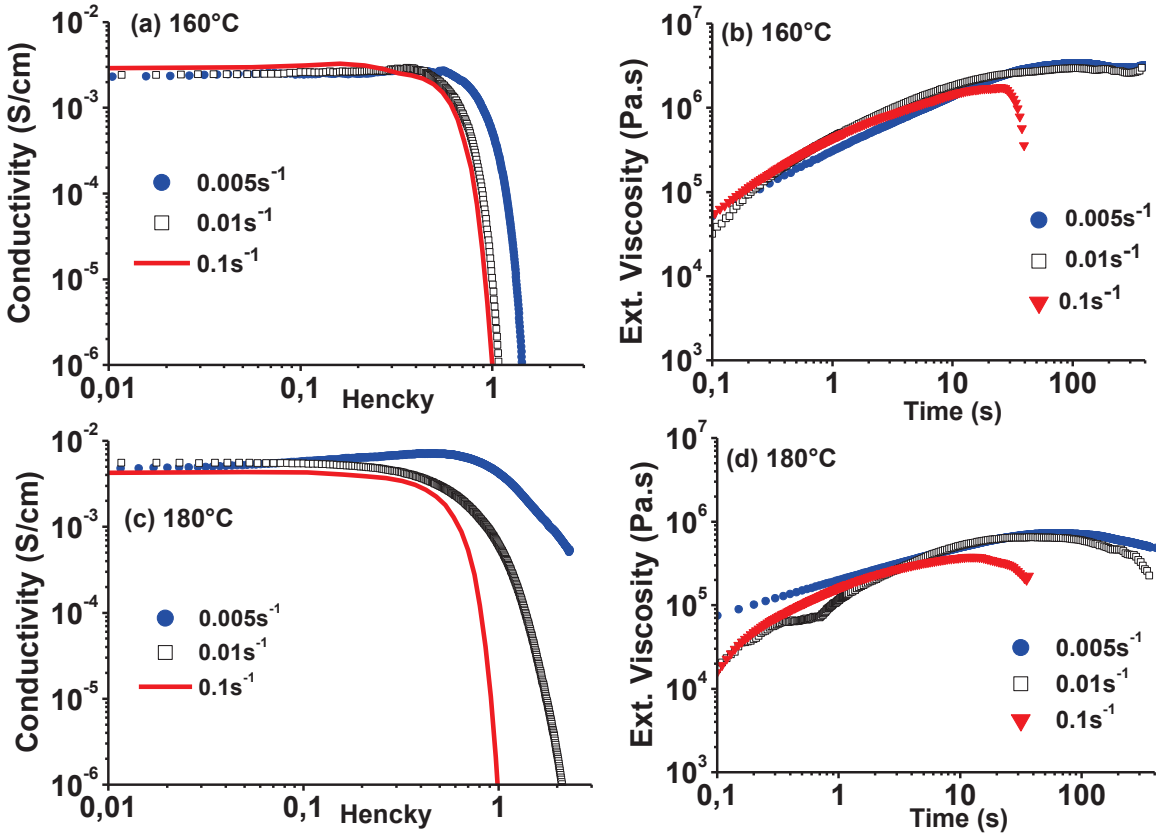

Figure 14: Conductivity variation at 160 °C (a) and at 180 °C (c) and their associated extensional viscsosities at 160 °C (b) and at 180 °C (d) for 3 extensional rates (0.005 s^{-1}, 0.01 s^{-1} and 0.1 s^{-1}) of PS filled with 0.79 vol%

In Figure 15 (a), (b) and (d) are presented the structures of those three samples after a Hencky deformation of 1. The structures obtained are truly different and corroborate with the conductivity variation. Indeed, at 0.005 s^{-1} the structure presents no specific orientation. Conversely, the structure obtained at 0.01 s^{-1} displays a slight orientation in the flow direction (less than the structure obtained at 160°C) and the structure obtained at 0.1 s^{-1} is similar to the one obtained at 160°C: strong orientation within the flow direction. After a Hencky deformation of 1.7, the material deformed at 180°C with an extensional rate fixed to 0.005 s^{-1} (see Figure 15 (c)) presents a structure similar to those obtained after lower deformation and higher extensional rates. Those observations highlight the concomitant influences of the temperature and the extensional rate on the deformation mechanism and steer the reflection on the predominant role played by the polymer molecular dynamics in the deformation mechanism of the CNT network.

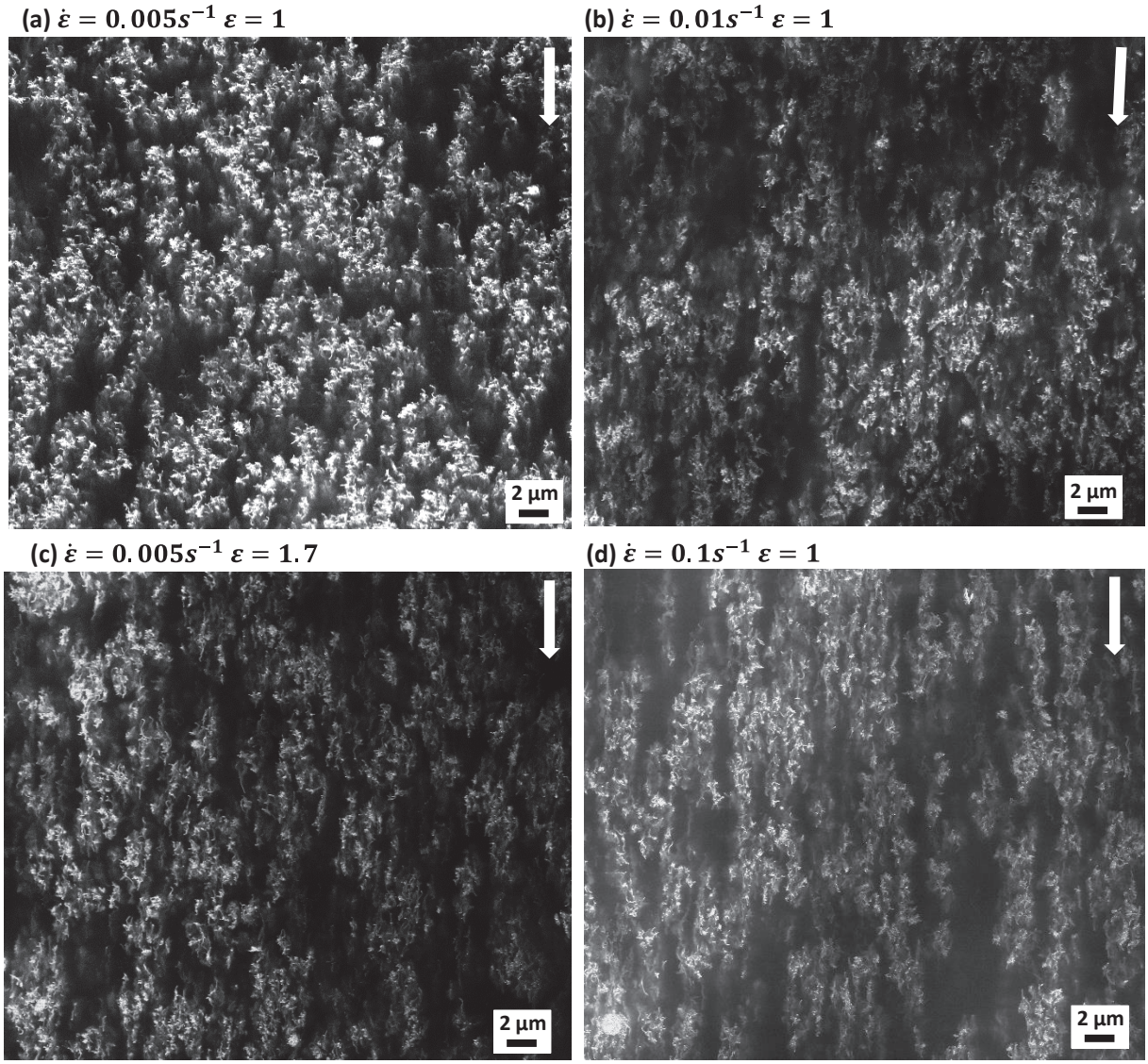

Figure 15: SEM observation with in-Lens detector, 20 kV, WD = 5mm x2 000. PS filled with 0.79 vol% at 180 °C extended to a Hencky deformation of 1 at extensional rates of (a) 0.005 s^{-1}, (b) 0.01 s^{-1} and (d) 0.1 s^{-1}. (c) Structure obtained after a Hencky deformation of 1.7 at an extensional rate of 0.005 s^{-1}.

Within the flow, the polymer orientation/deformation depends on its intrinsic characteristics such as its viscosity, chains reptation, relaxation behavior etc. In extensional flow, the polymer chains are drastically oriented and/or stretched. This stretching competes with the relaxation mechanism. At 160 °C all the W_i are large (see Table II), the stretch forces are predominant and the chains do not have enough time to fully relax. Moreover, the affinity between CNT and polymer chains is non-negligible due to strong interaction between Phenyl group and π-electron [44]. As a result, the CNT network is also oriented and stretched within the flow direction. Some experiments carried out at 140 °C and not detailed in this paper also confirm the results obtained at 160 °C. With rising temperature, the relaxation mechanisms are much faster and become predominant to the deformation dynamic. This transition is in good agreement with the W_i values obtained. For very low W_i, the network is not stretched and has no strong orientation. With the increase of the strain rate

the network becomes more stretched and oriented within the flow. In addition, the W_i coincide with the conductivity variations observed at 160 °C and 180 °C. Indeed, one can put in order the ε_σ obtained at the different extensional rates with their associated W_i. In other words one can shift the critical strain that nanocomposites can undergo by playing with both the temperature and the extensional rate. In that purpose, it is interesting to notice that the results obtained with a similar Weissenberg numbers (2.4 and 2.6) at different temperatures (respectively 160°C 0.005 s^{-1} and 180°C, 0.1 s^{-1}) lead to very close conductivity curves.

The polymer chains govern the filler network deformation. When the polymer chains can partially or fully relax, the filler network is not stretched and do not orient within the flow. The conductivity decrease is slow as the connections between aggregates are temporarily broken but conversely, the chains relaxation enables the regeneration of the inter-aggregates connections. This also explains the transition previously highlighted at extensional rate of 0.005 s^{-1} and a temperature fixed at 180°C (see Figure 14 (b)). The slight conductivity increase observed during the extensional test can now be attributed to a more predominant connections building mechanism than connection breaking. When the deformation becomes too important the encountered stretch exceeds the entropic elasticity of the coiled chains and the connection points of the filler network begin to break slowly (see Figure 15 (c)). It can be also highlighted that some big aggregates observable in SEM are not stretched. These are generally rich in CNT so that they are very rigid. Thereupon, these CNT are not stretched.

This proposal can also explain the results obtained within rotational flow. Indeed, during steady shear experiment, Hilarius *et al*.[6] have measured a conductivity decrease down to a stabilized non-zero value and even a conductivity increase. In this specific experiment, the polymer chains are stretched but significantly less than under extensional flow presented in this paper (decrease of the conductivity). The melt confinement in a constant volume and the possible chains relaxation mechanism might favor the apparition of a stabilized conductivity resulting from the equilibrium between the network break and the restructuration. In contrast, extensional deformation only drags apart the aggregates from each other.

IV. Conclusion

The presented new lab scale method gives access to the monitoring of the electrical conductivity of composites under extensional deformation. With a good repeatability, this method has shown that the electrical conductor-insulator transition occurs long before the sample breaks. It also makes possible the determination of the maximal Hencky uniaxial deformation that nanocomposites can undergo before becoming electrically insulating. Moreover, it has been shown that the addition of CNT shifts the insulating transition to higher Hencky deformation. SEM characterization of the material after extensional deformation has highlighted the stretching and the orientation of the CNT network.

The impact of both the temperature and the extensional rate has been investigated and has revealed the prevailing role played by the molecular dynamics in both quiescent experiment and dynamic regime. Within extensional flow, the polymer chains are stretched and oriented with the flow. Consequently, the CNT network is also stretched and oriented. In that specific case, the inter-aggregates connections are broken and the conductivity decrease is abrupt. Under appropriate conditions well described by the Weissenberg number, the polymer chains can partially or fully relax during the extensional test. This mechanism benefits to the CNT network as the aggregates are less stretched and the polymer chains relaxation triggers the inter-aggregates connection rebuilding. By consequence, the conductivity gradually decreases and the composites can undergo higher Hencky deformation before becoming electrically insulating. To go further, it will be interesting to carry out this experiment at higher temperatures and extensional rates to get closer of thermoforming conditions.

References

[1] Iijima, S., "Helical microtubules of graphitic carbon," Nature, **354**, 56-58 (1991).

[2] Dresselhaus, M.S. , G. Dresselhaus and P. Avouris, "Carbon Nanotubes: Synthesis, Structure, Properties and Applications," Vol. Springer Berlin Editions. (2001).

[3] Saito, R., G. Dresselhaus and M. S. Dresselhaus, "Physical properties of carbon nanotubes," Vol. Imperial College Press. (1998).

[4] Villmow, T., B.Kretzschmar.and P. Pötschke, "Influence of screw configuration, residence time, and specific mechanical energy in twin-screw extrusion of polycaprolactone/multi-walled carbon nanotube composites," Compos. Sci. Technol., **70**(14), 2045-2055 (2010).

[5] TabkhPaz, M. M. Mahmoodi and Mohammad Arjmand, "Investigation of chaotic mixing for MWCNT/polymer composites," Marcromol. Mat. Eng., **300**(5), 482-496 (2015).

[6] Hilarius, K., D. Lellinger., I. Alig, T. Villmow, S. Pegel and P. Pötschke, "Influence of shear deformation on the electrical and rheological properties of combined filler networks in polymer melts: Carbon nanotubes and carbon black in polycarbonate," Polymer, **54**(21), 5865-5874 (2013).

[7] Cassagnau, P., "Linear viscoelasticity and dynamics of suspensions and molten polymers filled with nanoparticles of different aspect ratios,". Polymer, **54**(18), 4762-4775 (2013).

[8] Moreira, L., R. Fulchiron., G. Seytre, P. Dubois and P. Cassagnau, "Aggregation of CNT in semi dilute suspension," Macromolecules, **43**, 1467-1472 (2010).

[9] Tiusanen, J., D.Vlasveld, and J. Vuorinen, "Review on the effects of injection moulding parameters on the electrical resistivity of carbon nanotube filled polymer parts," Compos. Sci. Technol., **72**(14), 1741-1752 (2012).

[10] Alig, I., P. Pötschke, D. Lellinger., T. Skipa, S. Pegel, G. R. Kasaliwal and T. Villmow, "Establishment, morphology and properties of carbon nanotube networks in polymer melts," Polymer, **53**(1), 4-28 (2012).

[11] Pegel, S., P. Pötschke , G. Petzold, I. Alig, S. M. Dudkin and D. Lellinger, "Dispersion, agglomeration, and network formation of multiwalled carbon nanotubes in polycarbonate melts," Polymer, **49**(4), 974-984 (2008).

[12] Alig, I., D. Lellinger, M. Engel, T. Skipa and P. Pötschke, "Destruction and formation of a conductive carbon nanotube network in polymer melts: In-line experiments," Polymer, **49**(7), 1902-1909 (2008).

[13] Allaoui, A., S.V.Hoa., P. Evesque and J. Bai, "Electronic transport in carbon nanotube tangles under compression: The role of contact resistance". Scripta Mater., **61**(6),628-631 (2009)

[14] Skipa, T., D. Lellinger, W. Böhm M. Saphiannikova and I. Alig, "Influence of shear deformation on carbon nanotube networks in polycarbonate melts: Interplay between build-up and destruction of agglomerates," Polymer, **51**(1), 201-210 (2010).

[15] Abbasi, S., P.J. Carreau., A. Derdouri and M. Moan, "Rheological properties and percolation in suspensions of multiwalled carbon nanotubes in polycarbonate," Rheol. Acta, **48**(9), 943 (2009).

[16] Kota, A.K., B. H. Cipriano, M. K. Duesterberg, A. L. Gershon, D. Powell, S. R. Raghavan and H. A. Bruck, "Electrical and rheological percolation in polystyrene/MWCNT nanocomposites," Macromolecules, **40**(20), 7400-7406 (2007).

[17] Martin, C. A., J.K.W. Sandier, M. S. P. Shaffer, M. K. Schwarz, W. Bauhofer, K. Schulte and A. H. Windle, "Formation of percolating networks in multi-wall carbon-nanotube–epoxy composites," Compos. Sci. Technol., **64**(15), 2309-2316 (2004).

[18] Marceau, S., P. Dubois, R. Fulchiron and P. Cassagnau, "Viscoelasticity of brownian carbon nanotubes in PDMS semidilute regime," Macromolecules, **42**(5), 1433-1438 (2009).

[19] Grillard, F., C. Jaillet-Bartholome, C. Zakri, P. Miaudet, A. Derré, A. Korzhenko, P. Gaillard and P. Poulin, "Conductivity and percolation of nanotube based polymer composites in extensional deformations," Polymer, **53**(1),183-187 (2012).

[20] Johannsen, I., K. Jaksik, N. Wirch, P. Pötschke, B. Fielder and K. Schulte, "Electrical conductivity of melt-spun thermoplastic Poly(hydroxyl ether of bispenol A) fibers containing Multi-Wall Carbon Nanotubes," Polymer, **97**(10), 80-94 (2016).

[21] Handge, U. A. and P. Pötschke, "Deformation and orientation during shear and elongation of a Polycarbonate/Carbon Nanotubes composite in the melt," Rheol. Acta, **46**(6), 889-898 (2007).

[22] ROUSSEAUX, D., O. Lhost, P. Lodefier and E.Scandino, "Masterbatches for preparing a composite materials with enhanced conductivity properties, process and composite materials produced," (2015); Available from: google.com/patents/WO2015014897A1?cl=en_2

[23] Li, W., S.T.Buschhorn., K. Schulte and W. Bauhofer, "The imaging mechanism, imaging depth, and parameters influencing the visibility of carbon nanotubes in a polymer matrix using an SEM," J. Carbon, **49**(6) (2011).

[24] Li, W.and W.Bauhofer, "Imaging of CNTs in a polymer matrix at low accelerating voltages using a SEM," Carbon, **49**(12), 3891-3898 (2011).

[25] Li, W., Y.Zhou, H.-J. Fitting and W. Bauhofer, "Imaging mechanism of carbon nanotubes on insulating and conductive substrates using a scanning electron microscope," J. Mat. Sci.,**46** (2011).

[26] Bird, R.B., R.C. Armstrong., O. Hassager, "Dynamics of polymeric liquids. Vol. 1, 2nd Ed. : Fluid mechanics," John Wiley and Sons Inc.,New York, NY; None. Medium: X; Size: Page: 784 (1987).

[27] Savvas, D. N., V. Papadopoulos and M. Papadrakakis, « The Effect of Interfacial Shear Strength on Damping Behavior of Carbon Nanotubes Reinforced Composites, » International Journal of Solid Structures, **49**, 3823-3837 (2012).

[28] Babaei, B., A. Davarian, K. M. Pryse, E. Elson and G. M. Genin, "Efficient and Optimized Identification of Generalized Maxwell Viscoelastic Relaxation Spectra," J. Mech. Behav. Biomed. Mater. , **55**,32-41 (2016).

[29] Herbert, A., G. L. Jones, E. Ingham and J. Fisher, «A Biomechanical Characterization of Acellular Porcine Super Flexor Tendons for Use in Anterior Cruciate Ligament Replacement: Investigation Into the Effects of Fat Reduction and Bioburden Reduction Bioprocesses,» J. Biomech., **48**(1), 22-29 (2015).

[30] Ferry, J.D., "Viscoelastic properties of polymers," Third edition ed. 1980.

[31] Cassagnau, P., J. P. Montfort, G. Marin and P. Monge, "Rheology of polydisperse polymers: relationship between intermolecular interactions and molecular weight distribution,". Rheol Acta, **32**(2), 156-167 (1993).

[32] Ferry, J. D., M. L. Williams and E. R. Fitzgerald, "The temperature dependence of relaxation mechanisms in amorphous polymers and other glass-forming liquids," JACS, **77**(14), 3701-3707 (1955).

[33] Bustos, F., P. Cassagnau and R. Fulchiron, "Effect of molecular architecture on quiescent and shear-induced crystallization of polyethylene,". J. Polym. Sci., Part B: Polym. Phys., **44**(11), 1597-1607 (2006).

[34] Watanabe, H., "Viscoelasticity and dynamics of entangled polymers," Prog. Polym. Sci., **24**(9), 1253-1403 (1999).

[35] Meissner J.and J.Hostettler, "A new elongational rheometer for polymer melts and other highly viscoelastic liquids," Rheol Acta, **33**(1), 1-21 (1994).

[36] Barroso, V. C., S. P. Ribeiro and J. M. Maia, "Unusual extensional behavior of a Polystyrene/HIPS blend," Rheol. Acta, **42**(5), 483-490 (2003).

[37] Marshall, L., C. F Zukoski IV and J. W. Goodwin"Effect of electric fields on the rheology on non-aquesous concentrated suspensions," J. Chem. Soc., **Faraday Transaction 1**(85), 2785-2795 (1989).

[38] Stauffer, D. and A. Aharony, "Introduction to percolation theory," Taylor and Francis, London, (1992).

[39] Bunde, A. and S. Havlin (Eds.), "Fractals and Disordered Systems," Springer Verlag, Berlin, Heidelberg,

(1991).
[40] Balberg, I. D. Azula and D. Toker, “Percolation and tunneling in composite materials,” Int. J. Mod. Phys. B, **18**(15), 1091-2121 (2004).
[41] Haward, S. J. and G. H. McKinley, “Instabilities in stagnation point flows of polymer solutions,” Phys. Fluids, **25**(8), 083104/21 (2013).
[42] Stary, Z., M. Papp and T. Burghelea, “Deformation regimes, failure and rupture of a low density polyethylene (LDPE) melt undergoing uniaxial extension,” J. Nonnewton Fluid Mech., **219**(3), 35-49 (2015).
[43] De Gans, B-J., L. Xue, U. S. Agarwal and U. S. Schubert, “Ink-Jet printing of linear and star polymers,” Macromol. Rapid Commun. **26**(4), 310-314 (2005).
[44] Liao, K. and S. Li, “Interfacial characteristics of a carbon nanotube-polystyrene composite system,” Appl. Phys. Lett. 79(25), 4225-4227 (2001).

Chapter 4

Effect of filler confinement for the generation of low-filled conductive composites

Abstract

The present work focuses on the analysis of two composites: a pure amorphous Polystyrene and a rubber modified Polystyrene (High Impact Polystyrene), both filled with Carbon Nanotubes (CNT) for generating Conductive Polymer Composites (CPC). Recently, the achievement of CPC with a filler content as low as possible has guided the researches on the volume confinement effect to force the filler segregation. This phenomenon enhances the contacts between fillers and consequently gives birth to conductive composites with ultra-low filler concentration.

In this work the two composites are analyzed using a specific set-up that gives the possibility to monitor both electrical conductivity evolution and the elongational stress in the melt state. This set-up allows determining the maximal deformation that nanocomposites can undergo before becoming insulating. In addition, the dynamic of the network evolution that is, its destruction and structuration has been analyzed. When the destruction is predominant, the two composites behave the same. However, we have observed a disparity when there is a possible competition between destruction and structuration during extensional deformation. This difference has been accounted to the presence of the nodules that might locally prevent the structuration mechanism during extensional deformation.

Keywords: Nanocomposites; Carbon Nanotubes, Extensional Viscoelasticity; Electrical conductivity.

Reformatted version of paper submitted in:

Macromolecules in February 2018

Generation of High Impact Polystyrene/ Carbon Nanotubes nanocomposites: an application of volume confinement strategy and their behavior under extensional deformation

Marjorie Marcourt, Philippe Cassagnau, René Fulchiron[a)],

Univ Lyon, Université Claude Bernard Lyon 1, CNRS UMR 5223, Ingénierie des Matériaux Polymères, F-69622, Villeurbanne Cedex, France

Dimitri Rousseaux, Olivier Lhost, Simon Karam

Total Research and Technology Feluy Zone Industrielle Feluy C 7181 Feluy, Belgium

I. Introduction

Owing to their good mechanical [1,2], electrical [3], and thermal [4] properties and their specific shape, Carbon Nanotubes (CNTs) are the ideal fillers for the generation of conductive polymer nanocomposites. This specific filler, due to its large aspect ratio, leads to composites with a lower percolation threshold compared to Carbon Black (CB). To push further the boundaries of percolation threshold, a new strategy has emerged. The idea is based on the tailored filler localization in the nanocomposite in order to enhance the formation of the percolated network by confining the fillers. The CNT network architecture design is based on the volume exclusion or on forced segregation.

One strategy is to use immiscible polymer blends in order to force the filler confinement by a privileged affinity between one polymer and the CNTs. The use of immiscible blends for the generation of Conductive Polymer Composites (CPCs) was first investigated by Sumita *et al.* [5,6] with CB. The goal is to generate at least one continuous phase in which the fillers will be located. This volume restriction will enhance the formation of a percolated network. Afterward, this strategy has been investigated in a lot for different kind of fillers [7-15]

Generally, the determination of the filler localization is achieved with only thermodynamic consideration. The minimization of the interfacial energy will drive fillers into the most energetically preferred phase. The localization may be predicted by the calculation of the interfacial energy. Considering a blend made of two polymers P_1 and P_2 and CNT fillers, the wetting parameter ω_{12} can

be calculated according to Young's equation for the adjustment of wetting angles on an ideal planes [16].

$$\omega_{12} = \frac{\gamma_{CNT-P1} - \gamma_{CNT-P2}}{\gamma_{P1-P2}}$$

Equation 1

with γ_{i-j} representing the interfacial tension between the components *i* and *j* which are alternatively the filler, the polymer P_1 or the polymer P_2. The value of ω_{12} forecasts the filler localization: if ω_{12} >1 MWCNT will be in the P_2 matrix, whereas, if ω_{12} < -1 they will be in the P_1 and finally if -1< ω_{12} < 1, MWCNT will be found at the interface of the different matrices.

The thermodynamic prediction is enough when considering two polymers with truly different polarities and surface energy [3,17-20]. However, to be more accurate, the kinetic aspect must be considered by taking into account the processing conditions, the physical properties of the CNTs, the filler dispersion state and the mixture procedure. For instance, some have observed that the addition of nanofillers can refine and even stabilize the continuous microstructure [21,22]. The best scenario for minimizing the percolation threshold is when the fillers are localized at the interface of the polymer phases. However, this specific case is quite hard to achieve. For instance, Gödel and coworkers have put in the light the impact of the filler shape. Indeed, fillers with a low aspect ratio (such as CB) segregated at the interface of Polycarbonate/SAN blend are more efficient to stabilize the morphology than CNTs. [10]

Nevertheless, the generation of composites with a controlled localization of the filler can be achieved and tuned by the functionalization of the filler to control the chemical affinity with a specific phase, by adapting the polarity [23], or grafting of polymer chains [24,25] or by kinetic consideration. [26,27-32]

Leaving apart all experimental conditions, the conductivity of such composites can be tuned by the blend composition (i.e. volume and morphology) of the phase containing the filler. For instance, Xu and coworkers have experienced an increase of five decades in conductivity by varying the blend composition [33]. Only few works dealt with the co-polymers of Polystyrene (PS). For instance, Moldenaers and coworkers [34,35] achieved to gain four decades in conductivity by playing on the molecular weight M_w and the structure of poly(styrene-random/block-methyl methacrylate) for the generation of PαMSAN/PMMA 40/60 filled with MWCNT. In addition, Mclory *et al*. [36] have dispersed MWCNT in High Impact Polystyrene (HIPS) (melt mixing strategy) and obtained a rather large electrical percolation threshold (≈2 wt%). By increasing the bead content from 30 to 60 wt% at a constant MWCNTs content of 0.6 wt% Shrivastava and coworkers [37] have obtained an increase of 2 decades of the electrical conductivity.

In addition to the increase of the electrical properties, the aggregates form an elastic network within the matrix. This is characterized by the storage modulus that becomes independent of the frequency in the low frequency range ($G' \propto \omega^0$; $G' = G_e$). In the literature the variation of the equilibrium modulus as a function of the filler concentration has been widely investigated [38-40] and it is well accepted that the value of the storage modulus illustrates the whole response of the

local contribution within the network, depending on the network structure and the filler-filler physical connections. More precisely, the filler concentration can be linked to the equilibrium modulus by combining fractal concept for the description of the filler structure and Kantor-Webman model that describes the elasticity of a chain made of particles. The concept of fractal is widely used for composites with filler in the nano to micrometric range [41-45]. Different models have been exposed. Among them, Heinrich and Klüppel have proposed a Cluster-Cluster Aggregation (CCA) model, that differs from the others with the assumption that fillers position can fluctuate around a mean value [46-48]. This assumption can be applied to CNTs because these fillers in the nanometer range are highly sensitive to the polymer chains mobility. Heinrich et al. have made the assumption that the clusters act as molecular springs with an end-to-end distance ξ, composed of N_B backbone units of length *d*. The backbone can be described as N_B with $d_{f,B}$ a fractal dimension that describes the backbone connectivity. From the expression of the constant force of the cluster backbone, they have obtained an elastic modulus of the cluster backbone and finally from scaling arguments they have obtained the evolution of the whole elastic modulus (considering three-dimensional case) as:

$$G_e \approx G_A \phi^{\frac{3+d_{f,B}}{3-d_f}}$$

Equation 2

where G_A is the elastic modulus of a cluster unit, Φ is the volume fraction, $d_{f,B} \approx 1.3$ for the smallest fractal dimension of the CCA-cluster backbone and $d_f \approx 1.8$, thereby the exponent $(3 + d_{f,B})/(3 - d_f) \approx 3.5$. [38]

However, the exponents reported in the literature for MWNT dispersed in both thermoplastic and thermoset matrix shows a great discrepancy. For instance, Pötschke *et al*. have obtained 0.2 and 2.5 for MWCNT dispersed in respectively Polyurethane [49] and Polycarbonate [50]. Hobbie and coworkers have observed a power law of 7.1 for MWNT dispersed in Polyisobutylene [51]. In addition, Esteban *et al*. [52] has observed a power law of 1.7 for MWCNT dispersed in unsaturated polyester resin.

This paper aims at studying the volume confinement effect in HIPS filled with CNT composites. The morphology will be compared to a more simple material: a pure PS matrix filled with CNTs. The percolation threshold, the structure of the filler network, the concentration dependence of the equilibrium modulus and the composites behavior under extensional deformation using a specific set-up will be analyzed. A particular attention will be devoted to the dynamic of the filler network structuration and its destruction during extensional tests.

II. Experimental section

A. Matrices and fillers

The CNTs are the NC7000, supplied by Nanocyl a Belgium company. They are characterized by a diameter *d* around 9.5 nm and a mean length of 1.5 µm. The two matrices used are a PS with a melt flow index of 2.4 and a High Impact Polystyrene (HIPS) with a melt flow index of 2.6 were both supplied by Total. In HIPS, nodules of Polybutadiene (PB) are included to improve the impact strength of the material. The composites are melt mixed using a masterbatches dilution strategy and were supplied by Total as pellets. The specimens were compression molded at 200°C.

B. Composites characterization

1. Morphology analysis

The morphologies have been investigated by Scanning Electron Microscopy (SEM) using a device LSM800 from Zeiss. The detection was ensured owing to in-Lens detector which is located inside the beam focusing lens. The observations have been carried out with a distance between the surface and the final condenser lens (the working distance WD) of around 5mm, an aperture size fixed at 30 µm and the accelerating voltage ranging from 10 kV to 20 kV. As the in-Lens detector is very sensitive to surface roughness, the sample surface has been cut with a diamond knife to prevent any roughness and promote the contrast between electrically conductor filler and insulating matrix. For the HIPS composite, the sample surface was firstly immerged in $Os0_4$ solution for at least four days in order to increase the phase contrast and make easier the specimen preparation by rigidifying the PB nodules. The observation technique will not be detailed in the paper, however the reader can refer to studies on this method [53,54]. In addition, Transmission Electron Microscopy observations have been carried out in order to complete the morphology characterization. Thin films have been cut at room temperature after the same specimen preparation as for the SEM characterization.

2. Conductivity measurement

Electrical properties analysis has been conducted on compression molded samples that have been additionally submitted to a quiescent treatment at 200°C for about 20 min. This supplementary thermal treatment enables the filler network to recover an equilibrium state in which most of the CNTs take part to the electrical conduction. Indeed, just after the compression molding, this state is

not obtained. A colloidal silver paste was applied on the surface sample to ensure a good contact between the electrodes and the specimen surface. Owing to a Keithley 237 power supply, a 10 volt Direct Current (DC) is delivered and the current passing through the sample is measured. The volume conductivity is then deduced using the specimen geometry as:

$$\sigma = \frac{L.I}{S.U}$$

Equation 3

with *U* the applied voltage, *I* the measured current, *L* and *S* respectively the specimen length and section.

3. Rheology

a. Dynamic rheology

Dynamic measurements were performed using an Ares rheometer (TA Instruments) equipped with parallel plates of 25 mm diameter under nitrogen atmosphere. The pure matrices where analyzed in the linear viscoelastic domain using the strain-controlled rheometer at different temperatures. Then following the time-temperature superposition principle, master curves have been built for a reference temperature of 200°C. The master curves were then described by a classical Maxwell *N* modes model [55]:

$$G'(\omega) = \sum_{i=1}^{N} \frac{G_i \omega^2 \lambda_i^2}{1 + \omega^2 \lambda_i^2}$$

Equation 4

$$G''(\omega) = \sum_{i=1}^{N} \frac{G_i \omega \lambda}{1 + \omega^2 \lambda_i^2}$$

Equation 5

where G_i is the modulus contribution corresponding to the relaxation time λ_i. For the fitting, the λ_i were fixed over the range of time constants corresponding to the reverse of the experimental frequency range. By means of an iterative method the G_i are deduced. The number of modes was fixed as the best compromise between the fitting quality and physically adequate (non -negative) values of the G_i. The frequency range for the HIPs matrix is chosen in order to characterize the relaxation mechanism of the PS phase. In Figure 1 the master curves are displayed fitted by a 5 modes Maxwell model for the pure PS matrix and by a 6 modes Maxwell model for the HIPS matrix.

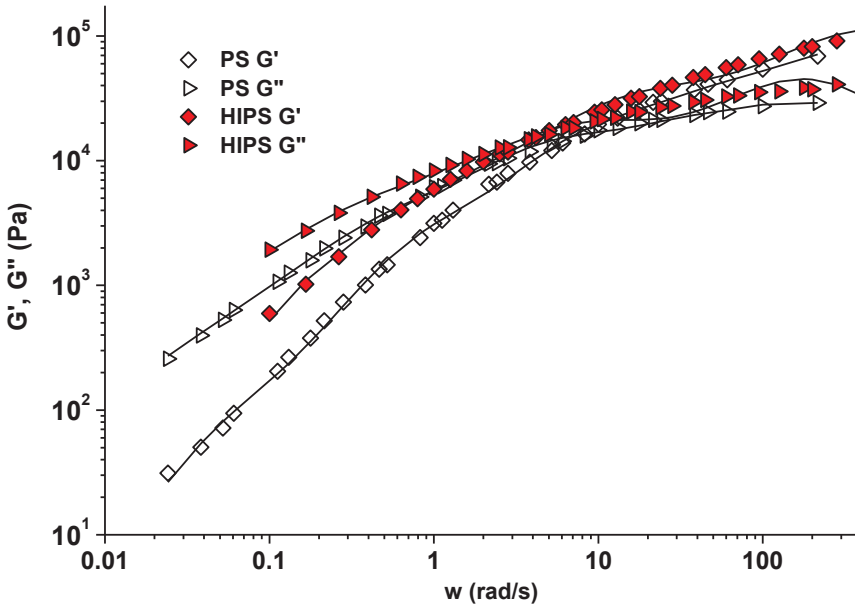

Figure 1 : Master curve of PS (filled symbols) and HIPS (open symbols) matrices built for a reference temperature of 200°C. Experimental data G' (diamond) and G" (triangle) and discrete Maxwell model (solid line).

The weight average relaxation time λ_w can be calculated from the λ_i and G_i parameters by:

$$\lambda_w = \frac{\sum_{i=1}^{n} G_i \lambda_i^2}{\sum_{i=1}^{n} G_i \lambda_i} = \eta_0 J_e^0$$

Equation 6

The build of the master curve gives access to the shift factors a_T, that follow the William Landel Ferry equation [56,57].

Table 1 displays the weight average relaxation time for the two matrices determined at different temperatures using the appropriate shift factor.

T°C	λ_w for the pure PS matrix (s)	λ_w of the PS in the HIPS matrix(s)
210	2.1	1.7
200	4.2	3.2
180	26	14
160	483	123

In addition, the viscoelastic behavior of the PS-MWCNT and HIPS-MWCNT filled with 0.15; 0.3; 0.6; 0.8; 1; 1.25; 1.5; 2; 3 wt% were analyzed at 200°C at a strain fixed to 1% chosen in the linear viscoelasticity domain. In order to control the aggregation state of the composites, the samples were first annealed for 20 min before the dynamic measurement. In an early study [58], we have shown that the filler concentration does not impact the dynamic of the polymer chains. In this work, the weight average relaxation time of the pure matrix will be used to calculate the Weissenberg number for the different extensional experiments. Indeed, we consider that the polymer molecular mobility

remains unaffected by the CNT network.

b. Extensional deformation combined with conductivity measurement

Extensional experiments were carried out with a commercialized Extensional Viscosity Fixture EVF (TA instruments) mounted on the ARES rheometer (TA instruments). The set-up was modified in order to measure the specimen conductivity during the extensional test. This specific set-up has already been detailed in an earlier work [58].

III. Results and discussion

A. Dispersion analysis

1. Morphology

The different morphologies of the composites will be first analyzed. Figure 2 shows a TEM micrograph of the HIPS/MWCNT. With interfacial energy from the literature, the wetting coefficient $\omega_{PS\text{-}PB}$ can be calculated and it is found equal to 2 at 200°C [59,60]. The thermodynamic prediction is $\omega_{PS\text{-}PB} > 1$; thus MWCNTs have a better affinity with PS than PB.

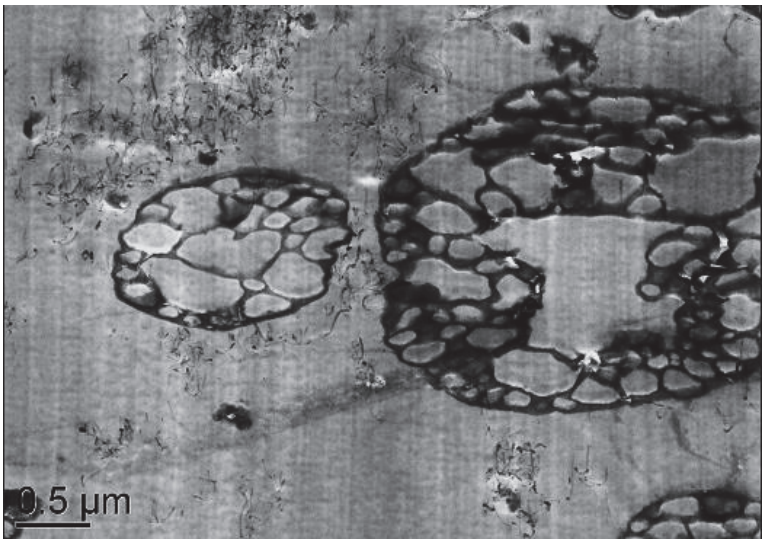

Figure 2: TEM micrograph of HIPS filled with 1.25wt% CNT

In this work, the CNTs were first melt mixed in a PS matrix for the generation of a highly filled masterbatch and then diluted with rubber-modified PS to obtain composites with a tailored filler concentration. CNTs are not expected to be found in the PS phase inside the PB nodules, because they should have to pass through the PB envelope. This is shown by the TEM micrographs where the CNTs are located in the PS phase outside the nodules.

Figure 3 shows two Scanning Electron Microscopy (SEM) micrographs of both composites filled with ~ 0.8 vol% of MWCNT. The observation is carried out with SEM with the in-lens detector. This detector gives the possibility to the observation of the CNTs thanks to enhanced contrast between the fillers and the matrix [53,54]. The bright dots are CNTs. The dark phase is the insulating PS matrix and the grey scaled phases are the PB nodules functionalized with OsO_4.

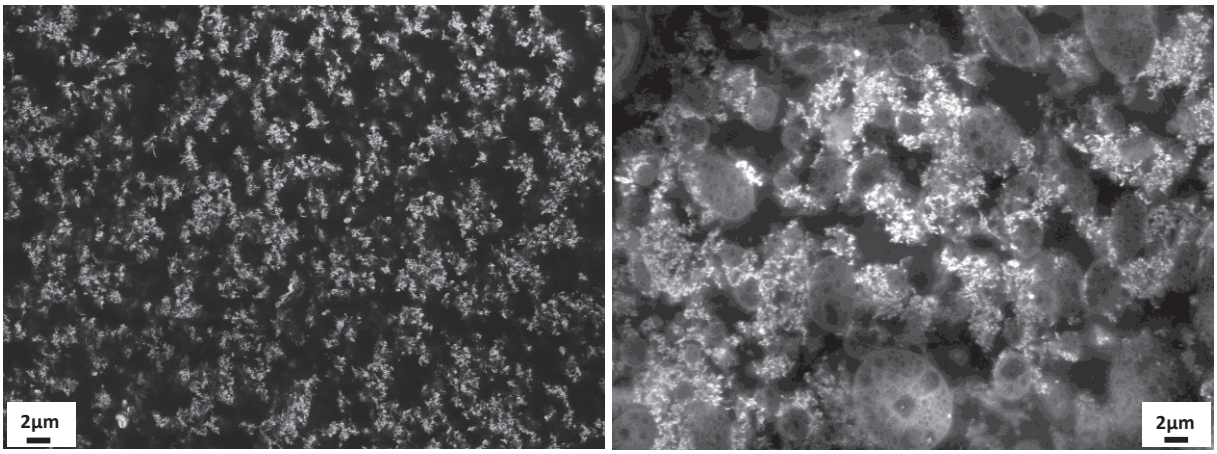

Figure 3: SEM micrographs of PS filled with 0.79 vol% MWCNT (left) and HIPS filled with 0.81 vol% MWCNT (right), magnification = x2000, WD 5mm 20 kV and in-lens detector.

In the PS matrix, the CNTs form a well percolated network of aggregates homogeneously distributed (Figure 3a). Figure 3b shows that in the HIPS matrix; the aggregates make a network in the PS rich phase around the nodules. The aggregates seem to be larger in the HIPS/MWCNT composites than in the PS/MWCNT composite. Due to not enough contrast within micrographs this assumption could not be confirmed by image analysis. In addition, the volume of the PB nodules in the HIPS has been estimated to 40 vol% by TEM analysis.

2. Effect of the nodules on the electrical conductivity

The conductivity in Conductive Polymer Composites arises when the fillers form a percolated network within the material [61,62]. Classical percolation theory has been applied in order to determine the percolation threshold of the two composites.

$$\sigma \quad = \sigma_0(\phi - \phi_c)^t$$

Equation 7

First of all, one must mention that during the melt mixing the CNT length can be reduced. The length distribution of the CNT after melt processing has been determined in TEM analysis on samples after the matrix has been removed with appropriate solvent. This analysis has only been carried out on the HIPS composite; as the processing conditions are quite comparable one can make the assumption that the length distribution is similar for the two matrices.

Fillers with aspect ratio in the range of 100 can theoretically generate composites with a percolation threshold a few lower than 0.1 vol% [63]. Experimentally, the two composites lead to slightly larger percolation thresholds than expected. The obtained exponent is 2.2 with a percolation threshold at 0.19 vol% of CNT for the PS/CNT composite and respectively 2.7 and 0.12 vol% for the HIPS/MWCNT

composite. The exponents illustrate the formation of a 3D network according to the percolation theory. As expected, due to the confinement of the fillers [5-7,9] the HIPS matrix generates composites with a lower percolation threshold than the PS matrix. In order to explain the difference between the two composites, the effective concentration of the CNT in the PS phase outside the nodules has been calculated with Equation 8:

$$Effective\ concentration\ of\ CNT\ (vol\%) = \frac{V_{CNT}}{V_{CNT} + V_{PS}} \times 100$$

Equation 8

where V_{CNT} is the volume occupied by CNT aggregates and V_{PS} is the volume occupied by PS. Taking into account the PS phase accessible to the fillers gives the possibility to explain the different percolation thresholds obtained. Figure 4 shows the conductivity evolution as a function of the CNT concentration in the accessible PS phase. The conductivity evolutions as a function of this corrected concentration for the two morphologies superimpose very well.

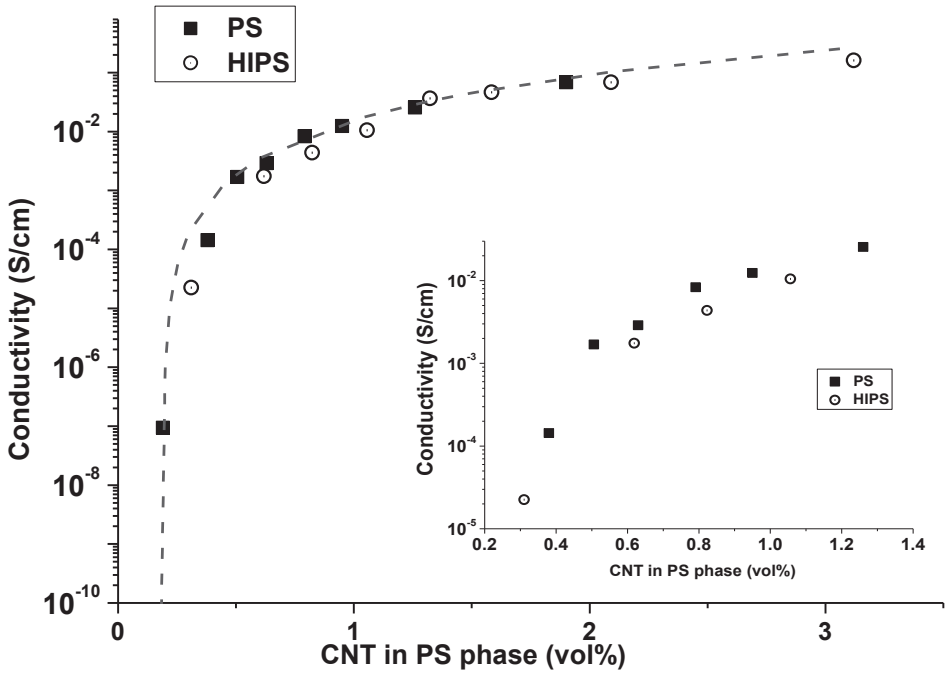

Figure 4: Evolution of the conductivity as a function of the volume concentration of MWCNT in PS continuous phase. Insert a zoom in on the conductivity evolution for a filler concentration in the range of 0 to 1.5 vol%. The data are fitted with a percolation law [61].

Hence, taking into account the effective volume concentration of the fillers in the PS phase for the HIPS composite, the matrices lead to similar percolation threshold. The nodules are randomly dispersed in the continuous PS phase. Thus, the conductivity of the material is preserved. Last, but not the least, the presence of the nodules which occupy around 40% of the total volume gives the possibility to decrease the CNT weight concentration of nearly 50%. It must be mentioned that,

everywhere in the following, the considered volume concentration of CNT will be the corrected concentration in the PS phase considering the restricted volume. However, it can be noticed in the insert of the Figure 4, that the HIPS conductivity is slightly lower than the PS composite conductivity, even with the correction of the filler concentration. This is certainly due to the effective section of electrical pattern which are smaller in the HIPS composite than in the pure PS.

3. Effect of the volume confinement on the filler network structure

The percolation theory applied to composites made of insulating matrix filled with electrically conductor particles gives the possibility to characterize the insulating/conductor transition. However, this concept does not give further details on the network structure. That is why, in addition to volume conductivity measurements, dynamic rheology measurements have been carried out on both composites in order to investigate the network formation and its evolution as a function of the CNTs concentration.

Like the evolution of the conductivity, the increase of the storage modulus can be described with a percolation law:

$$G_e \approx G_0(\Phi - \Phi_c)^t$$

Equation 9

The determination of the Φ_c has been achieved by the maximization of the correlation coefficient r^2 varying the three parameters (G_0, Φ_c and t). A value of Φ_c equal to 0.25% was obtained for the HIPS matrix and of 0.46% for the PS matrix. The generation of a percolated network occurs at a lower filler concentration in the HIPS matrix. Regarding the PS matrix, the formation of an elastic network occurs at a larger concentration than the electrical threshold and this threshold is much larger than for the HIPS composite. The formation of a percolated network exhibiting a macroscopic rigidity implies a larger concentration of connections within the material. It must be pointed out that, near the percolation threshold the network is so weak that its mechanical characterization without breaking the network is very difficult. Nevertheless, the difference between the two composites can be accounted for the presence of the nodules. The evolution of the equilibrium modulus is plotted as a function of the filler concentration in Figure 5.

First, attention has been paid on the modulus measurement since CNTs networks are very sensitive to the experimental conditions and especially to the melt history [64]. The aggregation state must be controlled in order to characterize a well-structured network. That is why in this work, the storage modulus has been measured after an annealing treatment of around 20min for the two composites. Surprisingly the equilibrium moduli of the HIPS composites are larger than these of the PS composites. Indeed, in that frequency range where the matrix modulus of PS or HIPS is negligible compared to the CNT network modulus the opposite was expected because of a “dilution” effect due to the PB nodules (the CNT concentration having been corrected). The composite modulus G* depends on the volume fraction and the elastic modulus of the different phases. The parallel model

(Voigt) (Equation 10) and the "series" model (Reuss) (Equation 11) mark the upper and lower bounds for the value of *G** out.

$$G^* = \left(1 - \phi_{PS/CNT}\right)G^*_{PB} + \phi_{PS/CNT}G^*_{PS/CNT}$$

Equation 10

$$\frac{1}{G^*} = \frac{1 - \phi_{PS/CNT}}{G^*_{PB}} + \frac{\phi_{PS/CNT}}{G^*_{PS/CNT}}$$

Equation 11

where G^*_{PB} is the complex modulus of the PB phase containing PS and $G^*_{PS/CNT}$ is the complex modulus of the PS containing the CNTs. The modulus $G^*_{PS/CNT}$ can be approximated by the Kernel model [65] as CNTs form aggregates. However, the composites modulus appears outside of theses limits and this will be attributed to the filler network. The use of such models fails at determining the elastic modulus of polymers filled with CNTs [65]. The filler network physical properties and especially its geometry are quite hard to take into account. That is why; the method proposed by Heinrich and Klüppel (see Equation 2) will be privileged for the analysis of the elastic modulus evolution as a function of the filler concentration. [66,67]

For the composites with the PS matrix, the exponent is in good agreement with the literature [68-70]. In addition, the d_f of the PS composite has been determined on threshold SEM micrographs thanks to the plugin FracLac developed for ImageJ software [71,72]. A d_f equals to 1.78 +/- 0.04 has been obtained, which is also pretty consistent with the literature. This is not surprising since the SEM micrographs of the PS/CNT composite (see Figure 3a) illustrates a network composed with aggregates similar to Carbon Black or Silica aggregates networks. However, the HIPS composites materials exhibit a different power law and a much larger equilibrium modulus (100 times larger). Indeed, the exponent and the elastic modulus of a cluster unit are lower than those obtained for the PS composite. Unlike the PS composite, it was impossible to determine the fractal dimension of the filler network in the HIPS composites. Nonetheless, this deviation and the larger equilibrium modulus obtained can be attributed to a different structure of the network in the HIPS composites. Indeed, as observed on the SEM micrographs (see Figure 3b), the aggregates are larger and denser which might lead to higher $d_{f,B}$ value and larger primary particles that form a cluster unit.

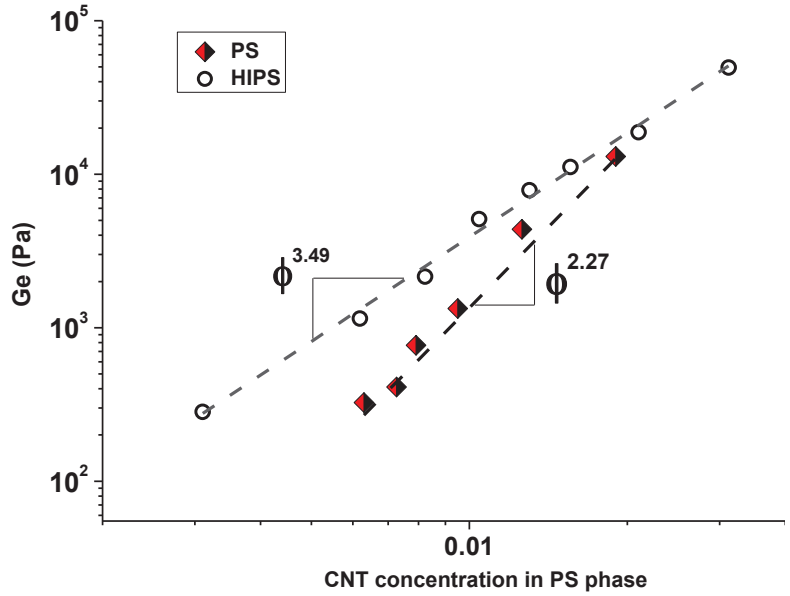

Figure 5: Variation of the equilibrium modulus as a function of the CNT volume fraction in PS continuous phase

The next section is aimed at analyzing the two composites under large extensional deformation.

B. Analysis of the filler network under extensional deformation

1. Composites under extensional deformation

The extensional viscosity of the materials have been measured at different temperatures in the range of 140°C to 210°C and different elongation rates between $0.01s^{-1}$ to $0.1s^{-1}$. In Figure 6 is plotted the ratio between the composites extensional viscosity at 180°C and $0.1s^{-1}$ and the zero shear viscosity of the unfilled material. For concentrations up to 1 vol% the obtained ratio is around 3 as expected for the classical Trouton's ratio. Thus, the presence of a percolated network does not influence the extensional viscosity. However, for the HIPS based composites at filler volume concentrations above 1 vol%, a large deviation is observed, whereas this deviation is not observed for the PS based composites. This deviation can be accounted for the confinement that enhances the formation of connections between the aggregates in the HIPS. Some have observed that the deviation from the Trouton's ratio of 3 occurs at a lower CNT content when using CNT with larger aspect ratio or highly filled suspension. [73,74] In addition, the analysis of the linear viscoelastic behavior has shown that the network strength is higher in the HIPS than in the PS. This denser filler

network has a crucial impact on the material flow ability. Concomitantly, with this large deviation, a smaller strain-at-break is observed for the HIPS based composites. In the literature, the PS strain-at-break is larger than for HIPS or even blend of PS and HIPS matrices [75]. Even if the filler content is quite low the generated interface volume is very large. The polymer chains embedded within the filler network do not have exactly the same behavior than in pure matrix. Their mobility is strongly reduces and the break appears at lower strains.

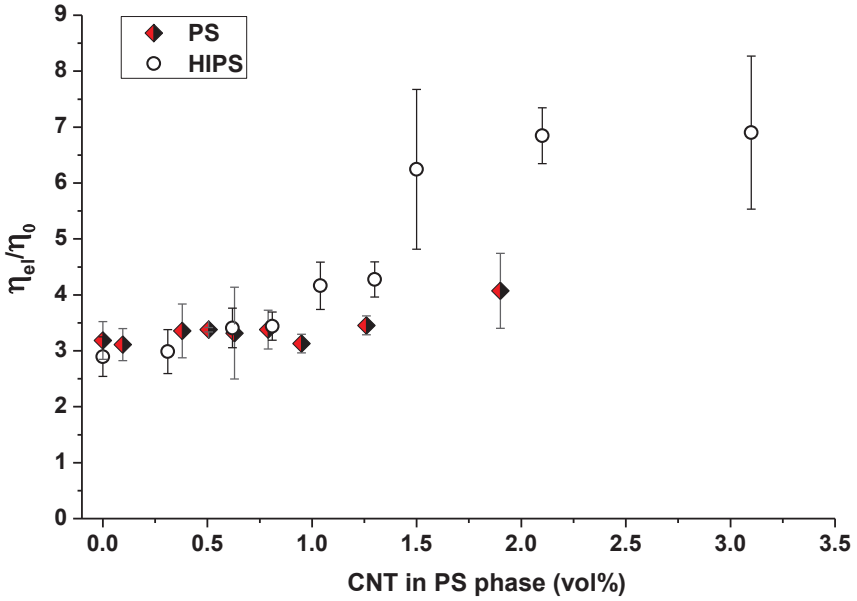

Figure 6 : Ratio between extensional viscosity at 0.1s^{-1} of the composites and the shear viscosity of the matrices at 180°C

At large filler concentration, the flow ability of the HIPS composite is dramatically impacted. From a pragmatic point of view, the use of nanofillers with large aspect ratio is motivated by their potential in the generation of conductive composites with low amount of fillers. Nevertheless, the small effect of the CNT on the measured extensional stress is not enough to provide valuable information on the filler network evolutions.

2. Conductivity variation under extensional deformation

The composites have been analyzed using a specific set-up of combined conductivity and extensional viscosity measurements. This set-up gives the possibility to measure the conductivity variation of the melt specimen which experiences an extensional deformation at a constant strain rate. Figure 7 shows the conductivity variation of two composites filled with about 0.8 vol% of CNT in the PS phase at 160°C and an extensional rate fixed at 0.01 s^{-1}. The slight concentration difference between the two composites and the fact that at a Hencky deformation ε equals 0, the two specimens are not at their equilibrium state have no strong impact on the following results.

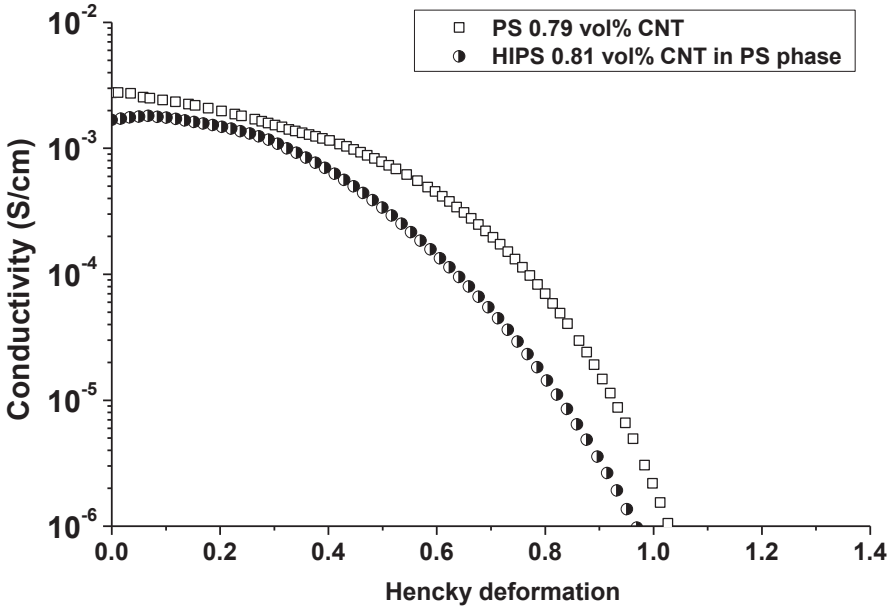

Figure 7 : Conductivity evolution under extensional deformation at 180°C for an extensional rate of 0.01 s^{-1}

For the two specimens, the conductivity decreases during the extensional experiment. As explained in our previous work [58], the conductivity decrease results from the progressive destruction of the filler network during the extensional test. The connections between the aggregates break due to the deformation of the sample. The two curves follow the same variation except that the HIPS composite shows a slightly faster decrease. Notwithstanding, this small difference is not enough significant to conclude.

The morphology of the two specimens after a Hencky deformation of 1 has been characterized. The two SEM micrographs are presented in Figure 8 where the white arrows illustrate the deformation direction. The structure of the PS composite (see Figure 8a) is made of aggregates stretched and oriented in the deformation direction. However; the structure of the HIPS morphology (see Figure 8b) is somewhat more difficult to characterize due to the presence of the PB nodules. First, the aggregates are stretched like in the pure PS matrix, but their orientation is less pronounced. Moreover, due to the PB nodules, the extensional rate is not homogeneous in the material and this can locally orient the aggregates in different directions than the whole deformation direction. In the following, the recovery mechanism and the competition between structuration and destruction mechanisms during the extensional deformation will be investigated more precisely.

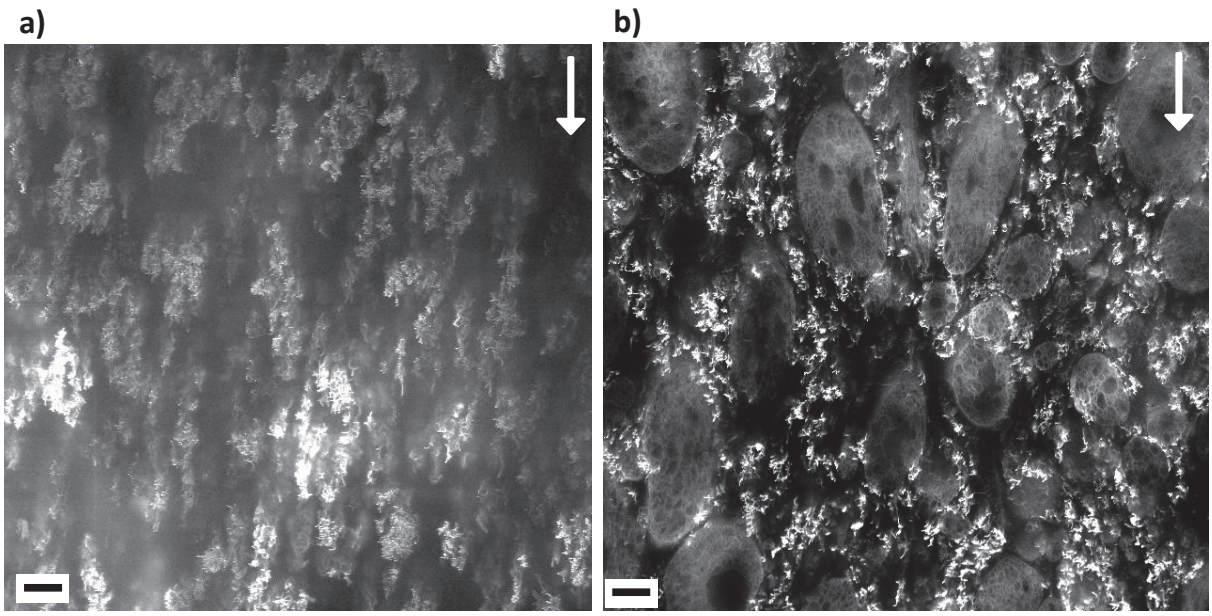

Figure 8 : SEM micrographs of the two composites after a Hencky deformation of 1 at 160°C and 0.01 s^{-1} a) PS filled with 0.79vol% CNT, b) HIPS filled with 0.81 vol% CNT in the PS phase and the conductivity is around 8.10^{-5} S.cm^{-1} for the two specimens. The scale is 2 µm.

3. Dynamic of the network restructuring

The conductivity recovery is a phenomenon largely addressed in the literature [76-80]. In our previous work carried out on PS filled with MWCNTs [58], we have shown that the polymer dynamics plays a major role in this mechanism. Indeed, the polymer chains govern the recovery mechanism as it gives sufficient mobility for isolated CNT or highly disentangled bundle of CNTs for the formation and reinforcement of the network. Here, the conductivity recovery has been analyzed for the HIPS composite following the same methodology. Specimens filled with about 0.80 vol% have been deformed in order to investigate the following conductivity recovery under quiescent conditions. This experience has been carried out at different temperatures. Like for the PS matrix composites [58], the conductivity recovery of the HIPS/CNT material fulfills a time-temperature superposition principle. A master curve of the conductivity recovery can be built and one obtains Williams Landel Ferry coefficients close to those obtained from rheological measurements (when using the same reference temperature). Figure 9 displays WLF plots of the a_T shift factors obtained respectively from the dynamic rheology of the pure matrices and from conductivity recovery experiments of both matrices filled with about 0.8 vol%. The reference temperature is 180°C. For the PS composites, the data from the dynamic rheology and conductivity recovery are very close. However, for the HIPS composite a slight difference can be observed between the a_T from the conductivity recovery and those from the dynamic rheology at high temperatures. The possible explanation of this result is that the shift factors obtained from rheology can be blurred because of the presence of the PB nodules which bring some uncertainty in the build of the master curve. Conversely, for the conductivity measurements, the PB nodules do not act in the CNT mobility. Thus, the network structuring is due

to the mobility given by the polymer chains. Figure 10 shows the conductivity recovery of the two composites after a Hencky deformation of 1 at 170°C and at 0.01 s^{-1}. The recovery of the two composites superimposes very well. The same results have been observed at higher and lower temperatures (not shown here).

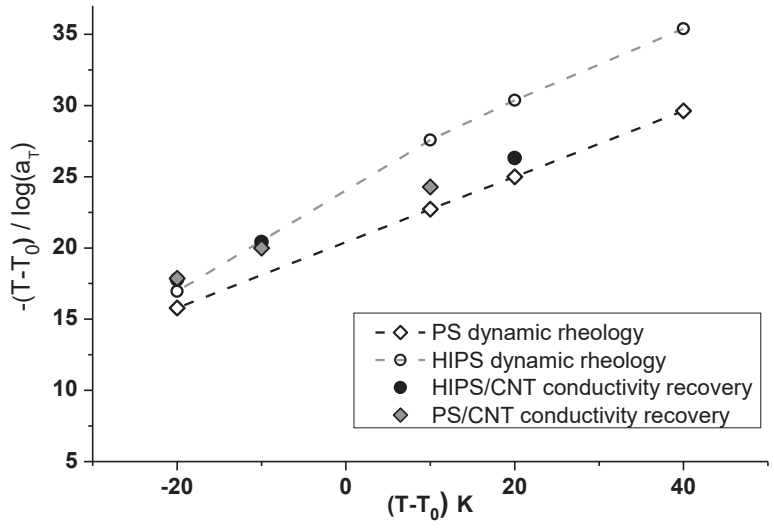

Figure 9 : WLF plot for the a_T shift factor from the build of the master curve of the pure matrices and from the build of the master curve of conductivity recovery. The reference temperature (T_0) is 180°C

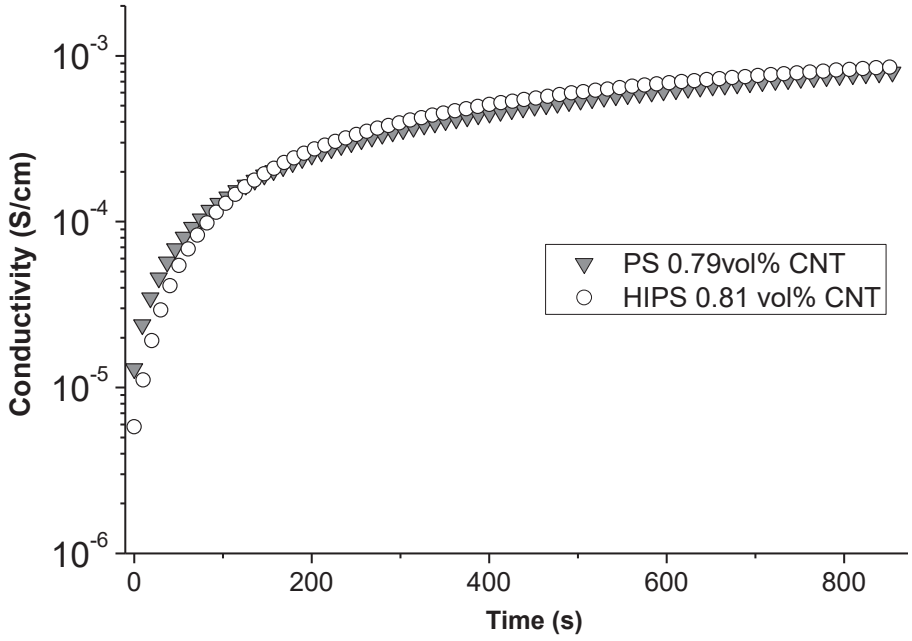

Figure 10 : Conductivity recovery under quiescent condition at 170°C of PS filled 0.79 vol% CNT and HIPS filled with 0.81 vol% CNT after a Hencky deformation of 1 at 170°C and 0.01s^{-1}

The filler reinforcement is driven by the same mechanism for the two composites. Disentangled and isolated CNT can diffuse and the attractive filler-filler interaction forces trigger the generation of

inter-particles connections.

4. Competition between restructuring and destruction of the filler network under extensional deformation

Under extensional deformation, a competition between destruction and restructuring of the network can occur. The use of the Weissenberg number ($\lambda_w \dot{\varepsilon}$) is useful for the determination of which mechanism is predominant. The contribution of the polymer chain mobility is taken into account thanks to the use of the weight average relaxation time of the pure matrix. Figure 11 illustrates the conductivity variations for the two composites under different experimental conditions that cover a wide range of W_i. It can be pointed out that they show different conductivity values at the beginning of the extensional test. This is due to the fact that the specimens are not fully aggregated and depending on the working temperature, they will tend to reach their equilibrium state (i.e state where all the CNTs take part to the conductivity) with more or less rapidity.

Table 1: Weissenberg number of the different extensional experiments for the two types of composites.

Temperature °C	Extensional rate (s^{-1})	PS/CNT	HIPS/CNT
160	0.01	4.8	1.2
160	0.1	48	12
180	0.01	2.6	1.4
180	0.1	26	14
200	0.1	0.4	0.3
210	0.1	0.2	0.17

At large W_i, all the measured conductivity curves merge to the same one. It is worth noting that the two materials exhibit the same limiting deformation (ε =1) before becoming insulating (under 10^{-6} $S.cm^{-1}$). Under those conditions, the relaxation mechanisms are too slow compared to the extensional rate. By changing the experimental conditions (playing on temperature and on extensional rate), the W_i can be reduced. In this specific case, a competition between restructuring and destruction can be theoretically observed and Figure 11 shows that the specimens can undergo larger deformation before becoming insulating. This shift to larger deformation observed for the two composites illustrates this competition.

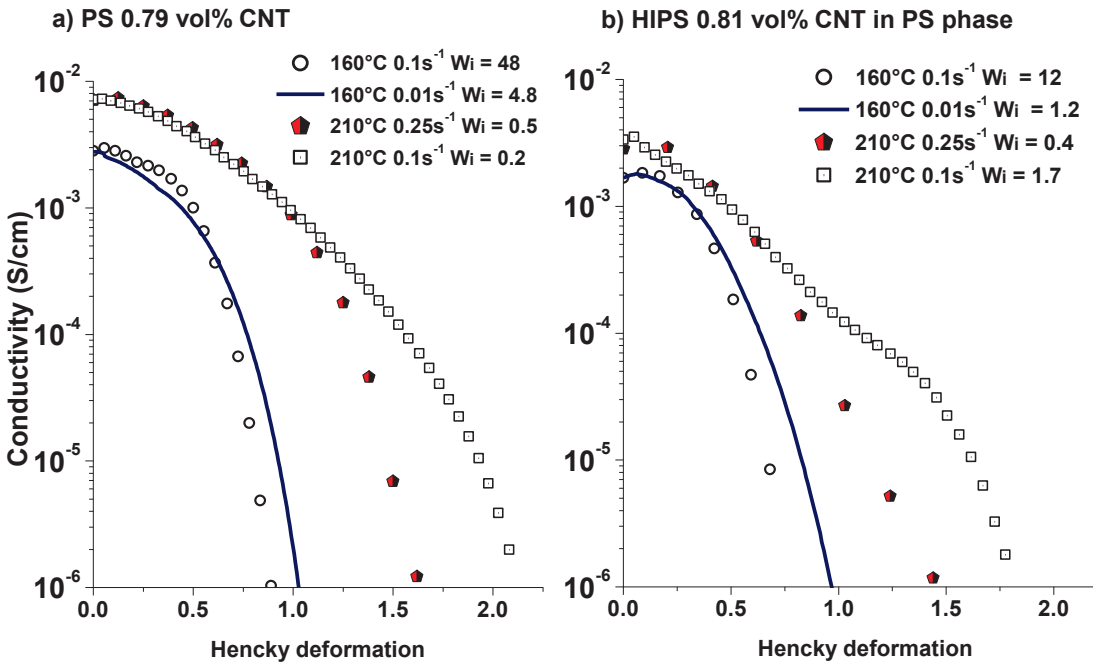

Figure 11: Conductivity variation for PS filled with 0.79 vol% CNT (a) and HIPS filled with 0.81 vol% CNT (b) under extensional conditions that lead to large and low W_i for the two composites.

In addition, a large range of CNT concentrations have been analyzed. Figure 12 and Figure 13 illustrate the conductivity variation during the extensional tests for an extensional rate fixed to 0.1 s^{-1} and two temperatures 180 °C and 200 °C. Moreover, the limiting deformation ε_σ when the specimen conductivity reaches 10^{-6} $S.cm^{-1}$ is plotted as a function of the filler volume fraction for different extensional conditions that cover low to large W_i (see Figure 14 and Figure 15). For the HIPS materials, only the results for specimens with filler concentrations lower than 2.1 vol% have been plotted. Indeed, the specimens filled with larger CNT concentrations were broken very early, that is, for deformations where the conductivity was still high. In Figure 12 and 13 show that the competition is not as pronounced for the HIPS composites than for the PS composites.

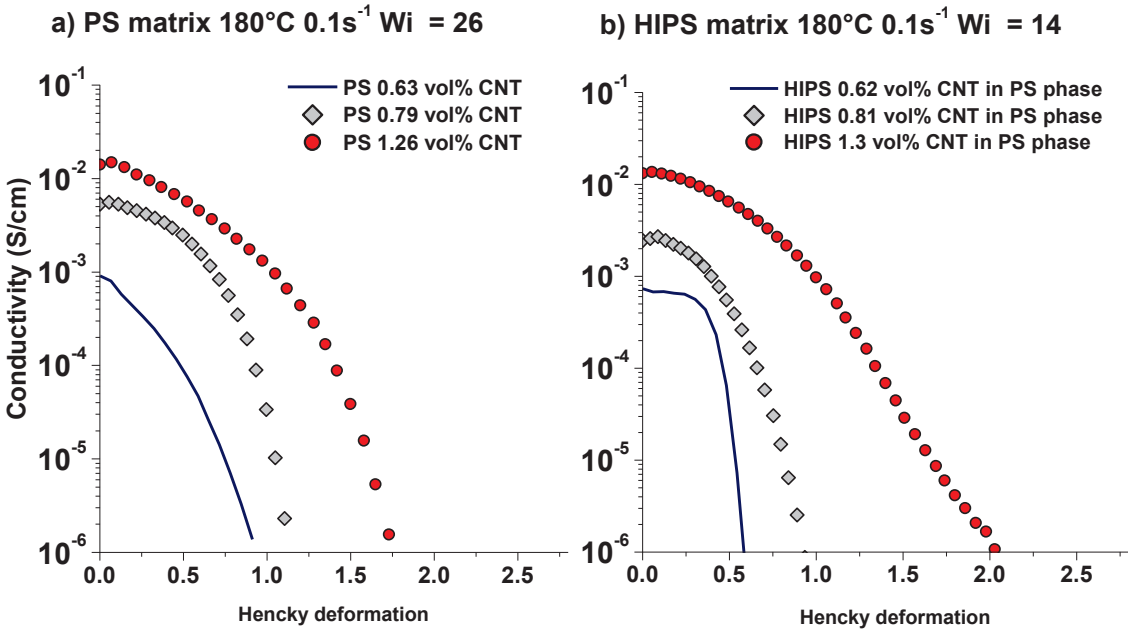

Figure 12: Conductivity evolution of composites under extensional rate fixed at 0.1 s^{-1} at 180 °C a) PS filled with CNT and b) HIPS filled with CNT

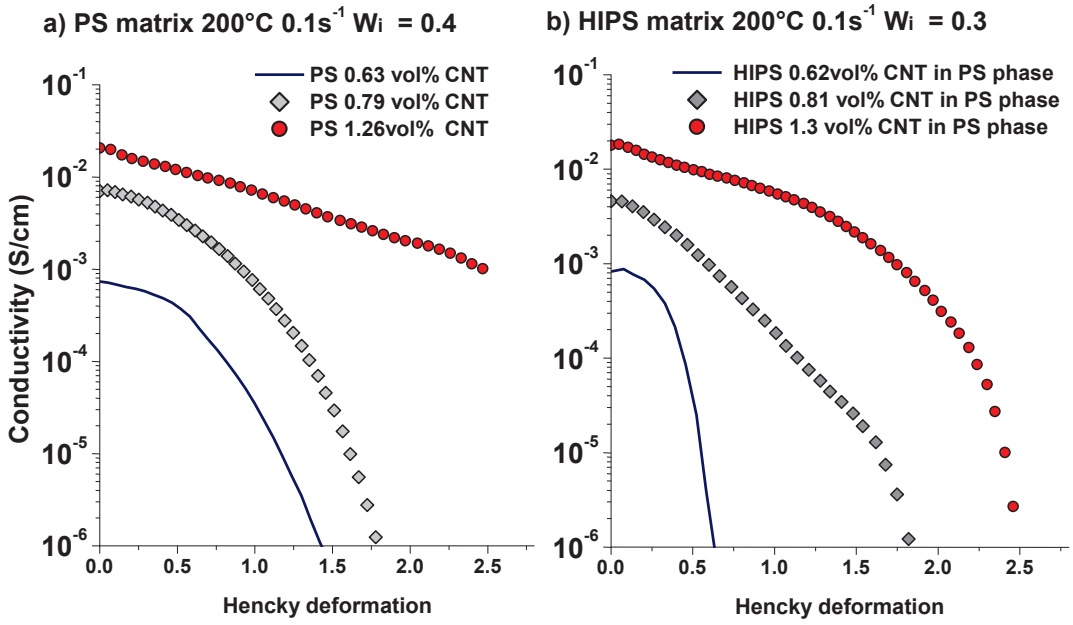

Figure 13: Conductivity evolution of composites under extensional rate fixed at 0.1 s^{-1} at 200 °C a) PS filled with CNT and b) HIPS filled with CNT

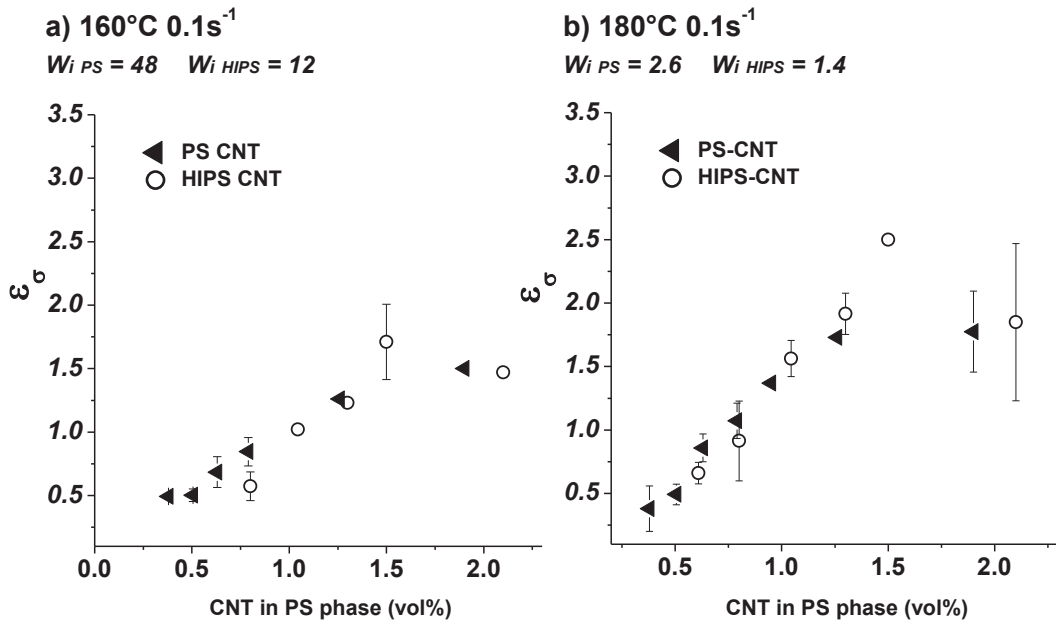

Figure 14 : Evolution of the Hencky strain value when the composites conductivity reaches 10^{-6} S.cm^{-1} as a function of the filler volume fraction for the two types of matrix for specimen under extensional rate fixed at 0.1 s^{-1} at 160 °C a) and at 180 °C b)

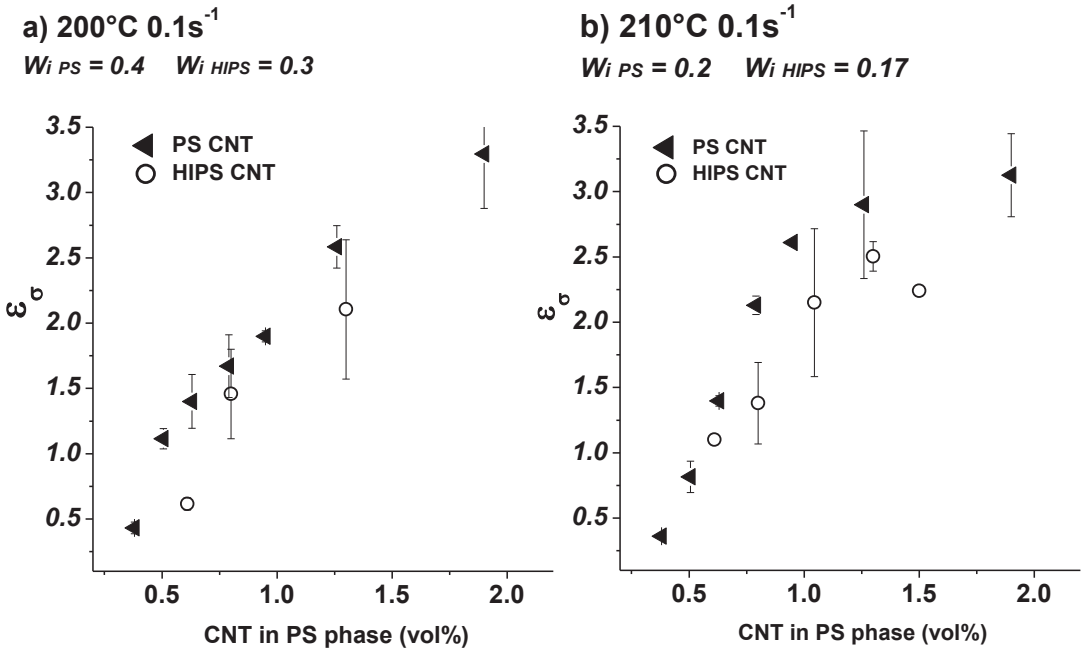

Figure 15 : Evolution of the Hencky strain value when the composites conductivity reaches 10^{-6} S.cm^{-1} as a function of the filler volume fraction for the two types of matrix for specimen under extensional rate fixed at 0.1 s^{-1} at 200 °C a) and at 210 °C b)

At low temperature, composites based on both matrices present close conductivity variations and the obtained ε_σ superimposed remarkably. However, with the increase of the temperature, the composites with the PS matrix show larger ε_σ than with the HIPS matrix. Even if λ_w is larger for the

pure PS than for the PS in the HIPS matrix (see Table 1), the restructuring phenomena appears more pronounced in the pure PS matrix.

The presence of the nodules and the difference in the aggregates size in the HIPS matrix can influence the network destruction under extensional deformation. Indeed, the deformation rate is not homogeneous within the sample. Because of the nodules which are less deformed, the deformation rate is larger in some locations of the PS phase. In addition, the presence of the nodules might strongly prevent the formation of connections between aggregates, especially in the deformation direction and consequently, enhance the destruction of the network. Finally, the difference in the filler dispersion state must be kept in mind as only isolated CNTs and disentangled group of CNTs can acquire sufficient mobility of the matrix. The concentration of this population may be different for the two matrices and may impact the restructuring mechanisms.

IV. Conclusion

In this work, two polymer matrices: a pure PS and a rubber-modified PS filled with Carbon Nanotubes have been analyzed in order to put in the light the influence of the restricted volume for the fillers. Indeed, it has been observed that the forces confinement of the filler in the PS continuous phase of the HIPS leads to the achievement of composites with a very lower percolation threshold. Indeed, the HIPS material which contains about 40 volume percent of nodules gives the possibility to decrease by a factor of about 2 the weight fraction of CNTs, while preserving the same conductivity compared to the pure PS matrix. The resulting elastic networks in the two composites are slightly different and this has been attributed to the difference in the dispersion state and more precisely the difference in the size and density of agglomerates that constitute the filler network.

The dynamics of the structuring and destruction of the filler network have been investigated in quiescent conditions and under extensional deformation. Like in the PS/CNT materials, the polymer dynamics in the rubber-modified matrix governs the structuring mechanism.

The competition between structuring and destruction of the network can be weighted thanks to the Weissenberg number defined as the product of the deformation rate and the weight average relaxation time of the matrix. When the restructuring is negligible during the deformation, the two composites have the same limiting deformation before becoming electrically insulating. However, at low W_i, when the restructuring mechanism can compete with the destruction induced by the deformation, the PS/CNT composite shows larger limiting deformation than the rubber-modified composite. Indeed, the restructuring phenomenon is limited for the HIPS/CNT specimens, even if the relaxation time is lower. This has been attributed to the presence of the nodules that can prevent locally the formation of connections between aggregates and induces non homogeneous deformation rate within the specimen.

In addition, a strong deviation from the Trouton's ratio of 3 combined with small strain at break has been observed for the HIPS/CNT specimens when the filler concentration is larger than 1.5 vol%. The amount of CNTs impacts the polymer chains mobility and consequently decreases the material properties.

References

[1] Demczyk, B. G.; Wang, Y. M.; Cumingd, J.; Hetamn, M.; Han, W.; Zettl, A.; Ritchie, R. O. Direct mechanical measurement of the tensile strength and elastic modulus of multiwalled carbon nanotubes. *Materials Sciences Engineering* A **2002**, 334, 173-178.

[2] Walters, D. A.; Ericson, L.M.; Casavant, M.J.; Liu, J.; Colbert, D. T.; Smith, K.A.; Smalley, R. E. Elastic strain of freely suspended single-wall carbon nanotube ropes. *Applied Physics Letters* **1999**, 74,3803-3805

[3] Yao, Z.; Kane, C.L.; Dekker, C. High-field electrical transport in single-wall carbon nanotubes. *Physical Review Letters* **2000**, 61, 2941.

[4] Berber, S.; Kwon, Y.-K.; Tománek, D. Unusually high thermal conductivity of carbon nanotubes. *Physical Review Letters* **2000**, 84, 4613–4616.

[5] Sumita, M.; Sakata, K.; Asai, S.; Miyasaka, K.; Nakagawa, H. Dispersion of fillers and the electrical conductivity of polymer blends filled with carbon black. *Polymer Bulletin* **1991**, 25, 265-271.

[6] Sumita, M.; Sakata, K.; Hayakawa, Y.; Asai, S.; Miyasaka, K.; Tanemura, M. Double percolation effect on the electrical conductivity of conductive particles filled polymer blends. *Colloid and Polymer Science* **1992**, 270, 134-139.

[7] Gödel, A.; Kasaliwal, G.; Pötschke, P. Selective localization and migration of multiwalled carbon nanotubes in blends of polycarbonate and poly(styrene-acrylonitrile). *Macromolecular Rapid Communications* **2009**, 30, 423-9.

[8] Périé, P.; Brosse, A. C.; Tencé-Girault, S.; Leibler, L. Co-continuous nanostructured nanocomposites by reactive blending of carbon nanotube masterbatches. *Polymer* **2012**, 53, 984-992.

[9] Thongruang, W.; Balik, C. M.; Spontak, R. J. Volume-exclusion effects in polyethylene blends filled with carbon black, graphite, or carbon fiber. *Journal of Polymer Science Part B: Polymer Physics* **2002**, 40, 1013–1025

[10] Warth H., M. Mechanical properties and electrical conductivity of carbon-nanotube filled polyamide-6 and its blends with acrylonitrile/ butadiene/styrene. *Polymer* **2004**, 45, 739–48.

[11] Pötschke, P.; Bhattacharyya, A.R.; Janke, A. Morphology and electrical resistivity of melt mixed blends of polyethylene and carbon nanotube filled polycarbonate. *Polymer* **2003**, 44 , 8061–9.

[12] Göldel, A.; Marmur, A.; Kasaliwal, G. R.; Pötschke, P.; Heinrich, G. Shape-Dependent Localization of Carbon Nanotubes and Carbon Black in an Immiscible Polymer Blend during Melt Mixing. *Macromolecules* **2011**, 44, 6094–6102.

[13] Pötschke, P.; Pegel, S.; Claes, M.; Bonduel, D., A novel strategy to incorporate carbon nanotubes into thermoplastic matrices. *Macromolecular Rapid Communications* **2008**, 29 (3), 244–251.

[14] Wu, M.; Shaw, L. L. J. On the improved properties of injection-molded, carbon nanotube-filled PET/PVDF blends. *Power Sources* **2004**, 136 (1), 37–44.

[15] Pötschke, P.; Bhattacharyya, A. R.; Janke, A., Morphology and electrical resistivity of melt mixed blends of polyethylene and carbon nanotube filled polycarbonate. *Polymer* **2003**, 44 (26), 8061–8069.

[16] Young, T. Philosophical Transactions of the Royal Society of London ; Works, edit by Peacock, 1805 Vol. 95, p 432.

[17] Baudouin, A.C.; Devaux, J.; Bailly, C.; Localization of carbon nanotubes at the interface in blends of polyamide and ethylene-acrylate copoly-mer. *Polymer* **2010**, 51, 1341–54.

[18] Göldel, A.; Marmur, A.; Kasaliwal, G.R.; Pötschke, P.; Heinrich, G. Shape-dependent localization of carbon nanotubes and carbon black inan immiscible polymer blend during melt mixing. *Macromolecules* **2011**, 44, 6094–102.

[19] Göldel, A.; Kasaliwal, G.; Pötschke, P. Selective localization andmigration of multiwalled carbon nanotubes in blends of polycarbo-nate and poly(styrene-acrylonitrile). *Macromolecular Rapid Communications*

2009, 30, 423–9.

[20] Zhang L.; Wan C.; Zhang, Y. Morphology and electrical properties of polyamide 6/polypropylene/multi-walled carbon nanotubes composites. *Composites Science and Technology* **2009**, 69, 2212–7.

[21] Li, L.; Miesch, C.; Sudeep, P.; Balazs, A.C.; Emrick, T.; Russell, T.P.; Hayward, R.C. Kinetically trapped co-continuous polymer morphologies through intraphase gelation of nanoparticles. *Nano Letters* **2011**, 11, 1997-2003.

[22] Chung, H.J.; Ohno, K.; Fukuda, T.; Composto, R.J. Self-regulated structures in nanocomposites by directed nanoparticle assembly. *Nano Letters* **2005**, 5, 1878-1882.

[23] Elias, L.; Fenouillot, F.; Majesté, J.-C.; Cassagnau, P. Morphology and rheology of immiscible polymer blends filled with silica nanoparticles, *Polymer* **2007**, 48, 6029-6040.

[24] Du, B.; Handge, U.A.; Wambach, M.; Abetz, C.; Rangou, S.; Abetz, V. Functionalization of MWCNT with p(mma-co-s) copolymers via atrp: influence on localization of MWCNT in SAN/PPE 40/60 blends and on rheological and dielectric properties of the composites. *Polymer* **2013**, 54, 6165-6176.

[25] Bose, S.; Bhattacharyya, A. R.; Kodgire, P. V.; Misra, A. Fractionated crystallization in PA6/ABS blends: Influence of a reactive compatibilizer and multiwall carbon nanotubes. *Polymer* **2007**, 48, 356-362.

[26] Feng, J. Y.; Chan, C. M.; Li, J. X., A method to control the dispersion of carbon black in an immiscible polymer blend. *Polymer Engineering & Science* **2003**, 43 (5), 1058–1063.

[27] Persson, A. L.; Bertilsson, H. Viscosity difference as distributing factor in selective absorption of aluminium borate whiskers in immiscible polymer blends. *Polymer* **1998**, 39(23), 5633–5642.

[29] Stickel, J.J.; Powell, R. L.; Fluid mechanics and rheology of dense suspensions. *Annual Review of Fluid Mechanics* **2005**, 37, 129–149.

[30] Van Puyvelde, P.; Vananroye, A.; Cardinaels, R.; Moldenaers P. Review on morphology development of immiscible blends in confined shear flow. *Polymer* **2008**, 49, 5363–5372.

[31] Baudouin, A.C.; Auhl D.; Tao, F.; Devaux J.; Bailly, C. Polymer blend emulsion stabilization using carbon nanotubes interfacial confinement. *Polymer* **2011**, 52, 149–56.

[32] Baudouin, A.C.; Bailly, C.; Devaux, J. Interface localization of carbon nanotubes in blends of two copolymers. *Polymer Degradation and Stability* **2010**, 95, 389–98.

[33] Xu, Z.; Zhang, Y.; Wang, Z.; Sun, N.; Li, H. Enhancement of electrical conductivity by changing phase morphology for composites consisting of polylactide andpoly (ε-caprolactone) filled with acid-oxidized multiwalled carbon nanotubes. *ACS Applied Materials & Interfaces* **2011**, 3, 4858-4864.

[34] Bharati, A.; Cardinaels, R.; Van der Donck, T.; Seo, J. W.; Wübbenhorst, M.; Moldenaers, P. Tuning the phase separated morphology and resulting electrical conductivity of carbon nanotube filled PaMSAN/PMMA blends by compatibilization with a random or block copolymer. *Polymer* **2017**, 108, 483-492.

[35] Bharati, A.; Cardinaels, R.; Seo, J. W.; Wübbenhorst, M.; Moldenaers, P. Enhancing the conductivity of carbon nanotube filled blends by tuning their phase separated morphology with a copolymer. *Polymer* **2015**, 79, 271-282.

[36] McClory, C.; Pötschke, P.; McNally, T. Influence of screw speed on electrical and rheological percolation of melt-mixed high-impact polystyrene/MWCNT nanocomposites. *Macromolecular Materials and Engineering*, **2011**,296, 59–69.

[37] Shrivastava, N. K.; Maiti, S.; Suin, S.; Khatua, B. B. Influence of selective dispersion of MWCNT on electricalpercolation of in-situ polymerized high-impact polystyrene/MWCNT nanocomposites. *eXPRESS Polymer Letters* **2014**, 8, 15–29.

[38] Klüppel, M.; Heinrich, G. Fractal structures in carbon black reinforced rubbers. *Rubber Chemistry and Technology* **1995**, 68, 623-651.

[39] De Gennes, P.G. On a relation between percolation theory and the elasticity of gels. *Journal of Physics* **1976**, 37, 1–2.

[40] Majeste, J.C.; Vincent, F. A kinetic model for silica-filled rubber reinforcement. *Journal of Rheology* **2015**, 59: 405–427.

[41] Moreira, L.; Fulchiron, R.; Seytre, G.; Dubois, P.; Cassagnau, P. Aggregation of Carbon Nanotubes in Semidilute Suspension, *Macromolecules* **2010**, 43, 1467–1472.

[42] Alig, I; Pötschke, P.; Lellinger, D.; Skipa, T.; Pegel, S.; Kasaliwal, G. R.; Villmow, T. Establishment, morphology and properties of carbon nanotube networks in polymer melts. *Polymer* **2012**, 53, 4–28.

[43] Ma, A. W. K.; Chinesta, F. ; Mackley, M. R. The rheology and modeling of chemically treated carbon nanotubes suspensions. *Journal of Rheology* **2009**, 53, 547–573.

[44] Jouault, N.; Vallat, P.; Dalmas, F.; Said, S.; Jestin, J.; Boué, F. Well-dispersed fractal aggregates as filler in polymer-silica nanocomposites: long-range effects in rheology. *Macromolecules* **2009**, 42, 2031-40.

[45] Jouault, N.; Dalmas, F.; Boué, F.; Jestin, J. Multiscale characterization of filler dispersion and origins of mechanical reinforcement in model nanocomposites. *Polymer* **2012**, 53,761-5.

[46] Klüppel, M.; Schuster, R.; Heinrich, G.; Structure and properties of reinforcing fractal filler networks in elastomers. *Rubber Chemistry and Technology* **1997**, 70, 243-255.

[47] G. Heinrich and M. Klüppel, Kautschuk, The role of polymer-filler interphase in reinforcement of elastomers. *Gummi Kunststoffe* **2004**,57, 452-454.

[48] Klüppel, M. The role of disorder in filler reinforcement of elastomers on various length scales. *Advances in Polymer Science* **2003**, 164, 1-86.

[49] Pötschke, P.; Haeussler, L.; Pegel, S.; Steinberger, R.; Scholz, G. K. Thermoplastic polyurethane filled with carbon nanotubes for electrical dissipative and conductive applications. *Gummi Kunststoffe* **2007**, 60, 432–437.

[50] Pötschke, P.; Abdel-Goad, M.; Alig, I.; Dudkin, S.; Lellinger, D. Rheological and dielectrical characterization of melt mixed polycarbonate-multiwalled carbon nanotube composites. *Polymer* **2004**, 26, 8863-8870.

[51] Hobbie, E. K.; Fry, D. J. Nonequilibrium Phase Diagram of Sticky Nanotube Suspensions. *Physical Review Letters* **2006**, 97, 036101.

[52] Esteban, E.; Ureña-Benavides, Kayatin, M. J.; Virginia, A. D. Dispersion and Rheology of Multiwalled Carbon Nanotubes in Unsaturated Polyester Resin. *Macromolecules* **2013**, 46, 1642−1650.

[53] Li, W., Buschhorn, S. T.; Schulte, K.; Bauhofer, W. The imaging mechanism, imaging depth, and parameters influencing the visibility of carbon nanotubes in a polymer matrix using a SEM. *Carbon* **2011**, 49, 1955-1964.

[54] Li, W.; Bauhofer, W. Imaging of CNTs in a polymer matrix at low accelerating voltages using a SEM. *Carbon* **2011**, 49, 3891-3898.

[55] Bird, R.B.; Armstrong, R.C.; Hassager, O. *In Dynamics of polymeric liquids. Vol. 1, : Fluid mechanics*, 2nd ed.; John Wiley and Sons Inc.,New York 1987; p 784.

[56] Ferry, J.D. *In Viscoelastic properties of polymers* Third edition 1980.

[57] Ferry, J. D.; Williams, M. L.; Fitzgerald, E. R. The temperature dependence of relaxation mechanisms in amorphous polymers and other glass-forming liquids. *Journal of the American Chemical Society* **1955,** 77(14), 3701-3707.

[58] Marcourt, M.; Cassagnau, P.; Fulchiron, R. An original combined method for electrical conductivity measurement of polymer composites under extensional deformation. *Journal of Rheology* **2017**, 61, 845.

[59] Barber, A.; Cohen, S.; Wagner, H. Static and dynamic wetting measurements of single carbon nanotubes. *Physics Review Letters* **2004**, 92, 186103.

[60] Yao Sun, Zhao-Xia Guo, Yu, J. Effect of ABS Rubber Content on the Localization of MWCNTs in PC/ABS Blends and Electrical Resistivity of the Composites. *Macromolecular Materials and Engineering* **2010**, 295(3), 263–268.

[61] Kirkpatrick, S. Percolation and conduction. *Reviews of Modern Physics* **1973**, 45,574–88.

[62] Bauhofer, W.; Kovacs, J. Z. A review and analysis of electrical percolation in carbon nanotube polymer composites. *Composites Science and Technology* **2009**, 69, 1486–1498.

[63] Balberg, I.; Binenbaum, N.; Wagner, N. Percolation thresholds in the 3-dimensional sticks system. *Physical Review Letters* **1984**, 52, 1465–1468.

[64] Rahatekar, S.S.; Koziol, K.K.; Kline, S.R.; Hobbie, E.K.; Gilman, J.W; Windle, A.H. Length-Dependent Mechanics of Carbon-Nanotube Networks. *Advanced Materials* **2009**, 21, 874–878.

[65] Alig, I.; Skipa, T.; Lellinger, D.; Pötschke, P. Destruction and formation of a carbon nanotube network in polymer melts: Rheology and conductivity spectroscopy. *Polymer* **2008**, 49 3524-3532.

[66] Shih, W.-H.; Shih, W. Y.; Kim, S.-I.; Liu, J.; Aksay, I. A. Scaling behavior of the elastic properties of colloidal gels. *Physical Review A* **1990**, 42, 4772−4779.

[67] Khalkhal, F.; Carreau, Scaling behavior of the elastic properties of non-dilute MWCNT–epoxy suspensions. P. *Rheologica Acta* **2011**, 50, 717−728.

[68] Mall, S.; Russel, W. Effective Medium Approximation for an Elastic Network Model of Flocculated Suspensions. *Journal of Rheology* **1987**, 31, 651–681.

[69] Chen, M.; Russel, W. Characteristics of flocculated silica dispersions. *Journal of Colloid and Interface* **1991**, 141, 564–577.

[70] Wolthers, W.; Vandenende Null, D.; Breedveld, V.; Duits M.; Potanin, A.; Wientjes R.; Mellema, J. Linear viscoelastic behavior of aggregated colloidal dispersions. *Physical Review E* **1997**, 56, 5726–5733.

[71] Schneider, C.A.; Rasband, W.S.; Eliceiri, K.W. NIH Image to ImageJ: 25 years of image analysis. *Nature Methods* **2012**, 9, 671-675.

[72] Smith Jr., T.G.; Lange, G.D.; Marks, W.B.; Fractal Methods and Results in Cellular Morphology. *Journal of Neuroscience Methods* **1996**, 69, 1123-126.

[73] Weinberger, C.B.; Goddard J.D. Extensional flow behavior of polymer solutions and particle suspensions in a spinning motion. *International Journal of Multiphase Flow* **1974**, 1, 465-486

[74] Krishnamoorti, R.; Ren, J.; Silva, A. Shear response of layered silicate nanocomposites. *The Journal of Chemical Physics* **2001**, 114, 4968–4973.

[75] Barroso, V. C.; Ribeiro, S. P.; Maia, J. M. Unusual extensional behavior of a polystyrene/HIPS blend. *Rheolica Acta* **2003** 42, 483-490.

[76] Alig, I.; Lellinger, D.; Dudkin, S. M.; Pötschke, P. Conductivity spectroscopy on melt processed polypropylene-multiwalled carbon nanotube composites: recovery after shear and crystallization. *Polymer* **2007a**, 48, 1020–1029.

[77] Alig, I.; Skipa, T.; Engel, M.; Lellinger, D.; Pegel, S.; Pötschke, P. Electrical conductivity recovery in carbon nanotube polymer composites after transient shear. *Physica Status Solidi B: Basic Solid State Physics* **2007b**, 244, 4223–4226.

[78] Alig, I.; Lellinger, D.; Engel, M.; Skipa, T.; Pötschke, P. Destruction and formation of a conductive carbon nanotube network in polymer melts: in-line experiments. *Polymer* **2008a**, 49, 1902–1909.

[79] Alig, I.; Skipa, T.; Lellinger, D.; Bierdel, M.; Meyer, H. Dynamic percolation of carbon nanotube agglomerates in a polymer matrix: comparison of different model approaches. *Physica Status Solidi B:Basic Solid State Physics* **2008c**, 245, 2264–2267.

[80] Alig, I.; Skipa, T.; Lellinger, D.; Pötschke, P. Destruction and formation of a carbon nanotube network in polymer melts: rheology and conductivity spectroscopy. *Polymer* **2008d**, 49, 3524–3532.

Chapter 5

Evolution of the Carbon Nanotubes network of molten nanocomposites under extensional deformation

Abstract

This work is dedicated to analyzing the variation of conductivity of polymer composites (polystyrene filled with Carbon Nanotubes) under extensional deformation. In a previous work, a conductor-insulator transition has been observed and the predominant role of the polymer dynamics has been brought to light. The evolution of the filler network within a polymer matrix can be described by a kinetic equation that takes into account a structuring mechanism that is controlled by the mobility in the melt matrix and a destruction mechanism that is induced by the extensional deformation. The solution of this equation that describes the filler network at a microscale is used in the percolation law to obtain the macroscopic conductivity of the composite. It turned out that the structuring parameter does not depend on the extensional deformation but only relies on the polymer matrix dynamics. In addition, the breaking parameter only depends on the Hencky strain, whatever the extensional rate. This model has been successfully applied for a large range of filler concentrations and experimental conditions from low to large Weissenberg numbers.

Keywords: Nanocomposites; Carbon Nanotubes, Extensional Viscoelasticity; Electrical conductivity; Modeling.

Reformatted version of paper submitted in:

ACS Applied Materials and Interfaces in February 2018

A model for the electrical conductivity variation of molten polymer filled with carbon nanotubes under extensional deformation

Marjorie Marcourt, Philippe Cassagnau, René Fulchiron[a)],

Univ Lyon, Université Claude Bernard Lyon 1, CNRS UMR 5223, Ingénierie des Matériaux Polymères, F-69622, Villeurbanne Cedex, France

Dimitri Rousseaux, Olivier Lhost, Simon Karam

Total Research and Technology Feluy Zone Industrielle Feluy C 7181 Feluy, Belgium

I. Introduction

The addition of electrically conductor nanofillers especially Carbon Nanotubes is a promising solution for the achievement of Conductor Polymer Composites (CPC). Owing to their large aspect ratio, only a small amount of fillers can turn an insulating polymer matrix to a composite with moderate electrical properties [1-3]. The preferred and reliable method for the filler incorporation is the melt mixing and more precisely the masterbatch dilution that can lead to suitable filler dispersion and distribution within the matrix [4]. Leaving apart all the parameters that must be taken into account (mixing duration, shear rates, filler functionalization) the generation of CPC with suitable electrical properties relies on the formation of a homogeneous network made of small aggregates, disentangled amounts of CNTs and individual CNTs [5-7].

The use of rheological analysis combined with conductivity monitoring has paved the way for the comprehension of the filler network behavior in molten composites under both quiescent and small shear strain [8]. Indeed, the “dynamic percolation” [5,9-13] and the conductor/insulator transition [14,15] have been brought to light. Those two specific mechanisms illustrate the huge capacity of the filler structure to evolve. The network build-up has been explained by Alig *et al*. [5] as the combination between strong dispersive interactions between nanotubes and depletion interactions between the diffusion of isolated CNTs that is made possible if the polymer viscosity is sufficiently low [16]. The network destruction is more complex and is intimately linked to the filler network structure. In fact, it has been observed that under shear deformation at large shear rates [17] or under extensional deformation [16] the agglomerates are stretched and orient in the deformation direction.

The aggregates network morphology changes in response to strains and, more precisely, its response

is linked to its initial morphology [15,18,19] Similarly to highly filled materials whose flow behavior depends on the filler network structure, the electrical properties of CPC are also intimately linked to the filler network structure. The structural evolution of highly filled material has been widely investigated and is well described by a kinetic equation introduced by Barnes [20] for heterogeneous materials as [21-26].

$$\frac{d\xi}{dt} = a(1-\xi)^b + c\xi\dot{\gamma}^d$$

Equation 1

where ξ is a structural parameter that describes the filler agglomeration state : ξ = 1 the network is at equilibrium and ξ = 0 the network is fully broken. The constants *a*, *b*, *c* and *d* are linked to the material. The first term describes the network reinforcement and the second depending on the sign of *c* illustrates the shear-induced agglomeration or the shear-induced destruction. For instance, Leonov *et al.* [26] have argued that the breakup depends on the second invariant of the rate of deformation $II_{\dot{\gamma}}$.

The description of the conductivity variation due to the CNT network evolution has been first investigated by Alig *et al*. [5,14].They combined a kinetic equation, which describes the evolution of the fraction of agglomerates which contributes to the conduction (φ_{eff}), with a percolation law which associates the filler microstructure to the electrical properties of the composite.

$$\frac{d\varphi_{eff}}{dt} = k_0(\varphi - \varphi_{eff})^n + k_1\left(\varphi - \varphi_{eff}\right) - k_2\varphi_{eff}$$

Equation 2

where φ is the filler total fraction, considering that, at equilibrium (when $t \to \infty$) all the CNTs contribute to the conductive network, φ_{eff} is the volume fraction of conductive agglomerates k_0, k_1 and k_2 are the kinetic coefficients for respectively quiescent agglomeration, shear-stimulated agglomeration and shear-stimulated destruction process. It must be noticed that k_1 and k_2 depends on the shear rate $\dot{\gamma}$. First Alig *et al*. argued that the network building was a second order mechanism (*n*=2) considering the agglomeration process as a clustering mechanism in which two non-conductive particles stick together to create an electrically conductor agglomerate. Later, Skipa and coworkers [19,20] have shown that the value of *n* equal to 1 leads to similar fit on their experimental data. Then, the solution of the kinetic equation is introduced into the percolation law that describes the macroscopic behavior of the composite. This model well fit the different conductivity evolutions observed under shear deformation at small shear rates. Indeed, it can, for instance, describe the interplay between build-up and destruction when the conductivity curve merges to a steady value [2, 20]. The evolution of k_0 remained unexplained even if the authors highlighted the influence of the

temperature on the conductivity recovery. In addition, Alig and coworkers [27] have observed large difference between the reaction rate k_0 for conductivity recovery experiments of comparable specimens. Surprisingly, for a shear-induced agglomeration that led to an increase of conductivity greater than six decades, they observed that the sum of the structuring parameter was very close to the breaking parameter. Moreover, they have proposed a destruction rate that depends on the shear rate (see Equation 2) [19,20] but did not deduce an obvious relation from the fitted parameters.

In this paper, the model proposed by Skipa [19,20] (see Equation 2) will be tested for extensional deformation on a polystyrene matrix filled with Carbon Nanotubes. Then, a new approach and, more precisely, a new form for the extensional-stimulated destruction will be introduced and applied to the composite under extensional deformation.

II. Experimental section

A. Materials description and characterization

1. Composites

The CNTs are the NC7000 supplied by Nanocyl, a Belgian company. They are characterized by a diameter *d* around 9.5 nm and a mean length of 1.5 µm. The matrix used is a polystyrene (PS) with a melt flow index of 2.4 supplied by Total. The composites were melt mixed using a masterbatch dilution strategy and were supplied by Total as pellets. The specimens were compression molded at 200°C following a specific protocol of temperature and pressure.

2. Conductivity measurement

Electrical properties analysis has been conducted on compression molded samples that have been additionally submitted to a quiescent treatment at 200°C for around 20 min. This supplementary thermal treatment enables the filler network to recover an equilibrium state in which most of the CNTs take part to the electrical conduction. Indeed, just after the compression molding, this state is not obtained. Colloidal silver paste was applied on the sample surface to ensure a good contact between the electrodes and the specimen. Owing to a Keithley 237 power supply, a 10 volt Direct Current (DC) is delivered and the current passing through the sample is measured. The volume conductivity is then deduced using the specimen geometry as:

$$\sigma = \frac{L.I}{S.U}$$

Equation 3

with *U* the applied voltage, *I* the measured current, *L* and *S* respectively the specimen length and section. From these experiments, the percolation law linking the conductivity to the effective CNT's fraction was determined on specimens that have been annealed [16]:

$$\sigma = \sigma_0(\varphi_{eff} - \varphi_c)^{\beta}$$

Equation 4

with $\varphi_{eff}$the volume fraction of CNTs which contribute to the conduction and φ_c the percolation

threshold. It must be added that, since the samples have been annealed to determine the parameters of this law, the efficient fraction (φ_{eff}) of CNTs can be assimilated to the total fraction (φ). The obtained exponent β is 2.2 with a percolation threshold φ_c at 0.19 vol% and a pre-factor σ_0 of 630 S.cm^{-1}.

3. Extensional deformation combined with conductivity measurement

Extensional experiments were carried out with a commercialized Extensional Viscosity Fixture EVF (TA instruments) mounted on the ARES rheometer (TA Instruments). The set-up was modified in order to measure the specimen conductivity during the extensional test. This specific set-up has already been detailed in an earlier work [16]. In some cases, the measurements have been carried out on samples directly after their compression molding without the annealing treatment. By this way, the structuring mechanism is not fully accomplished at the beginning of the experiment so that it can be caught during the measurements.

4. Data fitting

The kinetic equation was numerically solved using the software Scilab. All the fitting parameters presented in this work were obtained by the means of a non-linear least squares regression method.

III. Application of the model proposed by Skipa *et al.* [19,20]

A. Analysis of the model for large and low W_i

The model proposed by Skipa and coworkers was applied on our experimental data. Contrary to Skipa and coworkers who have analyzed the conductivity evolution of molten composites under shear deformation, here, the filler network evolution under extensional deformation is analyzed. In a previous work [16], it has been shown that the competition between network building and destruction can be described using the Weissenberg number (W_i) that is the product between a characteristic relaxation time of the material and the extensional rate. The characteristic time is taken as the weight average relaxation time deduced from a *N* modes Maxwell model applied on the master curve of the pure matrix [28-30]. At low W_i values, there is a strong competition between the two mechanisms, while at large W_i, the destruction is predominant. Contrary to shear deformation, no structuring network induced by the extensional deformation has been observed. Indeed, an insulating material will remain insulating under extensional deformation whereas under shear the conductivity can somehow increase [6]. Figure 1 and Figure 2 display the experimental data fitted by the model proposed by Skipa *et al*. respectively for large and medium W_i and low W_i. The factor k_1' which represents the kinetic factor for the network building is the sum k_0 and k_1 (see Equation 1) and k_2 is the factor for the network shear induced break.

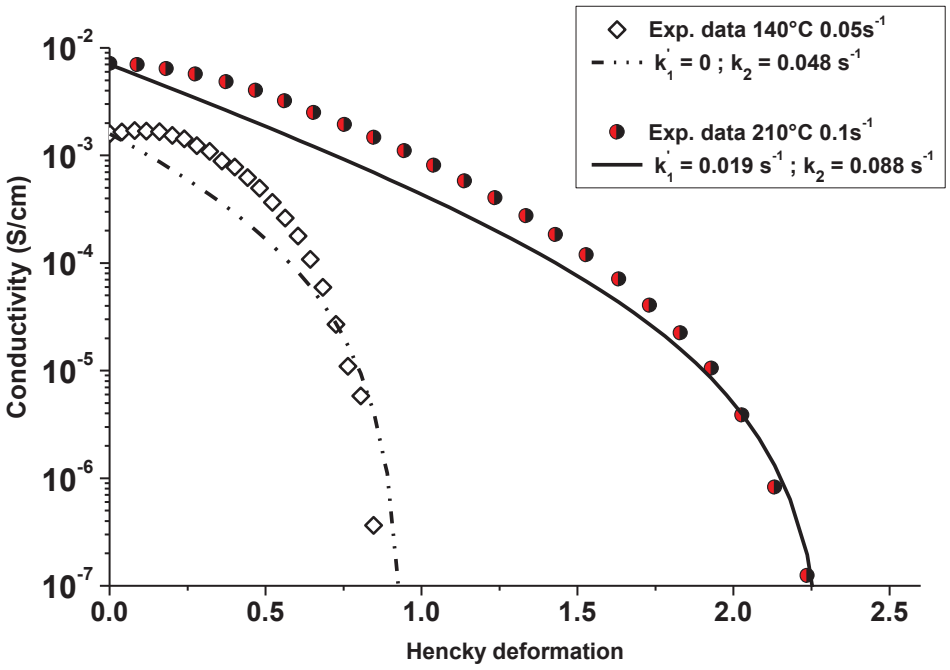

Figure 1: Conductivity variation as a function of the Hencky deformation of PS/MWCNT (0.79 vol% MWCNT) at 210°C, 0.1 s^{-1} and at 140 °C, 0.05 s^{-1}. The solid and dotted lines are the curves calculated by the model proposed by Skipa et al. [19,20]

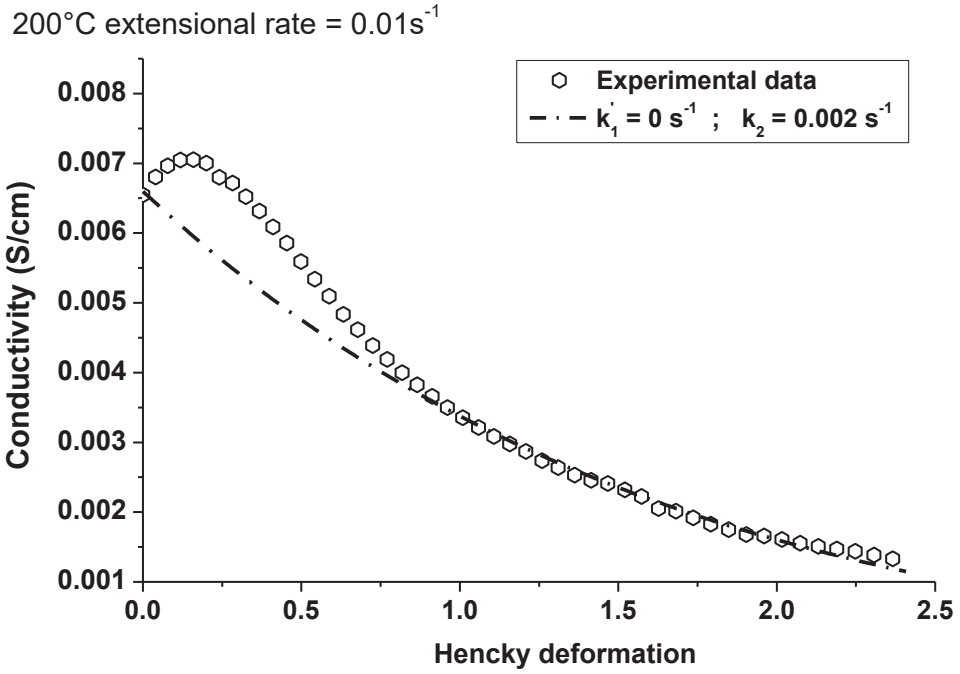

Figure 2: Conductivity variation as a function of the Hencky deformation PS/MWCNT (0.79 vol% MWCNT) at 200 °C, 0.01 s^{-1}. The semi-dotted line indicates the obtained best fit (which actually led to a value of k_1' of 0.

In Figure 1, the fitting is quite acceptable for the experimental conditions. In fact, experimental and calculated data merge. The deformation corresponding to the conductivity breakdown is well determined by the model. However, at low deformation, the difference between the experimental and calculated data is non-negligible.

At low W_i, the model of Skipa *et al.* shows strong limitations. Indeed, when there is a strong competition between network structuring and destruction (see Figure 2) the model fails at fitting the experimental data. A strong interplay between destruction and network build-up, which is characterized by a slight conductivity increase followed by a slow conductivity decrease is observed. However, the model of Skipa *et al*. cannot describe such a behavior. Indeed, the calculated result is inevitably monotonic so that a conductivity growth followed by a decrease cannot be taken into account. This is obviously in discrepancy with the experiment as the conductivity first increases illustrating strong network reinforcement. Moreover, for the experiment shown in Figure 2, if k_1' is not imposed to 0, the fitting leads to the prediction of a steady conductivity value for high deformations contrary to the experiment. The maximum observed in Figure 2 that illustrates the briefly predominance of the building mechanism could have been fitted by the enlargement of this model to different CNTs populations present in the specimen as proposed by Skipa *et al*. [20]. However, that would have induced an increase of the adjustable parameters. For instance, a model with a three-population of aggregates generates six parameters. Consequently, they concluded that the solution of the regression is not unique and it is hard to give a physical meaning to all the set of parameters.

In the following, a new form for the variation of the filler network under extensional deformation will be proposed.

IV. Description of the proposed model

A. Kinetic equation

1. Network structuring

The CNT network is made of aggregates that are connected together by individual CNTs or highly disentangled group of CNTs that constitute junctions between aggregates. Thermal diffusion triggers the formation of junctions and hence the filler network reinforcement [16]. The structuring rate depends on the difference from the equilibrium state in a manner analogous to the model of Skipa *et al.*. Even if we have been very cautious of the specimen's preparation, it remains possible that the initial state can slightly vary. The difference will be observed for specific specimens and will be detailed later in this work. The effective filler fraction that takes part to the conductivity is considered as the structural variable. Hence, the network structuring kinetic is given by:

$$\left.\frac{d\varphi_{eff}}{dt}\right|_{structuring} = k_{build}(\varphi - \varphi_{eff})$$

Equation 5

where φ_{eff} is the filler that belongs to the percolated network; φ is the total filler concentration in the specimen and consequently, the upper limit of φ_{eff}. It can be pointed out that ξ appearing in Equation 1 [20] would be φ_{eff}/φ in our notation. The parameter k_{build} has the dimension of the inverse time. The aggregation and the formation of connections can only be disrupted by deformation. Indeed, the theoretical energy required to counter the strong attractive forces between CNTs is around $1000k_BT$ (T is the temperature and k_B is the Boltzman's constant) [31]. The structuring mechanism is pretty complex and embraces different mechanism at different scale but for states relatively close to the equilibrium, Equation 5 is acceptable. The filler network can be seen as a 3D structure made of CNTs. All the CNTs can be considered as equivalent sites for the binding of isolated CNTs or small aggregates.

2. Network break-up

In our previous work, it has been shown that, under extensional deformation, the aggregates and CNTs of an isotropic filler network orientate in the deformation direction. Thus, it can be considered that, the CNT network is first stretched and then, the CNTs are strained apart from each other as indicated in Figure 3. The first step does not induce major conductivity evolution as the orientation does not or very slightly impact of connections within the network [32,33]. Thus it can be

assumed that extensional strains do not induce any increase of the number of connections. Depending on the experimental conditions, this stage can take more or less time. However, when the CNTs are fully extended, the deformation will progressively pull apart the CNTs and the aggregates from each other. The number of connections will progressively decrease and so will the conductivity.

Figure 3 : Evolution of the filler network under extensional deformation

In Figure 3, the number of connections that are represented by the grey circles does not vary in early stage but dramatically decreases when the CNTs are fully extended. In that sense, the destruction of the filler network will be considered as directly dependent on the Hencky strain. Thus, the network breakup is expressed by:

$$\varphi_{eff} = \varphi e^{-(k_{break}\varepsilon^2)}$$

Equation 6

where k_{break} is the adimensional breaking parameter. It can be noted that this last expression is a simple sigmoid decreasing from φ to 0.

For extensional measurements, where $\varepsilon = \dot{\varepsilon}t$, the time derivative of equation 4 leads to

$$\left.\frac{d\varphi_{eff}}{dt}\right|_{destruction} = -2k_{break}\dot{\varepsilon}^2\,\varphi_{eff}t$$

Equation 7

It can be added that, a priori, the breaking parameter k_{break} may be dependent on the extensional rate. This will be discussed further. The evolution of the CNTs that belongs to the percolated network is the sum of the building (Equation 5) and destruction (Equation 7) parts.

$$\frac{d\varphi_{eff}}{dt} = k_{build}\left(\varphi - \varphi_{eff}\right) - 2k_{break}\dot{\varepsilon}^2\,\varphi_{eff}t$$

Equation 8

The solution of the equation is then inserted into the percolation law (see Equation 4) to obtain the evolution of the conductivity as a function of the Hencky deformation or time. The initial filler effective concentration φ_0 is also determined by means of the percolation law, simply adjusting φ_0 to calculate the initial conductivity (if the material is not initially at equilibrium). Then, using a nonlinear least square regression algorithm, the two parameters k_{build} and k_{break} were fitted to the experimental data.

B. Analysis of the model under extensional deformation

1. Determination of the parameters

In previous work, we have shown that the conductivity variation of CPC under extensional deformation can be linked to the Weissenberg number expressed as:

$$W_i = \lambda_w . \dot{\varepsilon}$$

Equation 9

As the filler has no major impact on the whole composite rheological behavior, the weight average relaxation time of the pure matrix is taken as the characteristic time. For low W_i, there is a strong competition between the network restructuring and break. However, at large W_i, the destruction is predominant and from this point all the curves merge to the same maximal deformation, that is when the specimen become electrically insulating. Figure 4 shows on a linear scale the measured and calculated conductivities for low W_i. These results can be compared to those given by Skipa (-see Figure 2). Clearly, the model proposed in the present work better describes the experimental data. Figure 5 and Figure 6 display conductivity variation on a logarithmic scale of PS/MWCNT (0.79 vol %) under experimental conditions that comprise large and low W_i. Firstly, the breaking and building parameters have been determined for a large number of experimental data that cover low and medium W_i. In those specific conditions there is a strong competition between network building and breaking so reliable values of k_{build} and k_{break} can be determined. The obtained values are displayed in Table 1.

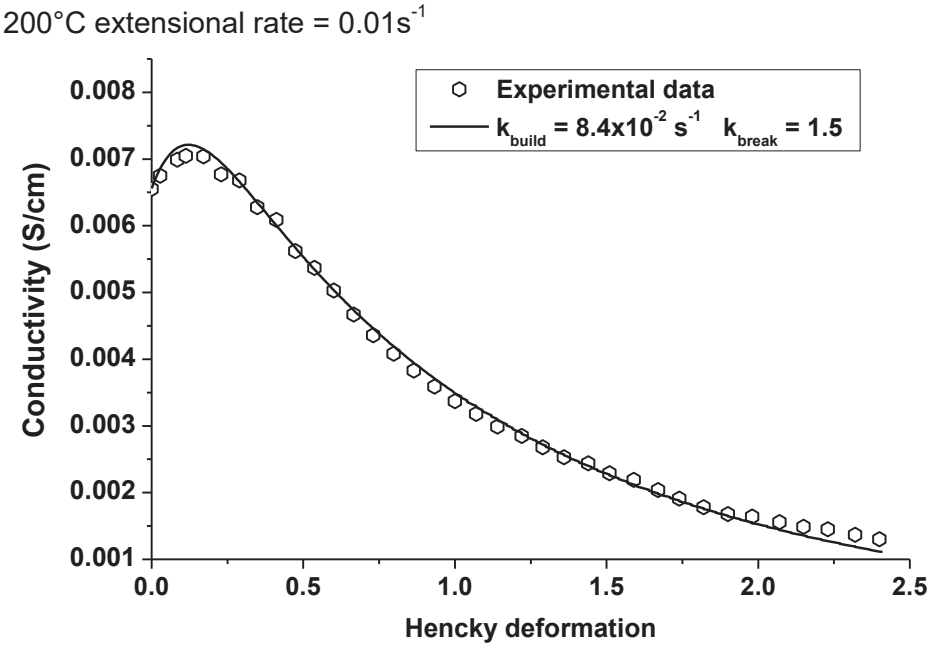

Figure 4: Conductivity variation as a function of the Hencky deformation of PS/MWCNT (0.79 vol%) for low W_i displays on linear scale. The unfilled symbols are the experimental data and the lines are the calculated curves.

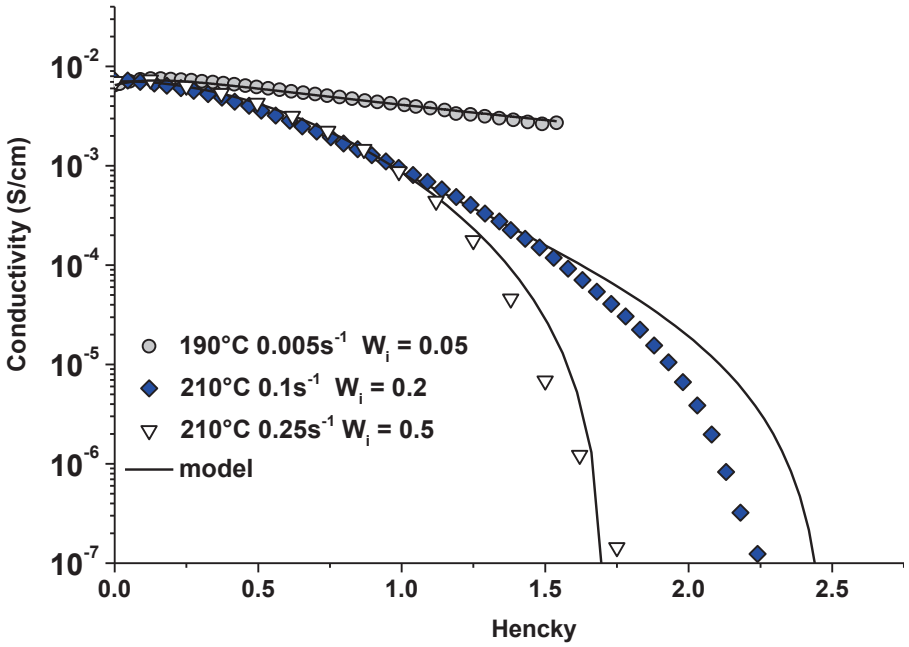

Figure 5: Conductivity variation as a function of the Hencky deformation of PS/MWCNT (0.79 vol%) for low W_i. The symbols are the experimental data and the solid lines are the calculated curves.

Table 1 fitted building and breaking parameters for large and low values of W_i

Specimens	Temperature °C	Extensional rate (s^{-1})	W_i	k_{break}	k_{build} (s^{-1})
PS+0.79 vol% CNT	200	0.01	$4.2x10^{-2}$	1.4	$8.4x10^{-2}$
	190	0.01	$9.5x10^{-2}$	0.6	$2.2x10^{-1}$
	190	0.005	$4.7x10^{-2}$	1.1	$3.8x10^{-2}$
	210	0.05	0.1	1.5	$1.9x10^{-1}$
	210	0.1	0.2	1.4	$2.0x10^{-1}$
	200	0.05	0.2	$7.8x10^{-1}$	$1.2x10^{-1}$
	180	0.01	$2.6x10^{-1}$	1.6	$1.6x10^{-2}$
	200	0.1	0.4	1.0	$9.3x10^{-2}$
	170	0.005	$4.6x10^{-1}$	$5.5x10^{-1}$	$2.2x10^{-3}$
	210	0.25	$5.3x10^{-1}$	$8.1x10^{-1}$	$1.5x10^{-1}$
	210	0.4	0.8	1.4	$1.9x10^{-1}$
	170	0.01	0.9	$8.5x10^{-1}$	$2.9x10^{-3}$
	180	0.1	2.6	1.2	$2.6x10^{-2}$
	180	0.1	2.6	1.1	$1.6x10^{-2}$
	190	0.4	3.8	1.4	$3.1x10^{-2}$

The results displayed in Table 1 show that the breaking parameter is practically independent of the temperature and the extensional rate. For very large W_i, that is for large extensional rates and low temperatures, it was not possible to adjust the structuring parameter because the structuring mechanism was not noticeable in the measured conductivity. In that specific case, only the breaking parameter has been determined.

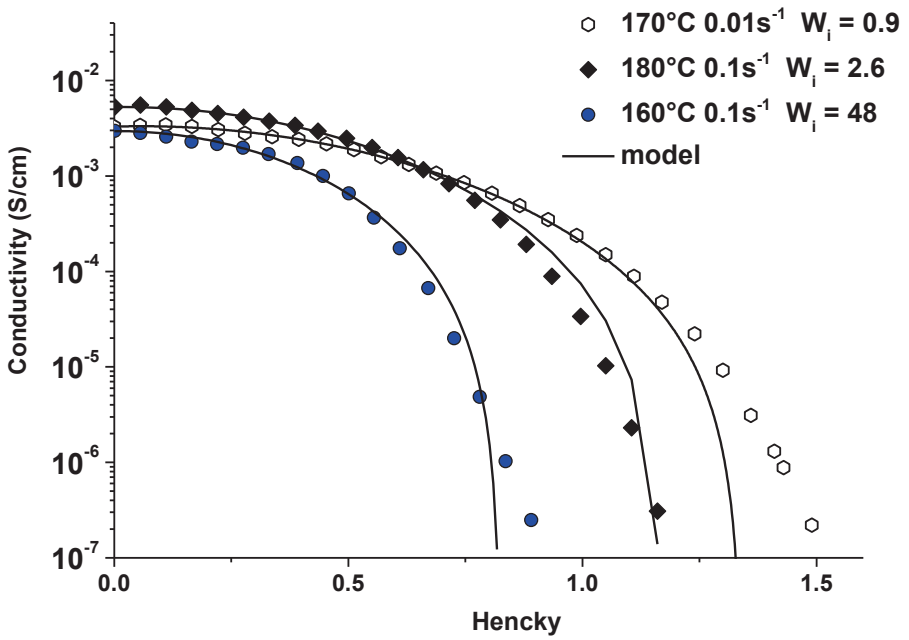

Figure 6: Conductivity variation as a function of the Hencky deformation of PS/MWCT (0.79 vol%) for large W_i. The symbols are the experimental data and the solid lines are the calculated curves.

First of all, it can be observed that the proposed model well describes the strong competition between network structuring and breaking that is observed in Figure 4 (for low W_i). At moderate and large W_i, (see Figure 5 and Figure 6) there is also a good description of the conductivity variation. Moreover, the obtained structuring parameter increases with the temperature and does not depend on the extensional rate (see Table 1). Furthermore, other results that are not detailed in this paper show that this structuring parameter is independent of the filler concentration. This corroborates the assumption that the building mechanism is mainly driven by the polymer mobility in the matrix.

2. Analysis of the structuring and breaking parameters

A large number of experimental data has been analyzed using the model. The dependence of the building and breaking parameters are respectively displayed in Figure 7a and 7b.

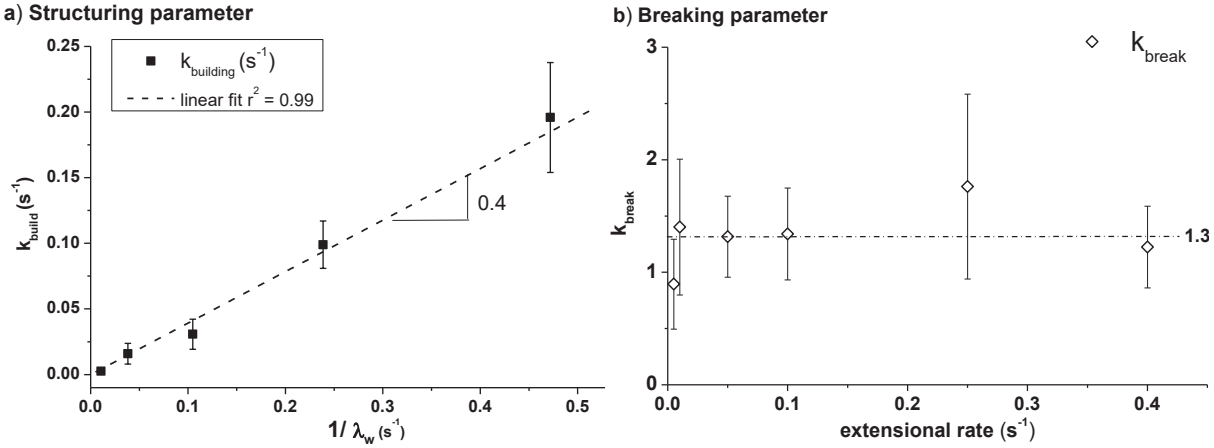

Figure 7: (a) Variation of the structuring parameter versus the inverse of the weight average relaxation time of the pure matrix and (b) the variation of the breaking parameter versus the extensional rate.

Figure 7a displays the variation of the building parameter as a function of the inverse of the weight average relaxation time which is given by the nature of the polymer matrix and the temperature using the Williams Landel Ferry equation [29,30]. The details of the rheological behavior of the used PS matrix are given in Reference [16]. The correlation is very clear indicating that the building coefficient increases with the temperature. Indeed, when the viscosity of the polymer decreases, the structuring mechanisms that are composed of diffusion of single CNTs and agglomeration of close aggregates are enhanced. Here, a linear dependence between the building parameter and the inverse of the characteristic time of the polymer is observed. Thus, at low temperature (140°C and 160°C), where the structuring parameter cannot be directly fitted on the experimental conductivity, it has been calculated from the relation displayed in Figure 7a. Nevertheless, this results show that the polymer dynamics dries the network structuring. Thus, the building parameter can be obtained from the relaxation time of the pure matrix and the Williams Landel Ferry coefficients for a given temperature.

The evolution of the breaking parameter is plotted in Figure 7b as a function of the extensional rate. No dependence is observed. However, this independence is consistent with the approach of Leonov [26] who considered a breaking mechanism dependent on the squared deformation rate. Indeed, in Equation 10 the squared elongation rate appears in the second member in an analogous manner to the Leonov's approach for the description of highly filled polymer under shear deformation at small shear rate. Indeed, they introduced the second invariant of the shear rate tensor in the kinetic equation for the evolution of the percolated network.

$$\frac{d\varphi_{eff}}{dt} = \frac{\alpha}{\lambda_{w-T_{ref}} a_T}\left(\varphi - \varphi_{eff}\right) - 2k_{break}\dot{\varepsilon}^2\varphi_{eff}$$

Equation 10

where α and k_{break} are dimensionless constants that depends on the material. In view of the results, it can be pointed out that α is a parameter characteristic of the matrix and k_{break} a parameter characteristic of the filler network.

C. Application of the model

1. Comparison with experimental data

The domain of validity of the proposed model has been tested. The model has been applied on different filler concentrations in the range between 0.38 vol% and 1.9 vol% of CNT in PS at different extensional rates. Here, for sake of simplification, it is assumed that the filler dispersion appearance is comparable for the different tested concentrations. However, it must be conceded that this assumption is questionable especially for large filler concentrations where there is a larger population of big agglomerates and at very low filler concentrations (lower than 0.5 vol%) where the fillers are more dispersed and consequently, the structuring mechanism are quite limited.

In a previous work, the Hencky deformation when the specimen conductivity reaches 10^{-6} S.cm^{-1} (ε_σ) has been introduced and used to characterize the composites behavior under different extensional conditions. Figure 8 displays experimental and calculated data obtained at 0.1 s^{-1} and 160, 180, 200 and 210 °C. The experimental data are chosen to cover both low and large W_i values.

For the calculated data, an initial efficient concentration φ_0 of CNTs that belongs to the percolated network has been set to 95% of the total filler concentration φ. This value corresponds to the initial measured value of conductivity and this illustrates the fact that the specimen is not totally at equilibrium at the beginning of the measurement.

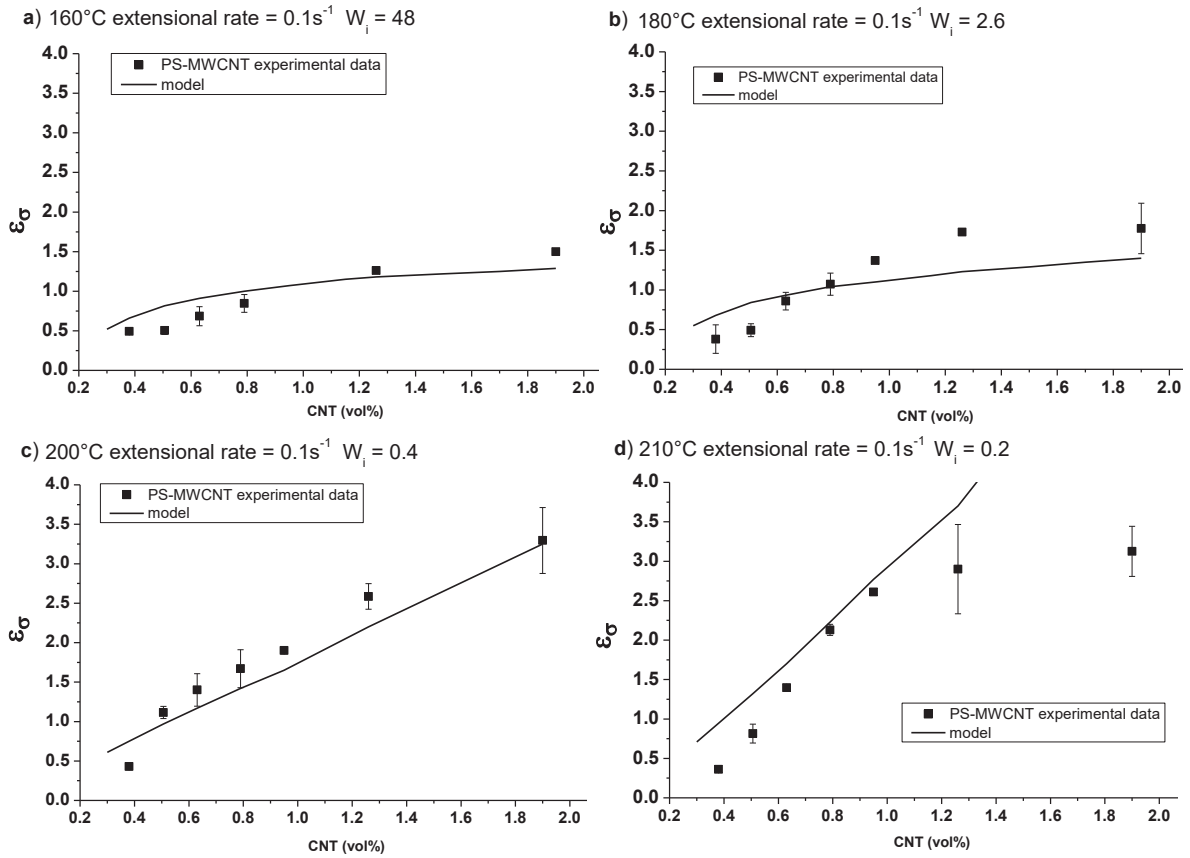

Figure 8 : Variation of the maximal deformation before conductive/insulating transition for PS filled with CNT (0.37 to 1.9 vol%) at an extensional rate of 0.1s^{-1} and at 160°C (a), at 180°C (b), at 200°C (c) and at 210°C (d). The filled squares are the experimental data and the solid lines are the calculated data.

At large W_i, (see Figure 8 a) and Figure 8 b)) the model correctly predicts the evolution of ε_σ for different filler concentrations and extensional conditions. Figure 8 c) and d) display ε_σ for close W_i values but obtained in different extensional conditions. At W_i = 0.4 there is a very good prediction of the model. However, at W_i = 0.2, the prediction of the model is acceptable, except for large concentrations (higher than 1.2 vol%). In those cases, the maximal deformation is overestimated and even predicts ε_σ that are larger than the specimen deformation at break. Indeed, under extensional deformation, the specimens break approximately after a Hencky deformation of 4, however, from a Hencky deformation of 3.5, the specimen becomes very thin and the homogeneity of the strain in the sample may not be ensured anymore. Consequently, the structuring mechanism may be disrupted while it is still considered in the model. Hence, at low temperatures, the building parameter is small so that it does not impact the prediction. However, at higher temperature (for instance 210 °C) the structuring factor is quite important and leads to an overestimation of the ε_σ.

2. Interplay between network structuring and breaking

Finally, the capability of the model to describe the competition between network structuring and breaking has been tested. Different calculated data have been generated in order to cover a large range of W_i and analyze the competition between structuring and destruction predicted by the model. The results are displayed in Figure 9.

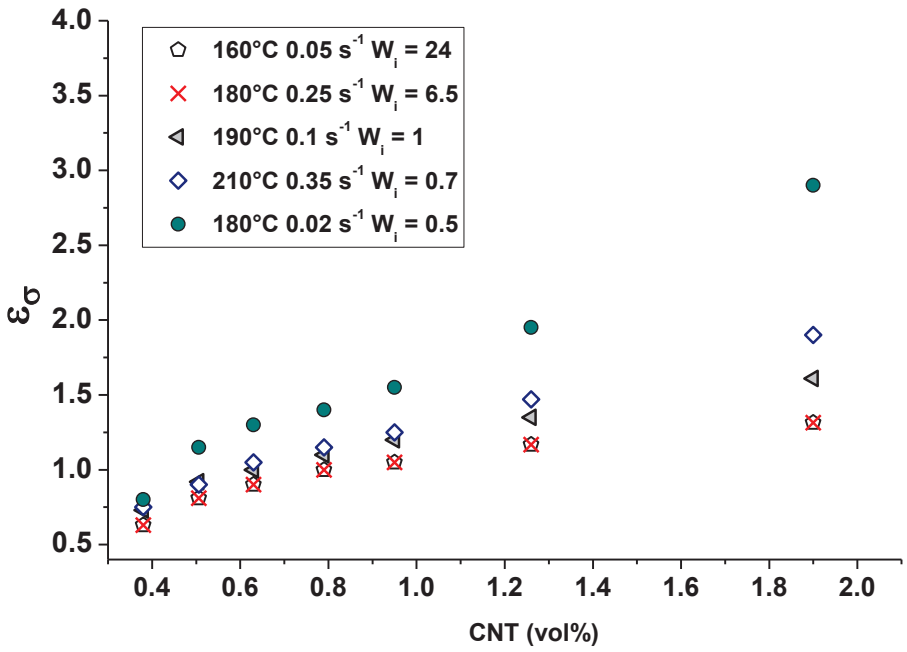

Figure 9: Model prediction of the maximal Hencky deformation before conductive/insulating transition for different W_i values.

In Figure 9 it can be observed that, for large W_i, (W_i = 24 and W_i = 6.5) all data merge to the same limiting Hencky deformation. Those results are in pretty good agreement with the experimental results. Indeed, it has been observed that, above a given W_i value, all the conductivity curves merge to the same Hencky deformation before conductive/insulating transition (here approximately 1.25). With the decrease of W_i, the material can undergo larger deformation before becoming electrically insulating (from W_i = 1). This transition from large to low W_i can be well observed in Figure 9.

V. Conclusion

In this work, a new model for the description of the conductivity variation of Conductive Polymer Composites under extensional deformation has been proposed and tested for large ranges of CNTs concentrations and extensional rates. First of all, the proposed model gives the possibility to describe the conductive to insulating transition for experimental conditions that cover a large range of W_i values. Indeed, it well describes the conductivity variation when the destruction is predominant but also when there is a strong competition between structuring and destruction of the network. We have also observed that the structuring mechanism only depends on the temperature and, more precisely, it is directly linked to the weight average relaxation time of the pure matrix. This means that the effect of the temperature on the building parameter can be determined using the Williams Landel Ferry equation applied to the polymer matrix. Hence, the temperature effect is solely in the structuring mechanism. Moreover, the breaking mechanism has been considered directly dependent of the deformation and it turned out that it was independent of the temperature and of the extensional rate. In some cases, the model overestimates the limit of the material. It occurs when the structuring parameter is quite large. After large deformation, the network structuring cannot be considered anymore as efficient as it would for an isotropic filler network.

This model presents a large domain of validity and gives the possibility to predict the limit of the composite under extensional deformation. We assume that the building and breaking parameters are linked to the type of CNTs and the dispersion state of the CNTs within the polymer matrix. In addition, this model can be extended to different kinds of composites. For example, it can be successfully applied to specimens made of High Impact Polystyrene matrix filled with CNT. Moreover, the model might be generalized to take into account other types of deformation such as planar flow or even shear.

References

[1] Kirkpatrick, S. Percolation and conduction. *Rev. Mod. Phys.* **1973**, 45, 574–588

[2] Bauhofer, W.; Kovacs, J. Z. A review and analysis of electrical percolation in carbon nanotube polymer composites. *Compos. Sci. Technol.* **2009**, 69, 1486–1498

[3] Pang, H.; Xu, L.; Yan, D.-X.; Zhong-Ming Li, Z.-M. Conductive polymer composites with segregated structures. *Prog. Polym. Sci.* 2**014**, 39, 1908–1933

[4] McNally, T.; Pötschke, P. Polymer-carbon nanotube composites. Preparation, Properties and Applications. Woodhead Publishing Limited 2011; Part I, pp 92-152

[5] Alig, I.; Pötschke, P.; Lellinger, D.; Skipa, T.; Pegel, S.; Kasaliwal, G. R.; Villmow, T. Establishment, morphology and properties of carbon nanotube networks in polymer melts. *Polym.* **2012**, 53, 4-28

[6] Moreira, L.; Fulchiron, R.; Seytre, G.; Dubois, P.; Cassagnau, P. Aggregation of Carbon Nanotubes in Semi-dilute Suspension. *Macromol.* **2010**, 43, 1467-1472

[7] Pegel, S.; Pötschke, P.; Petzold, G.; Alig, I.; Dudkin, S. M.; Lellinger, D. Dispersion, agglomeration, and network formation of multiwalled carbon nanotubes in polycarbonate melts. *Polym.* **2008**, 49, 974–984

[8] Obrzut, J.; Douglas, J. F.; Kharchenko, S. B.; Migler, K. B.; Shear-induced conductor–insulator transition in melt-mixed polypropylene–carbon nanotube dispersions, *Phys. Rev. B*, **2007**, 76, 195420/1-9

[9] Kharchenko S. B.; Douglas, J. F.; Obrzut, J.; Grulke E A, Migler, K. B. Flow-induced properties of nanotube-filled polymer materials. *Nat.*, **2004**, 3, 564–568

[10] Martin, C. A.; Sandler, J. K.; Shaffer, W.; Schwarz, M. S. P.; Bauhofer, W.; M. K.; Schulte, K.; Windle, A. H. Formation of percolating networks in multi-wall carbon nanotube epoxy composites. *Compos. Sci. Technol.* **2004**, 64, 2309–2316

[11] Ma, A. W. K.; Mackley, M. R.; Rahatekar, S. S. Experimental observation on the flow-induced assembly of carbon nanotube suspensions to form helical bands. *Rheol. Acta* **2007**, 46, 979–987

[12] Sandler, J. K. W.; Windle, A. H.; Martin, C. A.; Schwarz, M. L.; Bauhofer, W.; Schulte, K.; Shaffer, M. S. P. Percolation in multi-wall carbon nanotube-epoxy composites: influence of processing parameters, nanotube aspect ratio and electric fields on the bulk conductivity. *Contin. Nanophase Nanostruct. Mat.* **2004**, 788, 221–226

[13] Kovacs, J. Z.; Velagala, B. S.; Schulte, K.; Bauhofer, W. Two percolation thresholds in carbon nanotube epoxy composites. *Compos. Sci.Technol.* **2007**, 67, 922–928

[14] Alig, I.; Lellinger, D.; Dudkin , S. M.; Pötschke, P. Conductivity spectroscopy on melt processed polypropylene multiwalled carbon nanotube composites: Recovery after shear and crystallization. *Polym.* **2007**, 48, 1020-1029

[15] Bauhofer, W.; Schulz, S.C.; Eken, A.E.; Skipa, T.; Lellinger, D.; Alig, I.; Tozzi, E.J.; Klingenberg, D.J. Shear-controlled electrical conductivity of carbon nanotubes network suspended in low and high molecular weight liquids. *Polym.* **2010**, 51, 5024-5027

[16] Marcourt, M.; Cassagnau, P.; Fulchiron, R. An original combined method for electrical conductivity measurement of polymer composites under extensional deformation. *J. Rheol.* **2017**, 61, 845-851

[17] Villmow, T.; Pegel, S.; Pötschke, P.; Wagenknech, U. Influence of injection molding parameters on the electrical resistivity of polycarbonate filled with multiwalled carbon nanotubes. *Compos. Sci. Technol.* **2008a**, 68, 777–789

[18] Skipa, T.; Lellinger, D.; Saphiannikova, M; Alig, I. Shear-stimulated formation of carbon nanotube networks in polymer melts. *Phys. Status Solidi B*, **2009**, 246, 2453–2456.

[19] Skipa, T.; Lellinger, D.; Böhm, W.; Saphiannikova, M; Alig, I. Influence of shear deformation on carbon nanotube networks in polycarbonate melts: interplay between build-up and destruction of agglomerates. *Polym.* **2010**; 51: 201–210

[20] Barnes H., Thixotropy a review, *Journal of Non Newtonian Fluid Mechanics*, **1997**, 70, 1-33

[21] Chen, M.; Russel, W.B. Characteristic of flocculated silica dispersion. *J. Colloid Interface Sci.* **1991**, 141, 564-577

[22] Coussot, P.; Leonov, A.I.; Piau, J.M. Rheology of concentrated dispersal systems in a low molecular weight matrix. *J. Non-Newtonian Fluid Mech.* **1993**, 46, 94-114

[23] De Kee, D.; Code, R.; Turcotte, G. Flow properties of time dependent food stuffs. *J. Rheol*. **1983**, 27, 581-604

[24] Quemada, D. Rheology of concentrated dispersed systems and minimum energy dissipation principle. I Viscosity-concentration relationship. *Rheologica Acta*, **1977**, 16, 82-94

[25] Yziquel, F.; Carreau P.J., Tanguyn P.A. Non-linear viscoelastic behavior of fumed silica suspensions. Rheol. Acta, **1999**, 38, 14-25

[26] Leonov, A. I. On the rheology of filled polymers *J. Rheol.*, **1990**, 34, 1039-1068

[27] Alig, I.; Skipa, T.; Lellinger, D.; Pötschke P. Destruction and formation of a carbon nanotube network in polymer melts: Rheology and conductivity spectroscopy. *Polym.* **2008**, 49, 3524-3532

[28] Bird, R.B.; Armstrong, R.C.; Hassager, O. Dynamics of polymeric liquids. Vol. 1, 2nd Edition : Fluid mechanics, John Wiley and Sons Inc.,New York, NY; None. Medium: X; Size: 1987. Page: 784.

[29] Ferry, J.D. Viscoelastic properties of polymers, Third edition ed. 1980

[30] Ferry, J. D.; Williams, M. L.; Fitzgerald, E. R.; The temperature dependence of relaxation mechanisms in amorphous polymers and other glass-forming liquids, *JACS*, **1955**; 77(14), 3701-3707.

[31] Huang, Y.; Terentjev, E. M. Dispersion of Carbon Nanotubes: Mixing, Sonication, Stabilization, and Composite Properties. *Polym.* **2012**, 4, 275-295

[32] Chang, E.; Ameli, A.; Mark, L.H.; Park, C.B. Effects of uniaxial and biaxial orientation on fiber percolation in conductive polymer composites *AIP Conference Proceedings* **2015**, 1695, 020027

[33] Du, F.; Fischer, J.; Winey, K. Effect of nanotube alignment on percolation conductivity in carbon nanotube/polymer composites. *Phys. Rev. B* **2005**, 72, 121404/1-5

Additional content part 1

Application to thermoforming

I. Introduction

The goal of the PhD was to analyze and understand the behavior of conductive polymer composites during thermoforming. An innovative lab-scale set-up has given the possibility to analyze the conductivity variation of molten composites under extensional deformation. This experiment gave us precious results on the processing limits of specimen for the generation of composite parts with tailored electrical properties. In this chapter, we compare the lab-scale experiments to the thermoforming of composites. First, a complete presentation of the thermoforming machine and the characterization of the deformations and the strain rates will be carried out. Then, the results obtained will be compared to the developed model.

II. Experimental section

A. Materials and methods

1. Composites

The specimens are composites made of Polystyrene (PS) filled with 1.25 wt% of MWCNTs. The CNTs are the NC7000 supplied by Nanocyl, a Belgian company. They are characterized by a diameter d around 9.5 nm and a mean length of 1.5 µm. The matrix is fully amorphous with a melt flow index of 2.4 supplied by Total. The composites were melt mixed using a masterbatch dilution strategy and were supplied by Total as pellets.

B. Methods

1. Thermoforming

The sheets are 16x16 cm^2 with a thickness fix at 525 +/- 25 µm and obtained by compression molding. The thermoforming is carried out using a small thermoforming machine. The set-up is displayed in Figure 1. The thermoforming process consists of three stages. First, the sheet is clamped to the holder. The holder is fixed on the machine support (see Figure 1c), then the support translates to position a), where the sheet is heated by two IR radiants panels. The temperature of the sheet is by an infra-red imager that is located between the heating stage and the deformation stage (see Figure d)). So the temperature is only measured when the sheet translates to the deformation stage. In addition, this measure is carried out locally in the middle of the sheet. The determination of the sheet temperature required additional measurements in order to determine the sheet temperature as a function of the heating duration. This relation depends on the filler concentration, the sheet thickness, the radiant panel power and the matrix. During the heating stage, the holder can laterally move preventing large sagging. When the sheet has reached the appropriate temperature the holder moves to the stage (b). Here, a plug comes immediately into contact with the sheet and goes down to the targeted depth of the final cup. To give its final shape, the pre-form is forced against the mold by a vacuum.

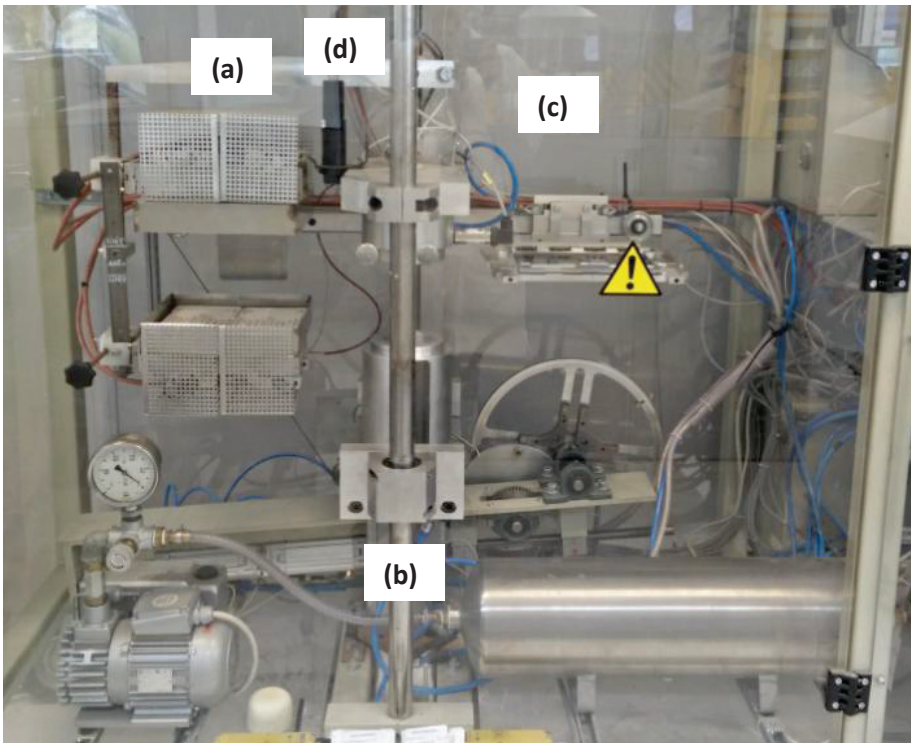

Figure 1; Details of the thermoforming machine (ALM) with respectively a) the heating area, b) the thermoforming zone, c) the sheet holder and d) the infra-red imager.

This machine allows large range of cup depths, plug speeds and pressures to accomplish the cup forming. However, the sheet temperature is not controlled during the deformation. Its temperature will decrease due to heat transfer during its shift position to the thermoforming area and when the plug comes into contact with it. The heat transfer is very important between the sheet and the plug as the plug is not thermally regulated. A detailed analysis of the heat transfer between the plug and the composite sheet was not carried out in this work. Moreover, if experiments are carried out one after the other, the enclosure heats up and so does the plug. Thus, the thermal history from one cup to the other may vary.

2. Deformation analysis

After the compression molding, the sheet is finely patterned (the ink is applied with a stencil). The square will give the possibility to measure the deformation after the thermoforming. Figure 2 shows the different stages of the sheet: (a) after the compression molding, (b) after that the plug went down to the targeted depth and (c) after the sheet was forced against the mold wall by vacuum.

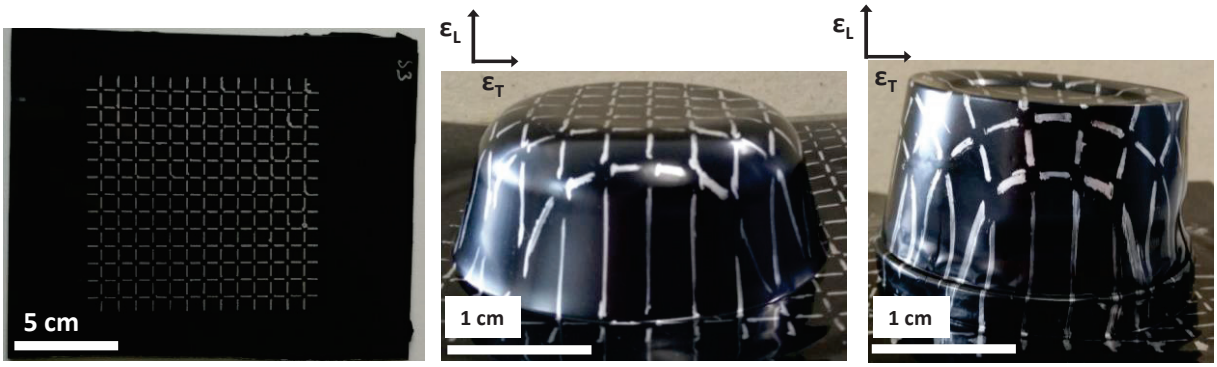

Figure 2: micrographs of a) the compression molded sheet with the pattern, b) the cup deformed by the plug and c) the cup after a plug and vaccum-assisted thermoforming.

The local strain is determined as:

$$\varepsilon = \ln(\frac{L}{L_0})$$

Equation 1

with L_0 the initial length of the pattern and L the measured length after the deformation. The strain analysis of the cup will take into account the longitudinal ε_L and the transversal deformation ε_T. The plug will mainly generate uniaxial deformations with $\varepsilon_L/\varepsilon_T > 10$ whereas; the last stage will induce a pure radial deformation near the cup bottom. Indeed, this last stage leads to $\varepsilon_L/\varepsilon_T \approx 3$.

To simplify the analysis and be able to compare the laboratory scale set-up to the thermoforming stage, the work will be restricted to the analysis of the deformation generated by the plug (analysis restricted to mainly uni-axial deformations). The variation of the deformation will be controlled by the descent of the plug. The cup bottom is slightly deformed. This area will be not analyzed.

3. Local strain analysis

The plug reaches a linear speed before coming into contact with the sheet. We assume that the stretching is done at a constant plug speed. The thermoforming machine prevents a precise analysis of the local strain which would be possible thanks to an in-line observation of the deformation (camera set-up). Another option, less precise was to determine the duration of the thermoforming with the monitoring of the strength applied on the plug. The strain rate is determined as the strain measured over the thermoforming duration as:

$$\dot{\varepsilon} = \frac{\varepsilon_L}{\Delta t}$$

Equation 2

with ε_L the local deformation in the longitudinal direction and Δt is the required time for the plug to complete descent. At the very beginning of the thermoforming, the force level remains low. It may not be measured by the force sensor inducing underestimation in the thermoforming duration. First, the evolution of the strain rate as a function of the plug speed has been analyzed in order to determine the appropriate range of strain rate to be close as possible to the extensional conditions of the lab-scale experiment. Figure 3 illustrates the evolution of the extensional rates as a function of the Hencky deformation measured for three plug speeds. Not surprisingly, the extensional rate increases with the plug speed, however, it also does with the Hencky deformation.

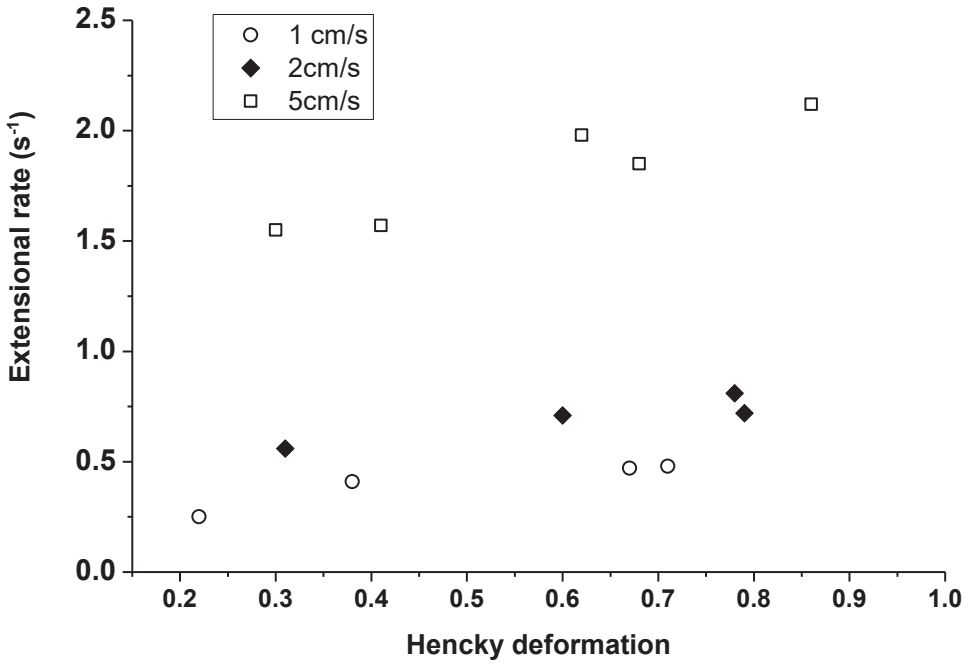

Figure 3: Variaiton of the extensional rate (measure on the cup side) as a function of the Hencky deformation for different plug speed (from 1 cm/s to 5 cm/s) at 190 °C

This method shows some drawbacks. First, the dimension of the square is too large compared to the cup depth. In some cases, illustrated in Figure 2 (b), the cup depth is not enough to perform a precise measure of both deformation and conductivity. Indeed, one can observe that only one square is deformed on the side of the cup. The not homogeneous temperature of the sheet will generate not homogeneous strain rate especially on the side of the cup. Figure 4 shows the strain rate as a function of the Hencky deformation for a plug speed fixed to 1 cm/s. The temperature varies between 180 °C and 210 °C. One can observe that the extensional rate increases with the deformation. From Hencky deformation around 0.6 the extensional rates finally merges to a constant value.

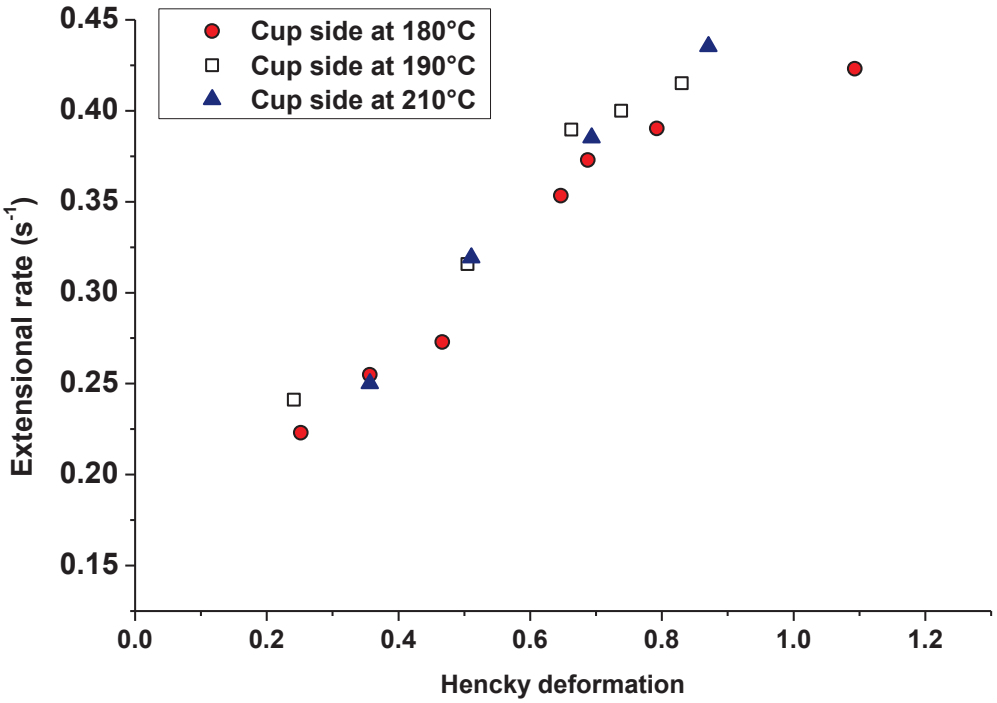

Figure 4: Evolution of the extensional rate as a function of the Hencky deformation at 210 °C, 190 °C and 180 °C. The plug speed is fixed to 1 cm/s. The deformations are measured on the side of the cup.

The Extensional Viscosity Fixture (EVF) combined with conductivity measurement presented earlier in this work gives the possibility to analyze the conductivity of molten composite under extensional deformation at a constant strain rate. The goal is to compare the lab-scale set-up to a semi-industrial thermoforming process.

C. Results and analysis

1. Variation of the thermoforming conditions

We played on the thermoforming conditions (temperature and plug speed) in order to identify the influencing parameters for the composites melt forming. The temperature mentioned in the text and in all Figure caption is the one measured during the transition from the heating stage to the forming stage. (see Figure 1 b)). We are truly aware that this assumption clearly overestimates the actual sheet temperature during the thermoforming. Conductivity measurements have been carried out where the deformation and the extensional were measured. Only surface conductivity could have been achieved due to the extremely brittle final parts. Indeed, even a small compression on a curved surface will dramatically leads to irreversible damage. We make the assumption that the conductivity does not variate a lot between the core and the surface. This is an appropriate

approximation as the semi products, generated by compression molding, are homogeneous. This would have been wrong considering calendared sheets. Indeed, the generation of composite sheets by calendaring leads to semi-products with non-homogeneous filer dispersion. There is a strong CNTs depletion at the extreme surface of the sheet which leads to differences between surface and volume conductivities.

Thermoforming have been performed at three temperatures from 180 °C to 210 °C for different plug speeds and cup depths to generate various extensional rates and Hencky deformations. Figure 5 displays two sets of conductivity values as a function of the Hencky deformation for two extensional rates: 0.25 s^{-1} and 0.4 s^{-1}. For each temperature, the Weissenberg number has been determined from the relaxation time corresponding to the measured temperature. The initial conductivity is measured after the thermoforming where the sheet is not deformed (see Figure 2). The conductivity at *t=0* is taken as the mean value of all conductivities measured specimen deformed with similar thermoforming conditions. In Figure 5a), we observe a distinction from the conductivity obtained at lower temperature and consequently at larger W_i. After Hencky deformation of 0.35 the conductivity is two decades lower. However, in Figure 5b) the distinction is less obvious. The W_i at 210 °C is clearly underestimated.

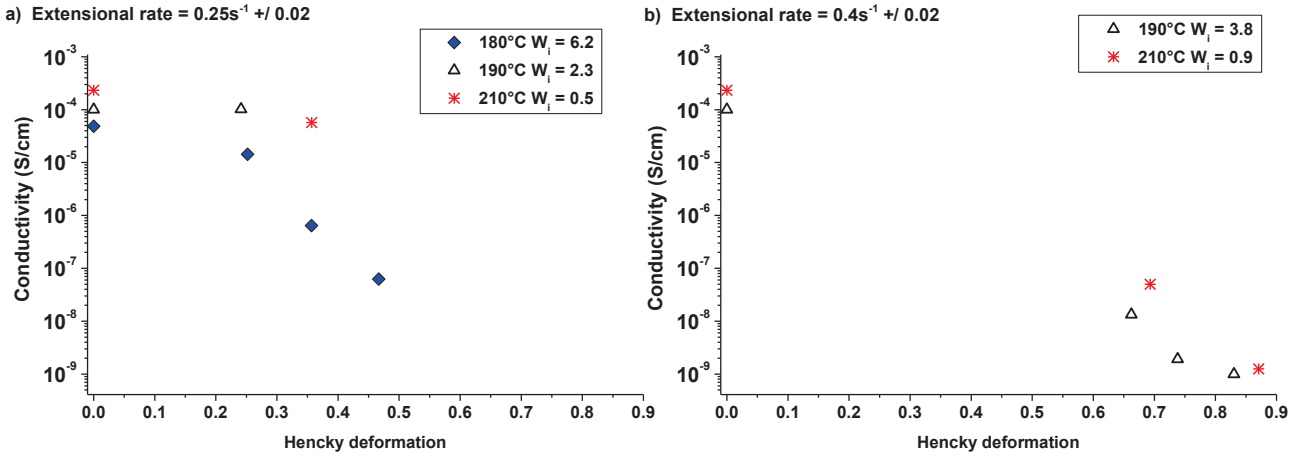

Figure 5: Conductivity variation as a function of the Hencky deformation of thermoformed composite sheets (PS filled with 0.79 vol% of CNTs). The extensional rate is around 0.25 s^{-1} a) and 0.4 s^{-1} b). The temperature varies from 180 °C to 210 °C.

A large number of thermoforming experiments have been carried out at 190°C. The data are displayed in Figure 6. We observe that all the data merge to the same curve. This result is quite comparable to those obtained with the EVF modified set-up. Indeed, from a W_i value, the conductivity variation is similar for different experimental conditions. The destruction mechanism becomes predominant over structuring mechanisms. The limiting parameter becomes the initial conductivity of the specimens. That is why, the experiments carried out at 180°C (see Figure 5 a)) with similar W_i than the experiments carried out at 190°C have lower conductivity for similar Hencky deformation. The initial conductivity is almost one decade lower.

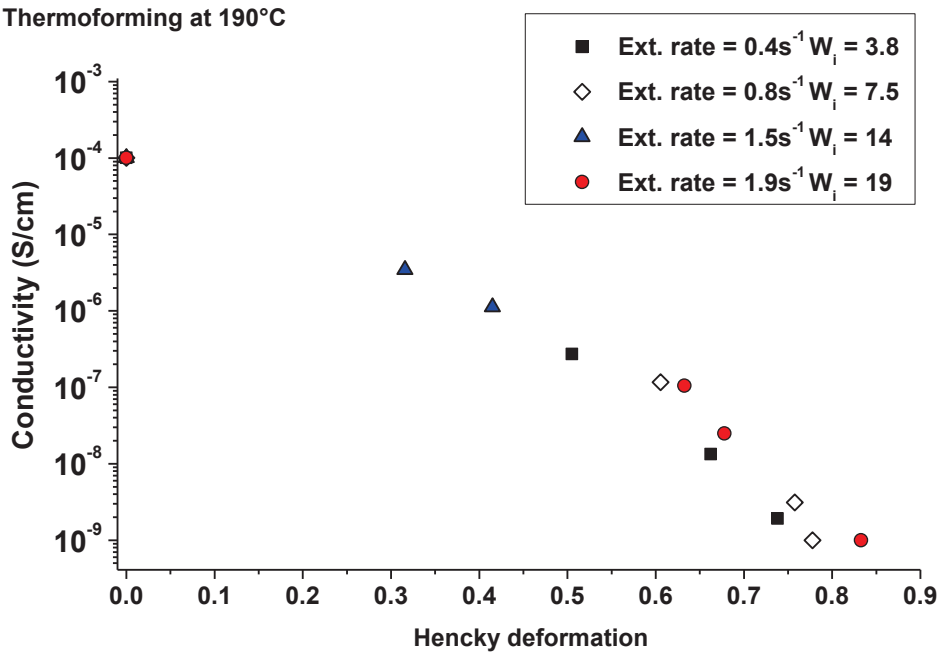

Figure 6: Conductivity variation as a function of the Hencky deformation of thermoformed composite sheets (PS filled with 0.79 vol% CNT) at 190 °C. The extensional rate varies from 0.4 s^{-1} and 1.9 s^{-1}.

During thermoforming, we hardly observe the impact of the temperature as observed thanks to the lab-scale experiments. However, we did observe the fact the filler network destruction is highly dependent on the Hencky deformation. We cannot directly compare the thermoforming data with those obtained with the modified extensional viscosity fixture. The initial conductivities are too much different (larger than one decade). This difference truly impacts the conductivity variation. That is why; we will compare data generated from the proposed model with thermoforming results.

2. Comparison with the proposed model

For each experimental condition, three initial conductivity values have been used: the mean, the lowest and the largest conductivity that are obtained from the characterization of not deformed area on different specimens.

The conductivity variation is deduced from those initial conditions. An envelope of the calculated data is displayed for each case. The breaking parameters are deduced from the relation presented in chapter 5.

$$Breaking\ parameter = 2k_{break}\dot{\varepsilon}^2$$

Equation 3

The building parameter is taken for a reference temperature 10 degrees lower than the temperature measured after the heating stage. This approximation was made to takes into account the decrease of temperature from the heating stage to the exact moment when the plug comes into contact with the composite sheet. In Figure 7 is displayed most of the experimental and calculated data obtained for three working temperatures.

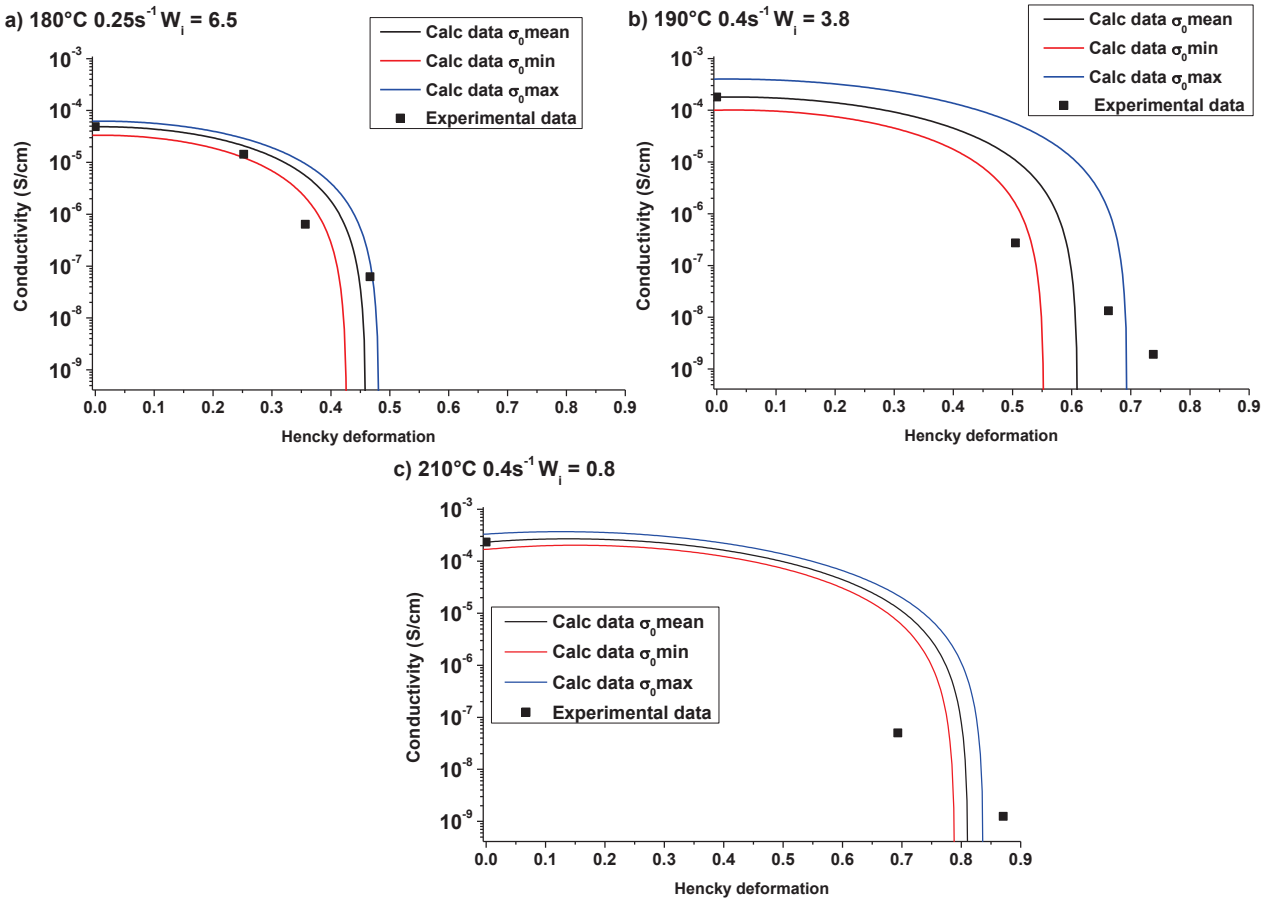

Figure 7 : Conductivity variation of thermoformed composite sheets (PS filled with 0.79vol% CNT) for different thermofroming conditions : W_i = 6.5 a), Wi= 3.8 b) and Wi = 0.8 c). For each conditions, the envelope of calculated data are displayed (solid lines), obtained from the lowest (red), the mean (black) and the largest initial conductivity (blue).

We observe that the experimental data are closed to the envelope of calculated data. Indeed, the extensional rate is not precisely known, the analyzed areas on the cup side are not deformed at a constant strain rate and the temperature is not homogenous. Moreover, the confinement leads to planar deformation whereas the EVF modified set-up induces uni-axial extensional deformation. Nevertheless, despite all these possible error sources, the model is in good agreement with experimental data and could be used for helping to predict the behavior of the material during thermoforming process.

III. Conclusion

In this study, we presented the strategy to analyze the conductivity variation of composite sheets as a function of the local Hencky deformation. The in-line observation of the cup during its thermoforming could not be achieved due to the mold that prevents the cup observation at the beginning of the thermoforming. Nevertheless, we determined the local extensional rate associated to the measure of the conductivity. We are truly aware that this measure is approximated as the cup side is not deformed at a constant strain rate and the temperature is not known or even controlled. Nevertheless, this study is consistent with the results obtained with the modified EVF. Indeed, at large Wi, the conductivity variation only depends on the initial conductivity value and the deformation. Moreover, the proposed model is in good agreement with the thermoforming data. It can be added that the model could be modified in order to take into account the planar deformation experienced during the thermoforming of the cup.

Additional content part 2

Various results

1. *Filler network analysis*

Determination of the agglomerate orientation

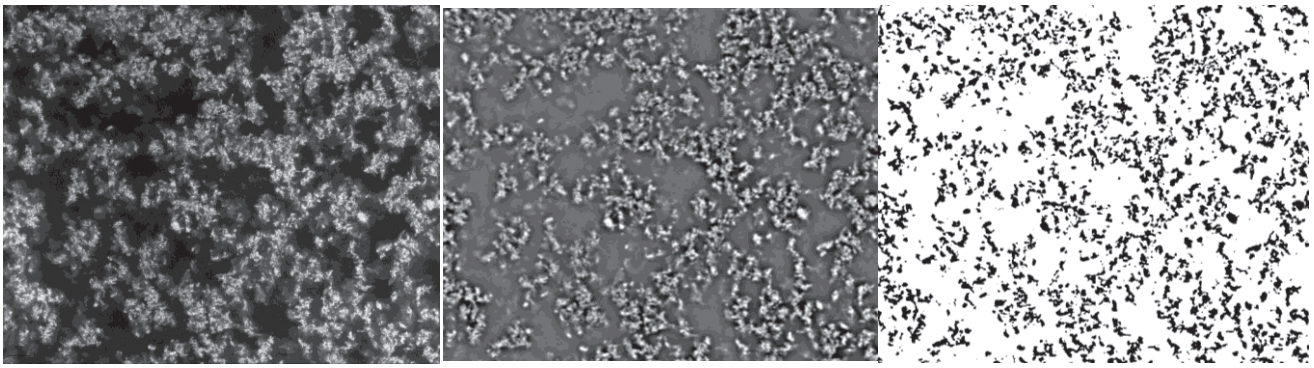

Figure 1: Image analysis using ImageJ. SEM image of compression molded specimen of PS+0.79vol% (left), image after noise reduction, contrast and edge improvement (middle), threshold image (right)

Evolution of the agglomerates orientation after extensional deformation.

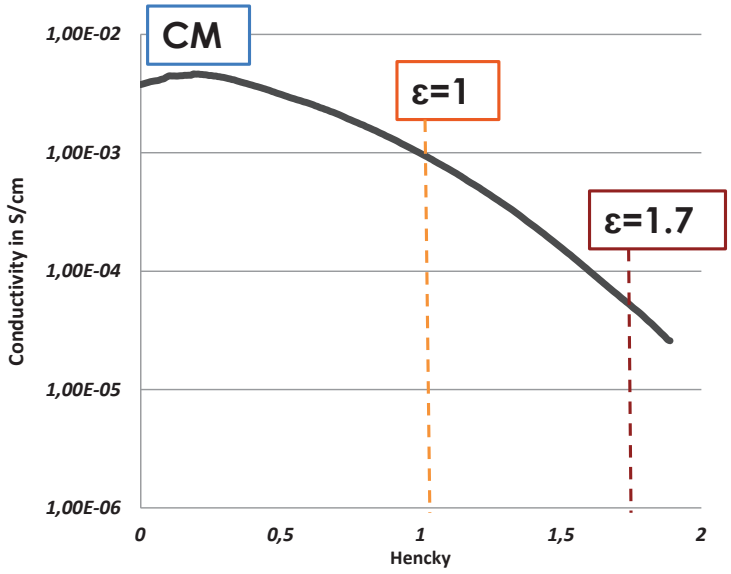

Figure 2: Conductivity variation of PS+0.79vol% (left) at 180°C and 0.01s^{-1}, Details of the analyzed specimen right after respectively compression molding (CM), 1 and 1.7 Hencky deformation

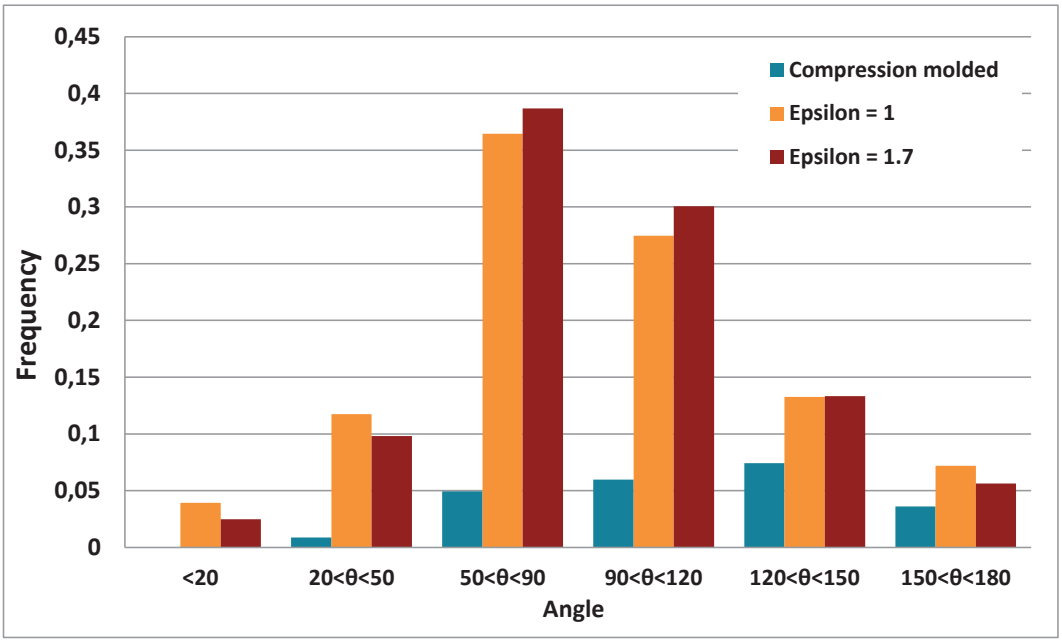

Figure 3: Analysis of the agglomerates orientation (determination of the Feret angle). 90° is the deformation direction of the extensional experiment. Specimen: PS+0.79vol% CNT, extensional conditions: 180°C and 0.01s⁻¹

Evolution of the agglomerates orientation of deformed specimen followed by quiescent treatment.

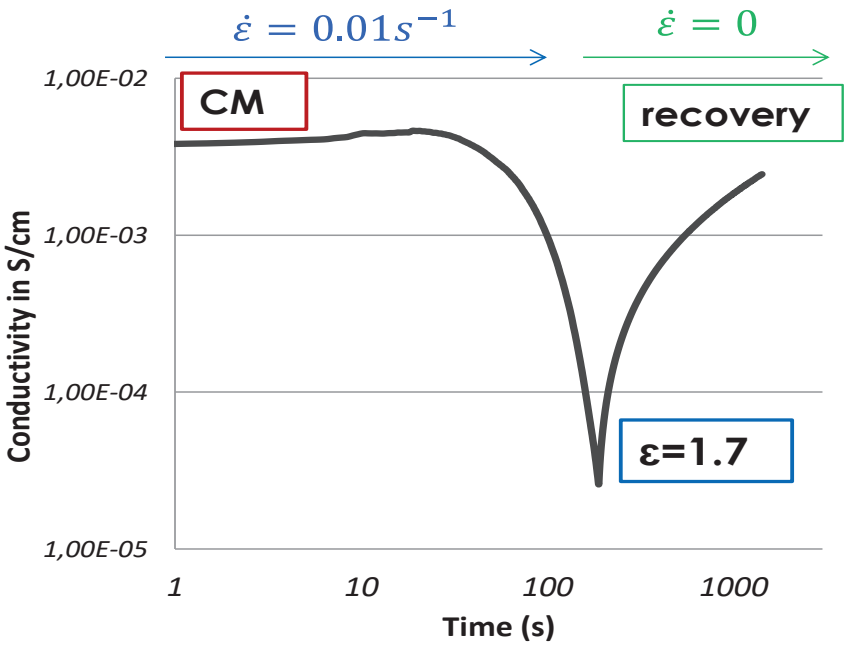

Figure 4: Conductivity variation of PS+0.79vol% (left) at 180°C and 0.01s⁻¹, Details of the analyzed specimen right after respectively compression molding (CM), 1.8 Hencky deformation and quiescent annealing at 180°C.

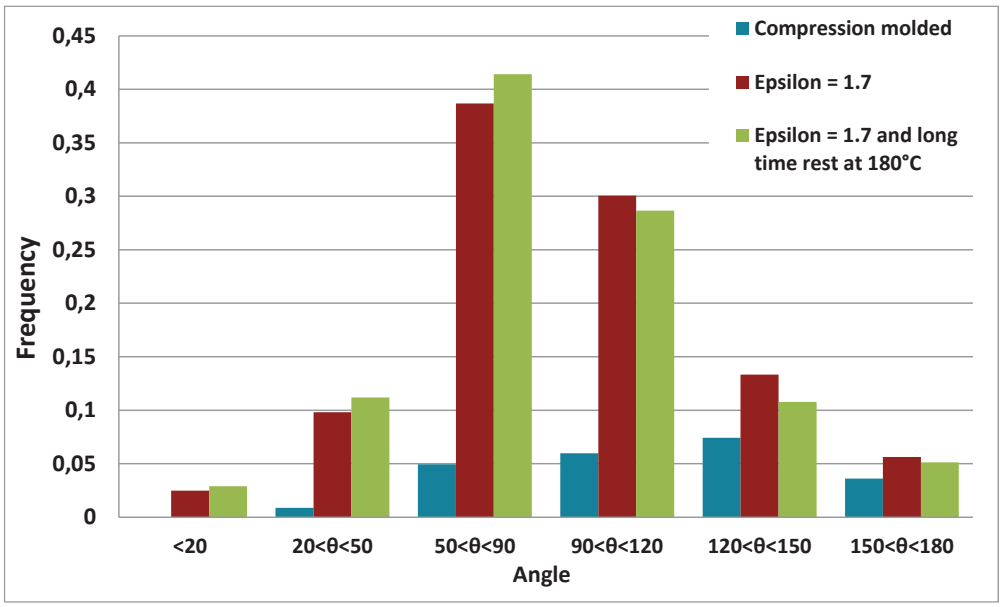

Figure 5: Analysis of the agglomerates orientation (determination of the Feret angle). 90° is the deformation direction of the extensional experiment. Specimen: PS+ 0.79vol% CNT. Extensional conditions: 180°C and 0.01s^{-1}

2. Additional results on the breaking and building parameters

Breaking parameters for HIPS filled with CNT composites

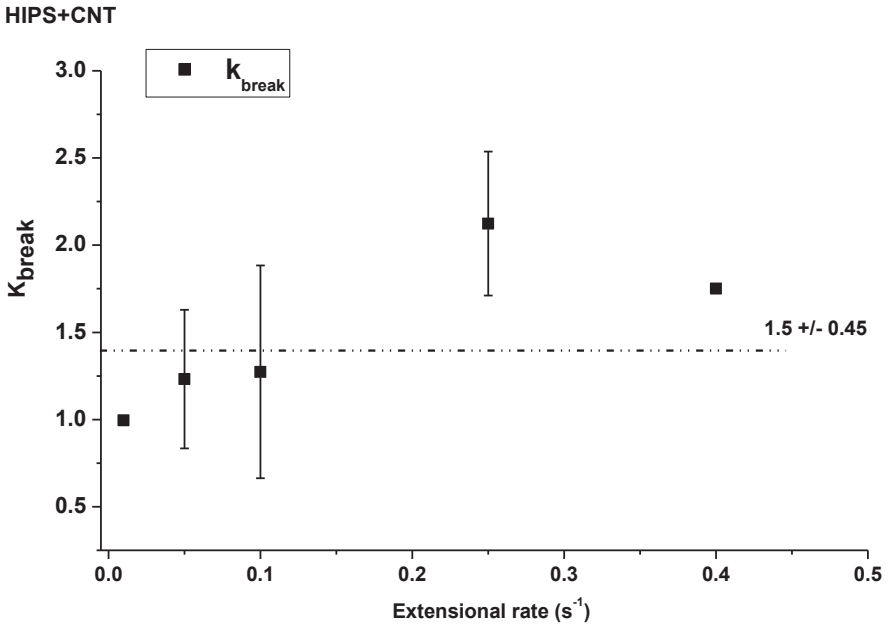

Figure 6: Variation of the breaking parameter versus the extensional rate for HIPS +0.82 vol% CNT composites.

Breaking parameter for PS filled with CNTs composites plotted as a function of the temperature.

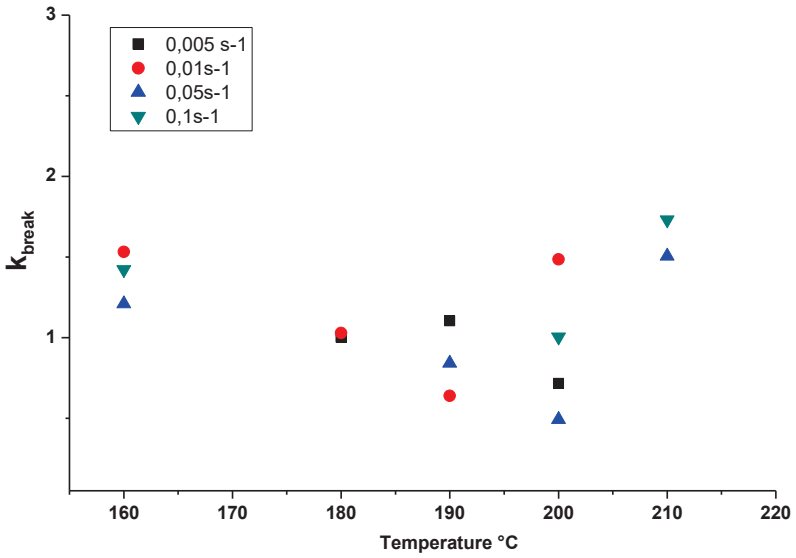

Figure 7: Variation of the breaking parameter versus the temperature for PS +0.79vol% CNT.

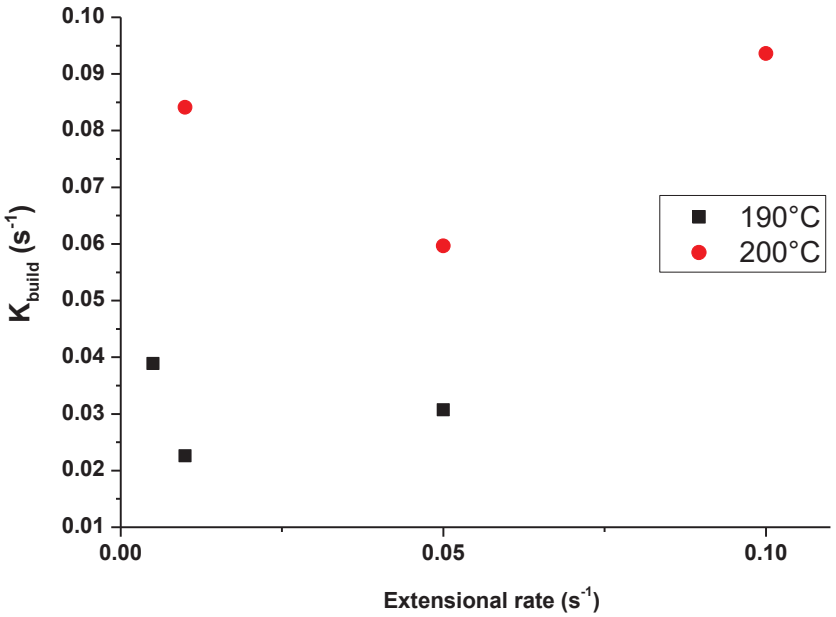

Figure 8: Variation of the structuring parameter versus the extensional rate for PS + 0.79vol% CNT.

Conclusion and outlooks

The purpose of this thesis was to investigate and to understand the conductivity evolution of molten composites under high elongational deformations. To do so, a new experiment that allows for the conductivity monitoring of specimen during extensional flow was developed. The use of this innovative set-up was combined with a complete Scanning Electron Microscopy analysis, which gave us precious information on the composites microstructure variation. Using these experimental methods, two composites were analyzed: a pure polystyrene matrix filled with Carbon Nanotubes (CNTs) and a more complex material: a rubber-modified polystyrene also filled with CNTs. Those composites are electrically conductor thanks to a percolated CNTs network within the polymer. When the composite flows, the filler network can be disrupted, altering the conductivity of the composite.

First of all, the precise analysis of the pure Polystyrene matrix filled with CNTs has highlighted the combined roles of the molecular dynamics in the polymer matrix and the extensional rate on the conductivity variation. We have shown that, when the composite flows the CNTs are oriented within the flow direction and are pulled apart from each other. The numbers of connections that constitute the filler network decreases, the percolated network that is responsible of the electron pathway is less dense and, consequently, the conductivity drastically declines. However, the way of the conductivity decreasing is closely linked to the extensional conditions.

Indeed, we have shown that the conductivity decreasing that is more or less fast can be linked to the Weissenberg number that takes into account the relaxation time of the polymer and the extensional rate. When the composite flows, the structure of the filler network is modified. A competition takes place between the network structuring via the formation of connections between CNTs and the network breaking that is illustrated by the orientation of the CNTs and the increasing remoteness between aggregates. The range of the Weissenberg number can describe how the composite loses its conductivity. Actually, for large Weissenberg numbers, the breaking mechanism will be the main phenomenon. However, when the relaxation time of the polymer chains is short, the simultaneous network building and breaking takes place. Thus, the composite can undergo larger deformation before losing its conductivity.

This analysis has been extended to more complex material: a High Impact Polystyrene filled with CNTs. In this material, the CNTs are confined in the Polystyrene phase outside the nodules. We have shown that the filler volume confinement gives the possibility to practically halve the CNT weight concentration for the generation of CPC without impacting there process-ability during

thermoforming. Indeed, considering the effective volume concentration of the filler in the Polystyrene phase, the two kinds of composites present very close volume conductivities. Moreover, for large W_i values, they show similar Hencky strain limit of the conductive behavior. However, under extensional conditions at low W_i values, the HIPS composite loses its conductivity before the PS composite. This phenomenon has been attributed to the presence of the nodules that alter the structuring mechanism during the extensional deformation.

All those results give us the possibility to propose a model that makes the link between the structural modification of the filler network and the conductivity variation of the composite. Indeed, the filler network evolution can be described by a kinetic equation that takes into account the molecular dynamics of the polymer that is responsible for the network building and the deformation that leads to the network breaking. In other words, knowing the temperature, the extensional rate and the initial conductivity, the composite conductivity can be determined as a function of the Hencky deformation. More precisely, we have shown that the building parameter can be determined thanks the William Landel and Ferry equation and the relaxation time of the polymer matrix. Moreover, this model can be applied on more complex composites such as HIPS matrix filled with CNTs. This model can certainly be used to predict the conductivity variation of composites made of various polymer matrices or fillers. Moreover, this model can be extended to other kinds of deformation such as planar or shear flows by simply modify the expression of the deformation in the breaking part of the basic differential equation.

This innovative set-up gave us the possibility to precisely describe the composites under extensional flow and to bring relevant results amongst the abundant literature dedicated on this specific topic. For an industrial point of view, this study confirms results obtained during the thermoforming of composites. Indeed, a conductive composite sheet can turn into an insulating finished part after its thermoforming. We observed the same conductive/insulating transition and we are now able to determine the optimal thermoforming conditions and limiting Hencky deformation for a given composite. In addition, this innovative set-up can be used for a wide range of temperatures, so that it can be easily extended for testing other conductive materials.